University of Southampton

Faculty of Engineering, Science and Mathematics
School of Civil Engineering and the Environment

Geoenvironmental impacts of construction dewatering

by

Marc A. Bevan, BSc

A thesis submitted for the degree of Engineering Doctorate

November 2005

UNIVERSITY OF SOUTHAMPTON

ABSTRACT

FACULTY OF ENGINEERING, SCIENCE & MATHEMATICS

SCHOOL OF CIVIL ENGINEERING AND THE ENVIRONMENT

Engineering Doctorate

GEOENVIRONMENTAL IMPACTS OF CONSTRUCTION DEWATERING

by Marc A. Bevan

Designing a suitable construction dewatering system can be difficult where ground conditions are uncertain. Furthermore, uncertainty relating to the performance of a construction dewatering system can also add complexity to an assessment of the environmental impacts.

Numerical models were used to investigate the influence of inhomogeneities in the Chalk on the performance of a large-scale construction dewatering system. It was found that permeabilities in the Chalk varied considerably within a large excavation. In addition, anisotropy was shown to be influential when dewatering within cut-off walls.

The potential environmental impacts of construction dewatering include saline intrusion and contaminant migration. Numerical models were used as a tool for interpreting groundwater quality data collected during the construction period. The modelling suggested that significant saline intrusion occurred as a result construction dewatering. Migration of cement kiln dust leachate may have also taken place, although concentrations were probably strongly attenuated by mixing and in some cases by ion exchange.

Consideration was given to the suitability of site monitoring programmes, in particular the location of monitoring wells, the sampling period and the vertical migration of contaminants caused by drilling of boreholes.

Contents

List of Figures

List of Tables

List of Symbols

Greek symbols

α_L	Longitudinal dispersion
α_{TH}	Transverse horizontal dispersion
α_{TV}	Transverse vertical dispersion
θ	Effective porosity
ρ_b	Bulk density
σ	Normal total stress
σ'	Effective stress
τ_f	Shear strength
ϕ'	Angle of shearing resistance

Latin symbols

A	Cross-sectional area
a	Excavation width
b	Excavation length
C	Factor for Sichardt's formula
C	Boundary conductance
C	Concentration
$Cseal$	Attenuation of tidal amplitude due estuary bed
D	Thickness of water-bearing stratum
D	Hydrodynamic dispersion
D^*	Effective molecular diffusion coefficient

d	Distance from model boundary to true recharge boundary
d	Average particle diameter
D_{10}	10% particle size
G	Dimensionless flowrate
H	Elevation of a piezomteric surface
h	Head
h_b	Boundary head
h_w	Elevation of the operating level of a pumping well
h_0	Tidal amplitude of the Thames
h_1	Tidal amplitude at a piezometer
K_d	Distribution coefficient
K_{ex}	Thermodynamic equilibrium constant
k	Soil permeability
k_b	Boundary hydraulic conductivity
k_{wall}	Diaphragm wall hydraulic conductivity
k_x	Horizontal hydraulic conductivity
k_z	Horizontal vertical conductivity
i	Hydrualic gradient
L_o	Distance of influence
M	Mean of residual errors
MA	Mean of absolute residual errors
Pe	Peclet number
Q	Discharge flowrate
q	Volumetric flowrate
R	Retardation factor
R	Product moment correlation coefficient
S	Radius ocoefficient
S	Sum of squares of residual errors
S_c	Specific capacity
S_y	Specific yield
s	Drawdown
T	Transmissivity
t	Time

t_{LAG}	Time lag for tidal response
t_0	Tidal period
u	Pore water pressure
V	Volume of water
v	True seepage velocity
x	Distance between piezometer and shoreline

Acknowledgements

I would like to express my sincere appreciation to my academic supervisor Professor William Powrie for his guidance, helpful advice, support and supervision.

I would like to express my deep gratitude to my industrial supervisor Dr Toby Roberts of WJ Groundwater Limited for the opportunity to carry out this research and for helping to direct the research.

I would like to thank Bridget Thorn of the Environment Agency for her guidance and support, particularly during the early stages of the research. The Environment Agency provided data and information to supplement the research.

I am indebted to all those people that assisted this research during my time working at the CTRL Thames Tunnel site. These include all the staff of WJ Groundwater Limited who kindly passed on their great experience of practical construction dewatering. In addition, I received help from many of the staff of Hochtief-Murphy Joint Venture and Rail Link Engineering when working on site.

Finally, I would like to express my deep gratitude to my family, friends and former housemates for providing encouragement and helping in many different ways during the last four years.

This research was funded through the Engineering Doctorate (EngD) programme of the Engineering and Physical Sciences Research Council (EPSRC). In addition, sponsorship was provided by WJ Groundwater Limited with support from the Environment Agency.

Chapter 1

Introduction

1.1 Background

The construction of new transport infrastructure below ground is becoming more common as space in urban areas is at a premium. Building underground is often preferable where over-ground alternatives bring unwanted environmental costs, such as noise disturbance and traffic pollution. Subsurface construction often means that groundwater is encountered, which presents a variety of challenges to geotechnical engineers. In urban areas such as London, Birmingham and Liverpool, the occurrence of groundwater problems will increase as the groundwater table rises due to the reduction in the water demand of a declining heavy industry (Johnson, 1994).

Construction dewatering is the process of lowering the groundwater level by means of a system of pumped wells, so that an excavation below the natural water table will remain dry and stable. It is an essential temporary works requirement during the early stages of many below-ground construction projects. Well-planned and closely monitored dewatering systems, using active pumping, allow the structure to be constructed efficiently and safely. Examples of recent underground infrastructure projects that required a construction dewatering system include the Channel Tunnel Rail Link (CTRL) Thames and London Tunnels and the Dublin Port Tunnel.

Using construction dewatering can offer significant cost savings compared to alternatives; for example a construction dewatering system designed to protect the Stratford CTRL station box from uplift was half the cost of using a piled solution (Whitaker, 2004). There is always a degree of risk assumed when carrying out construction dewatering which becomes more pronounced where inhomogeneous ground conditions are encountered. A dewatering system designed without a full appreciation of the ground conditions can lead to significant difficulties in achieving the required level of groundwater control. Consequently, dewatering can make a large contribution to the total construction cost.

The design of a construction dewatering system should consider potential off-site effects including consolidation settlement and environmental impacts. Dewatering systems will disrupt the natural, or existing, groundwater flow regime, which can lead to adverse impacts on the subsurface environment. These include degradation of groundwater quality and depletion of groundwater-dependent features (Preene and Brassington, 2003). For larger construction projects, it is a requirement to consider the environmental impacts of the construction methods by means of an environmental impact assessment. The Environment Agency (EA) is charged with regulating groundwater abstractions and acts within the scope of the Water Resources Act 1991. The Environment Agency has the power to object to abstractions if there is evidence that they will unacceptably introduce saline waters or polluted waters into an aquifer (Environment-Agency, 1998).

In light of the growing concern about the impacts of construction dewatering, a greater emphasis has been placed on the environmental monitoring. Environmental monitoring budgets are strained by the need to cut costs in a competitive market (Streetly, 1998). For large scale projects both the capital costs and ongoing operational costs can be significant. Therefore, there is a need to find a cost-effective approach to monitoring in which the value of the data is maximised.

1.2 Research objectives

Currently, very little information has been published on the magnitude of the environmental impacts of construction dewatering. A good assessment of the impacts of construction dewatering will be based upon the expected performance of the construction dewatering system. It will be shown how the performance of a construction dewatering system can be affected significantly by large-scale inhomogeneities, with reference to the CTRL Thames Tunnel southern approach excavation. The effect of changes in the groundwater regime will be demonstrated with respect to saline intrusion and leachate migration. The research presented here focuses on using numerical models as tools for interpreting site data.

The specific aims of the research were:

- To determine the potential scale of inhomogeneities that may be encountered during construction dewatering and how these can affect groundwater flows.
- To assess the magnitude of groundwater quality changes during the operation of a major construction dewatering scheme with respect to saline intrusion and leachate migration .
- To evaluate the limitations of a groundwater quality monitoring programme and to suggest how future monitoring can be improved.

1.3 Organisation of the thesis

The thesis is structured as follows:

Chapter 2 is a comprehensive review of construction dewatering processes, technologies and applications.

Chapter 3 introduces the case study site at the CTRL Thames Tunnel where a deepwell construction dewatering system was required for a large excavation. Some initial analysis is presented and some ideas are

put forward to account qualitatively for the performance of the dewatering system.

Chapter 4 describes the development and use of numerical models to explore the influence on groundwater flow of large scale inhomogeneities in aquifer material. The modelling results are discussed and the implications of variable ground conditions are discussed.

Chapter 5 reviews the need to protect groundwater and the current understanding of contaminant transport, which is relevant to the case study problem. The site monitoring programme is described and the baseline conditions are analysed.

Chapter 6 describes the development and application of a contaminant transport model. The results are presented and used to interpret the site groundwater quality data, with reference to the migration of cement kiln dust leachate from a nearby landfill and saline intrusion.

Chapter 7 discusses the implications of the contaminant transport results. A critical evaluation of the site monitoring strategy is presented and recommendations are made regarding the design of future site monitoring programmes and the interpretation of the collected data for practical use.

Chapter 8 draws together the conclusions from the two main themes of the research - groundwater flow and contaminant transport - and offers some recommendations regarding the future research.

Chapter 2

Dewatering processes and technology

2.1 Groundwater problems in geotechnical engineering

The difficulties of excavating below ground in water-bearing ground can be broadly categorised as:

1. Slope instability and ground settlement, caused by changes in effective stress.
2. Erosion or fluidization in excavations, caused by seepage.
3. Flooding of excavations.
4. Contact with contaminants when working in, or near to, contaminated land and or contaminant migration as a result of the altered groundwater regime.

2.1.1 Slope instability and ground settlement

The importance of groundwater in geotechnical engineering can be demonstrated using the principle of effective stress. The effective stress (σ') is the stress transmitted through the soil skeleton. For saturated soils, the

effective stress may be calculated using the following equation (Terzaghi, 1936):

$$\sigma' = \sigma - u \tag{2.1}$$

where u is the gauge pore water pressure, the pressure of water filling the void space between solid particles; and σ is the normal total stress on a plane within the soil mass. At the piezometric surface, or groundwater table, the pore water pressure is zero. During changes in the level of groundwater table, the normal total stress remains approximately unchanged so the effective stress increases or decreases to reflect the changes in the pore water pressure (Figure 2.1).

Soils with a high pore water pressure, and a low effective stress, will have a relatively low shear strength τ_f, according to the Mohr Coulomb failure criterion:

$$\tau_f = \sigma' tan\phi' \tag{2.2}$$

where ϕ' is the effective angle of soil friction of a dry soil. Horizontal seepage through a slope, into an excavation, reduces the maximum stable slope angle to about $\phi'/2$. For this reason, a principal aim of a construction dewatering system is to reduce pore water pressures in the soil surrounding an excavation, in order to achieve stability at a steeper angle.

Outside an excavation, vertical total stresses will remain largely unaffected, so a reduction in pore water pressure must result in an increase in vertical effective stress. The result is consolidation and settlement of the soil, as demonstrated in Powrie (1994), Preene (2000) and Forth and Thorley (1994). The potential for settlement depends on the soil stiffness. For relatively stiff soils, such as sand and gravels, settlement from dewatering is unlikely to be significant providing that measures are taken to minimise the loss of fines. Finer grained soils tend to be less stiff and the settlements may be greater. A major cause of settlement is pumping from an aquifer overlain by a compressible stratum (i.e confined conditions), which consolidates as a result of vertical flow into the pumped stratum

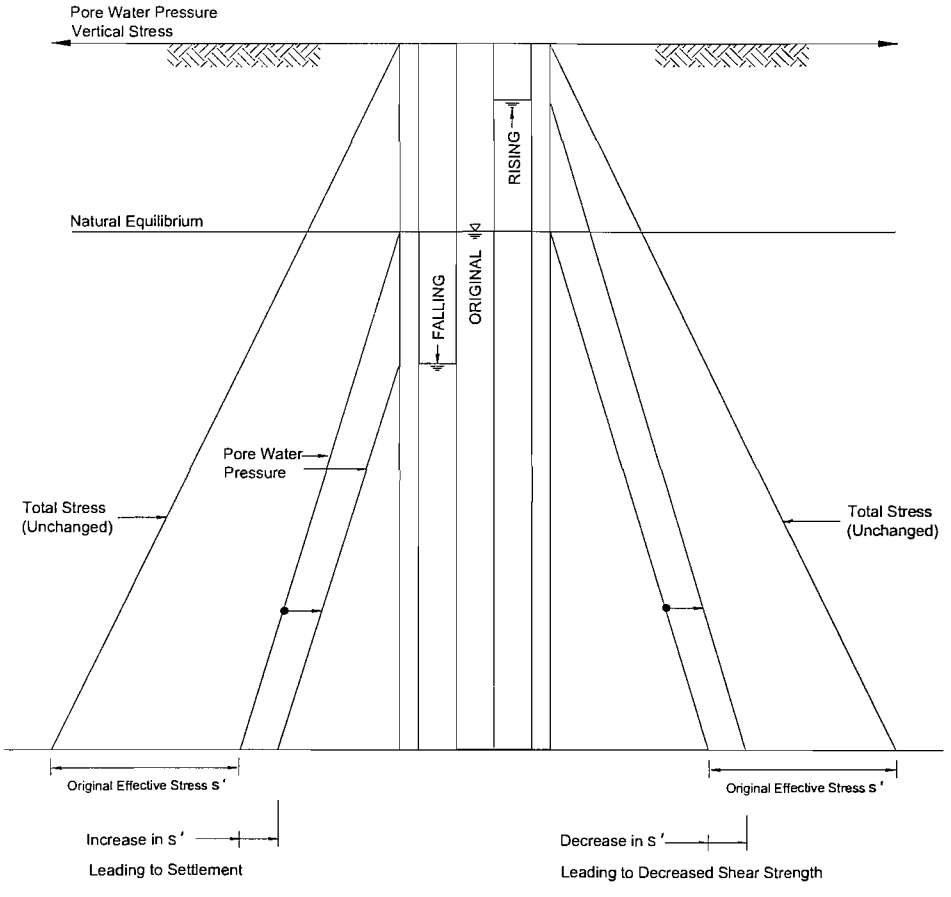

Figure 2.1: *The effect of changing groundwater levels on effective stress. Redrawn from Searle and Gammon (1993)*

(Powrie and Roberts, 1995). Settlement can cause damage to buildings and buried services. Differential settlements, as a result of the compressible stratum varying in thickness and containing inhomogeneities, tend to be more damaging to such structures.

Significant settlements can also be caused by ground loss during excavation and tunnel construction. However, settlements from groundwater control tend to occur over a much larger area than the localised settlements observed during tunnelling or excavation. For example, in one case described by Powrie (1994), settlement and consequent structural damage were observed at 500 m from an excavation

site. Observations of drawdown related settlement were also made during the excavation of the cut-and-cover approach tunnels at Tsuen Wan West Station, Hong Kong (Pickles, Lee and Norcliffe, 2003). Dewatering-related settlements can sometimes be mitigated by the careful recharge of groundwater outside an excavation.

2.1.2 Erosion and fluidization

During dewatering the flow of water through soil is governed by Darcy's Law (Darcy, 1856):

$$q = Aki \tag{2.3}$$

where q (m^3/s) is the volumetric flowrate, A (m^2) is the cross-sectional area of the flow, k (m/s) is the soil permeability and i is the hydraulic gradient. Darcy's Law forms the basis for flownet analysis, which permits the estimation of seepage flow into an excavation (e.g Cedergren (1989)).The derivation of the governing equation of groundwater flow can be found in any soil mechanics or hydrogeology text, and is summarised in §4.2. According to Darcy's Law, flow takes place down the hydraulic gradient, i.e. from high to low head. Upward seepage from below an excavation reduces the effective stress, leading to a decreased bearing capacity. Expansion of the soil may increase the permeability, and hence increase the flow. Eventually, a complete failure may occur as fluidization of the soil takes place. This condition is often referred to as quicksand.

2.1.3 Flooding of excavations

Safe access to an excavation is only possible if the area is dry. Unexpected flooding of an excavation can cost perhaps several hundred thousand pounds in replacing damaged plant and equipment, redesigning the structure and installing temporary works. To avert such occurrences, dewatering systems commonly include instrumentation that allows water levels to be monitored and alarms to be raised when trigger levels are

exceeded. Contingencies are made for plant failure including the provision of standby power in the case of duty power failure and additional pump capacity should a pump fail. A controlled switch-off test may be carried out to ascertain the rate of recovery of water levels inside an excavation.

2.1.4 Contact with contaminants

The risk of contact with groundwater contaminants can be mitigated by either remediating the affected groundwater or soil, or by placing an impermeable flow barrier between the contaminant source and the excavation. The risk of movement of contaminated groundwater into previously uncontaminated parts of an aquifer is the focus of the second part of this dissertation.

2.2 Dewatering technologies

Construction dewatering systems consist of arrays of wells which when pumped collectively allow the required level of groundwater control to be achieved. There are three common technologies which use active pumping: well points; deepwells (wells with submersible pumps); and ejector wells used to drain fine soils by generating a high vacuum at the base of wells (Table 2.2).The type of dewatering technology is chosen to suit the permeability of the subsoil and the drawdown that is required. It is important that the design is sufficiently flexible to accommodate the range of hydrogeological conditions present at the site (Roberts and Preene, 1994), which may vary spatially. Figure 2.2 shows the conditions for which each of the techniques is suitable.

In high permeability soils the purpose of dewatering will be to prevent uncontrolled inflow, whereas in lower permeability soils the primary aim is to reduce pore pressures to stabilize an excavation. It is the particle size and pore size of a soil that controls the permeability and the mechanism of dewatering. In gravels and coarse and medium sands, which have a relatively high permeability, water will flow out of pore spaces under

Table 2.1: *Typical design and performance characteristics of dewatering systems (Roberts and Preene, 1994).*

	Wellpoints	Deepwells	Ejectors
Well diameter	40 mm	100-300 mm	50 mm
Maximum operating depth	Up to 6 m	Unlimited	30 m typically
Typical spacing	1-3 m	10-100 m	2-15 m
Individual well yield	0.1 - 1 l/s	1-50 l/s	0-1 l/s
Relative efficiency	Good	Very good	Poor
Susceptibility to clogging	Low	Moderate	High

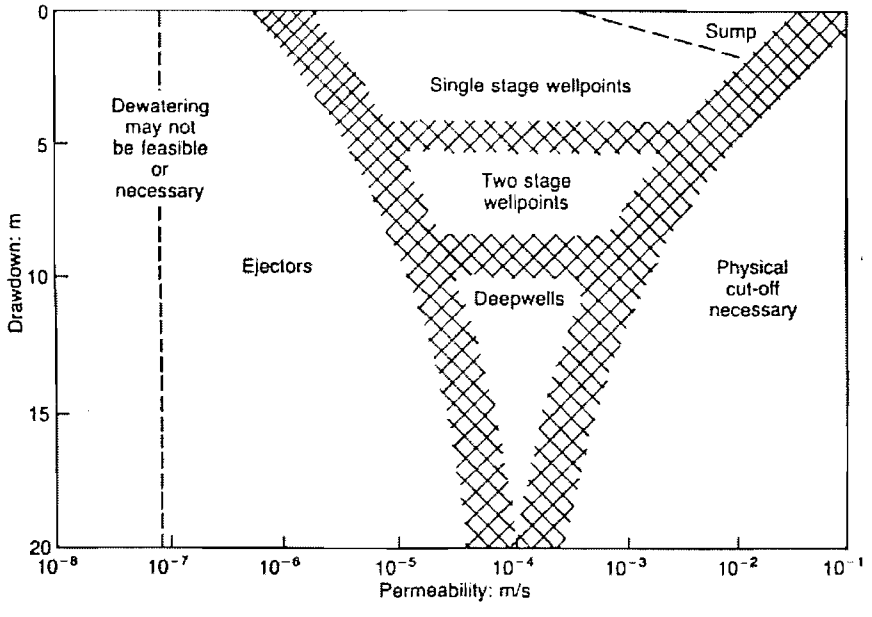

Figure 2.2: *Range of application of dewatering techniques (Roberts and Preene, 1994)*

gravity. In finer soils, capillary effects will result in water remaining within the pores at negative pore water pressures. In this case the soil remains saturated and drainage is by consolidation. As the pore size is decreased, the suction that a soil can hold while remaining saturated increases making dewatering more difficult.

Where the permeability of the ground is high (greater than 10^{-3} m/s),

a form of groundwater exclusion is probably required in conjunction with groundwater removal. For groundwater exclusion, common methods include sheet piling, contiguous bored piles, slurry trenches, diaphragm walls or ice-walls to form a physical cut-off to groundwater flow (Bell and Mitchell, 1986). In many cases the cut-off walls may form part of the permanent structure. Typically, temporary construction dewatering is required until the structure is made stable and the excavation base slab is cast and made waterproof.

Physical cut-offs are also beneficial in reducing drawdowns outside an excavation; the magnitude of external drawdowns can be a function of the diaphragm wall depth (Pickles et al., 2003). Therefore, cut-offs can help to mitigate potential settlement and environmental impacts.

2.2.1 Wellpoints

Wellpoints are suited to the control groundwater levels for shallow foundations and trench works in water-bearing granular soils. A wellpoint is a small well screen, approximately 40 mm in diameter and 0.5 m or 1.0 m long, attached to the base of a vertical riser pipe. The closely spaced wellpoints normally form an arrangement around the boundary of an excavation. Groundwater flows to the wellpoint under gravity and is drawn into a common header main, which is connected to one or more high-vacuum suction pumps. With the relatively shallow maximum operating depth (approximately 6 metres) it may be necessary to add a second stage of wellpoints as the excavation is deepened to achieve greater drawdowns (Figure 2.3).

The simplicity of the system allows a wellpoint system to be flexible and the design to be to some extent empirical; additional wellpoints can be placed in areas of high flows at relatively short notice. The wellpoints can be installed by jetting, using high-pressure water, where sands, gravels and silts are encountered. Where there is a superficial clay bed it is usually more effective to use drilling methods.

Valves are used to tune the performance of an individual wellpoint to

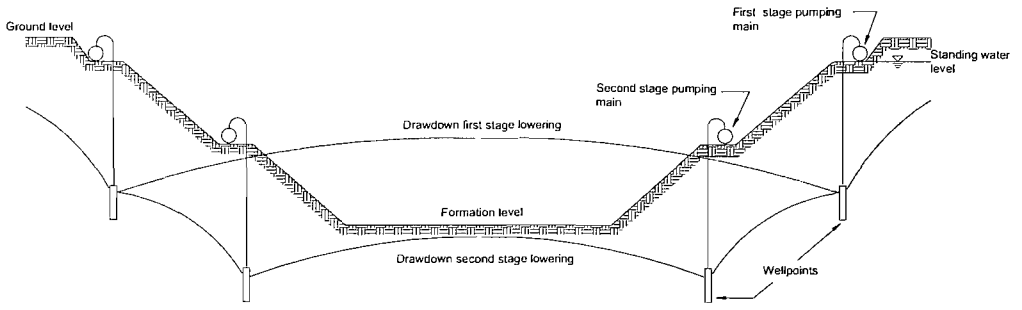

Figure 2.3: *A typical wellpoint dewatering system*

minimise the intake of air as the water table is lowered. If significant air is drawn the vacuum will reduce, limiting drawdowns in other areas of the excavation.

2.2.2 Ejectors

Ejectors can operate at relatively low pumped flowrates and are therefore appropriate for stratified low permeability fine soils where low volumes of water need to be removed to achieve stabilisation. The advantage of the ejector is that there is no limit on their operating depth. The ejector unit contains no moving parts and therefore is not subject to mechanical breakdown. Furthermore, the ejector remains operational even if all the groundwater in the borehole is extracted (Miller, 1988).

The simplest form of ejector is the dual-pipe configuration, however for most dewatering applications single pipe ejectors are commonly used. In the single pipe form, water is pumped down an annular supply passage at a prerssure typically in excess of 750 kPa. The water exits through a convergent nozzle within the ejector casing at a high velocity and a low pressure (close to zero absolute) and passes into the venturi section. This results in the entrainment of the surrounding groundwater, which is carried to the surface via a return riser (Figure 2.4). The creation of a vacuum inside the well facilitates drainage, drawing water into the well through the screen, and further reducing pore water pressures. The system uses either small high-pressure centrifugal pumps or more commonly a large pump

connected to a common supply main which is primed by water from a common return main. The excess water is discharged from the system.

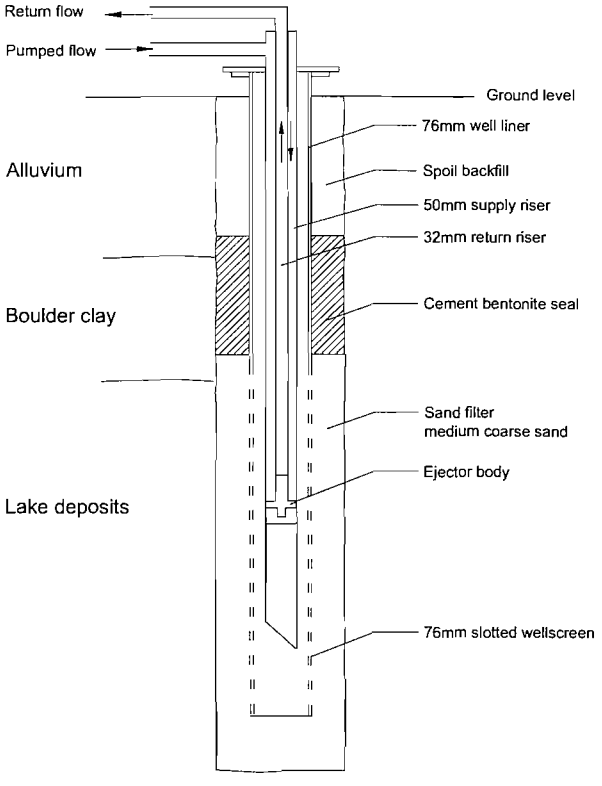

Figure 2.4: *A typical ejector well as used at the Conwy Crossing. (Powrie and Roberts, 1990)*

During the dewatering of casting basins for the Conwy immersed tube tunnel, ejectors were tested for their suitability to relieve pore pressures in laminated glacial deposits (Powrie and Roberts, 1990). Typically the extraction rates of the wells screened in lake deposits were less than 10 l/min (0.17 l/s) and vacuums were developed as water was drawn down 20 to 30 m. In wells penetrating the higher permeability North Wales till or bedrock, flowratres of 40-60 l/min (0.67 to 1 l/s) were achieved but drawdowns were limited to 6 to 8 metres.

2.2.3 Deepwells

Deepwells are used where required drawdowns exceed 10 metres and are widely used in relatively high permeability conditions such as the Chalk during dewatering for the Medway Tunnel (Leiper, Roberts and Russell, 2000) and The Brooks retail development in Winchester (Powrie and Roberts, 1995). Deepwells can be installed to an unlimited depth but a suitable electrical submersible pump, positioned at the base of the well, must be chosen to achieve the required water-lift. Water moves up a riser inside the well liner and is removed via a discharge main. A typical deepwell is shown in Figure 2.5. The well is usually screened below the final formation level of an excavation using a well liner with regular slots. The pump capacity of both an individual well and the system as a whole is likely to be far greater than the other dewatering methods. For example, dewatering of the Medway Tunnel casting basin required 40 wells installed to 25 to 30 metres below ground level, each capable of pumping 12 l/s, with the actual total system discharge being between 350 and 400 l/s to maintain the target drawdown of over 12 m (Leiper et al., 2000).

In general, the higher flows and possible greater drawdowns observed when using deepwells result in increased environmental risks where this type of system is employed. The application of deepwell dewatering systems will be discussed in detail in the main body of this dissertation.

2.3 System design and uncertainty

The purpose of the design process is to identify the well type, size, number and location. This information is then used to specify the required discharge infrastructure, power supply and monitoring system. The designs can be made using seepage flownet analysis, as shown for example by Powrie and Roberts (1995). Details of flownet analysis are given by Cedergren (1989). Other common methods used in the design of dewatering system are described in this section.

The design process is often complicated by the need to make

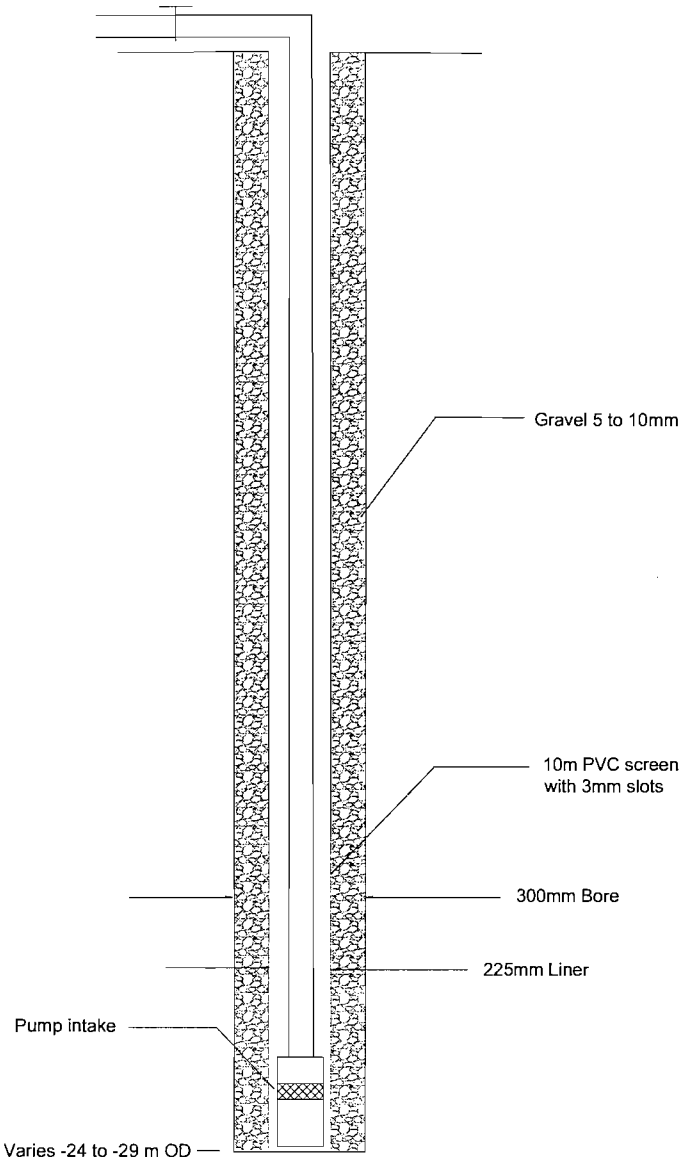

Figure 2.5: *A typical deepwell as used at the CTRL Thames Tunnel*

judgements as to the accuracy and reliability of the available permeability data. In this section, examples are used to demonstrate the uncertainty that can be associated with permeability data.

2.3.1 Methods of design

The theory of groundwater flow through permeable media was first introduced by Darcy (1856), Equation 2.3, and Dupuit (1863). The steady state flow rate (q) from a circular well required to achieve a drawdown level can be determined to a reasonable level of accuracy using Dupuit's formula. The Dupuit equation for the confined aquifer condition (Figure 2.6(a)) is:

$$q = \frac{2\pi kD(H - h_w)}{ln[(L_0 + r_w)/r_w]} \tag{2.4}$$

For unconfined conditions (Figure 2.6(b)), flow rate can be calculated using the Dupuit-Forcheiner equation:

$$q = \frac{\pi k(H^2 - {h_w}^2)}{ln[(L_0 + r_w)/r_w]} \tag{2.5}$$

where H is the elevation of the original piezometric surface above an impermeable base; h_w is the elevation of the operating level of the pumping well above the base; L_0 is the radius of influence; r_w is the radius of the borehole; and k the coefficient of permeability. For confined conditions, D is the thickness of the water-bearing stratum.

Using the Dupuit equations, a construction dewatering system comprising a ring or line of closely-spaced wells can be modelled as equivalent to a large single well (Cedergren, 1989; Powers, 1992). Powrie and Preene (1992) investigated the applicability of equivalent well analysis to different dewatering scenarios. The flow into a dewatering system of dimensions $a \times b$ can be either radial or plane depending on the excavation geometry (a/b) and the distance of influence (L_o/a). L_o is measured from the edge of the excavation, and can be estimated using Sichardt's empirical formula (Sichardt and Kyrieleis, 1930):

$$L_o = C(H - h_w)\sqrt{k} \tag{2.6}$$

where C is a factor between 1500 and 2000 for plane flow, and 3000 for radial flow, with L_o, H and h_w in metres and k in metres per second. However, where there are natural recharge boundaries, such as rivers and

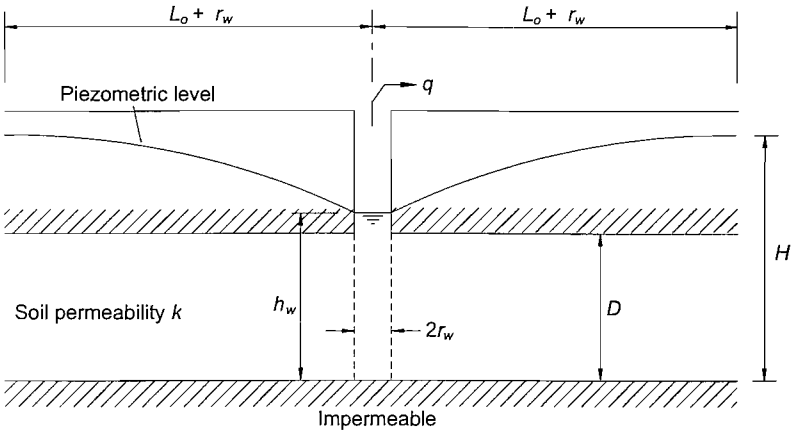

(a)

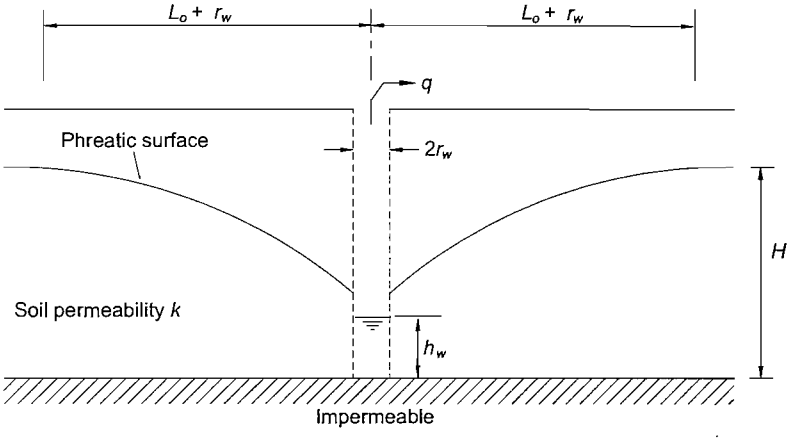

(b)

Figure 2.6: *Radial flow to a well: (a) confined conditions; (b) unconfined conditions*

lakes, at a distance less than the calculated L_o, it is normal to assume that L_o is equal to that distance.

Three example rectangular excavations, treated as equivalent wells, are shown in Figure 2.7. In each of the cases the analysis should use the following guidelines:

1. For rectangular excavations where a and b are in the same order $(1 < a/b < 5)$, and the distance to recharge boundary is relatively

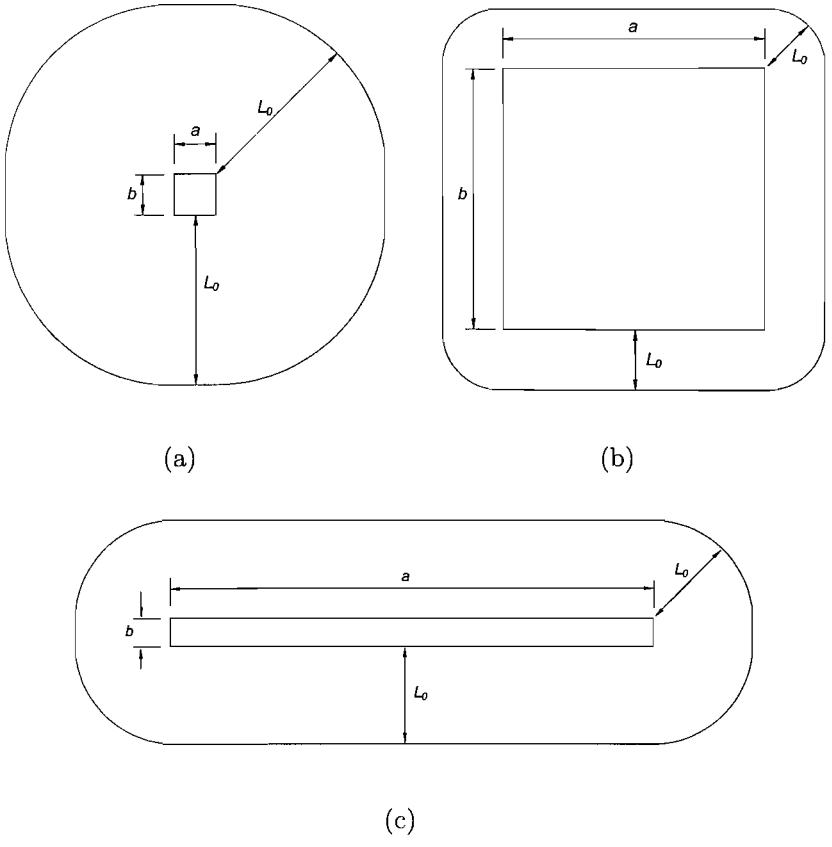

Figure 2.7: *Idealized flow patterns towards excavations treated as single equivalent wells: (a) Square wells with distant recharge boundaries; (b) Square wells with close recharge boundaries; (c) Long, narrow wells (redrawn from Powrie and Preene (1992)*

large ($L_o/a > 3$), as in Figure 2.7(a), flow is assumed to be radial. Flowrates can be estimated using Equation 2.4 or 2.5, where the radius of the equivalent well $r_e = (a + b)\pi$.

2. For rectangular excavations with close recharge boundaries ($L_o/a < 2$),as in(Figure 2.7(b), the combined plane and radial flow can be estimated using the equation:

$$q = kD(H - h_w)\Big([2(a + b)/L_0] + \pi\Big) \tag{2.7}$$

3. For long narrow excavations ($a \gg b$), as in Figure 2.7(c)), reasonable

estimates can be obtained using Equation 2.8 for confined conditions, or Equation 2.9 for unconfined conditions, when $0.1 < L_o/a < 2$.

$$q = 2kD(H - h_w)\Big([a/L_0] + [\pi/ln(2L_o/b)]\Big) \tag{2.8}$$

$$q = k(H^2 - {h_w}^2)\Big([a/L_0] + [\pi/ln(2L_o/b)]\Big) \tag{2.9}$$

If the excavation is very long compared to recharge boundary ($L_0 < 0.1a$), plane flow into long sides is dominant and end effects may be neglected. The term $([\pi/ln(2L_o/b)])$ can therefore be omitted from the calculation.

Other geometries can be analyzed by extrapolating the dimensionless flowrate G from Figure 2.8 and solving Equation 2.10 to find q.

$$q = GkD(H - h_w) \tag{2.10}$$

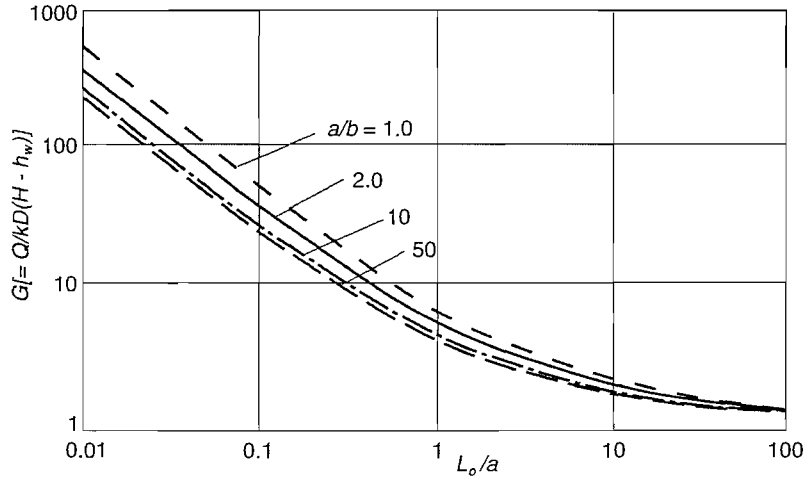

Figure 2.8: *Flow rates by finite element analysis for equivalent wells of various geometries (Powrie and Preene, 1992)*

Like flownet analysis, flowrates estimated using equivalent well analysis are highly sensitive to the soil permeability and distance of influence assumed. Furthermore, the equivalent well analysis follows the

same assumptions as the Dupuit equation: the aquifer is uniform and homogenous; flow is horizontal; the equivalent well penetrates the full aquifer. Powrie (2004) suggests that equivalent well analysis probably involves a greater degree of idealization than flownet sketching.

Another common method for designing a dewatering system is to apply the principle of superposition to the steady state drawdowns. This is often referred to as the cumulative drawdown method, which is described in a step-by-step guide by Preene and Roberts (1994). The flow-drawdown-distance relationship for a single well, determined from a pumping test, is used to estimate the drawdown of a group of wells. This method assumes that the wells do not interact with one another in terms of yield or drawdown; that is superposition is 100% and drawdowns can simply be added. Back-analysis carried out for number of projects suggests that for confined aquifer conditions a superposition of 80% or more may reasonably be assumed. In an unconfined aquifer, the transmissivity of the aquifer will be reduced as the drawdown is increased, so interference becomes more significant. Providing that the drawdown is no more than 20% of the initial aquifer thickness, it is expected that the degree of superposition will exceed 60%.

The key to successfully applying the cumulative drawdown method is having reliable pumping test data representative of the conditions across the site. This advantage of this method is that it avoids any complications which arise in the treatment of the aquifer boundary conditions.

The most advanced method of design is numerical modelling. Industry standard modelling codes include SEEP/W (finite element) and MODFLOW (finite difference). Numerical modelling offers considerable flexibility as variations in the stratigraphy and inhomogeneities can be incorporated if known, rather than assuming homogenous ground conditions. Individual wells and physical cut-offs can be modelled in addition to other boundary conditions including rivers and lakes. The disadvantage of this method is that preparing a groundwater model can be time consuming and some models take a long time to run. However, once the model has been set up it can be used to investigate systematically the

effects of boundary conditions and parameters on the design. The application of numerical modelling will be discussed later in this dissertation.

2.3.2 Sources of uncertainty

It is apparent that both the equivalent well analysis and numerical modelling methods of design are highly sensitive to the chosen soil permeabilities; any of design is only as good as the input parameters used. A reliable estimate of the soil permeability is required to enable the correct well type and design to be specified. The common methods of permeability estimation are listed in Table 2.2. For a given site, a range of permeabilities may be estimated, because of the heterogeneity of the substrata or errors in the method of estimation.

Hazen's formula (Hazen, 1892) can be used to estimate soil permeability from a particle size distribution (PSD) curve. Preene and Powrie (1993) shows that permeabilities derived from PSD curves may lead to an overestimation or underestimation of flow rates generally by a factor of less than 3 where soils contain less than 20% fines. For soils with more than 20% fines, there may be an underestimation by a factor of 100. Therefore, it is suggested that the PSD method of permeability estimation should only be used for isotropic soil containing less than 20% fines. Furthermore, it is suggested that tube samples are preferable to bulk samples, because often bulk samples experience washing out of fines during sample recovery.

There are two notable problems with using laboratory flow testing methods to determine soil permeability. Firstly, disturbance during sampling can disrupt the soil fabric. Secondly, the samples are of a limited size (75-250 mm in diameter) so scale effects may lead to an underestimation of the true permeability.

Small-scale *in situ* tests include falling head, rising head and constant head borehole tests. These methods only test a small volume around the response zone, frequently 1 or 2 m in length, which is likely to have

Table 2.2: *Methods of permeability estimation. (Preene and Powrie, 1993)*

Laboratory tests
Mechanical analysis of disturbed samples
- Hazen's method using particle size distribution curves
Flow testing of samples
- Permeameter
- Oedometer consolidation cell
- Rowe consolidation cell
- Triaxial cell
In situ tests
Small-scale
- Falling head, rising head and constant head tests in boreholes or piezometers
- Piezocone
- *In situ* permeameter
Large-scale
- Well pumping tests
- Dewatering trials
- Back-calculation from prototype systems

undergone considerable disturbance during the drilling. For example, in laminated ground, smearing of the borehole wall during drilling may reduce the connectivity between the more permeable layers and the well; in non-clay soils, the soil at the below the base of the borehole maybe loosened during drilling and soil particles may be rearranged; and in fractured rock, fine debris caused by drilling may block the fissures. During the construction of a lock at Chatham, Kent, borehole tests suggested a Chalk permeability of 10^{-6} to 10^{-5} m/s compared with a value of 1×10^{-4} m/s calculated by back-analysis of the dewatering performance (Roberts and Preene, 1990). For that small project, the borehole tests suggested an inflow into the excavation of 3 l/s, whereas the real inflow was 90 l/s. An advantage of small scale *in situ* tests is that they can be carried out at a number of depths in one borehole, by repeatedly testing and drilling deeper.

The most appropriate method of ascertaining the permeability is to conduct large scale *in situ* tests, because a larger volume of material is tested and disturbance of the ground becomes less significant. However, problems can still arise regarding how representative measurements are of the aquifer in general, particularly in inhomogeneous ground. Such difficulties are experienced when considering pumping test analysis in fractured rocks, such as Chalk, and special measures should be taken. The Chalk is a dual porosity aquifer with fractures that provide the permeable pathways for flow and matrix blocks which provide storage within the pores. As a well is pumped, the head in the fissures is reduced causing the water from the matrix to drain into the fractures, although only 2% or 3% of the matrix porosity is free draining (Reeves, 1979) because of its fine-grained nature. Measurements of the aquifer parameters may differ between boreholes a few meters apart because of the extent to which the borehole intersects the fractures that supply the most of the groundwater flow to the borehole (MacDonald and Allen, 2001). Solution development of dominant fractures can increase the disparity between high and low yielding boreholes. Similarly in construction dewatering the yields, hence the performance, of individual wells will be influenced by fracturing in the immediate locality of the well screen. Such influences were observed during

the dewatering of excavations at Port Solent Marina, Portsmouth and Mewsbrook Sewage Treatment Works, Littlehampton (Roberts and Preene, 1990), and also at the Brooks retail development, Winchester (Powrie and Roberts, 1995). Well tests carried out for the construction dewatering of the CTRL Stratford box, east London, showed a variation in specific drawdown (drawdown in well (m) divided by flowrate (l/s)) from 0.12 to 1.31 m/(l/s) (Whitaker, 2004).

To overcome these problems, a sufficiently large volume of the aquifer should be tested. Although there are no universally accepted guidelines, this normally means that piezometers shall be located so as to enable the distance of influence to be determined. Roberts and Preene (1990) recommend the use of 10 standpipe piezometers (5 boreholes, each with standpipes at two levels) to identify fully the drawdown patterns around the test well. To obtain relevant data the drawdowns in the piezometers 1-10m form the well should be at least 10% of the drawdown required for the dewatering scheme (Preene and Roberts, 1994). Large scale pumping tests can be expensive to carry out, but the costs can be minimised by testing wells which are likely to become part of the final dewatering system design. The pumping test procedure and the analysis are chosen as appropriate to the specific conditions. Tests in fine-grained soils may run over a longer period as water levels may take days or weeks to reach steady state; in contrast tests in coarse grained soils may reach a steady state very quickly.

For the design of large scale dewatering systems, a range of permeability data is often available and the design engineer needs to judge the quality of the data bearing in mind the limitations and shortfalls discussed above. This can be demonstrated with reference to unpublished permeability data at the site of the northern tunnel approach for the Docklands Light Railway Woolwich Arsenal Extension (DLR WAX), London (under construction at the time of writing). Figure 2.9 shows that there is a considerable variation in the permeability of the Terrace Gravels; PSD data suggest a permeability of 5×10^{-4} to 5×10^{-3} m/s while variable head tests (rising and falling) suggest a permeability of approximately 10^{-5} to 2×10^{-7} m/s. Combining both data sets gives values ranging across

approximately 4 orders of magnitude. PSD data were considered to overestimate of the actual permeability owing to the expected loss of fines during sampling, while the variable head tests permeability data were considered to be unrealistically low for the gravels, possibly as a result of borehole clogging and smearing. To determine a single permeability value for use in the design of a large scale dewatering and recharge system, an analysis of data from 2 pumping tests was made using a finite difference numerical model. The best fit between the model and field data was achieved with a permeability in the order of 4.6×10^{-4} m/s.

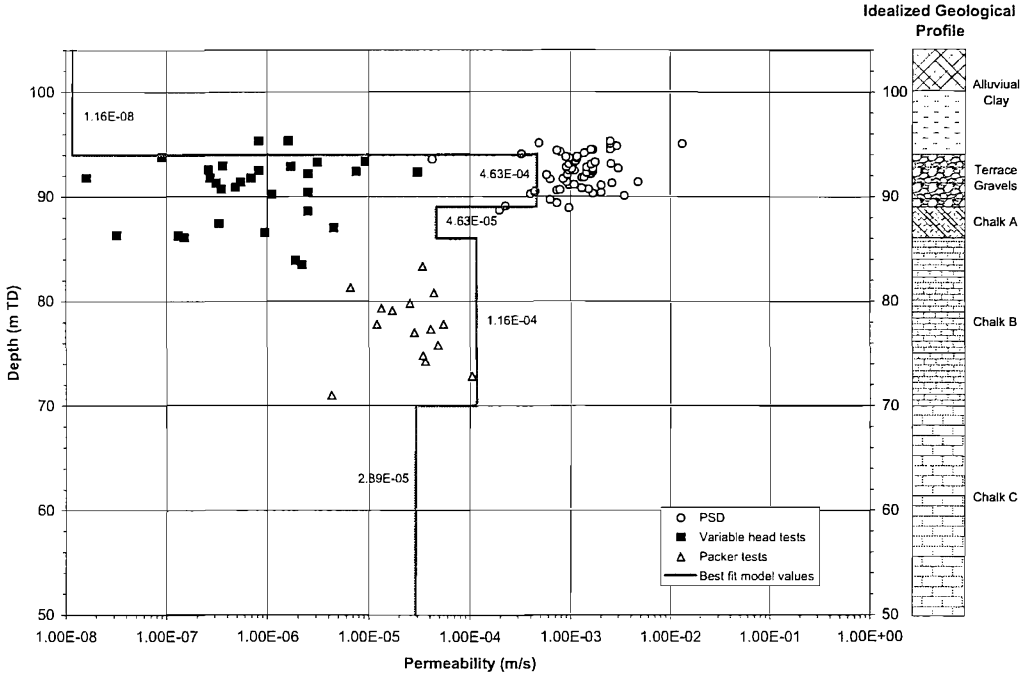

Figure 2.9: *Comparison of the permeability test data with the best fit values from a finite difference model of 2 pumping tests at the DLR WAX site (data provided by WJ Groundwater Limited)*

At the same site, packer tests were undertaken to determine the permeability of the Chalk strata. The best-fit pumping test permeability of Chalk B was higher than that shown by the packer test data (Figure 2.9). The explanation for this observation lies in the spacing of the fissures; the fissures may be spaced sufficiently as to be rarely present within the length

of the tested section of borehole, which is typically 2 to 3 m. However, such fissures contribute predominantly to the bulk permeability and so their influence would be observed if testing were to take place on a greater scale.

Similar observations can be made for an unpublished packer data set collected during site investigation for the proposed A303 Stonehenge Road Tunnel, as shown in Figure 2.10. In this case, a multiplication factor of 3 was applied to the calculated average depth profile in order to attain appropriate values for modelling.

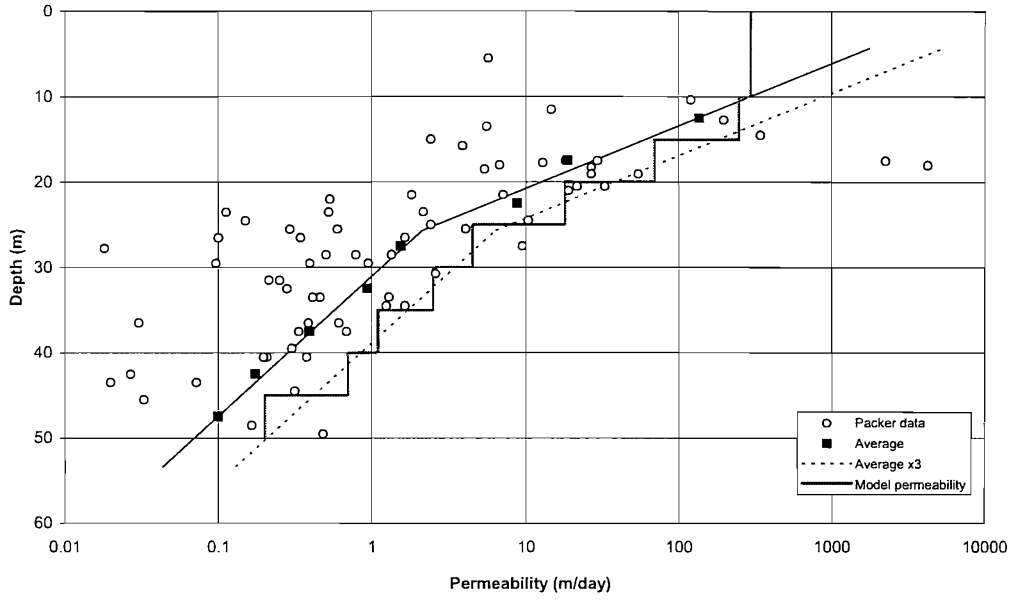

Figure 2.10: *Comparison of the packer test data with chosen values chosen for design using a finite difference model of the Chalk at the Stonehenge site(data provided by WJ Groundwater Limited)*

In addition to fractured rock such as the Chalk, problems of inhomogeneities are found with other soil types. For example, Powrie, Roberts and Moghazy (1989) demonstrated the profound influence of high permeability lenses on the performance of a wellpoint dewatering system, by means of a finite element analysis. In this analysis, a lens with a permeability 2 to 3 orders of magnitude greater than the surrounding soil causes a significant reduction in drawdown. The nature of lens, such as its length or depth, will affect its influence on the dewatering system.

Lenses commonly cause instability in excavations into the Lambeth Group, where fine-grained sand and silt inhomogeneities occur in the predominantly clay Woolwich Formation and Reading Formation. These conditions were encountered by Brunel during the construction of the original Thames Tunnel, at Rotherhithe (Skempton and Chrimes, 1994). Preene and Roberts (2002) give a very wide range of permeabilities for the Lambeth group as a whole (1×10^{-4} to 1×10^{-10} m/s), which have been estimated using in situ testing, PSD data and modelling studies. The problematic fine sand or silt layers within the Lambeth Group have an expected permeability of 5×10^{-5} to 1×10^{-7} m/s, but considerable local variations may occur. Identifying inhomogeneities during site investigation is difficult, hence further exacerbating the problem of choosing design input parameters for a pore water pressure relief system. Preene and Roberts (2002) demonstrate with reference to case histories, how groundwater control can be successfully carried out. For example, wellpoints can be targeted at the permeable layers, as on the London Underground Victoria Line at Euston Station, London (Morgan and Bubbers, 1969); although in this case the use of wellpoints was a reactive measure. Alternatively, vertical drains connecting the Lambeth Group to the more permeable lower aquifer allow underdrainage by deepwells, as at the Limehouse Link tunnel in east London (Stevenson and De Moor, 1994).

Laminated soils also present significant challenges as the layered structure of the deposits cause differences in the bulk permeability in the vertical and horizontal directions, sometimes of an order of magnitude or more. Such anisotropic conditions were encountered in a glacial lake deposit of silty clay with regular thin partings of silty fine sand during the construction of an immersed tube tunnel at the River Conwy crossing (Powrie and Roberts, 1990). Where the soil is known to contain regular alternating bands, the bulk horizontal permeability can be calculated by averaging the permeabilities over the entire thickness of the deposits. This requires knowledge of the thicknesses of well-defined bands throughout the deposits, which can be identified in recovered samples.

2.4 The observational approach

It is evident that measurements of permeability of the substrata can often range over several orders of magnitude. The problems discussed previously mean that the control of groundwater can be an inherently high-risk operation, particularly because dewatering is commonly required during the early stages of construction project and is relied on to facilitate other construction activities. In a review of over 130 groundwater control contracts Roberts and Deed (1994) found an average cost overrun of 35% while a doubling of the tender value was not uncommon (Figure 2.11). However, the cost overrun was primarily a result of an increased pumping period caused by general project delays rather than any problems with the dewatering; unforseen ground conditions had a bearing on the costs in only 8% of the cases.

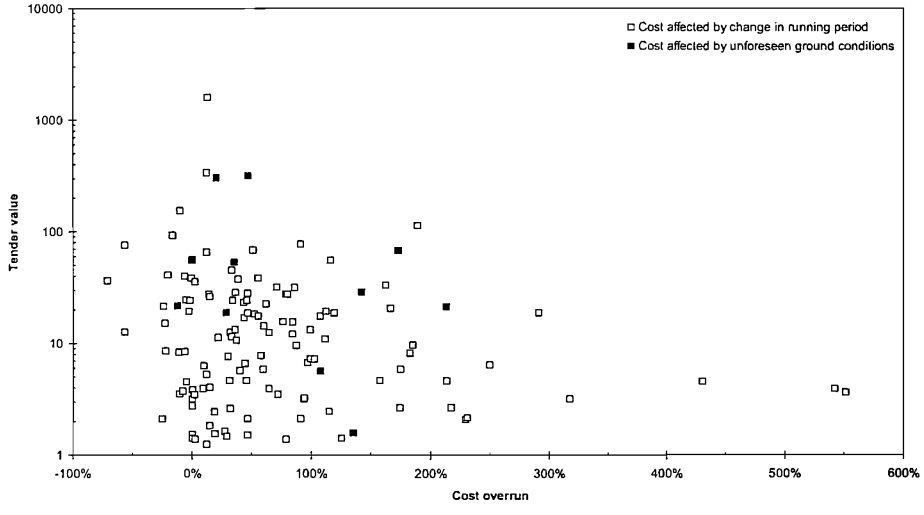

Figure 2.11: *Cost overun for construction dewatering projects (Roberts and Deed, 1994)*

For large civil engineering projects the cost of dewatering rarely accounts for more than 1% of the overall construction cost. Nevertheless, the dependence on groundwater control means that unforseen conditions may cause subsequent delays, disruption and cost increases for the construction project overall, which are not considered in Figure 2.11.

One way to reduce the uncertainty associated with construction dewatering is to carry out a more comprehensive ground investigation, which can typically only investigate a small proportion of the ground. Pumping tests are the most useful form of site investigation for the purpose of designing a dewatering system. However, pumping tests can be costly and so are generally only carried out for at one location on a site. On some smaller sites the cost of the pumping test can be a significant proportion of the total cost of the dewatering operations (Preene and Roberts, 1994).

Clayton (2001) stated that in the future it is unlikely that many clients will be willing to accept responsibility for 'unforseen ground conditions'. Therefore, designs should either be robust enough to accept the full range of expected ground conditions, or an observational approach should be taken. To deal with uncertainty, construction dewatering systems can be designed with large factors of safety; this will involve the installation of wells, discharge infrastructure and a power supply that, if the expected design is correct, will be redundant. This approach is undesirable if the aim is to provide a cost-effective design.

An alternative way to dealing with uncertainty to is to adopt the observational method approach. The observational method represents a more flexible approach allowing the management of risks and the controlling of costs. The objective is to achieve the best design in terms of safety, economy and time (Peck, 1969). The key principle is that by closely monitoring the system performance, especially during the early stages of commissioning, it can be seen whether the system is likely to meet its performance criteria, i.e. to achieve a specified drawdown for a given rate of abstraction. The data collected allows comparison with the predicted performance and this feedback enables the dewatering system to be modified as appropriate. In addition to adjustments to the the well array and well installations, there are a number of other areas where upgrading or downsizing should be considered including the discharge infrastructure, the pump controls and power supply and discharge and abstraction licences. Roberts and Preene (1994) discuss the application of the observational method for construction dewatering. Figure 2.12 demonstrates a continual

feedback system employed by the observational method as applied to construction dewatering by Sargent, Beckie and Smith (1998).

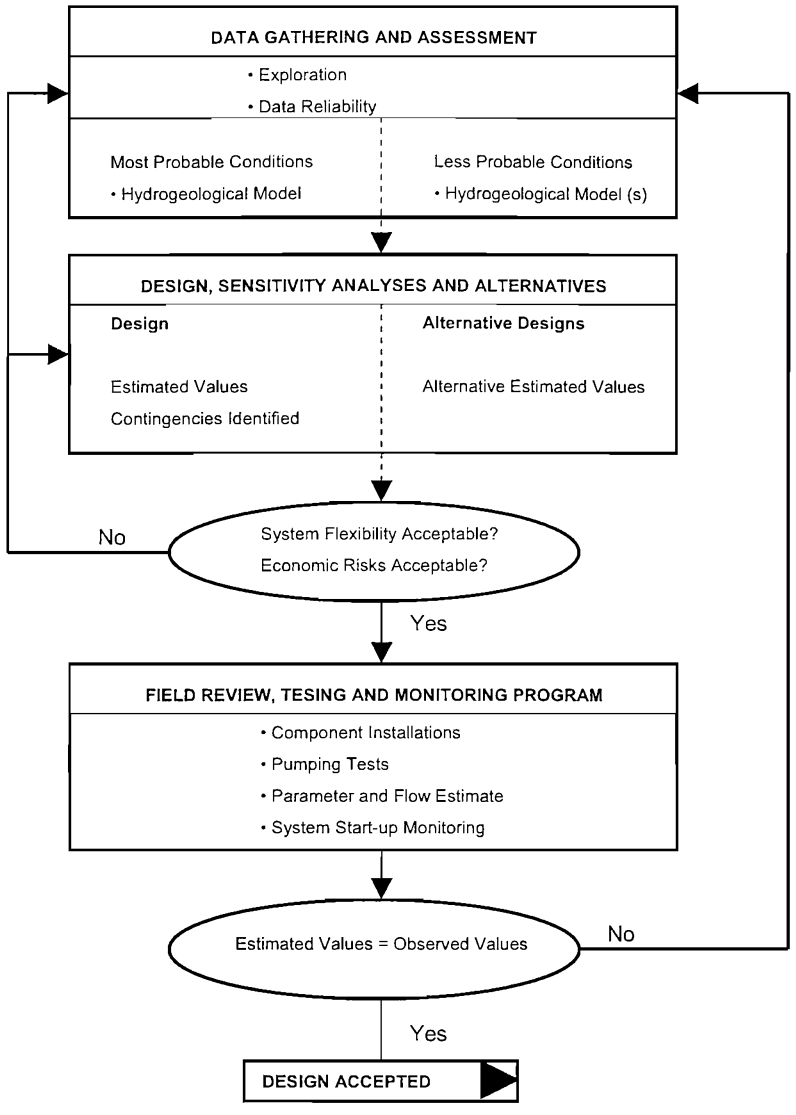

Figure 2.12: *The design and review process for temporary dewatering (Sargent et al., 1998)*

2.5 Areas requiring further work

When applying the observational method, all the possible contingencies should be identified during the design stage as shown in Figure 2.12. To successfully apply the observational approach it is necessary to understand both the mechanisms of a system failure and hence the risks. Roberts and Preene (1994) categorise the failure of construction dewatering systems in to five categories:

1. flow from the ground unexpectedly high
2. well yields unexpectedly low (i.e high well losses)
3. well/aquifer connection problems other than (2)
4. long-term performance deterioration
5. unacceptable off-site effects, such as consolidation settlement and environmental effects

A sound understanding of how unforseen inhomogeneities can impact on dewatering system performance will be beneficial to the design engineer. The first part of this thesis will demonstrate how large-scale inhomogeneities can have a major impact on local groundwater flows, and affect significantly the effectiveness of a construction dewatering system. A groundwater model for CTRL Thames Tunnel southern approach excavation is used to show that the observed performance of the construction dewatering system cannot adequately be explained unless such features are incorporated. The scales of variation that are potentially significant, and should be looked for in a site investigation, will be also be explored and discussed.

2.6 Summary

The purpose of construction dewatering can be considered to be threefold. It prevents instability of the soil at sides and base of an excavation by

reducing pore pressures, thereby increasing effective stresses; it prevents soil erosion due to uncontrolled seepage; and it prevents flooding of excavations. Active dewatering can be achieved by means of a wellpoint, deepwell or ejector system. Common methods of design analysis include equivalent well analysis, the cumulative drawdown method and numerical modelling studies. Equivalent well analysis and numerical modelling need reliable estimates of the soil permeability, whereas the cumulative drawdown method uses the assumption that the ground is uniform across the site.

Permeability data can often be unrepresentative of the site as a whole, due to both problems with the method of permeability estimation and the natural heterogeneity of the ground. The observational method represents a more flexible approach allowing the management of risks associated with unforseen ground conditions and the controlling of costs. However,the application of the observational method requires an understanding of the nature of the potential features that can affect the performance of dewatering system. The first part of this feature will demonstrate the significance of large scale inhomogeneities with reference to the CTRL Thames Tunnel southern approach excavation.

Chapter 3

The case study

When completed, the CTRL will provide the UK's first high-speed rail link, connecting London to the Channel Tunnel with a journey time of approximately 35 minutes. Section 2 of the CTRL will link London's St Pancras station to the existing high-speed line (Section 1) at Fawkham Junction, northwest Kent. Construction of the Thames Tunnel (Contract 320) involved boring twin 8.15 m diameter tunnels up to 25 m below the bed of the Thames from Swanscombe, Kent to West Thurrock, Essex.

3.1 Excavation geometry

Each tunnel drive used a separate tunnel boring machine (tbm) attached to a 200 m long drive train, and commenced from a southern launch chamber on the Swanscombe Marshes. The southern launch chamber was part of a longer excavation for the tunnel's southern approach, which will carry service trains from the ground surface to the tunnel portal. The southern approach structure is 445 m long and 26 to 29 m wide, and was constructed within diaphragm walls as either a cut-and-cover tunnel or a retained cut. Construction dewatering was required to lower groundwater levels to 1 m below formation level. As this varied along the length, the southern approach structure was divided into four separate dewatering cells by means of cement/bentonite slurry cross-wall cut-offs. The excavation geometry and target drawdowns are summarized in Figure 3.1 and Table

Table 3.1: *Design specifications for the four dewatering cells*

	SLC+SCC1	SCC2
Description	TBM launch chamber, cut and cover	cut and cover
Length (m)	75	135
Width (m)	29 to 26	26 to 28
Ground level (m OD)	+1.3	+1.3
Toe of d-wall (m OD)	-29	-26 to -21
Formation level (m OD)	-17 to -14	-14 to -11
Target drawdown (m OD)	-18 to -15	-15 to -12

	SCC3+SRC1	SRC2+SRC3
Description	cut and cover + 25 m retained cut	retained cut
Length (m)	115	120
Width (m)	28	29
Ground level (m OD)	+1.5 to +2.0	+2.0 to +3.2
Toe of d-wall (m OD)	-21 to -19	-17 to -12
Formation level (m OD)	-11 to -7.25	- 7.25 to -4.5
Target drawdown (m OD)	-12 to -8.25	-8.25 to -5.5

3.1. Figure 3.2 shows the construction of the deepest dewatering cells.

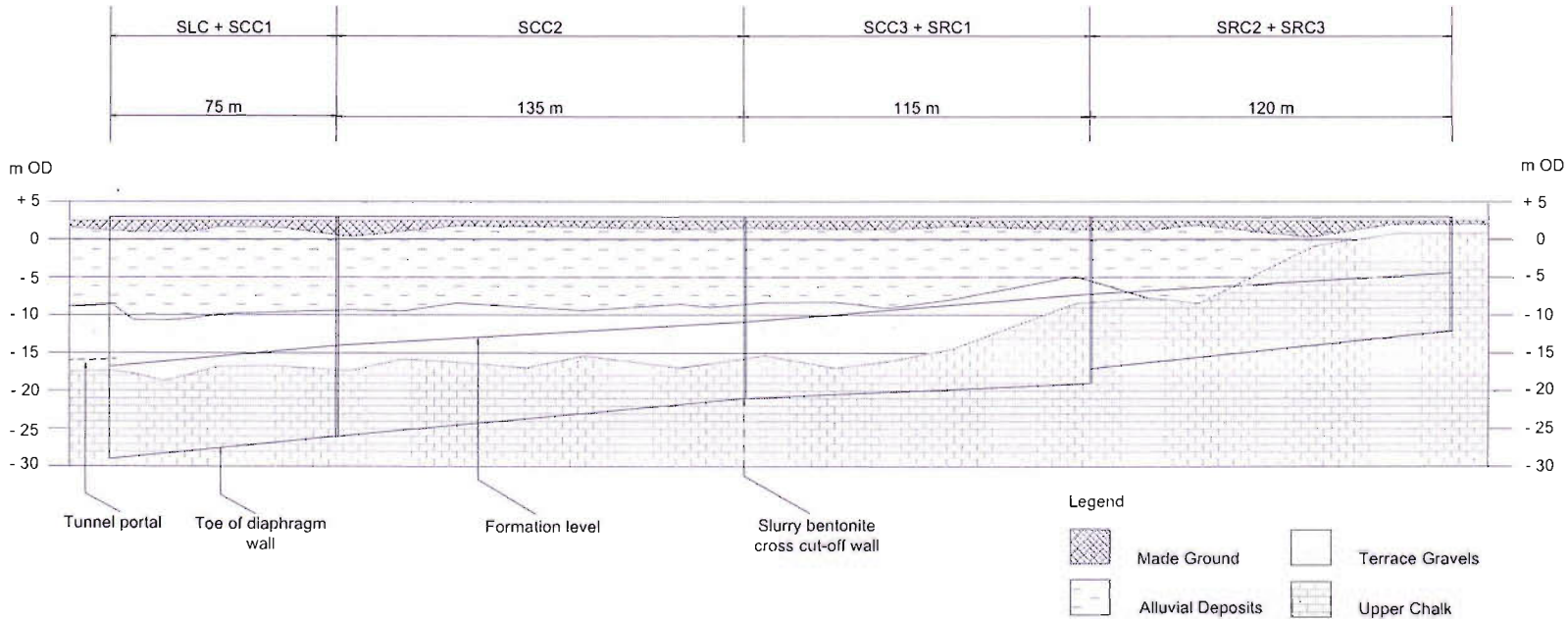

Figure 3.1: *Longitudinal profile of the approach structure and geological strata derived from borehole logs*

3.2 Ground conditions

3.2.1 Stratigraphy

The main water bearing strata at the site are the Terrace Gravels and the underlying Upper Chalk, which are generally in hydraulic connection. The Chalk was eroded and weathered prior to deposition of the Terrace Gravels during the interglacial periods of the Pleistocene epochs as sea levels rose. The Terrace Gravels are comprised of medium dense, fine, medium and coarse sandy gravel. Superficial alluvial deposits consisting of soft silty clay with peat horizons were formed subsequently, during minor sea level recessions in the Flandrian interglacial, and act as a confining layer for much of the site (Figure 3.3). Detailed descriptions of the Lower Thames geological succession are given by Marsland (1986) and Gibbard (1994).

The depth profile shown in Figure 3.4 is typical of much of the site, with ground level at approximately +2 m OD. The thickness of the confining alluvial layer is in the order of 9-10 m, with approximately 7 m of Terrace Gravels below. The thickness of both the alluvium and Terrace Gravel decreases towards the shallow end of the excavation, further away from the Thames, as shown in Figure 3.1.

The chalk outcrops to the south of the site, close to the southern end of the excavation, as shown in Figure 3.3. The extent of the chalk outcrop was determined from borehole logs and is consistent with the geological map (BGS, 1997). An outline of the chalk geology associated with the CTRL project is given by Warren and Mortimore (2003).

3.2.2 Permeabilities

The Upper Chalk encountered during construction was of the Seaford Chalk formation. Typically there was 1 to 2 m of structureless chalk at the interface with the Terrace Gravels. Below this the Chalk was generally classified as Grade B2 or B3 using the CIRIA grading scheme (Lord, Clayton and Mortimore, 2002), indicating that discontinuity apertures are less than 3 mm and the discontinuity spacing is between 60 and 200 mm.

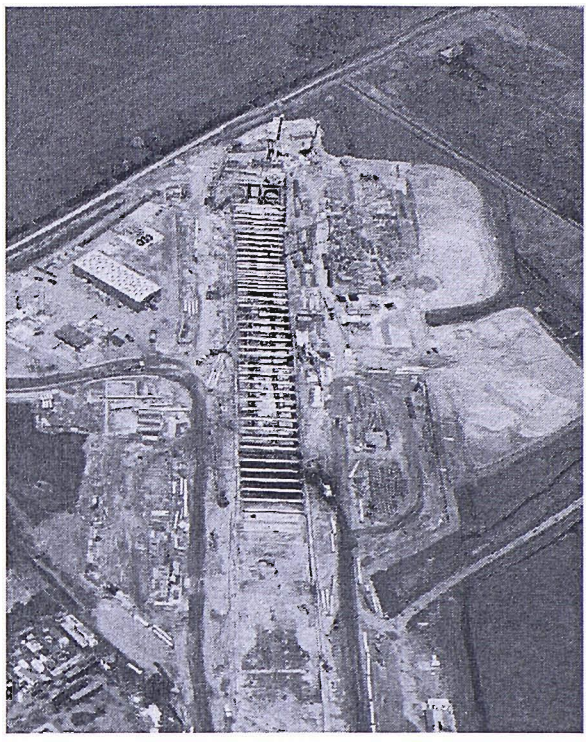

Figure 3.2: *Aerial photograph of the construction of cells SLC+SCC1 and SCC2*

This corresponds to Mundford grade III (Spink, 2002), which suggests a bulk permeability of 10^{-5} to 10^{-3} m/s (Roberts and Preene, 1990).

The dewatering system was designed using estimates of permeability based on limited data from pumping tests carried out some distance away from the actual excavation. Analysis of the pumping test data from a single well indicated a uniform permeability of 1.7×10^{-4} m/s (14.7 m/day) for the gravel and the chalk above a level of -65 m OD. The level of -65 m OD was taken as the aquifer base since the productive zone of the chalk aquifer is generally taken as the top 50 to 60 m (Price, Downing and Edmunds, 1993). Analysis of the data could not detect any significant change in permeability between the gravel and the chalk, or with depth in the chalk.

After the dewatering system had been designed, more detailed pumping test data including tests in piezometers with defined response zones and borehole packer tests became available from the site of the

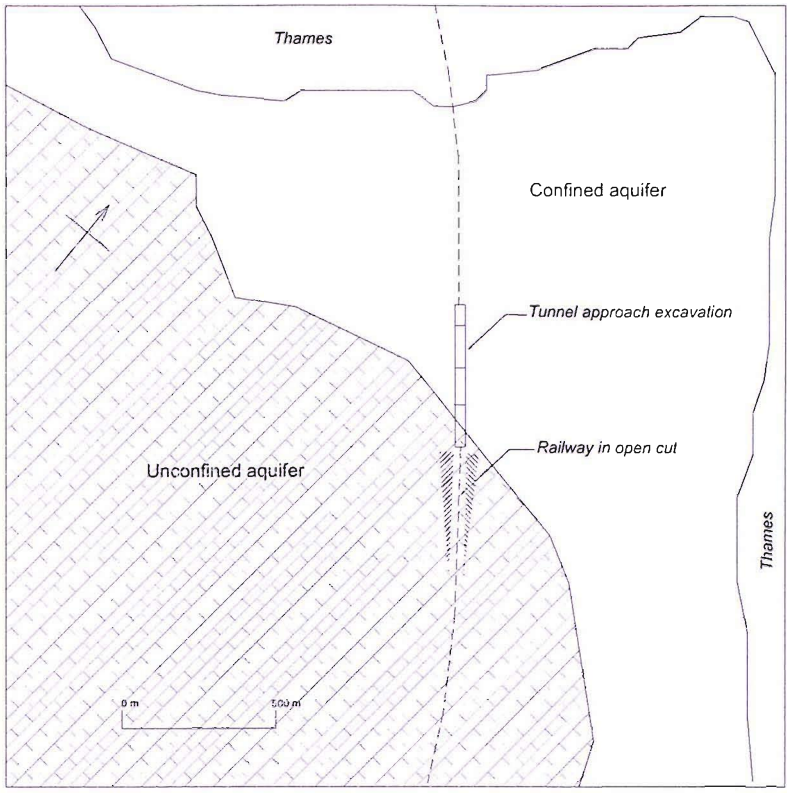

Figure 3.3: *Schematic diagram of the Swanscombe Peninsula showing the confined and unconfined areas of the Chalk aquifer*

northern tunnel approach on the opposite bank of the river Thames. These types of test draw water from a limited and reasonably well defined horizon, and may therefore be used to determine any variation in permeability with depth. The stratigraphy and formative geological processes for the two sites are almost identical so it would seem reasonable to assume that the data (shown in Figure 3.5) are likely to be apply to the south side of the river as well. The data indicate a clear decrease in the permeability of the chalk with depth. Simple statistical analysis of the Chalk permeabilities revealed a significant boundary at approximately -25 m OD, marking the interface between the more weathered surface chalk and the base chalk. Table 3.2 shows the mean hydraulic conductivity of the surface chalk to be 3.1×10^{-4} m/s, compared with 4.7×10^{-6} m/s for the base chalk. The permeability of the surface chalk appears to be more

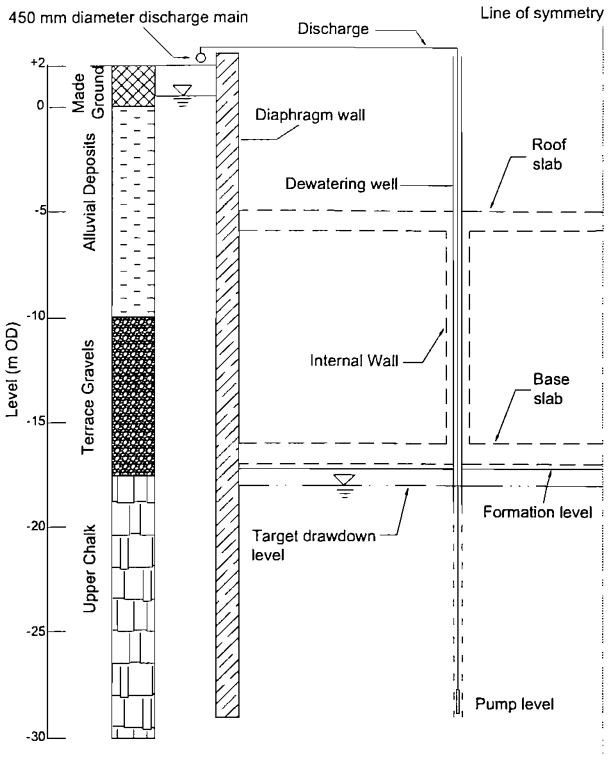

Figure 3.4: *Idealised cross-section through the cut and cover section of the approach*

spatially variable, which may reflects increased localised fissuring.

Analysis of constant flow pumping tests suggested that the permeability of the Terrace Gravels was generally in the range 2.2×10^{-3} to 4.6×10^{-3} m/s (190 to 400 m/day). This is broadly consistent with an estimate based on the D_{10} particle size and Hazen's formula (Hazen, 1892):

$$k = 0.01(D_{10})^2 \tag{3.1}$$

(where k is the permeability in m/s and D_{10} is in mm), which with 0.2 mm $\leq D_{10} \leq$ 0.6 mm suggests a permeability range from 4×10^{-4} to 3.6×10^{-3} m/s (34 to 306 m/day). It is also comparable with the estimate of 2×10^{-4} to 1×10^{-2} m/s (17 to 864 m/day) given by Marsland and Randolph (1978) for bulk samples taken at Crayford Marshes, 4 km upstream. At the same site pumping tests indicated a horizontal permeability of 5×10^{-3} m/s (432

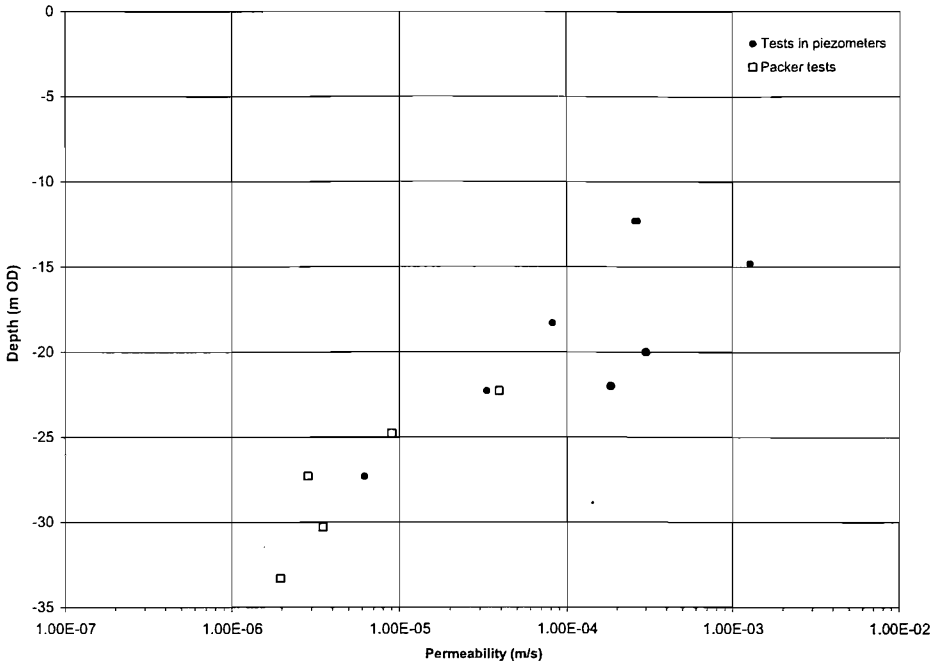

Figure 3.5: *Permeability depth profile of the Chalk at the northern approach site*

Table 3.2: *Values of hydraulic conductivity (k) of the chalk in m/s (m/day)*

	Surface chalk (8 samples)	Base chalk (5 samples)
Depth (m OD)	-12 to -25	-25 to -35 m OD
Mean k	3.06×10^{-4} (26.47)	4.71×10^{-6} (0.41)
Standard deviation	4.08×10^{-4} (35.21)	2.88×10^{-6} (0.29)
Min k	3.30×10^{-5} (2.85)	1.96×10^{-6} (0.17)
Max k	1.28×10^{-3} (110.59)	6.21×10^{-6} (0.54)

m/day).

3.3 *In situ* groundwater conditions

Natural groundwater levels across the Swanscombe Peninsula are generally in the range 0 to +1 m OD. They are affected by the tidal fluctuations of the Thames to varying degrees, depending on the geological conditions, as indicated in Figure 3.6 (piezometer locations are given in Figure 3.7). The magnitude of the tidal influence must be taken into account in assessing the acceptable residual error of a groundwater model. It is also important to establish the tidal variation when designing a dewatering system to meet specified target drawdown. In addition, analysis of tidal influence can aid the understanding of the site hydrogeology and provide useful estimations of aquifer characteristics to support other data. The mean tidal range of the Thames, as recorded at the Tilbury tidal gauge, is approximately 4.5m, with the maximum variation being between +6.7 m OD and +0.3 m OD (Figure 3.6(a)).

SR5945 (Figures 3.6 and 3.7) was situated in the confined part of the aquifer and comprised a dual installation with two separate piezometers screened and sealed in each of the Terrace Gravels and in the Upper Chalk. The monitoring data sets from the two piezometers are virtually identical in Figure 3.6; both data sets show a tidal peak-to-peak amplitude of approximately 0.5 m. The closeness of the data from each stratum was observed throughout the confined area, suggesting a good hydraulic connection between the gravels and the chalk and the absence of low permeability putty chalk at the gravel/Chalk interface. The maximum recorded tidal amplitude was 2.50 m at the closest piezometer to the shoreline, SR1232, at a distance 50 m from the shoreline. In comparison Figure 3.6 shows amplitudes of approximately 1.5 m for the piezometer SA5981, approximately 270 m from the shore.

The tidal amplitude is reduced to < 0.2 m close to the boundary between the confined and unconfined areas, as shown by the data for AC1919 and NBH5 (Figure 3.6). In unconfined aquifers tidal fluctuations

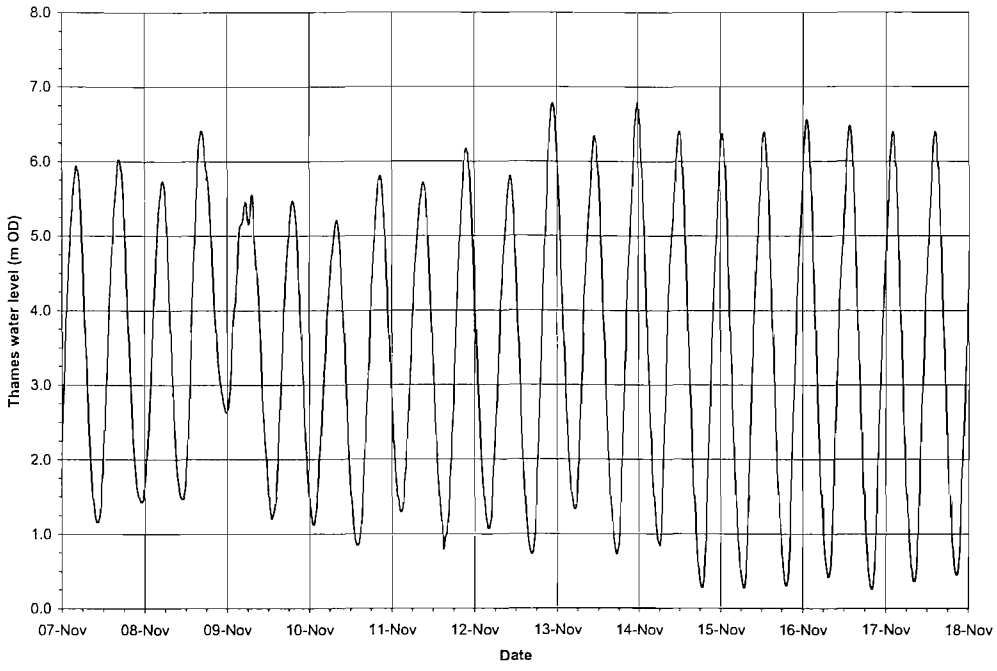

(a) Thames

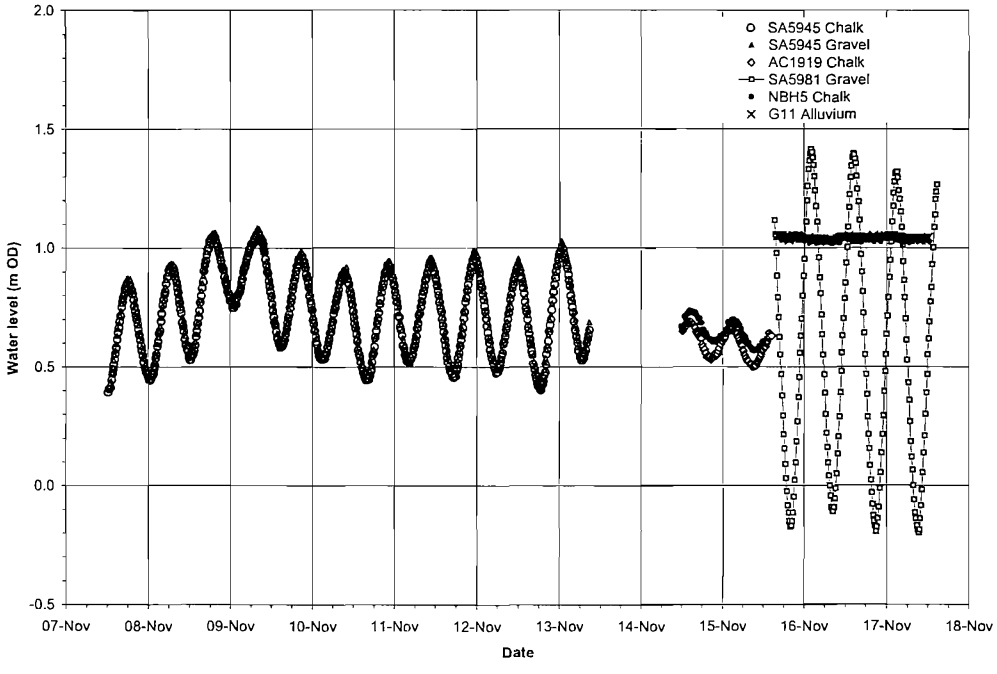

(b) Example piezometer responses

Figure 3.6: *Tidal influence on water levels in piezometers: (a) Thames water level, logged at 10 min intervals at Tilbury tidal station; (b) example piezometer responses, logged at 15 minute intervals*

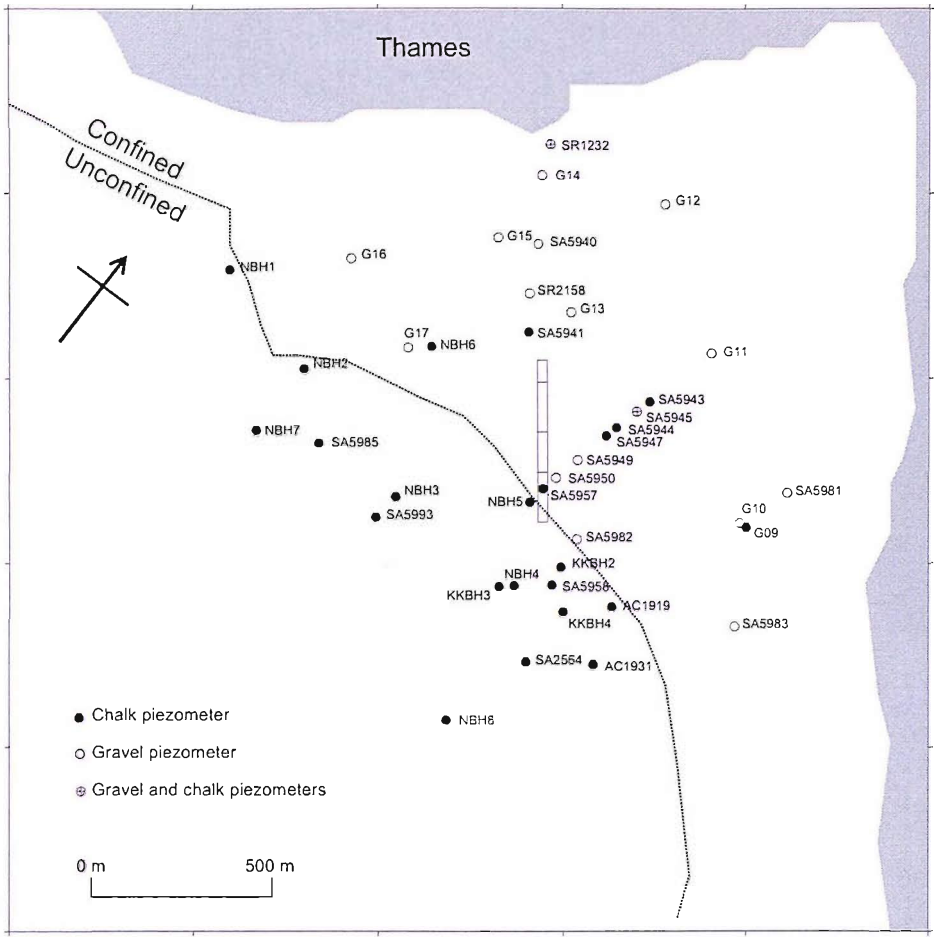

Figure 3.7: *Location of remote standpipe piezometers around the Swanscombe Peninsula*

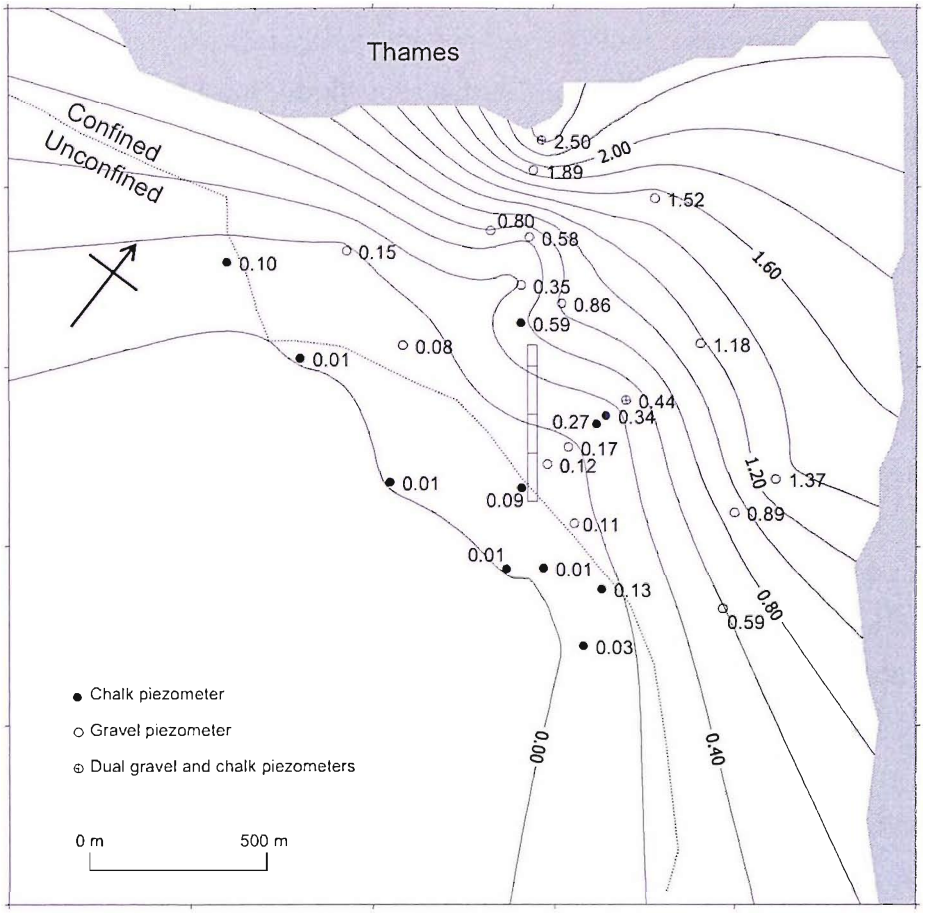

Figure 3.8: *Mean amplitude of tidal oscillations (m) recorded in the remote standpipe piezometers where data are available*

are damped more readily because of their greater storage capacity. Hence the fluctuations for the unconfined standpipe piezometers further south, away from the river, are negligible (Figure 3.8).

Although tidal data are not available for inside the excavation prior to dewatering, it is expected that the diaphragm walls attenuate the tidal effects. Therefore, the model errors attributable to tidal effects should be less for internal piezometers located inside the excavation. Pickles et al. (2003) found that diaphragm walls also significantly isolated piezometers on the landward side of an excavation from tidal effects. Damping of the tidal response by diaphragm walls was also observed by Erskine (1990).

The methods described by White and Roberts (1993) and Erskine (1990), based on the theory set out by Ferris (1951), were used to interpret the attenuation of tidal amplitudes across the confined area. The attenuation is related to the aquifer transmissivity T and storage coefficient S as follows:

$$\frac{h_2}{h_1} = \exp\Big(-\sqrt{\frac{S\pi}{t_o T}}(x_2 - x_1)\Big) \tag{3.2}$$

where t_o is the tidal period (12.5 hours, or 45000 seconds), $x_2 - x_1$ is the horizontal distance between two standpipe piezometers and h_2/h_1 is the ratio of the mean tidal amplitudes recorded at the two piezometers. At this site, for piezometers that lie along lines approximately perpendicular to the centreline of the Thames channel this equation adequately describes the attenuation ($R^2 = 0.95$), as shown in Figure 3.9, where $T = 9.35 \times 10^{-3}$ m^2/sec (808 m^2/day) and $S = 0.00229$. The transmissivity is based on the uniform permeability of 1.7×10^{-4} m/s times an aquifer thickness of 55 m, as used in the dewatering system design.

According to White and Roberts (1993) a value $T/S = 4.08$ indicates partially confined conditions, similar to those observed during construction of the Medway immersed tube tunnel, where similar stratigraphy and formative geology was encountered (Leiper et al., 2000). The T/S relationship cannot provide absolute values for T and S, but may be useful in determining$S$ once the permeability has been investigated in more detail.

The time lag could be determined, for most piezometers, by a least squares fit method, as used by Erskine (1990) to analyse tidal fluctuations during a large scale construction dewatering operation for the Sizewell 'B' Nuclear Power Station. For this method, the piezometer fluctuations were amplified using a tidal efficiency factor h_1/h_0, where h_1 is the piezometer tidal amplitude and h_0 is the Thames amplitude. The fluctuations were then shifted so that the mean piezometric level $\overline{h_1}$ was equal to the mean tidal level $\overline{h_0}$. This transformation can be represented by the equation:

$$h_1'(t) = \overline{h_0} + \frac{h_1(t) - \overline{h_1}}{h_1/h_0} \tag{3.3}$$

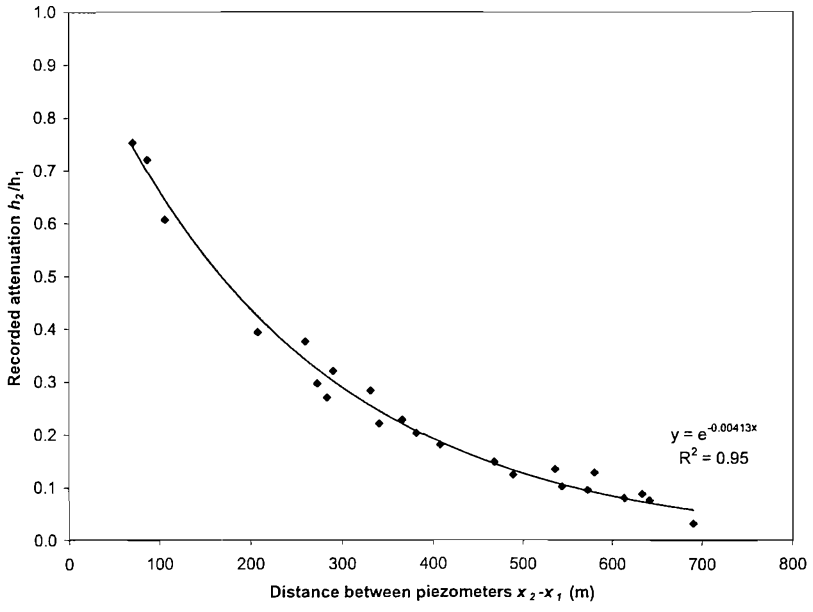

Figure 3.9: *Attenuation of tidal fluctuations through the aquifer, where* $T = 9.35 \times 10^{-3}$ m^2/sec *and* $S = 0.00229$

where $h_1(t)$ is the piezometric level at time t (m) and $h_1'(t)$ is the shifted piezometric level at time t (m). The time lag factor t_{LAG} was then varied by increments of 5 minutes to find the minimum sum of squared residuals SSQ between the two datasets:

$$SSQ = \Sigma[h_0'(t) - h_1'(t - t_{LAG})]^2 \tag{3.4}$$

Figure 3.10 shows examples of the transformed piezometer water levels. As expected, the time lag t_{LAG} increases with distance from the shoreline (Figure 3.11), with lags of approximately 180 minutes (3 hours) observed at a distance of 1000 m. Using the time lag data it is possible to make a second estimate of the T/S ratio from the following equation (Ferris, 1951):

$$t_{LAG} = x\sqrt{\frac{t_o S}{4\pi T}} \tag{3.5}$$

Figure 3.11 compares the data to the relationship of $T/S = 4.08$, as determined from the attenuation analysis. The data indicates that the storage coefficient may be an order of magnitude greater than previously

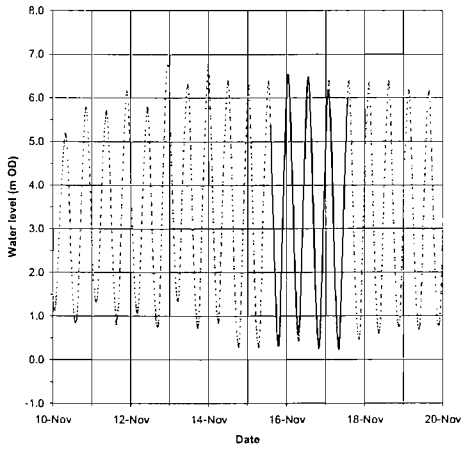

(a) SA5981; $E = 0.255, t_{LAG} = 65$

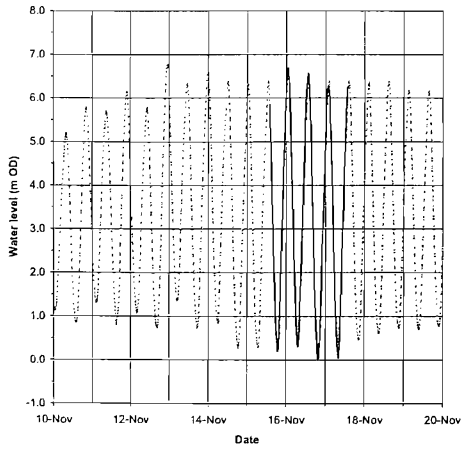

(b) G10; $E = 0.160, t_{LAG} = 75$

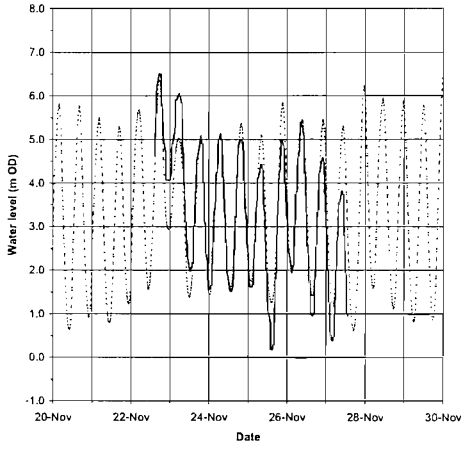

(c) G15; $E = 0.150, t_{LAG} = 100$

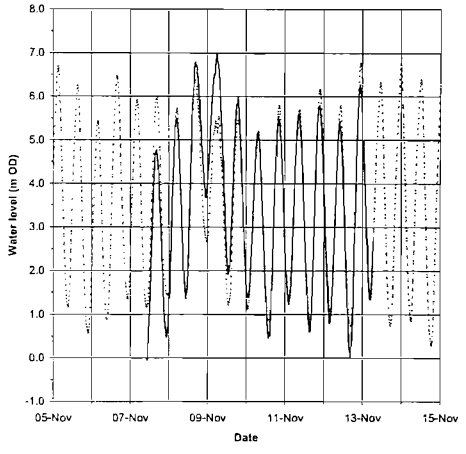

(d) SR5945; $E = 0.095, t_{LAG} = 110$

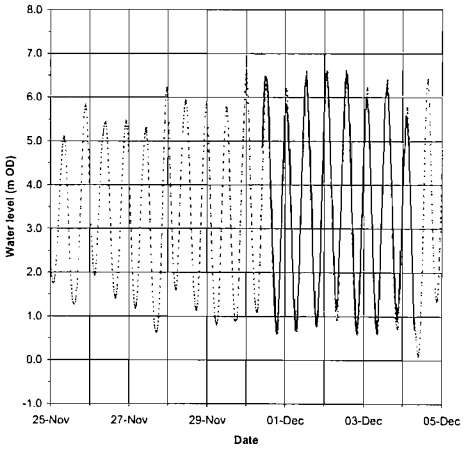

(e) SA5944; $E = 0.075, t_{LAG} = 115$

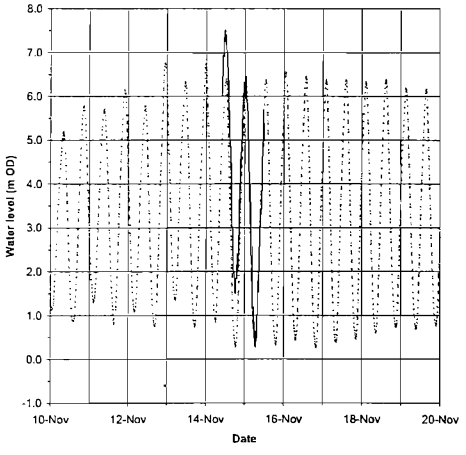

(f) AC1919; $E = 0.026, t_{LAG} = 145$

Figure 3.10: *Transformed piezometer fluctuations (solid line) and the tidal water level (dashed line) during November and December 2001.* t_{LAG} *is given in minutes.*

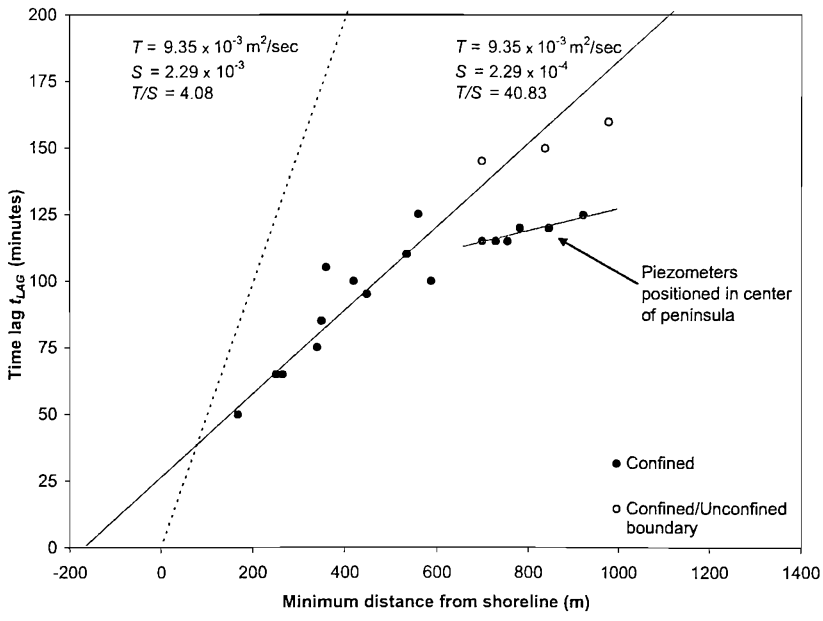

Figure 3.11: *Time lag vs distance from the shoreline*

suggested. The data fit reasonably well to a relationship with $T/S = 40.83$, except for the of piezometers located centrally within the peninsula at distances greater than 700 m where the time lags are less than expected. This is presumed to be a result of the inteference between groundwater pressure waves propagating from either side of the L-shaped shoreline; the work of Ferris assumes the wave propagates from a single straight shoreline.

An order of magnitude discrepancy between the storage coefficient determined by the attenuation and time lag analysis was also found by Erskine (1990) during the Sizewell 'B' Nuclear Power Station construction. It was suggested that the partially confined nature of the aquifer was responsible for the disparity; the presence of a phreatic surface was thought to have a greater effect on the dampening of amplitudes than on the time lags. Further evidence of discrepancies is given by Reynolds (1987), who failed to match simulated and observed tidal responses with both correct tidal efficiency and correct time lags. It was found that matching the time lag provided a better estimation of the actual storage coefficient values.

To give a reasonable fit to the data, the $T/S = 40.83$ line had to be

shifted to intercept the y-axis at approximately 25 minutes. This was caused by two factors. Firstly, there will have been a lag in the tidal cycle between the tidal gauge at Tilbury and the point along the shoreline from which the distance was measured. The size of that lag will have been varied along the peninsula shoreline according to speed that the tidal 'wave' propagates along the Thames. Based on the approximate 35 minute time lag between the high tides at Tilbury and the high tides at the North Woolwich gauge, which is approximately 25 km upstream, it is roughly estimated that the tide will travel around the peninsula in approximately 7 minutes. Given that the t_{LAG} for each piezometer is estimated to the nearest 5 minutes, this level of error is relatively small. The second more significant factor is the nature of the hydraulic connection between the Thames and the aquifer. It is assumed that the aquifer is in connection with the sea at the shoreline, but in reality the two may only be in hydraulic connection close to the centre of the Thames because the alluvial clay and silt deposits that form the bed of the Thames are likely to inhibit the hydraulic connection. Figure 3.11 indicates that the effective source may be approximately 150 m past the shoreline.

Further analysis of hydraulic connection between the Thames and the aquifer was made by examining the tidal efficiency. The relationship between the tidal efficiency (h_1/h_0) data and the distance from the shoreline x_1 is given by:

$$\frac{h_1}{h_0} = \exp\Big(-\sqrt{\frac{S\pi}{t_o T}}x_1\Big) \tag{3.6}$$

However, for $T/S = 4.08$, the best fit was achieved by applying the factor C_{seal}, which does not affect Equation 3.2 or Figure 3.9, but does alter Equation 3.6 to become:

$$\frac{h_1}{h_0} = C_{seal}\exp\Big(-\sqrt{\frac{S\pi}{t_o T}}x_1\Big) = \exp\Big(-\sqrt{\frac{S\pi}{t_o T}}(x_1 + x_e)\Big) \tag{3.7}$$

where x_e is the additional distance to the effective tidal source. A C_{seal} factor of 0.86 gave the best least squares fit to the data shown in Figure 3.12. This equates to $x_e = 36.5$ m, which is a shorter distance than

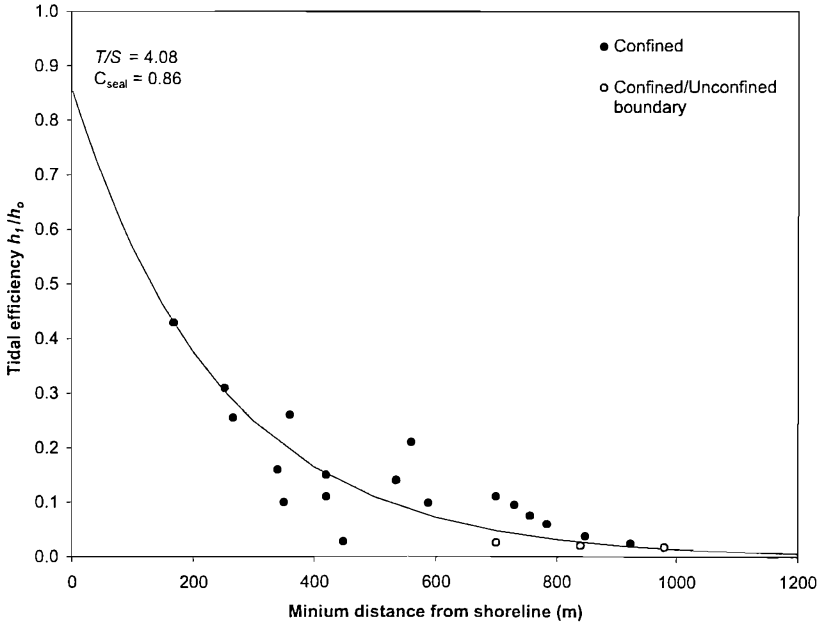

Figure 3.12: *Tidal efficiency vs distance from the shoreline*

suggested by the tidal lag analysis. These factors suggest that partial seal between the Thames and aquifer is relatively small or ineffective compared to other sites, including the Medway tunnel site where White and Roberts (1993) calculated a C_{seal} coefficient of 0.21. Site investigation records indicate that the alluvial bed of the Thames was only present within 300 m of the shoreline, where the Thames is approximately 1200 m wide. This analysis also indicated that the aquifer may be especially prone to the intrusion of higher salinity water from the Thames as as result of the dewatering operations, which is discussed in the second part of this dissertation. The nature of the boundary between the Thames and the aquifer will be important when developing groundwater models of the site.

3.4 Dewatering system design

In view of high flowrates anticipated, a deepwell system was installed to lower the groundwater levels within the tunnel approach structure. The dewatering contractor proposed a design incorporating 42 wells (W01 to

Table 3.3: *Distribution of pump capacity within the excavation*

Dewatering cell	Length (m)	Number of wells	Pump size (l/s)		Capacity (l/s)
			20	12	
SLC+SCC1	75	16	16		320
SCC2	135	14	4	10	200
SCC3+SRC1	115	6		6	72
SRC2+SRC3	120	6		6	72
Totals	445	42	20	22	664

W42), located as indicated in Table 3.3 and Figure 3.13. The additional wells W43 to W58 will be discussed later.

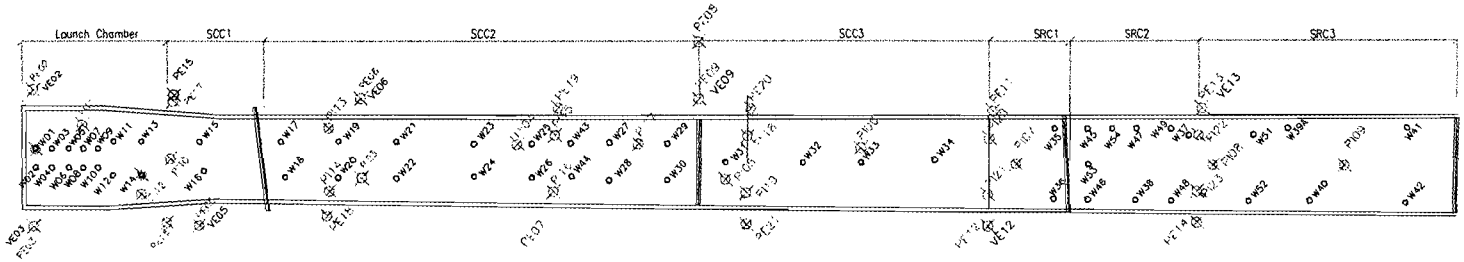

Figure 3.13: *Layout of wells and piezometers*

The design provided increased pumping capacity at the deeper end of the excavation, where the required drawdown was greatest. Either a 15 kW or 9.2 kW electrical submersible pump, with flow capacities of 20 and 12 l/s respectively, was installed in each well. Wells were installed to a depth of between -29 and -24 m OD using the cable percussion method, and screened from one metre below formation level to the bottom with an annular pea gravel filter, as shown in Figure 2.5 - §2.2.3. Well installation, pumping and excavation started at the deep end of the tunnel approach (cell SLC+SCC1) to enable the TBM to be prepared at the earliest possible stage. Dewatering and excavation then progressed towards the shallow end.

3.5 Instrumentation

The dewatering system was monitored by means of standpipe piezometers both inside the excavation (the PI series) and outside but close to the diaphragm walls (the PE series). The PE series included dual installations into the gravel and the Chalk strata. Pore pressures in the alluvial layer were monitored using pressure cells installed into the Clay (VE series). All of these piezometers (PI, PE and VE) incorporated a vibrating wire transducer linked to a Campbell Scientific CR10X datalogger to record hourly water level readings. The instrument locations are shown in Figure 3.13. The instruments were calibrated against manual dip readings and corrected for the effects of changes in barometric pressure. Piezometers and cables that became damaged during construction were repaired where possible; cases of instrument breakdown and repair are indicated by a gap in the data record.

Remote standpipe piezometers in the chalk and gravel, at the locations shown in Figure 3.7, were monitored manually using a dip meter. In addition to a selection of the site investigation piezometers, the monitoring programme required the installation of standpipe piezometers in the Chalk (NBH series) and in the gravel (G series). Pore pressures in the alluvial clay were monitored by pressure cells installed at the G series locations. In general, the remote standpipe piezometers were monitored once every two

to five days during commissioning of the dewatering system, reducing to once every seven to fourteen days once the system was fully operational and flows had stabilized. Baseline data of *in situ* groundwater levels were recorded by monitoring each remote piezometer for at least 24 hours, using a stand-alone pressure transducer and datalogger, to establish the tidal range (as shown in Figure 3.6).

Groundwater abstraction flow rates from the dewatering system were monitored with in-line electro-magnetic flowmeters installed in each of the two discharge mains, each of which was capable of delivering 300 l/s of water from the excavation to the discharge outfall into the Thames. The flowmeters were logged by the datalogger unit at hourly intervals. Initially, air in the discharge main, which was drawn in when pumps drew down to the pump intake level, could result in an erratic incorrect measurement. This was resolved by trimming back individual wells using the valve at the well-head, and by installing air escape valves in the discharge main.

3.6 Dewatering system performance

The dewatering system was commissioned in mid-November 2001 with all 16 wells in SLC+SCC1 pumped briefly, giving an initial flow in excess of 200 l/s (Figure 3.14). It was immediately evident that this cell could be dewatered to the target level (approximately -18 m OD) by pumping from just 2 of the 16 wells. Dewatering in SCC2 began on 1 January 2002, with the pumps being switched on progressively from this date. By the end of January the discharge flow was approximately 200 l/s, but two additional wells, W43 and W44 (Figure 3.13) were required to achieve the target drawdown.

Dewatering of SCC3+SRC1 began in March 2002, increasing the total extraction flowrate (from all cells) to about 370 l/s. The required drawdown in the retained cut sections (SRC1 or SRC2+SRC3) could not be achieved with the designed pumped capacity, and twelve additional wells (W45 to W49 and W51 to W58) had to be installed in this area. The required drawdowns were achieved across the entire southern approach structure

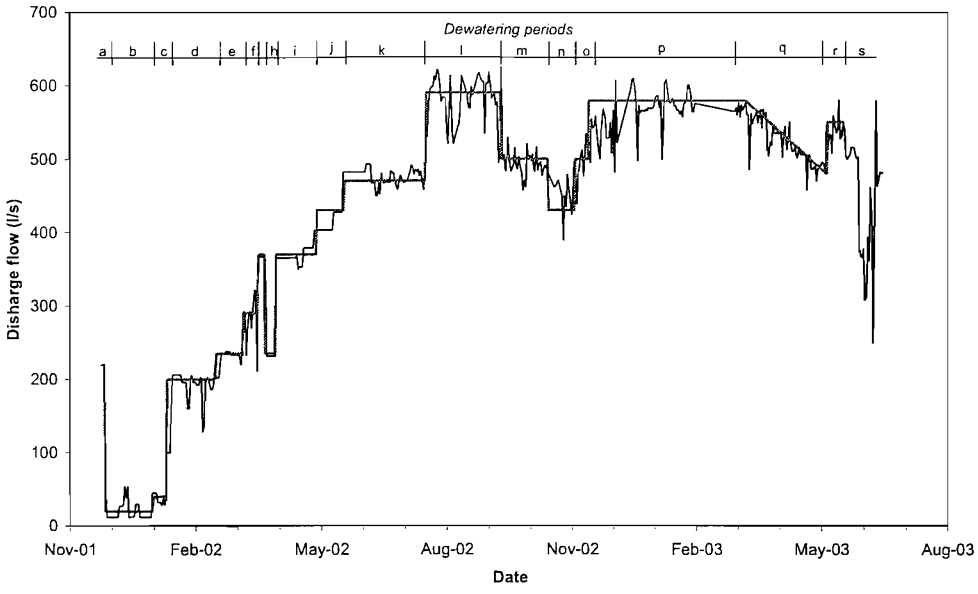

Figure 3.14: *Total abstraction of groundwater by the dewatering system. A description of the dewatering schedule is given in Table 3.4*

with a total abstraction rate of just under 600 l/s.

3.7 Evidence of large scale inhomogeneities

3.7.1 Horizontal definition

During the commissioning of wells in the retained cut section, it became clear that locally the ground was far more permeable than expected. This is indicated by the variation in the specific capacities of the wells across the excavation as a whole (Figure 3.15). Specific capacity (S_c) is defined as:

$$S_c = \frac{Q}{s} \tag{3.8}$$

where Q is the yield measured in m^3/day and s is the drawdown in m, and so S_c has units m^2/day. The yield and drawdown data were recorded during the commissioning of most of the wells. Specific capacity depends on both well depth and diameter and on the permeability of the ground. In this case the well depth and diameter did not vary greatly across the site so the

Table 3.4: *Description of dewatering schedule and approximate total system flowrates*

Period	Start Date	Description	Flow (l/s)
a	26-Nov-01	Wells in SLC+SCC1 commissioned	220
b	27-Nov-01	Only wells W04 + W12 operational	20
c	01-Jan-02	First pumping in SCC2 using wells W19 +W20	40
d	11-Jan-02	Wells W21 to W30 started	200
e	18-Feb-02	Additional wells W43 + W44 started	235
f	08-Mar-02	First pumping in SCC3+SRC1 using wells W32 to W34	290
g	19-Mar-02	All wells in SCC3+SRC1 operational	370
h	24-Mar-02	All wells in SCC3+SRC1 stopped	235
i	01-Apr-02	All wells in SCC3+SRC1 operational	370
j	01-May-02	First pumping in SRC2+SRC3 using wells W37+ W38	430
k	21-May-02	Wells W39 to W42 started. Wells W41+ W42 then permanently decommissioned	470
l	20-Jul-02	Additional wells W45 to W54 started	590
m	13-Sep-02	Wells W47 to W54 stopped, except W52	500
n	18-Oct-02	Wells W45 and W46 stopped	430
o	07-Nov-02	Additional wells W55 to W58 commissioned	500
p	17-Nov-02	All wells in SRC2+SRC3 operational	580
q	12-Mar-03	Gradual decline in flow rate from SRC2+SRC3 as dewatering operations are scaled down to allow drawdown recovery	580 to 490
r	10-May-03	Increase in pumping in SRC2+SRC3, to prevent temporary leakage of base slab	550
s	22-May-03	Decline in pumping rate and start of gradual system decommissioning	550 to 370

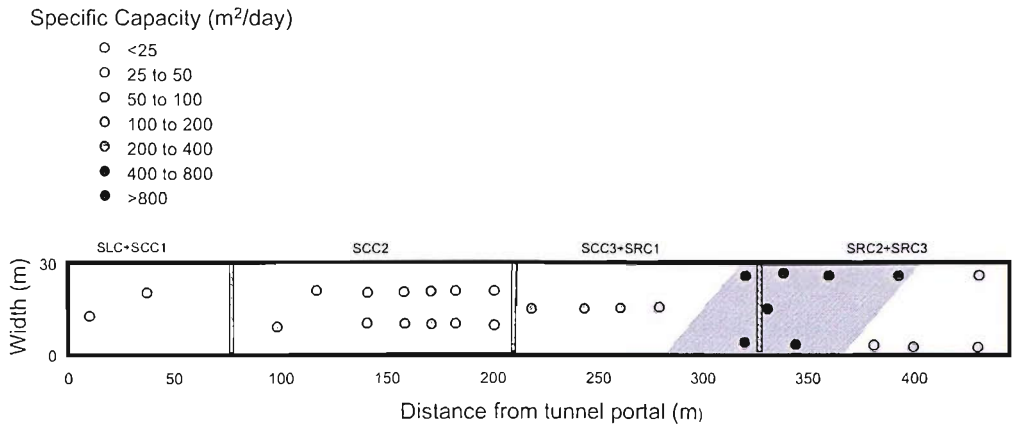

Figure 3.15: *Distribution of specific capacity inside the southern approach excavation, where data are available (not to scale). Estimated extent of the high permeability zone depicted by the shaded area*

distribution of specific capacity provides a good indication of zones of increased permeability. It is apparent from Figure 3.15 that a zone of increased permeability runs diagonally across the excavation between 300 and 400 m from the tunnel portal.

The validity of using specific capacity as a proxy where there are gaps in transmissivity data has been the subject of considerable investigation. Several empirical relationships between T and S_c are listed in Table 3.5. Commonly, the solutions are specific to the data set or geological conditions being investigated; general correlations were not found, primarily because of the influence of well head losses, which vary with geology. Logan's approximation, $T = 1.22S_c$, (Logan, 1964), is the most widely used general relationship. However, a study by MacDonald and Allen (2001) suggests that Logan's approximation underestimates transmissivity at low specific capacity in the Chalk, and a weak empirical relationship $T = 12.5(S_c)^{0.71}$ was found. In this case, the empirical equations listed in Table 3.5 are likely to underestimate T since the diaphragm walls will reduce the apparent S_c (increase the well drawdown for a given flow rate) and the variable toe depths add to the complexity. Furthermore, these relationships cannot account for any variation in anisotropy, which was thought to be an

Table 3.5: *Some empirical relationships between transmissivity (T) and specific capacity (Sc)*

Investigators	Relationship	Aquifer Type
Logan (1964)	$T = 1.22S_c$	General
MacDonald and Allen (2001)	$T = 12.5(S_c)^{0.71}$	Chalk
El-Naqa (1994)	$T = 1.81(S_c)^{0.92}$	Fractured carbonate
Fabbri (1997)	$T = 0.785(S_c)^{1.07}$	Fractured carbonate
Mace (1997)	$T = 0.76(S_c)^{1.08}$	Karstic
Razack and Huntley (1991)	$T = 15.3(S_c)^{0.67}$	Alluvial

explanation of the low inflows into the cell SLC+SCC1. Despite the absence of a universally applicable relationship, Monkhouse (1995) found it was possible to map specific capacity to provide a conceptual understanding of the relative transmissivity variation of the Chalk of the London Basin. A similar approach is useful for the excavation (Figure 3.15), where S_c varies over approximately two orders of magnitude (9.3 to 888 m^2/day).

The variable performance of two dewatering wells is compared in Figure 3.16. For each test, only one well was pumped in the cell until steady state conditions were achieved, although dewatering was taking place in other cells. Flow measurements were taken at the well head, using a mechanical turbine flowmeter, and water levels inside the pumped well and an observation well were measured manually using a dip meter. For well W34 in cell SCC3+SRC1 (see Figure 3.13), the water level inside the well casing was drawn down by approximately 14.5 m to after 40 minutes, and the flowrate stabilised at 23.4 l/s after 90 minutes. Drawdown at the observation well was limited, indicating a steep cone of depression around the pumped well. In contrast, W38 in cell SRC2+SRC3 was pumped at a rate of 27.5 l/s, but the drawdowns achieved were minimal (less than 0.2 m), despite the presence of the diaphragm wall cut-off. In fact, any changes in water levels may have been caused by tidal fluctuations.

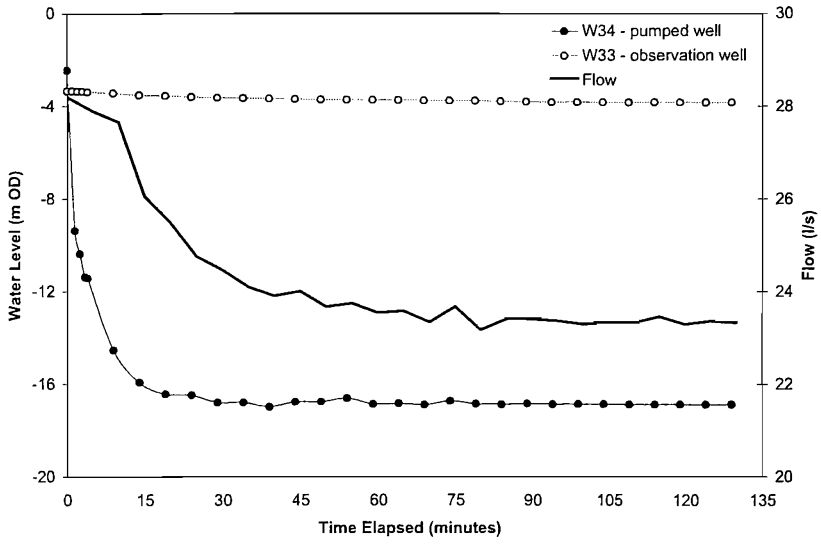

(a) W34

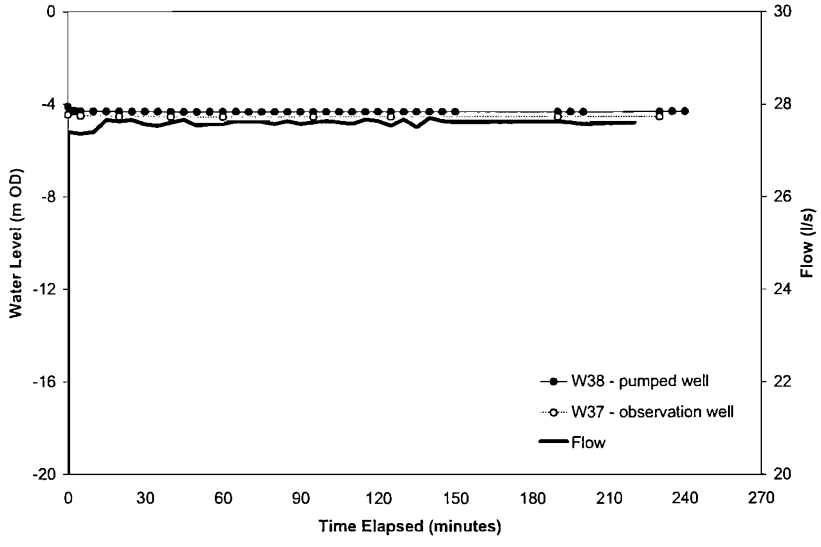

(b) W38

Figure 3.16: *Well performance test data: (a) well W34 in cell SCC3+SRC1; (b) well W38 in SRC2+SRC3*

3.7.2 Vertical definition

As discussed previously, the Upper Chalk is predominantly of CIRIA grade B2 or B3. At the high permeability zone, the Chalk was more difficult to classify but is described as 'possibly Grade C4-C5' for the top five metres. This implies a discontinuity aperture greater than 3 mm and a discontinuity spacing less than 60 mm, suggesting a more permeable material.

Further evidence of an increased permeability in the chalk at the retained cut end of the approach excavation was provided by the analysis of core samples taken during the pre-construction site investigation. Figure 3.17 compares the quality of the core samples for two rotary drilled boreholes: SR5957, located within the proposed high permeability zone; and SR5958, located on the exposed Chalk outcrop to the south of the site. The locations of the boreholes are shown in Figure 3.7. Caution must be exercised in assessing the state of rock cores, because they are largely a function of the drilling method and the care taken by the driller during boring and extraction (Clayton, Matthew and Simons, 1995). However, the total core recovery (TCR) gives an indication of the presence of natural voids and is expressed as a length of the core recovered during a single coring run given as a percenatge of the sample length. The solid core recovery (SCR), which is the length of full diameter core recovered during a single coring run, given as a percentage of the core length, gives an indication of the fracture state.

Figure 3.17 suggests a high degree of fracturing in the top 5 metres of the chalk at SR5957. At this location the SCR generally appeared to increase, suggesting a decrease in fracturing, with depth. Overall, the profiles suggest a greater degree of fracturing at the high permeability zone (SR5957) than at the Chalk outcrop (SR5958), particularly above -22 m OD where the SCR is less than 60% in the high permeability zone. The TCR data indicates that significant voids are absent at both locations.

With hindsight this analysis of the core samples helps to validate the idea of a zone of high permeability Chalk at the site. However, it is probably unrealistic to think that such an interpretation could have been

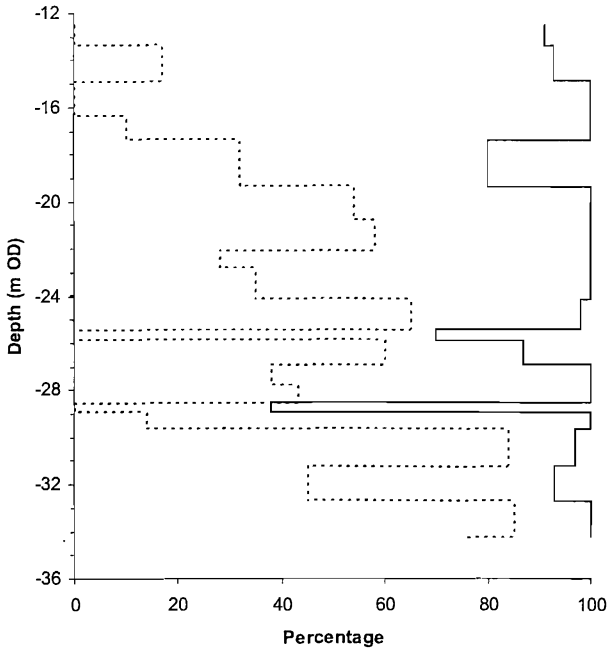

(a) SR5957

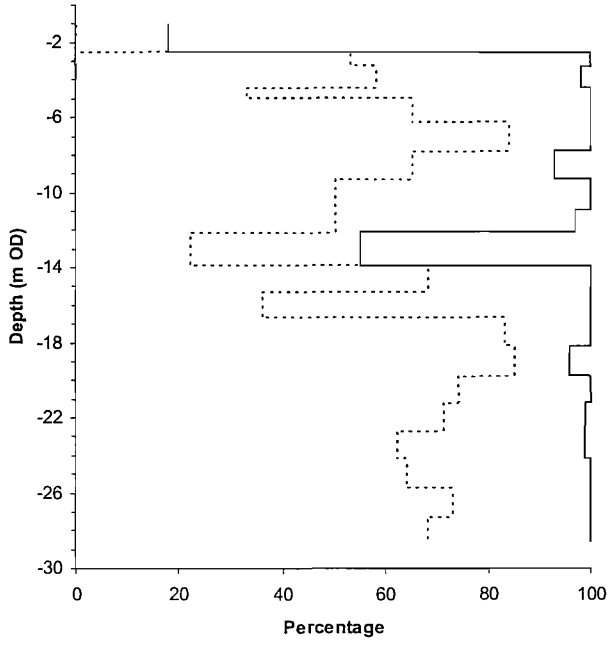

(b) SR5958

Figure 3.17: *The quality of chalk cores as shown by total core recovery (solid line) solid core recovery (dashed line):(a) boreholes SR5957 in the high permeability zone; (b) borehole SR5958 on the outcrop chalk. Borehole locations shown in Figure 3.7*

made based on these samples alone.

3.7.3 Zone formation

The high permeability Chalk lies at the extremity of the Thames floodplain in the old river valley. An increase in transmissivity of Chalk in valleys has been widely observed, most notably by Ineson (1962). Several mechanisms have been proposed that may lead to enhanced permeability of the Chalk:

Concentration of groundwater flux: In homogenous and isotropic Chalk, flowlines converge towards the valley leading to an increase in flow velocity near the point of discharge. As a result a single major fissure or fissure zone is formed (Rhoades and Sinacori, 1941; Connorton, 1976; Robinson, 1976; Owen and Robinson, 1978; Price, 1987; Price et al., 1993). This explanation is applied to the Thames Tunnel site in Figure 3.18 and can be related to the existing topography of the site in Figure 3.19. This process is likely to have taken place during periods of high sea level in the Upper Pleistocene, before the Terrace Gravel and alluvial deposits were laid down by the Thames. Small changes in the sea level and the level of the water table would have shifted the position of the discharge point, hence the approximate 100m width of the high permeability zone.

Chalk structure: Early studies, including Ineson (1962), suggested that rivers follow zones of structural weakness in the Chalk, which have a high fracture frequency. Furthermore, it is postulated that the removal of Chalk by erosion causes additional fracturing as the overburden pressure is released. In this explanation, it is fracture frequency which determines the permeability. This mechanism is possible at the Thames Tunnel site as the valley side would have been eroded by the Thames, but it fails to explain the well-defined nature of zone. Although at this site a considerable mass of Chalk has been removed by quarrying the valley side, which may have caused pressure-release fracturing, again this would have had a greater effect on the outcrop

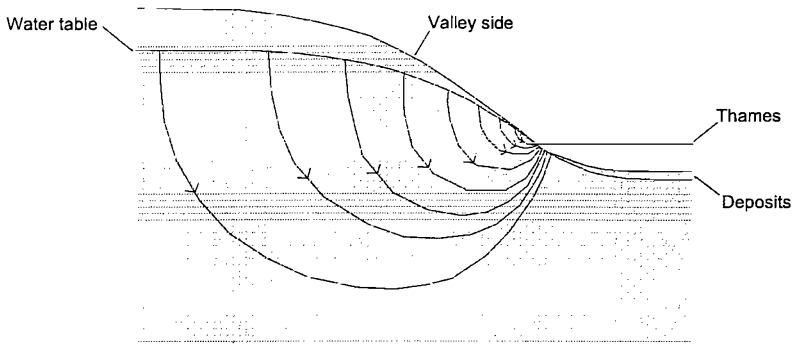

(a) Pleistocene

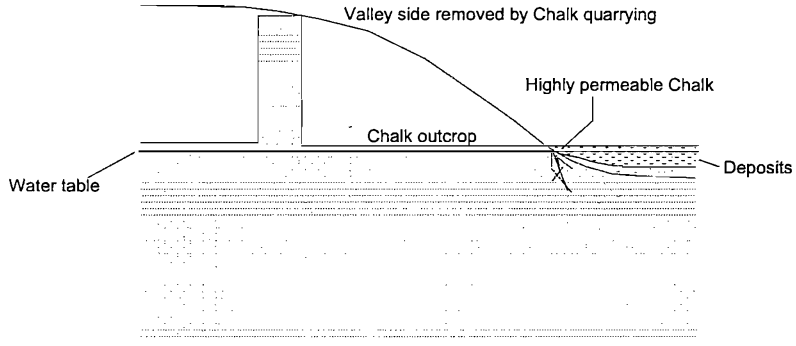

(b) Time of construction

Figure 3.18: *The possible development of enhanced permeability in the Chalk at the CTRL Thames Tunnel site: (a) Converging flow lines during the Pleistocene; (b) Fissure zone created at the edge of the outcrop. Based on Price et al. (1993)*

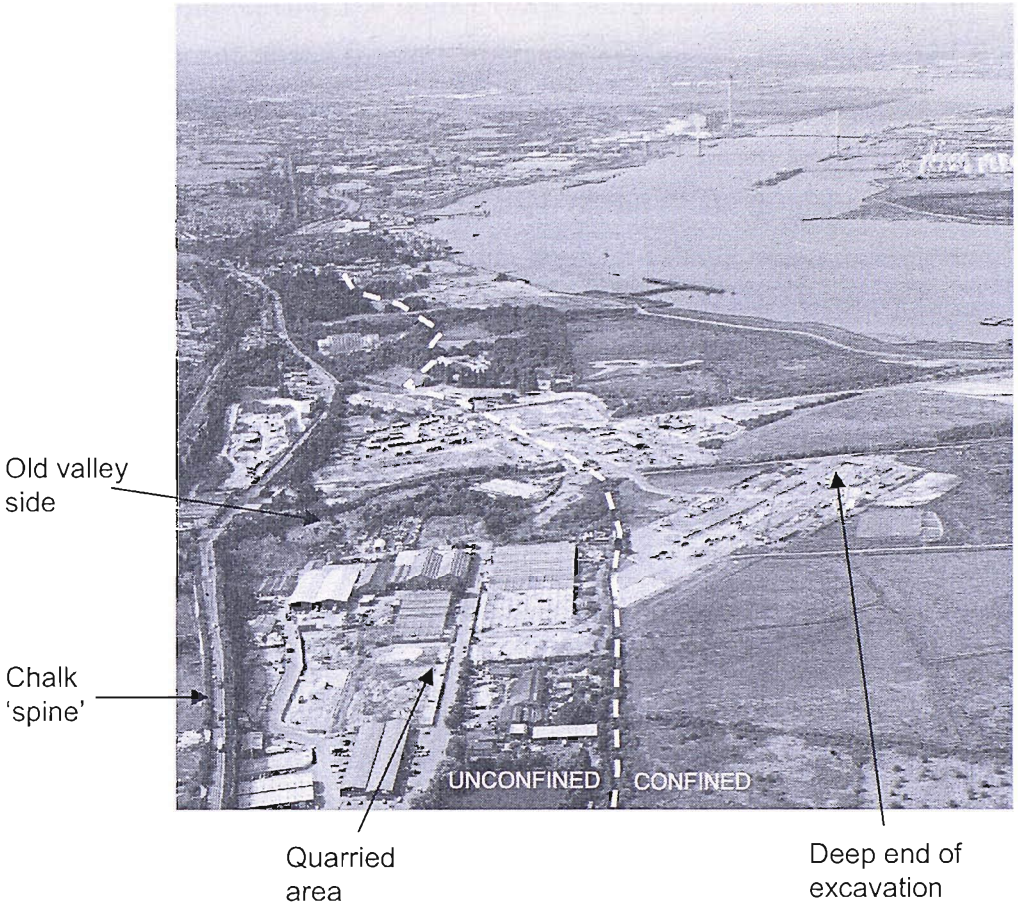

Figure 3.19: *Aerial photograph showing the topography of the site*

than on the confined part of the site where the zone is found. Pressure-release fracturing is a process normally found in igneous and metamorphic rocks, rather than sedimentary, because of the residual stresses caused by being buried at great depths (Younger, 1989).

Periglacial erosion: Younger (1989) states that there is no evidence to suggest that there is increased fracture frequency in valleys. Instead, it is proposed that the higher chalk permeabilities are a result of enlargement of the fracture aperture. Williams (1987) suggested that the high permeability of the main river valleys may be caused by the deep mechanical weathering by repeated formation and permafrost which is responsible for brecciation of the Chalk druing the Devensian periglacial conditions. However, Younger (1989), when investigating the spatial variability of Chalk permeability in the Middle Thames Valley, argues that brecciated chalk is normally confined to seasonally dry tributary valleys. Instead it is suggested that while groundwater flow in the interfluve areas would have been restricted by permafrost, substantial flows of cold groundwater would have occurred in talik zones beneath major river channels. The result would have been far greater enlargement of fissures by carbonate dissolution in the taliks leading to zones of high permeability. However, this explanation is only generally applicable to narrow river valleys with a few deep braided channels. In wider valleys, such as the Lower Thames, shallow anabranch channels would probably have frozen in the winter, preventing groundwater circulation and therefore chalk dissolution. The annual freeze-thaw cycle would have destroyed the Chalk structure leading to putty chalk (defined as structureless chalk that is devoid of fractures) at the gravel/Chalk interface, rather than high permeability zones. During the construction of a shaft at Tilbury for the Thames Cable Tunnel, unexpectedly high water ingress was experienced due to the complete disintegration of the top 6.1 m of the Chalk, which Haswell (1969) suggests could be the result of permafrost.

Chemical weathering: The enlargement of the fissure component of the Chalk has an important role in increasing the permeability. Carbonate dissolution takes place when the Chalk comes into contact with water having a high dissolved carbon dioxide concentration, especially at low temperatures. This process is known as acid hydrolysis and is described by the following equation:

$$CaCO_{3(s)} + CO_{2(g)} + H_2O \rightleftharpoons Ca^{2+} + 2HCO_3^- \tag{3.9}$$

In addition, carbon dioxide may be released during the mixing of waters which are both saturated with respect to calcite but have different concentrations of HCO_3, hence further dissolution may take place(Bogli, 1964). Carbonate dissolution is thought to be particularly vigorous at outlets along river valleys because of the mixing of different solutions. This form of dissolution can lead to the formation of macrofissures and karst, including sinkholes and dissolution pipes. This mechansism would have probably worked in conjunction with the convergence of flow as shown in Figure 3.18 (Price et al., 1993).

3.8 Summary

To enable the construction of an approach structure for the CTRL Thames Tunnel, a deepwell construction dewatering system was designed and installed. The Chalk aquifer was partly confined by alluvial clay deposits and partly unconfined. Analysis of the tidal response of piezometers proved useful in confirming the part confined aquifer conditions. In addition, the tidal data indicated that there might not be a significant alluvial seal on the bed of Thames, making the aquifer vulnerable to contamination by saline water.

The design for the dewatering system was based on limited permeability data and it was assumed that the Chalk was isotropic and contained no inhomogeneities. When commissioning the system it was found that there were unexpectedly low inflows at the deepest part of the

excavation (cell SLC+SCC1), but unexpectedly high inflows in a well-defined zone close to the boundary between the confined and unconfined parts of the site. Chalk core sample data were re-examined which may indicate a zone of highly fractured chalk. It is possible that this zone was created by a number of mechanisms including the convergence of flow at at the valley and chemical weathering.

Chapter 4

Modelling aquifer inhomogeneity

4.1 Modelling aims

A numerical model was developed to help understand the hydrogeology at the CTRL Thames Tunnel site and to assess the level of complexity required in analysis for the design of a large scale dewatering system. In particular, the influence and effect of three large scale features was investigated. These were:

- a high degree of anisotropy of the surface chalk, though to be responsible for unexpectedly low flowratres in the cell SLC+SCC1;
- a generally high permeability zone, leading to unforeseen high flowrates in the retained cut sections; and
- a transition zone between the high permeability zone and the anisotropic surface chalk, which led to the need to install the additional wells (W43 and W44) in the cell SCC2.

The matrix in Table 4.1 shows the four steady state models that were tested, where *MODEL 1* includes all three features and *MODELS 2 to 4* each have one feature omitted. For each model the hydraulic conductivities of the hydrostratigraphic units were varied, within the limits of the

Table 4.1: *Features included in the steady state groundwater models*

Model	Anisotropy of surface chalk	Isotropic high permeability zone	Transition zone
MODEL 1	✓	✓	✓
MODEL 2	✓	✓	✗
MODEL 3	✓	✗	✓
MODEL 4	✗	✓	✓

expected permeability ranges, to find the best calibration (i.e the best fit between calculated and observed piezometer levels).

The models were developed using Groundwater Vistas (Rumbaugh and Rumbaugh, 1996), a windows interface for processing input and output files for the three dimensional finite difference code MODFLOW (McDonald and Harbaugh, 1988). The steady state model represented a dewatering period 'l' (Figure 3.14 and Table 3.4), when the dewatering system was yielding its maximum flow. This was a relatively stable period in terms of both flows and drawdowns.

Further models were produced to investigate certain aspects in more depth. These models are based on *MODEL 1* and will be described in the course of the discussion. The findings described in this chapter are also relevant to the investigations made in the second part of this dissertation.

4.2 Governing equations

The governing equation for groundwater flow is derived from combining the water balance equation with Darcy's Law (Darcy, 1856). A cube of porous material known as a representative elementary volume (REV) is used to derive the governing equation. The volume of the REV is equal to $\Delta x \Delta y \Delta z$ (Figure 4.1). The water balance equation states that:

$$\text{outflow} - \text{inflow} = \text{change in storage} \tag{4.1}$$

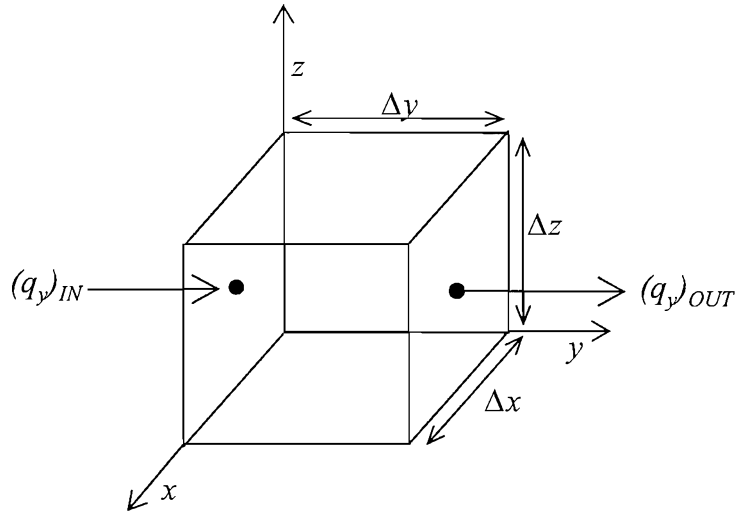

Figure 4.1: *The representative elementary volume (REV) used for the derivation of the governing equation. The components of flow are shown for the y coordinate axis. The flow of water is expressed in terms of discharge rate q.*

For flow along the y axis in Figure 4.1, the influx through the face $\Delta x \Delta z$ is equal to $(q_y)_{IN}$ and the outflow is $(q_y)_{OUT}$. The volumetric outflow rate minus the volumetric inflow rate along the y-axis can be written as:

$$\frac{(q_y)_{OUT} - (q_y)_{IN}}{\Delta y}(\Delta x \Delta y \Delta z) \tag{4.2}$$

or alternatively:

$$\frac{\partial q_y}{\partial y}(\Delta x \Delta y \Delta z) \tag{4.3}$$

This expression can also be written for the change in flow rates along the x and z axes. Therefore the water balance for the REV can be expressed as:

$$\Big(\frac{\partial q_x}{\partial x} + \frac{\partial q_y}{\partial y} + \frac{\partial q_z}{\partial z}\Big)(\Delta x \Delta y \Delta z) = \text{change in storage} \tag{4.4}$$

However, water may be removed or added to the REV where there is a sink, such as a pumped well, or a source of recharge. The volumetric inflow rate is represented by $R\ \Delta x \Delta y \Delta z$, where R is positive when describing a source:

$$\Big(\frac{\partial q_x}{\partial x} + \frac{\partial q_y}{\partial y} + \frac{\partial q_z}{\partial z} - R\Big)(\Delta x \Delta y \Delta z) = \text{change in storage} \tag{4.5}$$

The change in storage is represented by the specific storage (S_s) of the porous medium, which determines the volume of water released from storage (ΔV) per unit drop in head (Δh) per unit volume of the aquifer. For the REV the rate of change in storage is:

$$\frac{\Delta V}{\Delta h} = -S_S \frac{\partial h}{\partial t}(\Delta x \Delta y \Delta z) \tag{4.6}$$

Equations 4.5 and 4.6 can be combined to give the final water balance equation:

$$\frac{\partial q_x}{\partial x} + \frac{\partial q_y}{\partial y} + \frac{\partial q_z}{\partial z} = -S_S \frac{\partial h}{\partial t} + R \tag{4.7}$$

The equation is more useful when expressed in terms of head (h), which can be measured directly unlike q. The relationship between h and q is defined by Darcy's Law in the three dimensions:

$$q_x = k_x \frac{\partial h}{\partial x} \qquad q_y = k_y \frac{\partial h}{\partial y} \qquad q_z = k_z \frac{\partial h}{\partial z} \tag{4.8}$$

where k is the hydraulic conductivity. The Equations 4.8 are substituted into the Equation 4.7 to give the governing equation:

$$\frac{\partial}{\partial x}\left(k_x \frac{\partial h}{\partial x}\right) + \frac{\partial}{\partial y}\left(k_y \frac{\partial h}{\partial y}\right) + \frac{\partial}{\partial z}\left(k_z \frac{\partial h}{\partial z}\right) = -S_S \frac{\partial h}{\partial t} + R \tag{4.9}$$

The x, y and z-axes are assumed to be in parallel with the major axes of hydraulic conductivity.

Darcy's Law applies to porous media where flow is laminar rather than fractured aquifers such as the Chalk where flow can be turbulent. However, the simplest and most common way to model the Chalk is to treat as an equivalent porous media whereby it is assumed that both the fracture density and the scale of the study area are sufficiently great so that groundwater flow takes place in accordance with Darcy's Law. Scanlon, Mace, Barrett and Smith (2003) concluded that equivalent porous media models could be used even in karst systems.

4.3 Numerical methods

With the exception of very simple applications, analytical solutions are not practical, so numerical methods are commonly used to achieve approximate

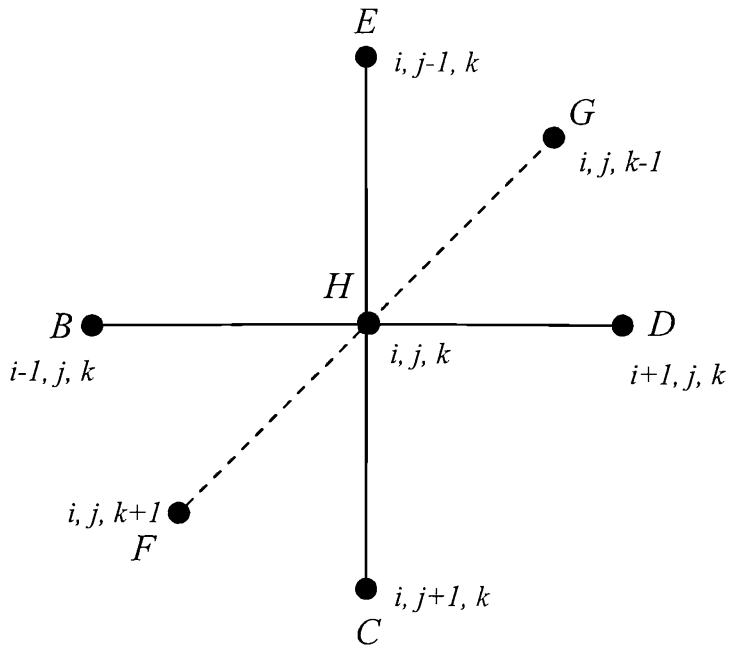

Figure 4.2: *Three-dimensional finite difference computational molecule (redrawn from Anderson and Woessner (1992)).*

solution of groundwater problems. MODFLOW uses the continuity equation (Equation 4.9) in finite difference form, which is discussed in detail in McDonald and Harbaugh (1988). The finite difference method computes a value for the head at the node of each cell of a grid, and that head represents the average head for the cell. A block-centered approach is used where the node is located in the centre of the cell. Each node is indexed by an i,j,k system, where the i subscript represents the number of the row within the grid, j the column number and k the layer number.

The finite difference expression for the computational molecule, shown in Figure 4.2, is written as:

$$\begin{aligned} &Bh_{i-1,j,k} + Ch_{i,j+1,k} + Dh_{i+1,j,k} + Eh_{i,j-1,k} \\ &+ Fh_{i,j,k+1} + Gh_{i,j,k-1} + Hh_{i,j,k} = RHS_{i,j,k} \end{aligned} \tag{4.10}$$

The head at each node i,j,k is influenced by the heads of the of the six surrounding nodes (i.e the hydraulic gradients between adjacent cells). The coefficients B to G represent the hydraulic conductivity between the nodes. In addition the coefficient H is also a function of storage. The storage,

sources and sinks are specified on the right hand side of the equation. A similar equation is used in MODFLOW.

MODFLOW uses iterative techniques to obtain a solution to the finite difference equation for each time step. After each iteration the largest head change of all the nodes in the grid is compared to the convergence criterion, which is specified by the user. If the head change is smaller than the convergence criterion the iteration stops for that time step, otherwise it continues until the criterion is met. The criterion should be set at an order of magnitude smaller than the required accuracy of the computed head. For the models presented here, an accuracy of 0.01 m was prescribed.

4.4 Model development

4.4.1 Grid discretisation and the diaphragm wall

Each model represented an area 2.5 km long by 2.5 km wide with the excavation situated close to the centre. The grid was orientated so that the diaphragm walls around the excavation were aligned approximately with the x and y axes. Cells of varying size were used to allow more closely spaced nodal points inside the excavation (4 m by 4 m) than at the model boundaries (33.33 m by 33.33 m), as shown in Figure 4.3. This gave an increased sensitivity in the zone where the hydraulic gradients were greatest without using an impractically large number of nodal points. The widths of adjacent cells did not differ by a factor of more than 1.5.

The vertical spacing of the layers of the three dimensional model was dictated by the need to be able to simulate approximately the variable depth of the diaphragm walls and the levels of the interfaces between each of the hydrostratigraphic units. The base of the model, which was assumed to be impermeable, was set at -65 m OD, as it is the upper 50-60 m of saturated Chalk that comprises the effective aquifer (Price et al., 1993). Figure 4.4 shows the discretisation into horizontal layers, together with the stepped diaphragm wall profile. This profile led to a small discrepancy in the surface area of the diaphragm walls when compared to the actual wall

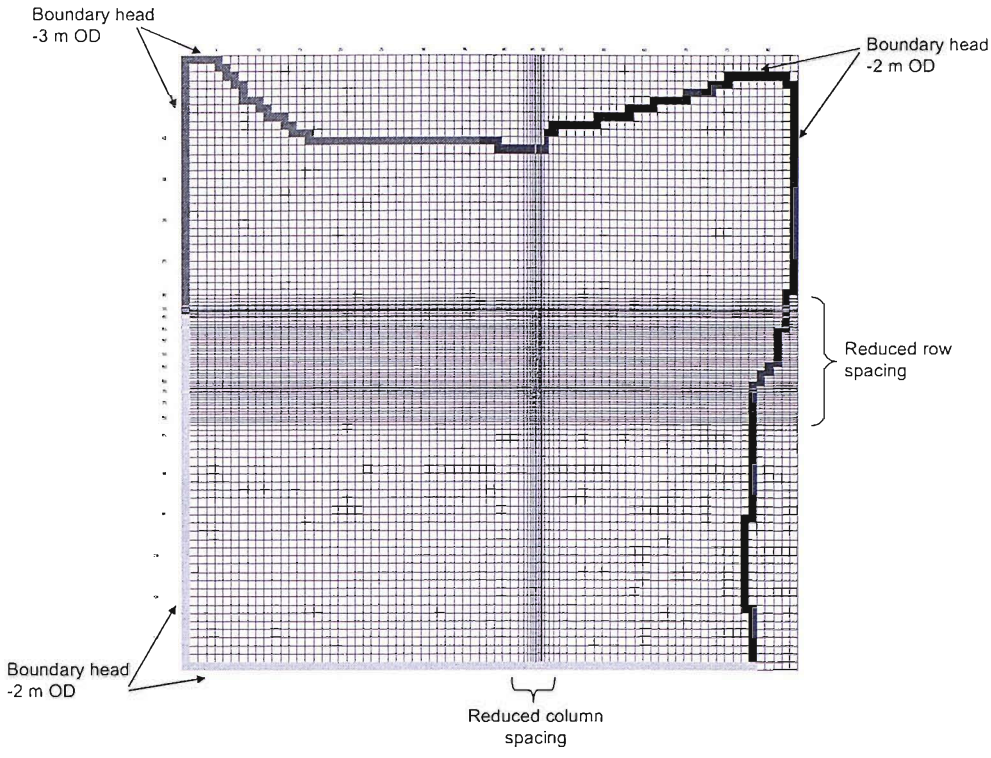

Figure 4.3: *The reduced spacing of cells around the excavation and the initial boundary heads for the model layers 3 to 12*

configuration. Furthermore, the very small curvature along the length of the excavation and the variable width of the excavation could not be reproduced in the model without significantly increasing the number of nodes. For the excavation as a whole, the difference in the surface areas of the actual and modelled diaphragm walls was approximately 1.5% (Table 4.2). The diaphragm walls and cut-off cross walls were incorporated into the model using the MODFLOW horizontal flow barrier package, as elements of thickness of 1.2 m and hydraulic conductivity 10^{-7} m/s (0.01 m/day).

4.4.2 Parameters

Zones of potentially different hydraulic conductivity were incorporated into the grid as indicated in Figure 4.5. The chalk between -17 to -26 m OD was

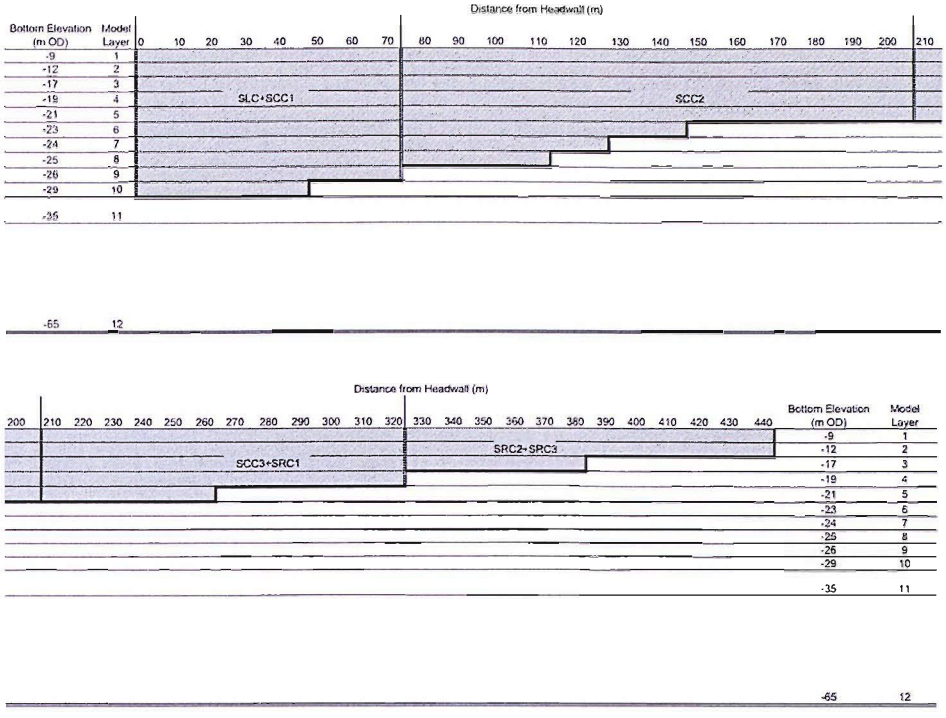

Figure 4.4: *Layer discretisation and the stepped diaphragm wall profile*

Table 4.2: *Comparison of actual and modelled diaphragm wall surface areas* (m^2) *for each cell. Percentage error* $= 100(1 - \frac{Actual}{Modelled})$

Cell	Actual surface area	Model surface area	Percentage error
SLC+SCC1	6257	6449.5	+2.98
SCC2	8581	8533.5	-0.56
SCC3+SRC1	6370	6617	+3.73
SCR2+SRC2	5273	5291.5	+0.35
Total	26481	26891.5	+1.53

split into an anisotropic surface chalk zone and a transition zone, as shown. For all the zones it is assumed that $k_x = k_y$, so from this point forward the horizontal permeability will be signified by k_x. It was assumed that the high permeability zone followed the line of the chalk outcrop and old river valley. The depth of the high permeability zone was investigated during the modelling.

4.4.3 Initial heads

The mean standing water level for each available piezometer in the Terrace Gravels and the Chalk was contoured, as shown in Figure 4.6. The levels range from +1 to +0.5 m OD with a general decrease in the level towards the Thames. These levels were used in the model as the initial heads. In the alluvium the initial heads were set to +0.5 m OD.

4.4.4 Model boundaries

Groundwater flows between the modelled aquifer area and adjacent parts of the aquifer were controlled by head-dependent flux boundaries, with the exception of the boundaries surrounding the alluvium, which were constant head boundaries. As drawdown was not observed, or expected, in the confining alluvium, the boundaries surrounding this material were set a head of +0.5 m OD. For head-dependent flux boundaries, the flux into or out of a boundary cell is computed by the model as follows:

$$Q = C(h_b - h_m) \tag{4.11}$$

where Q is the flowrate (m^3/day), C is the boundary conductance (m^2/day), h_b is the boundary head (m OD) and h_m is the head computed by the model (m OD). Both the conductance and the boundary head must be set for each cell.

The boundary conductance (C) can be determined by:

$$C = k_b \frac{(a \times b)}{d} \tag{4.12}$$

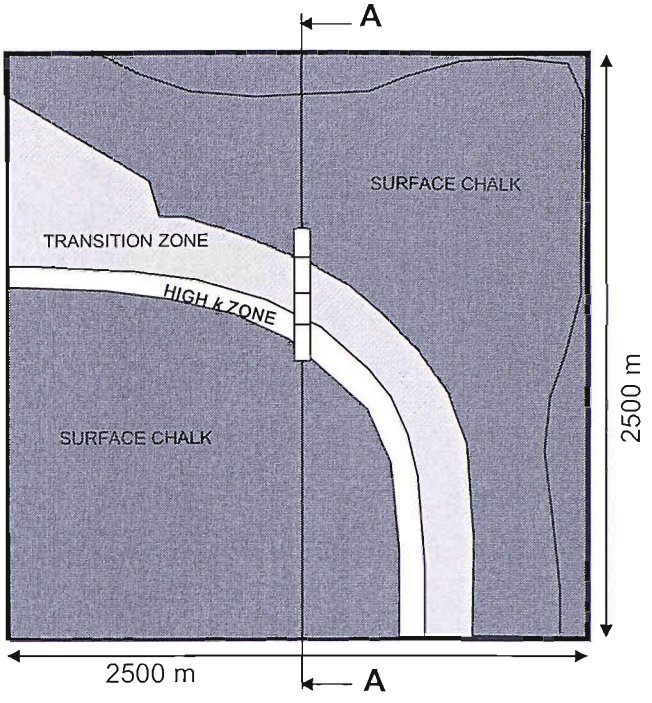

(a) Plan: -17 to -23 m OD

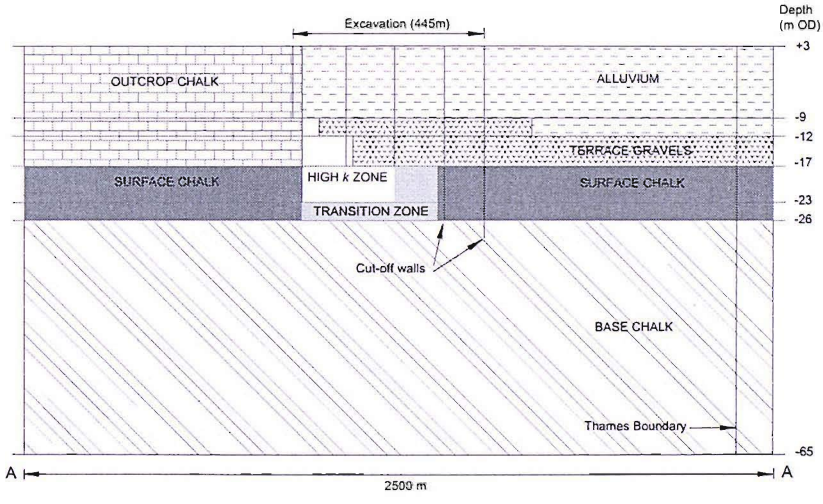

(b) Cross-section AA

Figure 4.5: *The hydrogeological zones of the model (not to scale): a) plan; b) cross section*

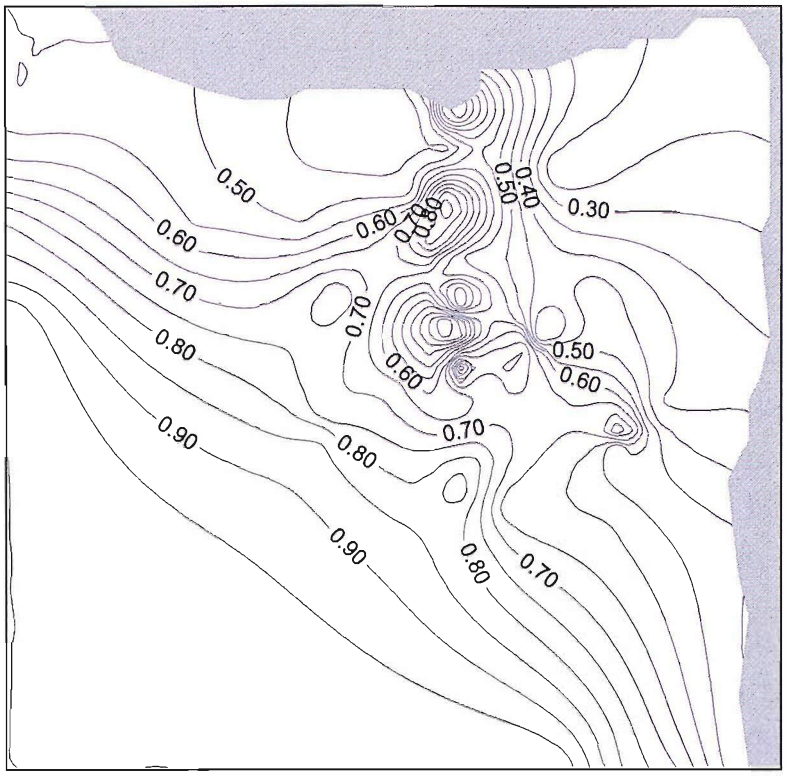

Figure 4.6: *Contours of the mean standing water levels in the aquifer (m OD)*

where k_b is the hydraulic conductivity of the boundary material (m/day), a is the width of the boundary cell (m), b is the thickness of the boundary cell (m) and d is the distance from the model boundary to the true recharge boundary (m).

The model boundary positions, shown in Figure 4.3, should be sufficiently far away from the excavation to exceed the estimated distance of influence (L_o), as calculated using Sichardt's empirical formula (Equation 2.6). Assuming a drawdown of 18 m and a permeability (k) of 3.4×10^{-4} m/s, which is twice the design value, the estimated distance of influence should be of the order of 1000 m for radial flow. The Thames shoreline was used to define the boundary around the upper and right sides of the model and is at least 850 m from the centre of the excavation. The landward boundaries represented the extent of the area of interest for this study and

are between 1200 and 1900 m from the centre of the excavation. Measured drawdowns suggested that the distance of influence extends beyond these positions. Initially, the boundary heads were set to -2 m OD or -3 m OD, as shown in Figure 4.3, within k_b equal to the k_x of the surrounding aquifer material and d set to 1 m. This allowed a first calibration to be made and gave the opportunity to gain a conceptual understanding of the effects of the boundary flows.

After exploring the boundary conditions, the boundary properties were set as listed in Table 4.3 and as shown in Figure 4.7. The conductance of the Thames boundary was assumed to be uniform around the shoreline, although it was varied with depth. Modelling suggested inflows from around the landward boundary were variable, so four reaches were created (L1 to L4). During the process of exploring the boundary conditions a number of observations were deduced from the model:

- Boundary conductance, and in turn inflows, generally decreased with depth in accordance with the concentration of transmissivity in the upper layers of the aquifer.

- Inflows from reach L1 were very low. This is probably a result of groundwater lowering to between -7.5 and -10 m OD at a quarry approximately 2 km south-west of the site (DBC, 2002). This influence may also explain the lower conductance of reach L2 compared to reach L3 in layers 1, 2 and 3.

- The highest inflows came from reach L4 in layers 2 and 3 where flow was through the gravels.

- Inflows through the gravels from the Thames boundary are much lower than the reach L4. This could be attributed to the reduction in the thickness of the gravels below the Thames shoreline, as shown in Figure 4.8. The relatively low k_b values are likely to reflect the nature of the hydraulic connection between the Thames and the aquifer, which appears to be inhibited, although the tidal analysis perhaps suggests otherwise (see §3.3).

- The conductance data indicate that larger flows within the high permeability zone are likely to have originated from the south-east of the site rather than the south-west.

- The distance (d) has been calculated for the required conductance value based on an assumed hydraulic conductivity (k_b). Since other values of d and k_b can give the same conductance, it is difficult to determine these properties with certainty. With the exception of reach L1 and the upper layers in reaches L3 and L4 , $d \approx 500$ m, and the values of k_b are within the likely ground permeability ranges. The shorter distances in the upper layers of reaches L3 and L4 help to encourage a more radial drawdown pattern, which was necessary to match the drawdowns of some remote piezometers close to the bottom left corner of the model area. The distance of influence is clearly greater than indicated by Sichardt's formula; this may be a result of high permeability features not accounted for in the calculation, or the inadequacy of the formula when used for relatively deep aquifers. The distance drawdown data recorded in December 2002, when drawdowns were greatest, are shown in Figure 4.9. The data indicate that flow was not radial, possibly as a result of inhomogenieties. The distance of influence interpolated from the data is unrealistically large ($L_o > 10000$ m), which suggests a highly permeable aquifer receiving low surface recharge flows.

By assuming the excavation is equivalent to a single large well, the data in Figure 4.9 were used to estimate the aquifer transmissivity T using the Jacob straight-line distance-drawdown method:

$$T = \frac{(2.3Q)}{2\pi\Delta(h_o - h)} \tag{4.13}$$

where Q is the total dewatering system flowrate and $\Delta(h_o - h)$ is the change in water level over one log cycle of distance. If $Q = 51840$ m^3/day (600 l/s) and the water level at the excavation is taken as -18 m OD (as a conservative estimate), then for the best fit line $T = 5500$ m^2/day, or 6.4×10^{-2} m^2/s. This estimate is approximately 7 times the design value of

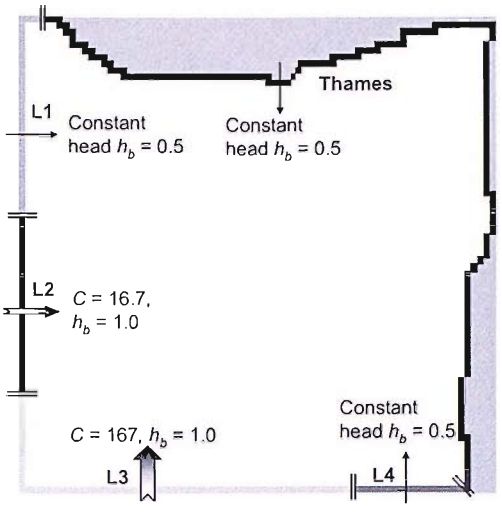

(a) Layer 1

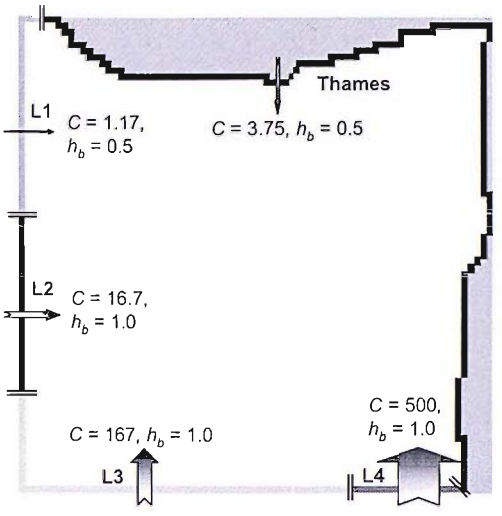

(b) Layers 2 and 3

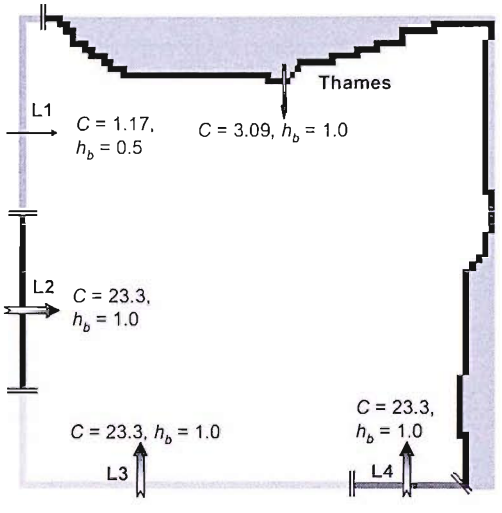

(c) Layers 4 to 9

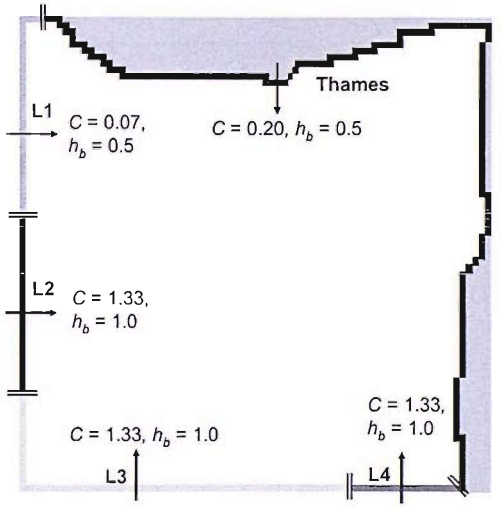

(d) Layers 10 to 12

Figure 4.7: *Boundary conductance (m^2/day) and heads (m OD)applied to the models. Boundary proprieties are given in Table 4.3.*

T = 810 m^2/day. However, the discrepancy is probably a result of the high permeability feature, hence the new estimate is not representative of the whole site.

Table 4.3: *Boundary properties used to achieve a good calibration. The properties are defined in Equations 4.12 and 4.11*

	Reach	C	k_b	a	b	d	h_b
		m^2/day	m/day	m	m	m	m OD
Layer 1	Thames	CH					0.5
	L1	CH					0.5
	L2	16.67	25	33.33	10	500	1
	L3	166.65	50	33.33	10	100	1
	L4	CH					1
Layers 2 and 3	Thames	3.75	7.03	33.33	8	500	0.5
	L1	1.17	50	33.33	8	11395	0.5
	L2	16.67	30	33.33	8	480	1
	L3	166.67	50	33.33	8	80	1
	L4	500	150	33.33	8	80	1
Layers 4 to 9	Thames	3.09	5.15	33.33	9	500	0.5
	L1	1.17	35	33.33	9	8973	0.5
	L2	23.33	35	33.33	9	450	1
	L3	23.33	35	33.33	9	450	1
	L4	23.33	35	33.33	9	450	1
Layers 10 to 12	Thames	0.2	0.08	33.33	39	500	0.5
	L1	0.07	0.5	33.33	39	9285	0.5
	L2	1.33	0.5	33.33	39	489	1
	L3	1.33	0.5	33.33	39	489	1
	L4	1.33	0.5	33.33	39	489	1

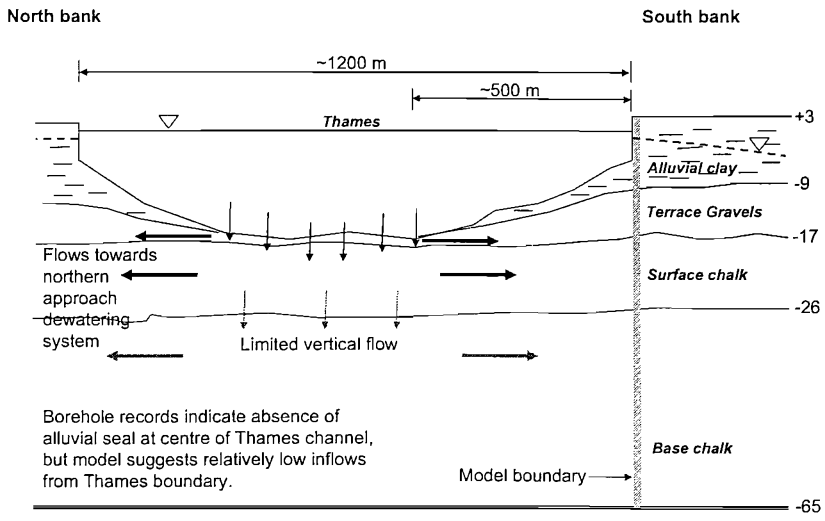

Figure 4.8: *The conceptual understanding of the Thames boundary. Section is along the tunnel alignment. Stratigraphy based on RLE (2001)*

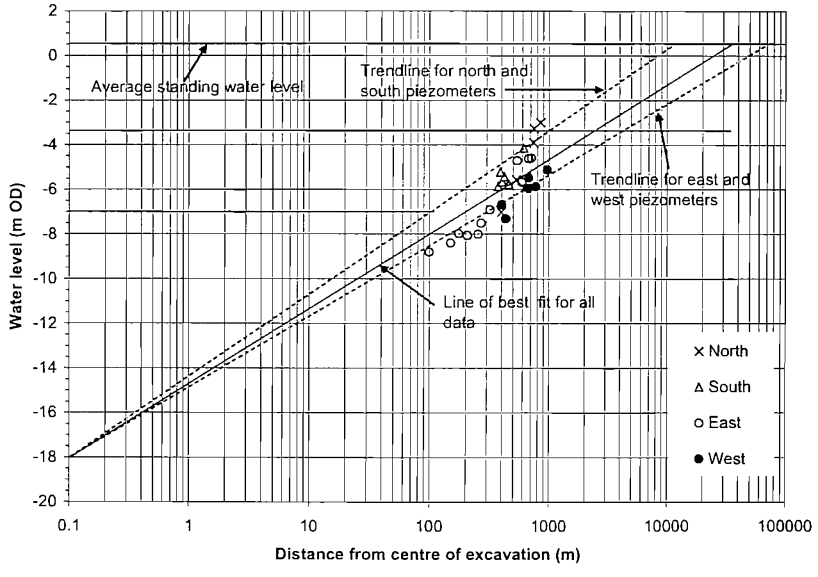

Figure 4.9: *Distance-drawdown data for December 2002 indicating a very large distance of influence. Piezometers are grouped in relation to the true north-south axis shown in Figure 3.7*

4.4.5 Analytical elements

Each dewatering well was represented by an analytical well (a well that is incorporated in the model, but is independent of the model grid Rumbaugh and Rumbaugh (1996))in the model, with the well coordinates and the depth of well screen specified in accordance with site records. The flow of each well was specified to match those recorded during the period that was modelled. These ranged from approximately 3 to 29 l/s (200 to 2500 m^3/day), with higher flows generally recorded for wells in cells SCC3+SRC1 and SRC2+SRC3, as shown in Figure 4.10 The total system abstraction rate for the period was 592 l/s (51149 m^3/day).

To calibrate the model, the drawdowns at 60 target locations, corresponding to the response zones of 12 internal, 16 external and 32 remote piezometers installed in the field, were compared with those recorded. (The recorded piezometer levels for the modelled period were taken as the mean measured water levels over the period, in each piezometer). For internal and external piezometers, the mean level was based on a large volume of continuous data recorded at hourly intervals. For the remote piezometers, the mean was calculated on the basis typically only 2 to 4 manual dip measurements made over the period in question, as shown in Figure 4.11.

4.4.6 Recharge

Recharge of the aquifer by the infiltration of rainfall was not included in the model. The effect of omitting infiltration on the model was checked by carrying out a simple calculation using rainfall and evaporation data for 2002 (WeatherOnline, 2006):

1. Average recorded UK rainfall: 700 mm/year
2. Average recorded UK evaporation: 600 mm/year
3. Infiltration: 100 mm/year
4. Total model area: 2500 m $\times$ 2500 m = 6250000 m^2

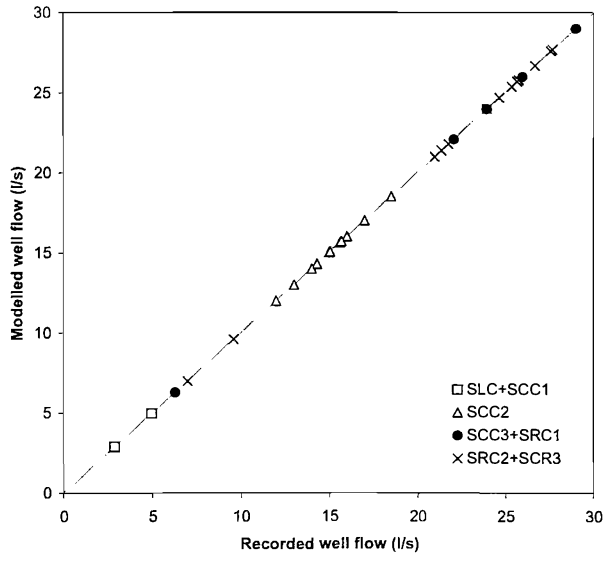

Figure 4.10: *Comparison of simulated analytical well flows and recorded well yields used for the four models.*

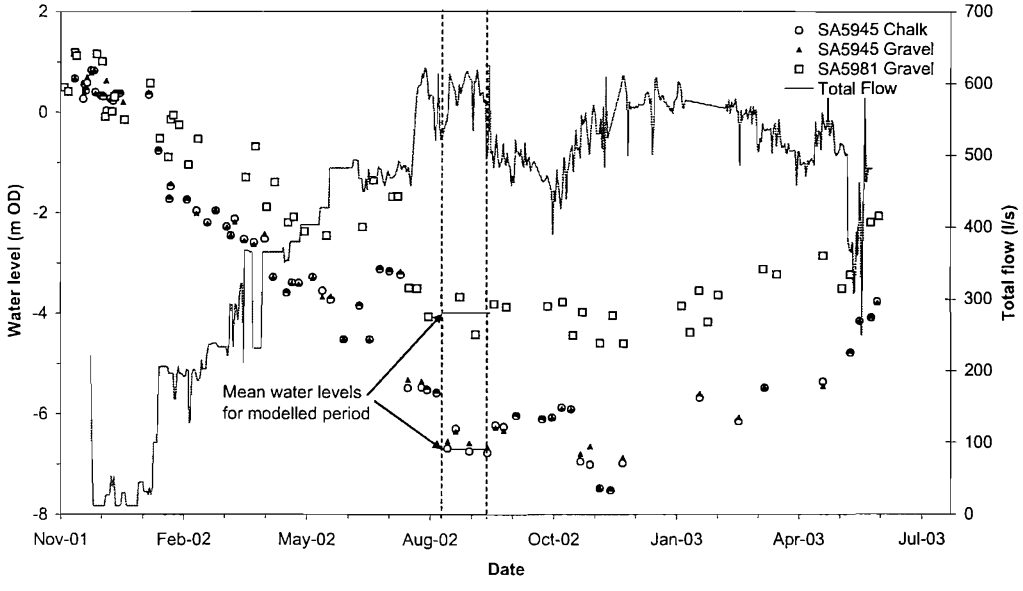

Figure 4.11: *Example piezometer hydrographs. The mean water levels used in the model are shown for the steady state period from 10th August 2001 to 13th September 2002.*

5. Approximate proportion of total model area which is unconfined: 35%

6. Unconfined model area: 6250000 $\times$ 0.35 = 2187500 m^2

7. Volume of water infiltrated in a year: 2187500 $m^2 \times$ 0.1 m/year = 218750 m^3/year

   or 599 m^3/day or 6.9 l/s

8. Approximate proportion of total inflows (600 l/s) from infiltration:

$$6.9/600 = 0.01$$

The calculation demonstrated that infiltration is insignificant when compared to both the lateral inflow through model boundaries and the dewatering system abstraction flow. The lateral recharge through landward boundary may have allowed for the contribution of rainfall to the model

4.4.7 Model calibration

The calibration of *MODEL 1* was initially by trial-and-error, whereby the k_x and k_z parameters of each zone were adjusted manually within a range broadly in accordance with the site investigation data (§3.2). The gradual refinement of the model was aided by a sensitivity analysis in which each parameter was varied systematically. A number of techniques, graphical and statistical, were used to investigate the match of the modelled data to the recorded data. The first step was to match the internal drawdowns, which was best achieved by plotting the water level profile along the excavation.

The simplest overall comparison of modelled and recorded drawdowns was made by calculating the mean of residual errors (M), defined as:

$$M = \frac{1}{n} \sum_{i=1}^{n} (x_i - y_i) \tag{4.14}$$

where x_i is the recorded piezometer water level (m OD), y_i is the modelled water level (m OD), and n is the number of samples (piezometers) - for the steady state model this was 60. This measure of fit can indicate the

whether there is a general underestimation or overestimation of drawdowns for the whole model. However, where both negative and positive residuals occur, they can cancel each other and give the impression of a good fit. To overcome this problem the mean of absolute residual errors (MA) was calculated as follows:

$$MA = \frac{1}{n}\sum_{i=1}^{n} \mid x_i - y_i \mid \tag{4.15}$$

For the sensitivity analysis the effects of changes on the overall model fit were compared by calculating the sum of squares of residuals (S)

$$S = \sum_{i=1}^{n}(x_i - y_i)^2 \tag{4.16}$$

S gives an indication of the total discrepancy between the model and the field performance of the dewatering system. An ideal calibration would be achieved when M, MA and S are all equal or as close as possible to zero. If a residual of 0.5 m is set as an acceptable level of error for each piezometer, S should not exceed 15, (within n = 60) although this assumes that the residuals are distributed evenly.

The relationship between the modelled and recorded data was established using linear regression analysis. A least squares method was used to plot the regression line on a scattergram the form of $y = bx$, where the line was forced through the origin. The gradient (b) is calculated as follows

$$b = \frac{\sum xy}{\sum x^2} \tag{4.17}$$

For an ideal model fit b will equal 1.

Finally, the product moment correlation coefficient (R) was calculated as follows

$$R = \frac{n\sum xy - \sum x \sum y}{\sqrt{[n\sum x^2 - (\sum x)^2][n\sum y^2 - (\sum y)^2]}} \tag{4.18}$$

During the calibration process it was attempted to move as close to $R = +1$ as possible, as this indicates a perfect positive correlation between

Table 4.4: *Correlation coefficient (R) values required for a statistically highly significant ($P = 0.01$) relationship between recorded and modelled data*

	No. of piezometers (n)	Degrees of freedom	$\pm R$ at $P = 0.01$
Internal piezometers	12	10	0.708
External piezometers	16	14	0.590
Remote piezometers	32	30	0.449
All piezometers	60	58	0.325

Table 4.5: *Values of hydraulic conductivity (m/day) for each of the models*

Zone	*MODEL 1*		*MODEL 2*		*MODEL 3*		*MODEL 4*	
	k_x	k_z	k_x	k_z	k_x	k_z	k_x	k_z
Alluvium	0.1	0.01	0.1	0.01	0.1	0.01	0.1	0.01
Terrace Gravels	150	150	150	150	150	150	150	150
Surface chalk	35	0.1	35	0.1	35	0.1	**1.25**	**0.83**
Transition zone	55	36.5	**35**	**0.1**	55	36.5	**90**	**57**
Outcrop chalk	50	5	50	5	50	5	50	5
High k zone	4800	4800	4800	4800	**55**	**36.5**	4800	4800
Base chalk	2	0.02	2	0.02	2	0.02	2	0.02

the recorded and modelled data. Table 4.4 gives values of R required for the correlation to be statistically highly significant, where $P = 0.01$.

4.5 Results and discussion

MODEL 1, with all the large scale features, shows a good fit between the recorded and modelled internal drawdowns (Figure 4.12) and this model represented the overall hydrogeology convincingly (Figure 4.13(a) and Table 4.6). The modelling suggested that the hydraulic conductivity of the Terrace Gravels (150 m/day) (Table 4.5) was slightly lower than expected based on pumping tests (190 to 400 m/day), but within the estimated

Table 4.6: *Summary table of statistics for the steady state model simulations (M is the mean of residual errors, MA is the mean of absolute residual errors, and R is the correlation coefficient)*

	Internal $n = 12$	External $n = 16$	Remote $n = 32$	Overall $n = 60$
MODEL 1				
M (m)	-0.09	0.10	0.07	0.04
MA (m)	0.32	0.28	0.34	0.32
Linear relationship	$y = 0.989x$	$y = 1.012x$	$y = 1.012x$	$y = 1.001x$
R	+0.99	+0.94	+0.97	+0.99
MODEL 2				
M (m)	3.92	0.84	-0.07	0.92
MA (m)	3.93	1.12	0.34	1.22
Linear relationship	$y = 1.326x$	$y = 1.106x$	$y = 0.987x$	$y = 1.176x$
R	+0.86	+0.84	+0.97	+0.94
MODEL 3				
M (m)	10.66	8.13	3.92	6.32
MA (m)	10.66	8.13	3.92	6.32
Linear relationship	$y = 1.7146x$	$y = 1.923x$	$y = 1.764x$	$y = 1.778x$
R	-0.28	+0.63	+0.92	+0.82
MODEL 4				
M (m)	0.21	0.81	0.57	0.55
MA (m)	0.50	0.81	0.05	0.67
Linear relationship	$y = 1.001x$	$y = 1.096x$	$y = 1.104x$	$y = 1.053x$
R	+0.97	+0.84	+0.93	+0.96

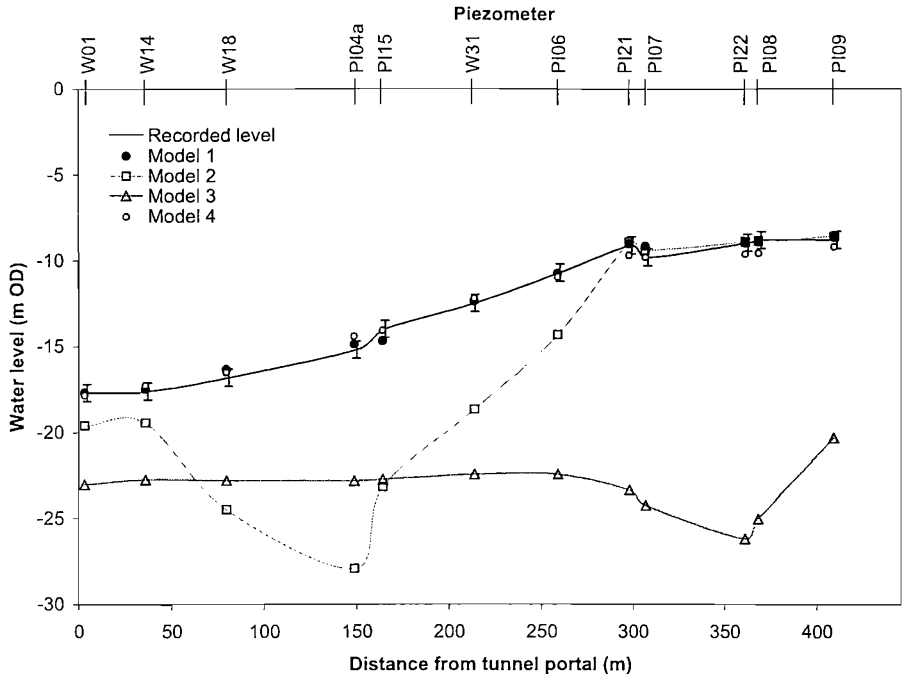

Figure 4.12: *Drawdown profile inside the excavation for each of the models. The recorded levels are shown with error bars of +/- 0.5 m.*

range based on particle size distribution (PSD) curves (34 to 306 m/day). It is normally expected that the permeability derived from PSD curves is higher than in reality and that pumping tests give a better estimation, as discussed in §2.3.2.

To achieve the recorded drawdown in the cell SLC+SCC1, an anisotropic permeability ratio of 350 (k_x/k_z = 35/0.1 m/day) had to be applied to the surface chalk. Assuming a low anisotropy ratio of just 1.5 for the surface chalk, a k_x in the order of 1.25 m/day was required to achieve the same drawdown in the cell SLC+SCC1, as shown for *MODEL 4*. Such a low horizontal hydraulic conductivity in the top 9 metres of the Upper Chalk could be indicative of a significant putty chalk presence. Putty chalk is term to describe structureless chalk that is devoid of fissures, or where fissures are infilled with clay-sized chalk fragments, hence the chalk has a low permeability similar to that of the Chalk matrix. Permeabilities of putty chalk are typically 10^{-9} to 10^{-7} m/s, or 8.6×10^{-5} to 8.6×10^{-3}

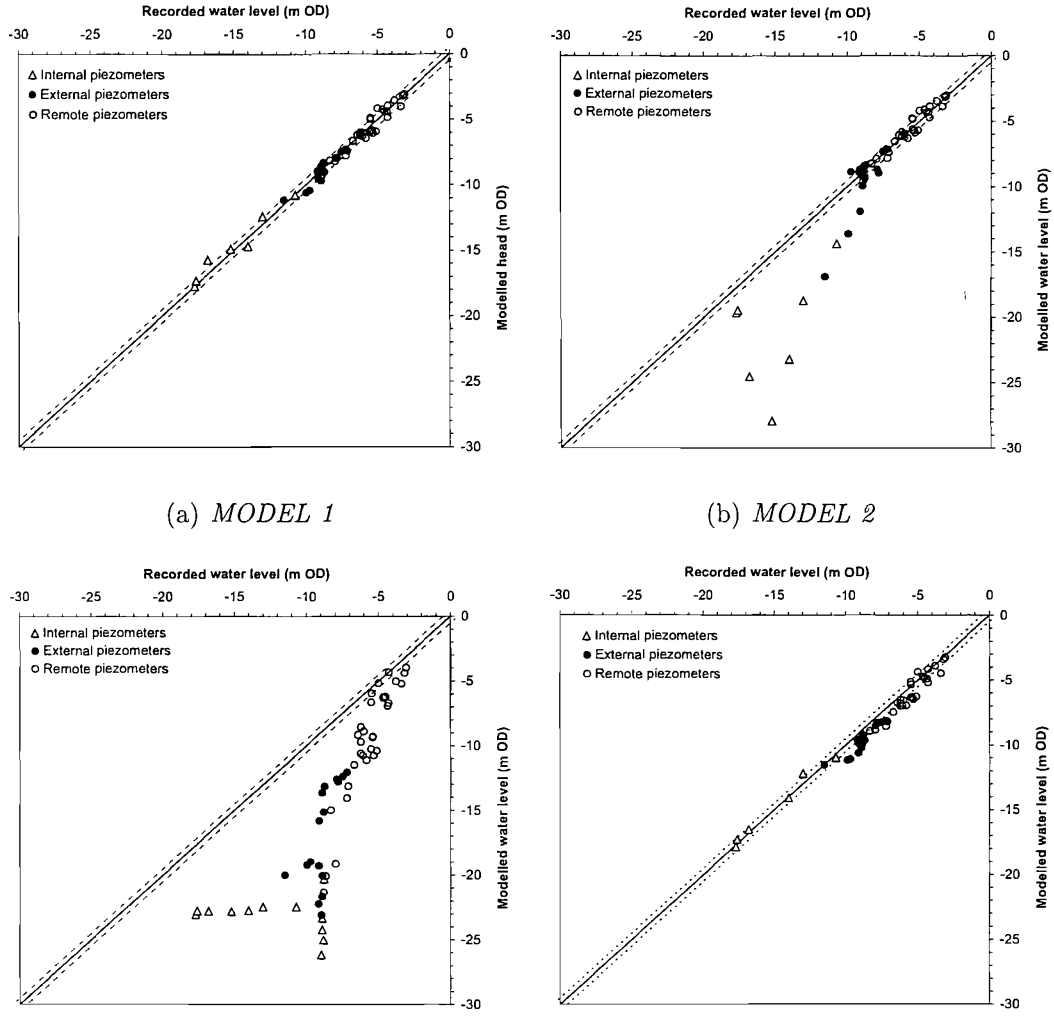

(a) *MODEL 1*

(b) *MODEL 2*

(c) *MODEL 3*

(d) *MODEL 4*

Figure 4.13: *Comparison of recorded and modelled piezometric heads for each model. The solid line indicates the ideal correlation and the dashed lines represent an error of +/- 0.5 m.*

m/day (Roberts and Preene, 1990). At floodplain sites, putty chalk is often observed at the chalk/gravel interface (Younger, 1989), but little if any thickness of this material was observed at this site. Roberts and Preene (1990) state that putty chalk can inhibit gravity drainage, but the cell SLC+SCC1 was drained quickly with a flat drawdown response throughout the cell; this indicates a good hydraulic connection between the wells and aquifer material. To avoid a significant overestimation of drawdown along the cell SCC2 in *MODEL 4*, the permeability of the transition zone was increased (Table 4.5).

In *MODEL 1*, the degree of anisotropy in the transition zone was low (1.5), and the horizontal permeability, at 50 m/day, was slightly greater than the surface chalk. Omitting the transition zone, as in *MODEL 2*, overestimates of the internal drawdowns in the cell SCC2 by up to 12.5 m at P104a (Figure 4.12), and overestimates some external drawdowns. However, the fit of the remote drawdowns remains largely unaffected (Figure 4.13(b), Table 4.6), suggesting that anisotropy only has a significant influence on drawdowns in and immediately around excavations where cut-off walls restrict horizontal flow.

In addition to the four steady state models, a study of the dewatering of the cell SLC+SCC1 was used to confirm the anisotropy of the surface chalk zone. A transient model, with the same grid design and conceptual hydrogeology as *MODEL 1*, was constructed to simulate a period of dewatering in December 2001 when only this cell was being dewatered. Records showed that a pumping rate of 20 l/s, evenly distributed between wells W04 and W12, lowered water levels in the standpipe piezometer PI01 to -9.2 m OD. Doubling the pumping rate to 40 l/s achieved water levels of -18.5 m OD. A series of transient model runs was carried out with different levels of anisotropy of the surface chalk, where k_x was constant at 35 m/day. All other zones were assigned the hydraulic conductivities of *MODEL 1*, as listed in Table 4.5. Figure 4.14 shows that the drawdown inside the cell is most sensitive to anisotropy k_x/k_z at ratios between 10 and 1000, and suggests that a ratio between 350 and 750 is appropriate for the surface chalk zone, giving $0.047 < k_z > 0.1$ m/day. This is consistent

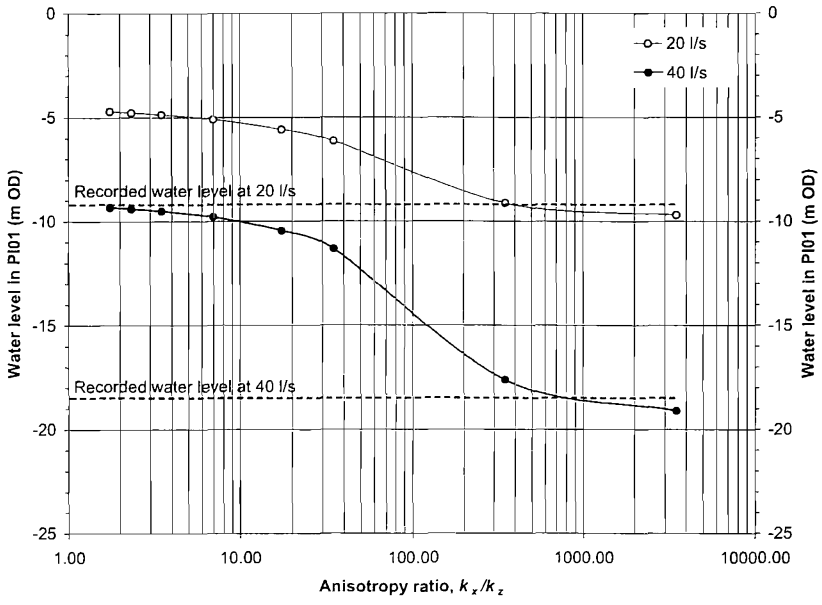

Figure 4.14: *The drawdown at the standpipe piezometer PI01 for different anisotropy ratios of the surface chalk, when extracting groundwater at two pumping rates from the cell SLC+SCC1.*

with the level of anisotropy applied in *MODEL 1.* The models were largely insensitive to any anisotropy of the base chalk over the same range.

It is clear from this analysis that anisotropy can have an important influence on drawdowns inside excavations bounded by cut-off walls. In this case the effect is particularly pronounced since the diaphragm walls extend into the less permeable base chalk, which means horizontal flow below, as well as around the toe, is limited. It is possible that the anisotropy is largely determined by the orientation of fractures, as suggested by Toynton (1983) in a study of Norfolk Chalk. Bedding-parallel fractures, related to the deposition of the Chalk, occur at an angle approximately equal to the mean plane of dip and trace lengths persist across the full extent of the formation; contrastingly the trace length of bedding-normal fractures are typically less than 1 m (Younger and Elliot, 1995). Warren and Mortimore (2003) show that the bedding planes at this location are near horizontal. Solution development of such fractures may lead to a greater horizontal conductivity than vertical conductivity, particularly if the connectivity

between bedding-parallel fractures (though by bedding-normal fractures) is low. Similar degrees of anisotropy were found to be influential on the performance of a wellpoint dewatering system during a modelling study by Powrie et al. (1989). They found that a high permeability lens extending horizontally within an otherwise moderately permeable aquifer caused significant increases in flows and decreases in drawdowns for anisotropy ratios above 100.

The remote drawdowns at the case study are highly sensitive to the hydraulic conductivity of the high permeability zone, which dominates most of the hydrogeological system. In *MODEL 1* the isotropic hydraulic conductivity of this feature is estimated to be approximately 4800 m/day. In *MODEL 3*, which omits the high permeability feature completely there is large overestimation of drawdowns centered on the retained cut sections where internal drawdowns exceed the recorded values by up 16 m at PI08 (Figure 4.12). Excessive drawdowns in this area caused increased drawdowns throughout the excavation.

While it is possible to determine the approximate width of the high permeability zone using specific capacity data (Figure 3.15), the depth is less clear. *MODEL 1* suggests a transmissivity of $T = 53400$ m^2/day for the effective aquifer (-9 m OD to -65 m OD) at well W38, in the retained cut, where the high permeability zone extends to depth of -23 m OD (Figure 4.5). In contrast, $T = 1593$ m^2/day for the cut and cover sections of the tunnel approach. The base of the high permeability zone cannot be above 21 m OD otherwise the zone would not extend laterally into the SRC1 section, because of the sloping profile of the gravel/chalk interface (Figure 4.5). It is unlikely that the zone would extend below -35 m OD given the improved chalk core quality at borehole SR5957 below -30 m OD (Figure 3.17). Figure 4.15 shows that varying the thickness of high permeability material, whilst maintaining the same overall transmissivity, appears have a minimal impact upon the fit of the model. For these model runs the vertical hydraulic conductivities were unchanged from the starting permeabilities listed in Table 4.5 for *MODEL 1*.

For the *MODEL 1* starting permeabilities, the sum of squares of

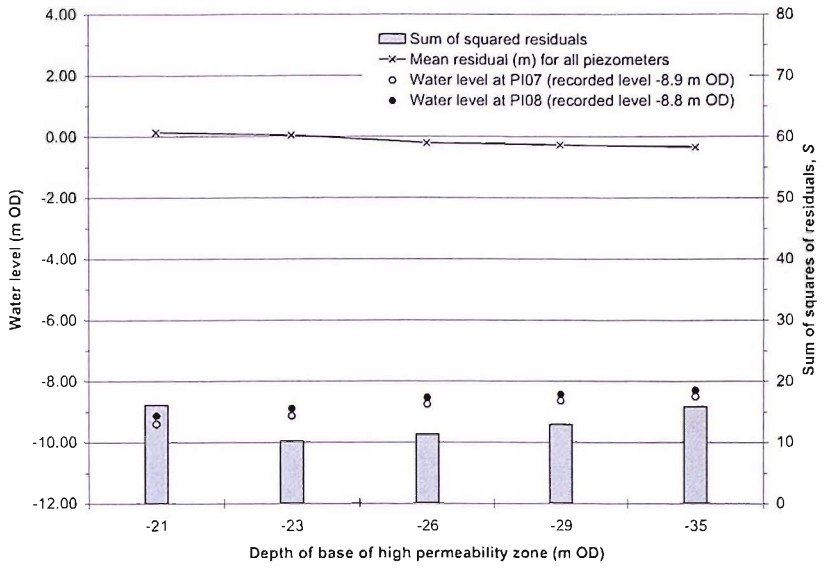

Figure 4.15: *The model fit and internal drawdown in the retained cut sections for different thicknesses of the high permeability zone. The transmissivity of the effective aquifer is constant for each configuration.*

residuals $S = 9.95$ and for each of the model runs in Figure 4.15 $S \leq 15$, indicating a satisfactory match between the model results and the recorded data. The best fit was achieved using a depth of -23 m OD for the high permeability zone, but this was inevitable given that the hydraulic conductivities of the other zones were calibrated using this configuration; improved fits for the other configurations could be achieved if small changes were made to the hydraulic conductivity of the Terrace Gravels, for example. The internal drawdowns at standpipe piezometers PI07 and PI08 show a maximum variation of 0.9 m for the different zone configurations, and the mean of residual errors (M) for all the 60 modelled piezometers varies by just 0.38 m.

This analysis suggests that the hydraulic conductivity of the high permeability zone is in the range of 2300 to 5850 m/day (2.7×10^{-2} to 6.8×10^{-2} m/s), implying that the zone consists of karstic chalk or a network of enlarged macrofissures. The karstic behaviour of the Chalk is characterised by high velocity flow through dissolution pipes, which provide pathways for the rapid transport of water (Banks, Davies and Davies,

1995; MacDonald, Brewerton and Allen, 1998). Significant conduits are common in the area; during a regional hydrogeological study of the Chalk (Thames-Water, 2003), dissolution features were observed in a chalk quarry that lies 2km to the southwest of the site. Reeves (1979) defined enlarged macrofissures as having an aperture greater than 3 mm and a spacing between 2 and 20 m, which can contribute to hydraulic conductivity of the order of 1000 m/day. Examination of chalk cores for borehole SR5957 suggested a closer spacing (less than 60 mm) of similar size apertures, which is consistent with the even greater hydraulic conductivities apparently identified here by the modelling studies.

4.5.1 Sensitivity analysis

A formal sensitivity analysis for *MODEL 1* was carried out, which confirmed the findings already discussed. The starting parameter values were those listed in Table 4.5. The impacts of each model zone were investigated in turn by varying the hydraulic conductivity parameter, whilst maintaining the other parameters unchanged. The relative sensitivity of the model to each of the parameters is shown by the gradient of the sensitivity curve (Figure 4.16); for example, the model drawdown was influenced significantly by the horizontal permeability of the high permeability zone but was insensitive to the horizontal permeability of the base chalk. The vertical hydraulic conductivity (k_z) is expressed in terms of the anisotropy ratio (k_x/k_z) , where k_x is kept constant and equal to the starting parameter value. The anisotropy of the surface chalk, transition zone and base chalk zones all influence the model fit, as explained previously with regard to the internal drawdown. The apparent insensitivity of the model to the permeability of the outcrop chalk means that the model could be simplified by treating this zone as an extension of the surface chalk zone with the same parameter values. The Terrace Gravels and high permeability zone would be expected to be isotopic in reality, and applying an anisotropy ratio of less than 50 has a negligible impact on the overall model fit.

The models presented in this chapter make the assumption that the

large variation in transmissivity through the excavation is due to inhomogeneities in the surface chalk (-17 to -26 m OD) and that the Terrace Gravels and base chalk zones are homogeneous. It is possible to achieve a similar, or perhaps even better, calibration by a combination of increasing the permeability of the Terrace Gravels and counteracting this with a decrease in the horizontal permeabilities of the underlying chalk zones. In view of the number of model zones and parameters it is not possible to find a unique solution, which is a limitation of this type of model. However, the relative differences in the permeability of between the surface chalk, transition zone and high permeability zone must still apply, as shown for the simulations presented in Figure 4.17.

4.5.2 Further modelling

Further modelling was carried out to demonstrate that as the designed dewatering system could have dealt adequately with the inflows for a more homogenous aquifer. A new model, based on *MODEL 1*, was developed in which the surface chalk, transition zone, high permeability zone and outcrop chalk (Figure 4.5(b)) were treated as one zone of uniform hydraulic conductivity. This simplified model will be referred to as *MODEL 5*. Two simulations were carried out in which:

a) the uniform surface chalk and the base chalk were assumed to be relatively isotropic, with $k_x/k_z = 35/20$ m/day, and $k_x/k_z = 2/1.15$ m/day respectively.

b) the uniform surface chalk and the base chalk were assumed to be anisotropic, with $k_x/k_z = 35/0.1$ m/day and $k_x/k_z = 2/0.02$ m/day respectively.

MODEL 5a) represents the conceptual hydrogeology on which the dewatering system was based, although the values of transmissivity are different at the centre of the excavation $T = 1600$ m^2/day (1.9×10^{-2} m^2/s) in the model, approximately double the design value of $T = 810$ m^2/day

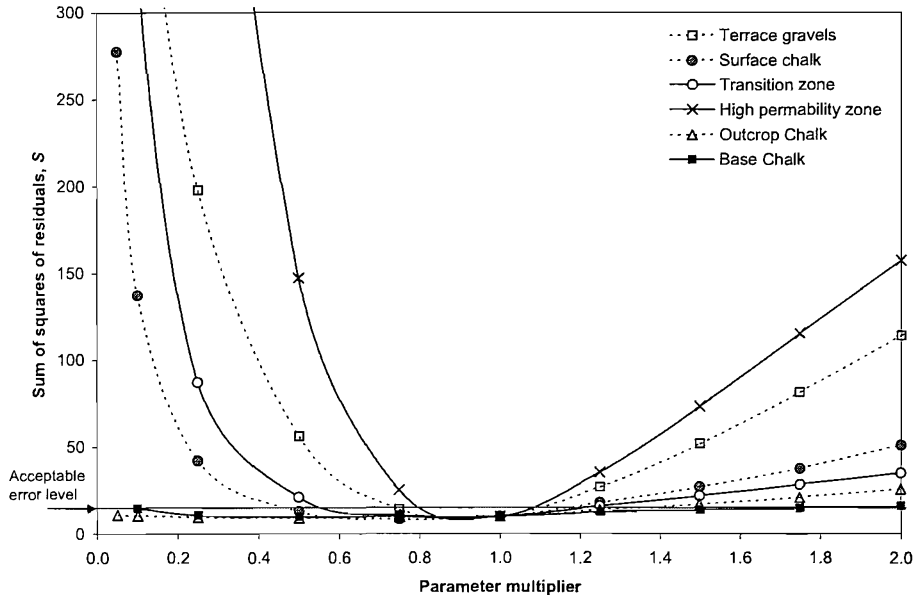

(a) k_x

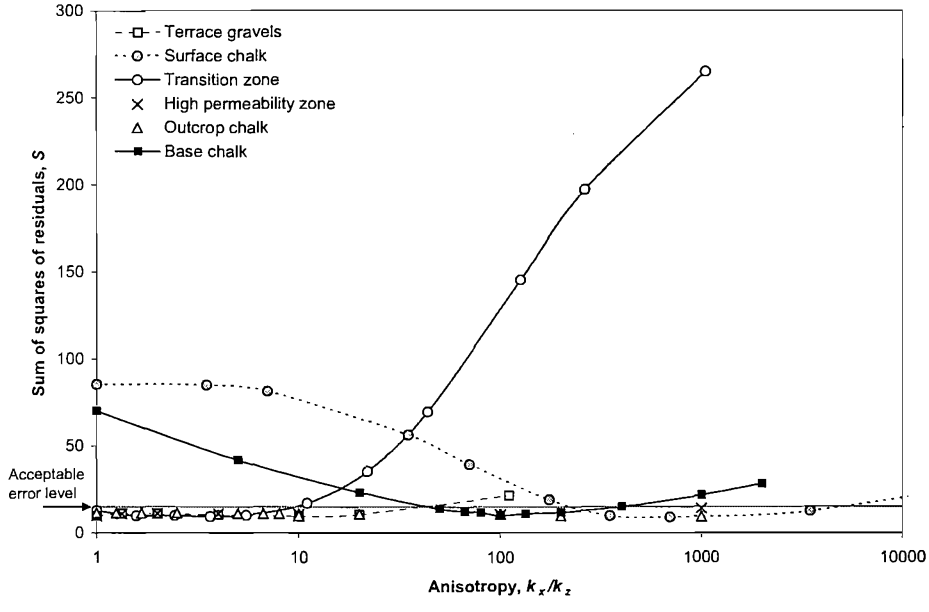

(b) k_z

Figure 4.16: *Sensitivity curves for hydraulic conductivity: (a) k_x; (b) k_z*

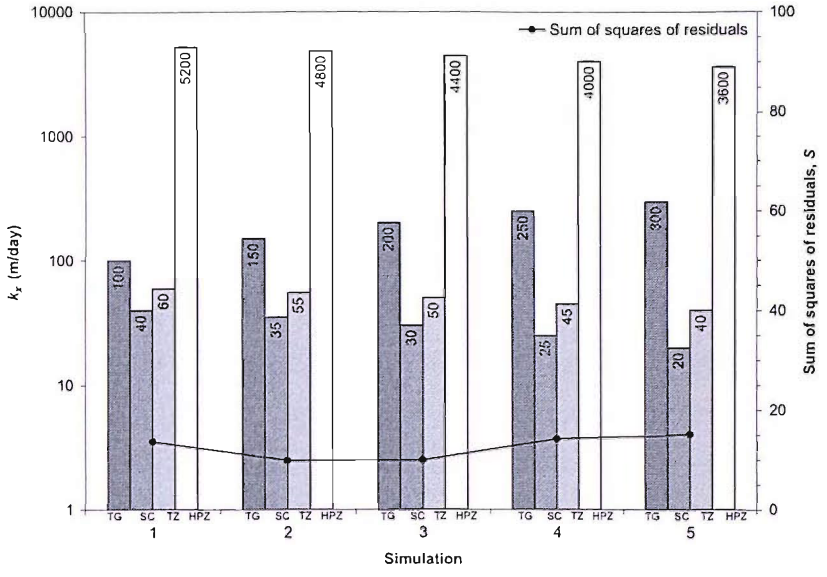

Figure 4.17: *Horizontal hydraulic conductivities (k_x) used to achieve good calibrations of* MODEL 1, *i.e.* $S \leq 15$. *The k_x of the Terrace Gravels (TG), surface chalk (SC), the transition zone (TZ) and the high permeability zone (HPZ) have been varied, while the outcrop chalk, base chalk and alluvium are kept constant at the starting values (Table 4.5). Anisotropy was applied at the same ratios used for the starting values.*

(9.4×10^{-3} m^2/s). The boundary conditions were as indicated in Figure 4.7 and Table 4.3.

Both of the simplified model runs gave internal water levels that approximately matched the recorded values, as shown in Figure 4.18. The corresponding calculated individual well flows are summarised in Table 4.7. Only the design wells (W01 to W42) were used in these model runs, although not all were required. It is noticeable that even when the surface chalk is relatively isotopic, as in *MODEL 5a)*, there was a large amount of redundancy in cell SLC+SCC1. The high pump capacity in this cell was installed because of uncertainty about the depth of the interface between the surface and base chalk; failure to achieve the drawdown in this cell would have led to significant delays in the construction of launch chamber and in turn the boring of the tunnel. The design flow from cell SCC2 had a factor of safety of 2; in *MODEL 5a)* the as-built flows are close to the

design flow as a result of the modelled transmissivity (T) value being twice the design T value. A larger factor of safety was applied for the remaining cells, because the design engineers were mindful of the potential for high flows close to the confined-unconfined boundary based on previous experience (Leiper et al., 2000). In this case, that allowance was clearly not adequate to deal with the high permeability zone.

The results for *MODEL 5b)* confirm that the influence of anisotropy is limited to the parts of the excavation with deeper diaphragm walls; the anisotropy reduces flows by a factor of approximately 3 compared with *MODEL 5a)*in cells SLC+SCC1 and SCC2 and has little or no effect in the remaining cells.

In *MODELS 5a)* and *5b)* the flow is radial. The flow pattern is more complex in *MODEL 1*, in which the Chalk was modelled as inhomogeneous, as shown in Figure 4.19. The high permeability zone intercepts much of the flow south of the excavation and channels flow into the retained cut area of the excavation. In *MODEL 1*, the contours spread along the high permeability zone and therefore the remote drawdowns are approximately 1 m greater than in *MODEL 5a)*. The effect of the anisotropy in *MODEL 5b)*, combined with the cut-off walls, is to reduce the hydraulic continuity between the excavation and the external aquifer. As a result, remote drawdowns are significantly lower for the anisotropic case, and the distance of influence generally occurs within the model area.

4.6 Model integrity

A number of studies were carried out to investigate the integrity of the model design. As well as the ground conditions, both the boundary conditions and the permeability of diaphragm walls could have an influence on the model calibration. In addition, a series of model runs were made to determine the impact, if any, that finite difference grid spacing had on the accuracy of the model solution.

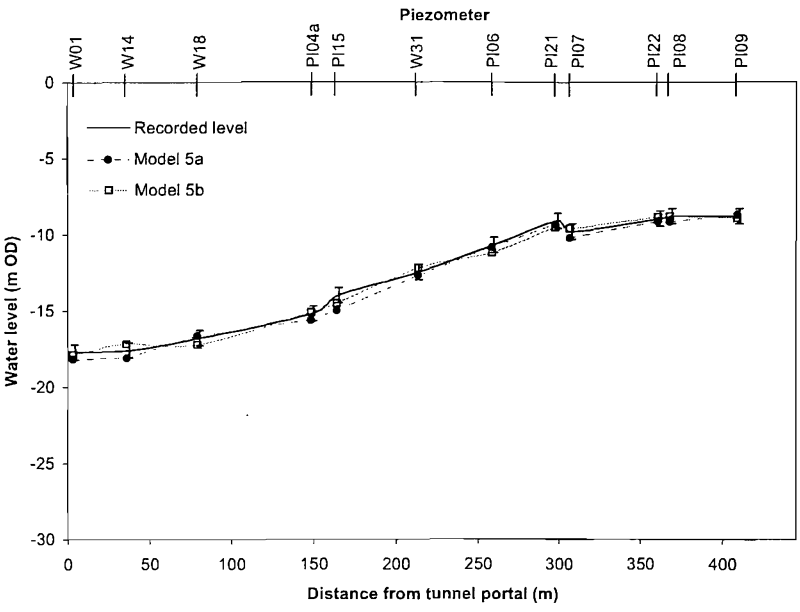

Figure 4.18: *The internal drawdown profile for the simplified model* - MODEL 5

4.6.1 Boundary conditions

The groundwater models were calibrated by assuming the boundary conditions described in Figure 4.7, where the conductance (C) varies between the boundary reaches. The distribution of inflows (Q) into *MODEL 1* is shown in Figure 4.20 for the best fit case. The proportion of the total inflow from the Thames boundary is 0.25. When the length of the boundary is taken into account, the inflow from the Thames is low compared with the other reaches with the exception of reach L1.

In a steady state model, the flow into the model through the boundaries must balance the flow removed by the dewatering system, assuming that there is no recharge by rainfall infiltration. A study was carried out to establish the effect of increasing and decreasing inflows from the Thames boundary. This will be important in assessing the contamination of the aquifer by saline water from the Thames as a result of the dewatering, which will be discussed later in the dissertation. Figure 4.21 shows that to achieve a good calibration ($S \leq 15$), the proportional inflows through the Thames boundary must be within a narrow range of 0.22 and

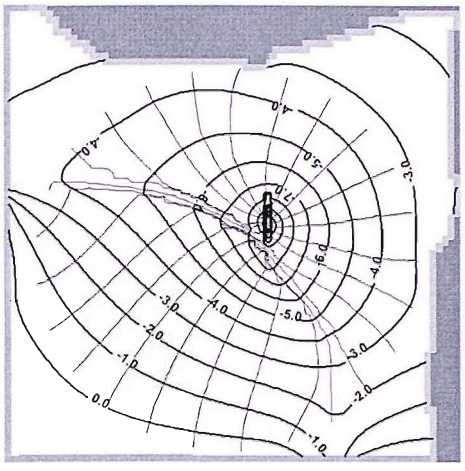

(a) *MODEL 1* -the inhomogeneous case

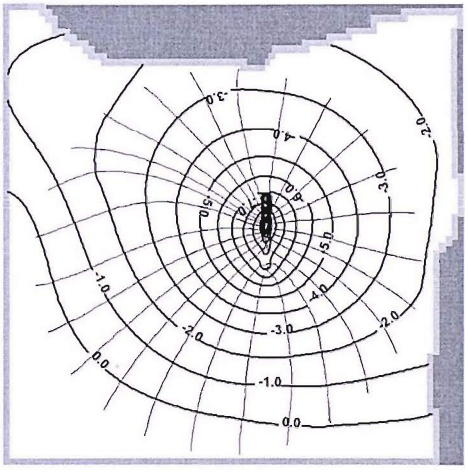

(b) *MODEL 5a)* - the isotropic case

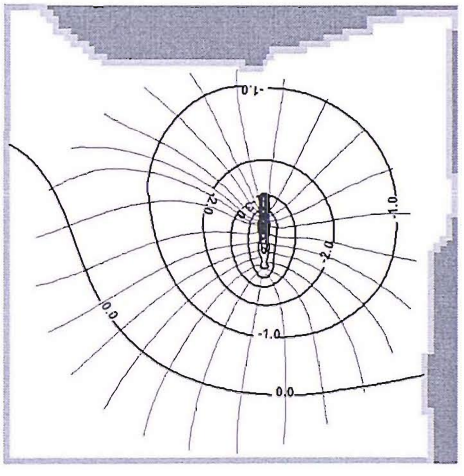

(c) *MODEL 5b)*- the anisotropic case

Figure 4.19: *Water level contours (m OD) and flowpaths in the surface chalk for the 2500 m by 2500 m model area*

Table 4.7: *Comparison of flows (l/s) during steady state full system operation*

	Design		*MODEL 5a)*	
	No. wells	Flow	No. wells	Flow
SLC+SCC1	16	320	4	23.3
SCC2	14	200	14	170
SCC3+SRC1	6	72	6	37
SRC2+SRC3	6	72	6	45
Total	42	664	30	275

	MODEL 5b)		As-built	
	No. wells	Flow	No. wells	Flow
SLC+SCC1	2	8.1	2	8.1
SCC2	13	55	14	189
SCC3+SRC1	6	29	6	120
SRC2+SRC3	6	45	14	274
Total	27	137	36	592

0.28, or a total flow of 130 to 166 l/s. The distribution of the Thames boundary inflows to the gravel, surface chalk and base chalk layers is shown in Figure 4.22. Inflows are greater in the surface chalk layers than the gravel layers. The inflows to the base chalk layers may be limited by the low vertical flows in the Chalk. This indicates that the rate of migration of saline water from the Thames boundary is likely vary with depth.

4.6.2 Diaphragm wall permeability

For each of the previously discussed model runs, the diaphragm wall had been assigned a hydraulic conductivity of 10^{-7} m/s. As the actual as-built permeability could not be established, it was necessary to consider the influence of the diaphragm wall permeability on the model. For this study, it was assumed that the permeability of the wall was uniform throughout

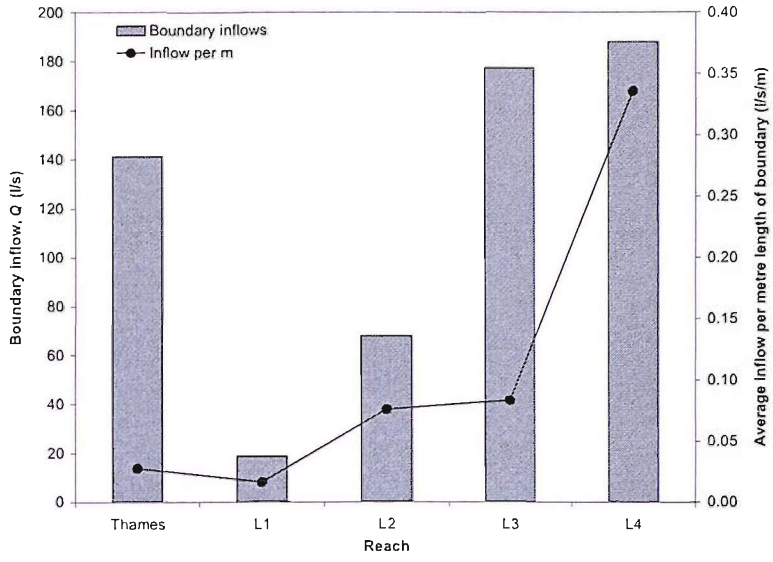

Figure 4.20: *The distribution of the total model inflow between the boundary reaches of* MODEL 1

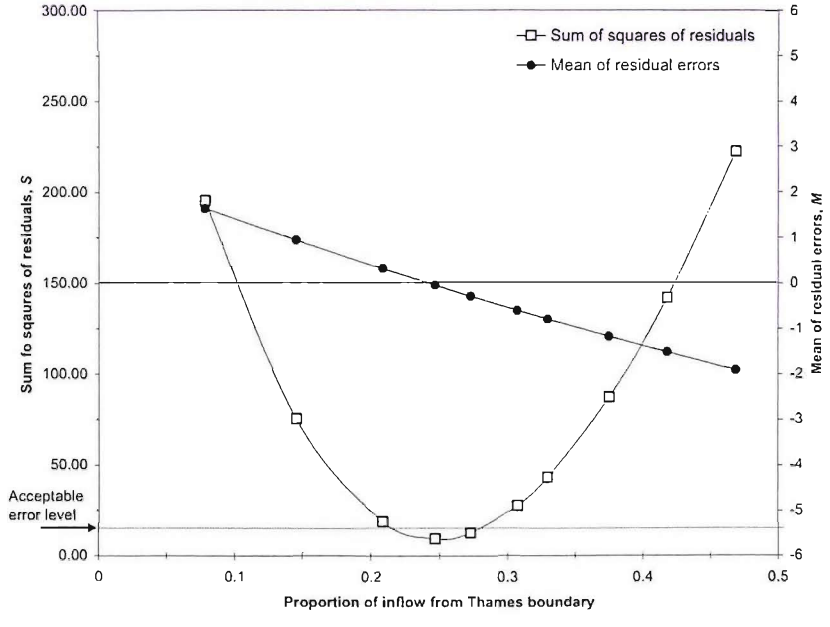

Figure 4.21: *The effect of different inflows from the Thames on the model fit*

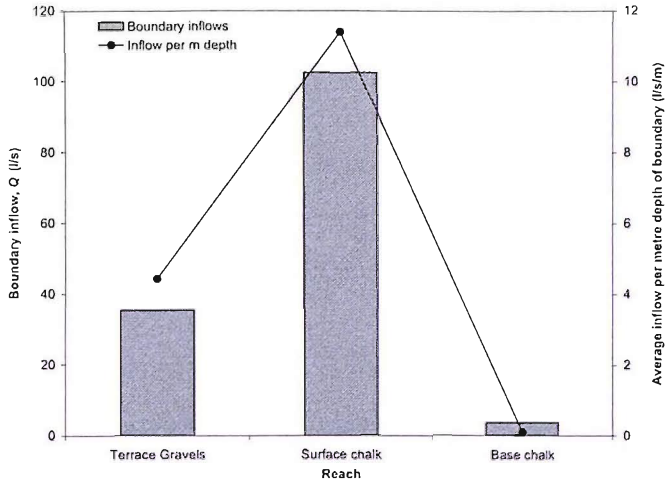

Figure 4.22: *The distribution of the Thames boundary inflow between the strata*

with no localised defects. Bell and Mitchell (1986) state that significant leakages are rare, probably because of the presence of a bentonite filter cake around the panel joints, but leakages may occur where there are differential deflections between wall panels, which are more prevalent near corners of an excavation. However, Greenwood (1994) gives greater consideration to leakages through diaphragm walls. It is suggested that panel joints are not of above-ground structural quality and that wall deformations during excavation will lead to openings at joints, hence some leakage should be expected. Knight, Smith and Sutton (1996) considered the influence of diaphragm wall permeability on the construction dewatering at the Sizewell B nuclear power station, where the specified design permeability was 1.5×10^{-8} m/s. A modelling study, using an electrical resistance network analogue model, was used to show that drawdown outside the diaphragm wall was particularly sensitive to increases in the wall permeability between 10^{-7} and 10^{-5} m/s.

Figure 4.23 shows the impact of changing the wall permeability (k_{wall}) on drawdown both inside and just outside of the excavation for each of the four dewatering cells, at selected piezometers. The results indicate that the wall permeability is less significant in the shallower cells, but the internal drawdown of cell SLC+SCC1 is particularly sensitive to the wall

permeability. In this area of the excavation the wall toes into the base chalk, whose low horizontal and vertical permeabilities restrict water ingress from around the toe, thereby giving added importance to leakage through the wall. The relative influence is high because of the low inflows into the excavation. Conversely, where flows around the toe are greater, the leakage through the diaphragm wall contributes a much smaller proportion of the total inflows.

The results suggest that within a more effective cut-off, the degree of anisotropy of the Chalk must be significantly reduced to achieve the same drawdowns in the cell SLC+SCC1. In light of this information, the model was re-calibrated for wall permeabilities of 10^{-6}, 10^{-8} and 10^{-9} m/s. For each calibration, only the k_z of the surface chalk and base chalk was changed to achieve the recorded drawdown in the cell SLC+SCC1. Table 4.8 shows that the internal drawdown could be matched in each of the cases. However, the only calibration that allowed a good match of the recorded drawdown at the external piezometer PE17-C (shown in Figure 3.13), installed to a depth of -31 m OD, was the original *MODEL 1* calibration where $k_{wall} = 10^{-7}$.

The effect of the diaphragm wall in the high permeability zone was shown to be negligible by removing it completely for the cell SRC2+SRC3 and removing the cross cut-off wall between cell SRC2+SRC3 and SCC3+SRC1. Figure 4.24 shows that a good match to the recorded steady state internal drawdown profile could still be achieved with this section of the wall absent, but within the high permeability zone having a permeability of 4000 m/day rather than 4800 m/day as in *MODEL 1*. This seems to imply that the presence of such a high permeability material made the construction of this section of the diaphragm wall of little value in terms of forming an effective groundwater cut-off. However, it must be noted that the high permeability zone was present below the toe of the relatively shallow diaphragm wall.

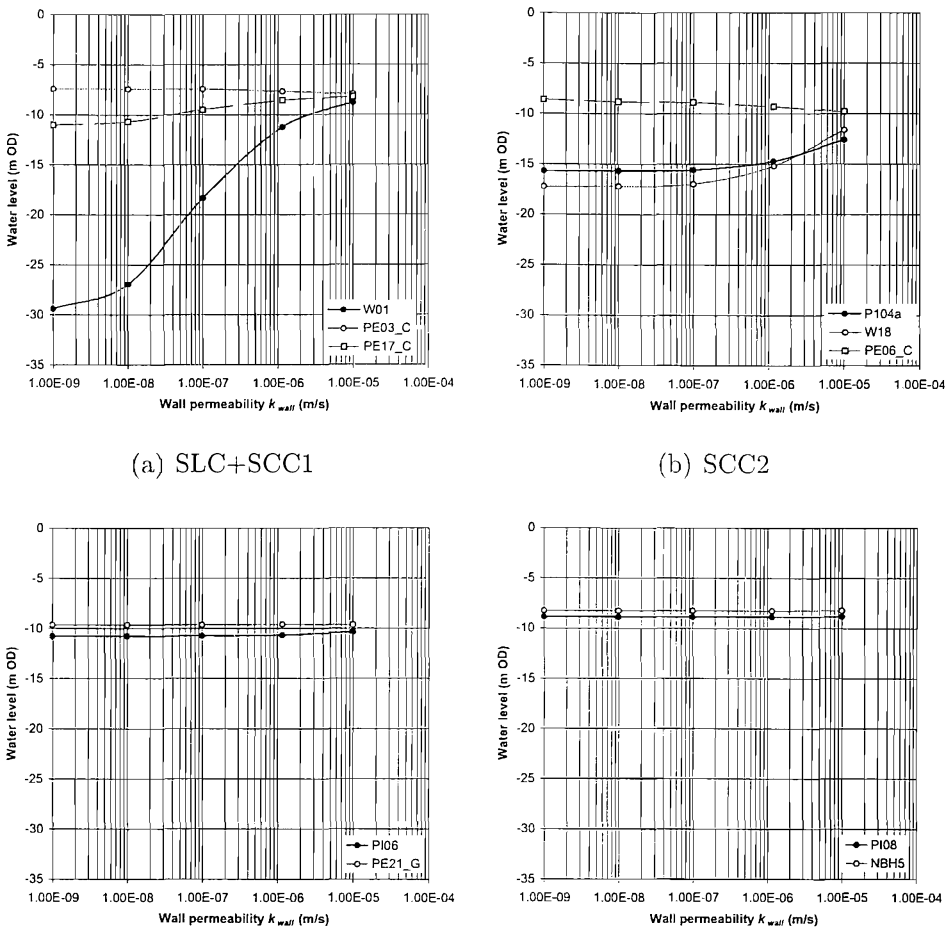

(a) SLC+SCC1

(b) SCC2

(c) SCC3+SRC1

(d) SRC2+SRC3

Figure 4.23: *The effect of changing diaphragm wall permeability (k_{wall}) on drawdowns at selected piezometers*

Table 4.8: *Degrees of anisotropy required to achieve the recorded drawdown inside and outside of cell SLC+SCC1 for different values of k_{wall}*

K_{wall}	Surface chalk			Base chalk			Residual error (m)	
	k_x	k_z	k_x/k_z	k_x	k_z	k_x/k_z	W01	PE17-C
10^{-9}	35	0.5	70	2	0.15	13.3	0.26	1.66
10^{-8}	35	0.5	70	2	0.12	16.7	-0.25	1.55
10^{-7}	35	0.1	350	2	0.02	100	-0.02	-0.33
10^{-7}	35	0.01	3500	2	0.005	400	-0.29	-1.94

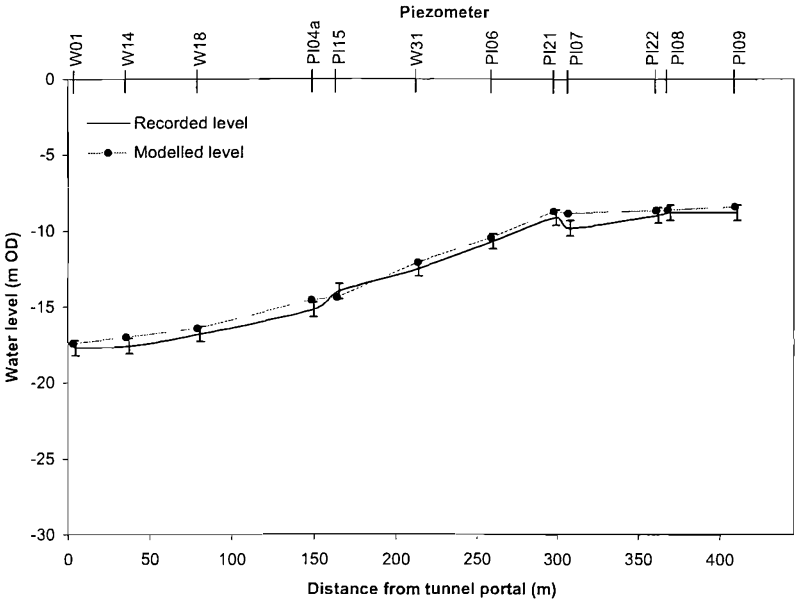

Figure 4.24: *The internal drawdown profile without diaphragm walls for cell SRC2+SRC3 and where the high permeability zone is k = 4000 m/day*

4.6.3 Grid resolution

The accuracy of the modelled water levels for the internal and external piezometers might be affected by the resolution of the model nodes around the excavation area. Grid design 1, which was used in all the previous model simulations, is specified in Table 4.9. Two additional grid designs were applied to *MODEL 1*, but the impact on the model calibration was found to be negligible, as shown in Figure 4.25.

4.7 Transient model

The understanding of the site hydrogeology was developed using steady state models. Further modelling was required to ensure the permeability parameters are still applicable when pumping at different rates. A transient model also allowed the boundary conditions to be examined for different flow regimes. *MODEL 1* was used as the basis for transient model, with same boundary conditions, hydraulic conductivities, initial heads and diaphragm wall arrangement being applied. The transient model represents

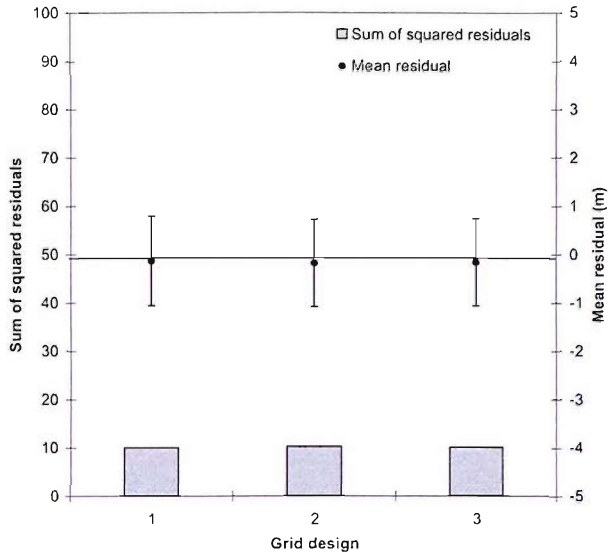

Figure 4.25: *The influence of grid spacing on the model calibration, using the designs specified in Table*

Table 4.9: *Grid designs tested during the modelling. Design 1 was used for all previous model simulations.*

	Grid design		
	1	2	3
Number of rows	114	141	163
Number of columns	83	95	103
Total number of nodes	113544	160740	206412
Max nodal spacing (m)	33.33	33.33	33.33
Min nodal spacing (m)	4	2.5	1.6

the period between 26th November 2001 and 8th May 2003.

4.7.1 Wells and revised grid design

Each well was represented by a drain in a 1 m by 1 m cell. In MODFLOW, drains are a type of head-dependent boundary condition which only remove water from the model. Drain cells were inserted into the model layers in which the well was screened and the drain head was set according to the recorded water levels inside the wells. Additional rows and columns had to be inserted to the grid to allow the insertion of the 1 m by 1 m drain cells. The flow Q into the well was automatically calculated by the model as follows:

$$Q = C(h_m - h_w) \tag{4.19}$$

where Q is the flowrate (m^3/day), C is the specified drain conductance (m^2/day), h_d is the specified head in the drain cell (m OD) and h_m is the head computed by the model (m OD). The conductance is a function of the hydraulic connection between the aquifer and well screen through the pea gravel filter. For drains in the high permeability zone, $C = 512$ was found to give a good match of the recorded well yield. For all the wells outside the high permeability zone $C = 51200$ m^2/day. The well heads were set to match the measured internal drawdowns. Flows from individual wells and the system were therefore an output of the model, which could be compared to the recorded flow.

4.7.2 Stress periods

The dewatering period was divided into 18 stress periods, each representing a time interval during which the well heads were constant. These periods are broadly the same as those given in Figure 3.14 and described in Table 3.4. Each stress period was divided into a number of time steps with the length of each subsequent time step increasing as determined by the multiplier (Table 4.10). Water levels and flows were calculated for each time step of the model simulation.

Table 4.10: *Stress periods details of the transient model*

Stress period	Start Date	Period length (days)	Number of time steps	Time step multiplier
1	01-Jan-02	36	30	1.4
2	11-Jan-02	10	20	1.4
3	18-Feb-02	38	30	1.4
4	08-Mar-02	18	20	1.4
5	19-Mar-02	11	20	1.4
6	24-Mar-02	5	20	1.4
7	01-Apr-02	8	20	1.4
8	01-May-02	30	20	1.4
9	21-May-02	20	20	1.4
10	20-Jul-02	60	20	1.4
11	14-Aug-02	25	20	1.4
12	12-Sep-02	29	20	1.4
13	18-Sep-02	35	20	1.4
14	08-Oct-02	20	20	1.4
15	18-Oct-02	10	20	1.4
16	13-Feb-03	118	30	1.4
17	15-Mar-03	30	20	1.4
18	14-Apr-03	24	20	1.4
Total		533		

4.7.3 Storage

In a steady state model simulation there is no requirement to specify storage parameters for the aquifer. For a time-dependent model the storage properties of the aquifer will influence the period of time taken for groundwater water levels to adjust to a change in the flow regime. The storage of an aquifer is described by three properties:

- Porosity θ is the maximum volume of groundwater that can be stored in a saturated material, expressed as the proportion of a volume of soil or rock which is represented by its interstices or voids. The Chalk matrix has a moderate to high porosity of 0.2 to 0.4.

- Specific yield S_y is the volume of water that can freely drain from a saturated rock or soil, expressed as a proportion of the total volume. In the Chalk, gravity drainage from the pores is inhibited by the small pore throats (Price, Bird and Foster, 1976), therefore the specific yield is typically between 2 to 3% of the porosity (Reeves, 1979).

- The storage coefficient S is the volume of water released or taken into storage per unit surface area of aquifer per unit change in head. As the piezometric level falls water is released as a consequence of the slight compression of the granular structure of the aquifer and a very small expansion of the water. For unconfined conditions the specific yield is the same as the storage coefficient.

It is difficult to investigate the storage properties of the aquifer as the model cannot replicate exactly the site pumping programme and data. In the model, wells are switched on or off simultaneously in groups and their performance is fixed for each stress period, whereas in reality pumps were started individually at different times. Furthermore, ongoing maintenance of the system meant that the system was only operating at a true steady state for short periods. However, the transient model does allow the overall trends to be examined. For the model, the storage coefficient and specific yield values listed in Table 4.11 were found to be most appropriate. These

Table 4.11: *Storage parameters used for the transient model*

Zone	Storage coefficient	Specific yield
Alluvium	0.0045	0.1
Terrace Gravels	0.0045	0.25
Surface chalk	0.0045	0.01
Transition zone	0.0045	0.01
Outcrop chalk	0.01	0.01
High k zone	0.008	0.1
Base Chalk	0.001	0.005

values are consistent with those suggested by Reeves (1979) and MacDonald and Allen (2001).

4.7.4 Results

The approximate dewatering system flow record was successfully replicated by the transient model (Figure 4.26). For each stress period, the dewatering flows reached steady state within 2 or 3 hours of the wells being switched on, which is consistent with low specific yield. Flows from the cells SLC+SCC1 and SCC2 were relatively steady throughout the dewatering period compared with cell SRC2+SRC3 where more variable flows took place because of the modification of the well array and the upgrading of pump sizes.

The model inflows strongly reflected the dewatering system pumping rate with any difference being attributed to a small change in the aquifer storage (Figure 4.27. The record of the yield from storage shows positive spikes immediately after wells were switched on and water levels were drawn down. As the drawdown propagates through the aquifer the yield from storage continues at lower rates for each stress period. Negative spikes indicate water going into storage as water levels recover following a reduction in pumping rate. If the storage coefficient were to be reduced, the drawdown would propagate through the aquifer more quickly leading to an increase in the size of the initial spikes followed by decreased lower levels.

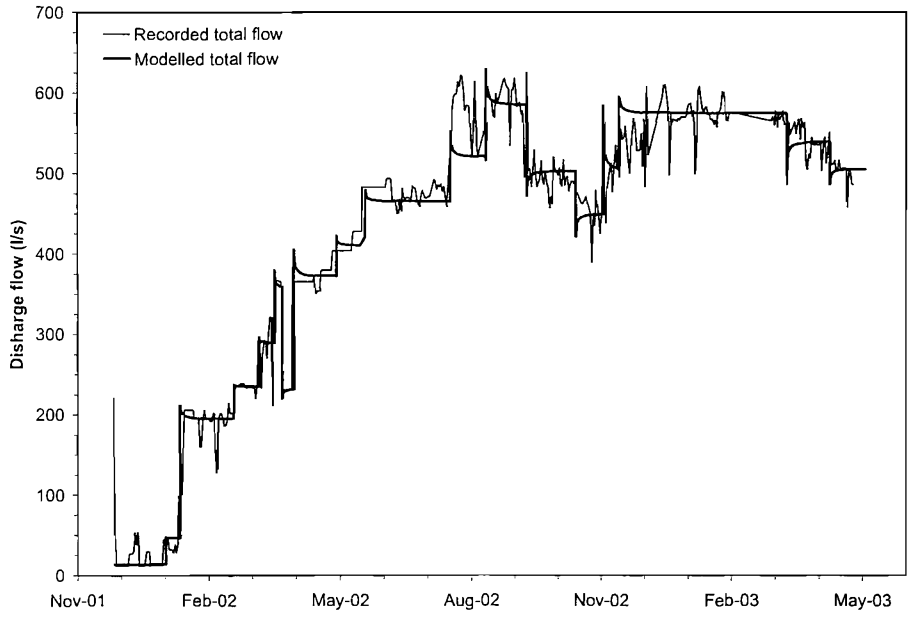

(a) Total flows

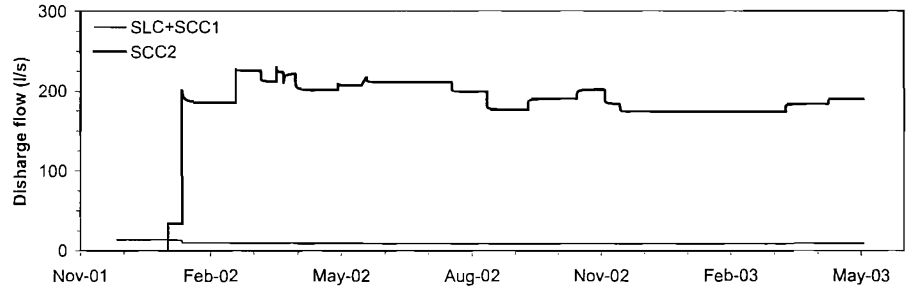

(b) Cells SLC+SCC1 and SCC2

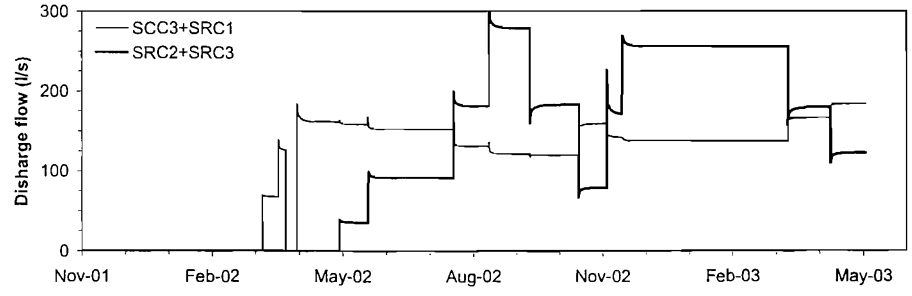

(c) Cells SCC3+SRC1 and SRC2+SRC3

Figure 4.26: *The modelled flows from the dewatering system*

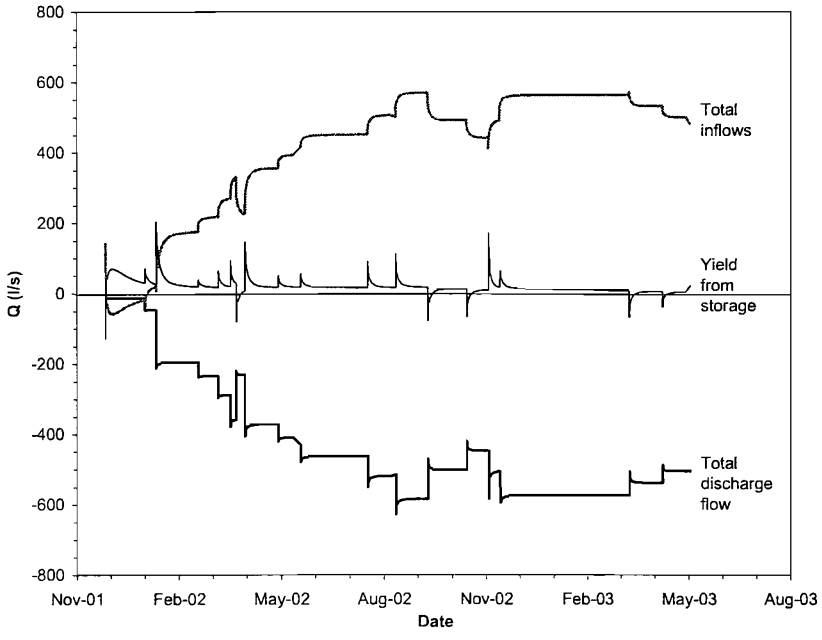

Figure 4.27: *The mass balance of groundwater flows*

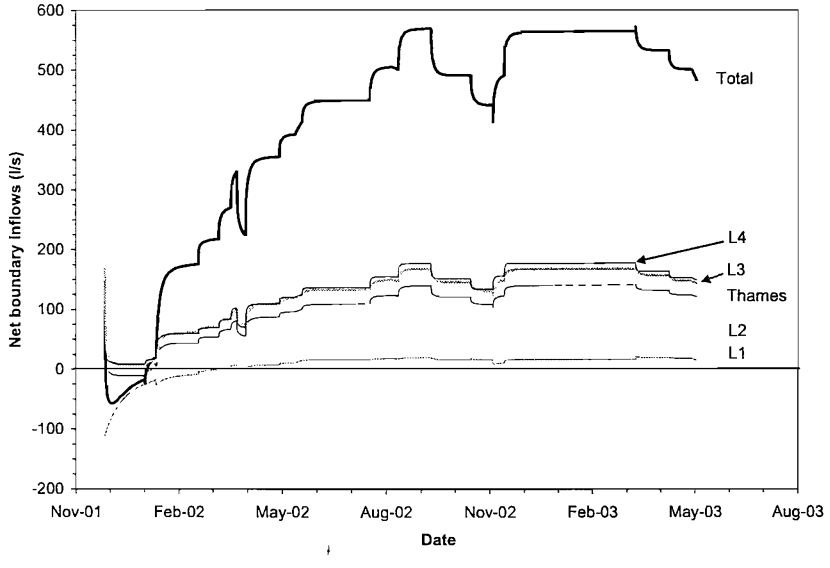

Figure 4.28: *The inflows from the model boundaries*

The contribution of each boundary reach to the total model inflow is shown in Figure 4.28. The initial water levels specified in the model cause some removal of water from the model through the boundaries during the early stages of dewatering. These outflows occur through the Thames boundary and the L1 boundary and reflect the natural groundwater regime. By February 2002, the increased pumping rate meant that the hydraulic gradient for all parts of the model only allowed flow into model. No recharge by infiltration was applied to the model as reliable rainfall or infiltration data was not available. It has been demonstrated in §4.4.6 that infiltration would have been negligible compared to the lateral boundary flows, but some seasonally variable infiltration would have taken place in the unconfined areas.

Examples of remote piezometer responses are shown in Figure 4.29 for the gravel and Figure 4.30 for the chalk. The model is able to replicate the general drawdown trend quite well. Achieving an improved fit between the recorded and modelled data is not possible without using a greater number of stress periods and adding to the model complexity, to an extent unwarranted by the detail of the data available.

The recorded and modelled drawdown profiles inside the excavation are compared for three dates during the dewatering operation in Figure 4.31. The modelled data reflects the actual drawdowns reasonably well, although residual errors up to 2 m were common as shown in Figure 4.32(a). Similar levels of error were calculated for the external and internal piezometers (Figure 4.32). The statistics in Table 4.12 indicate that the model does not perform as well as the steady state *MODEL 1*. For example, the mean of absolute residual errors (MS) is 0.65 m for the transient model compared with 0.32 m for *MODEL 1* for all piezometers. This probably reflects the actual variation in the dewatering system flows within each stress period, which cannot be modelled. Nevertheless, the transient model does confirm the understanding of both the spatial distribution of permeability and the model boundaries.

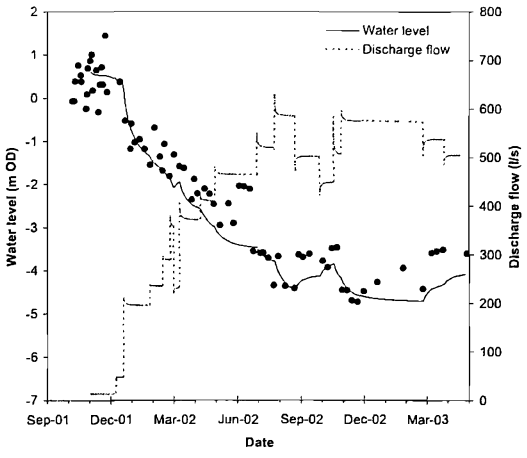

(a) G11

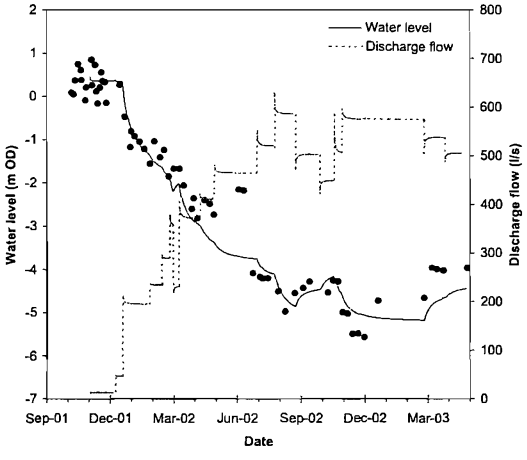

(b) G15

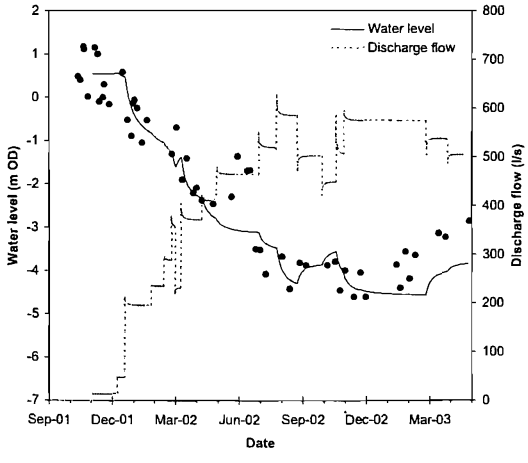

(c) SA5981

Figure 4.29: *Drawdowns at selected remote standpipe piezometers in the gravel*

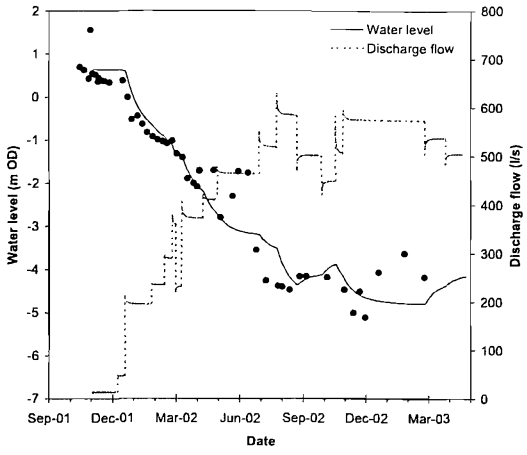

(a) NBH1

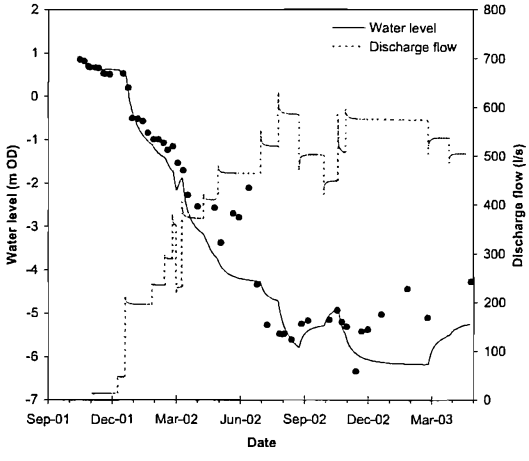

(b) NBH3

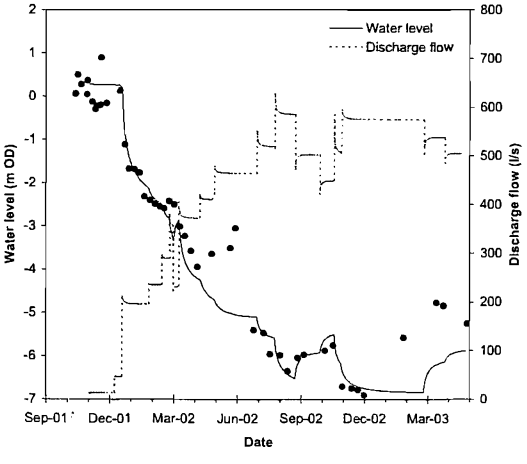

(c) SA5943

Figure 4.30: *Drawdowns at selected remote standpipe piezometers in the Chalk*

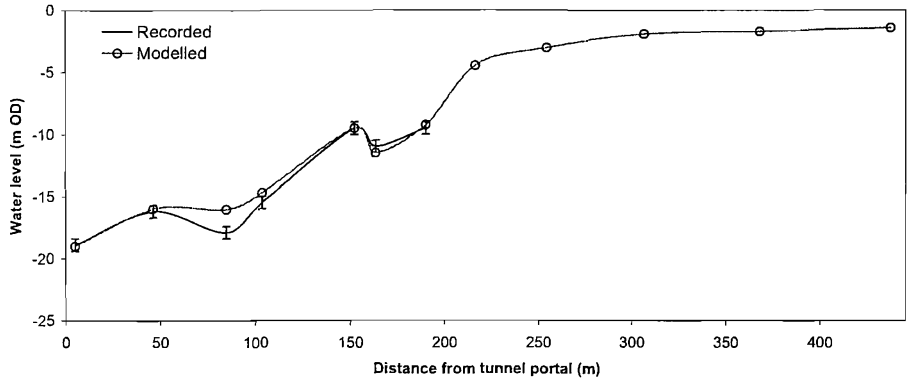

(a) 25 January 2001

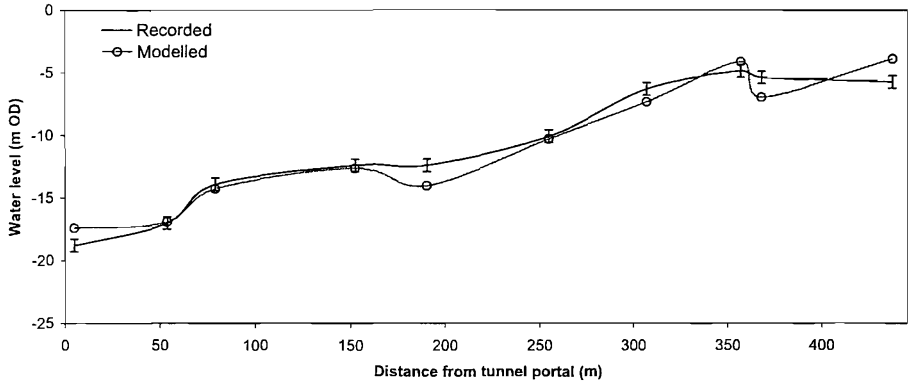

(b) 6 June 2002

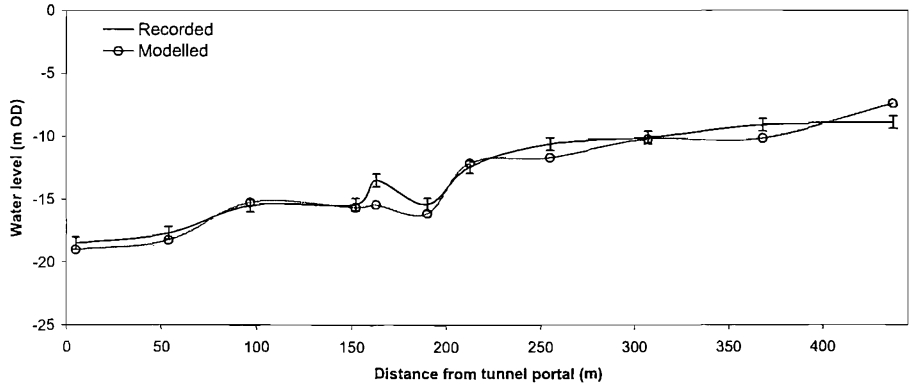

(c) 2 October 2002

Figure 4.31: *Internal drawdown profiles*

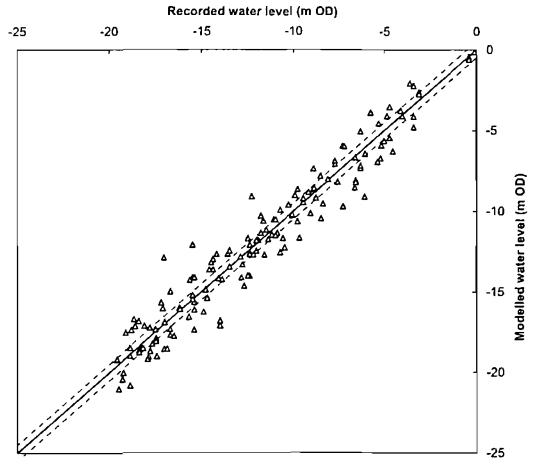

(a) Internal piezometers

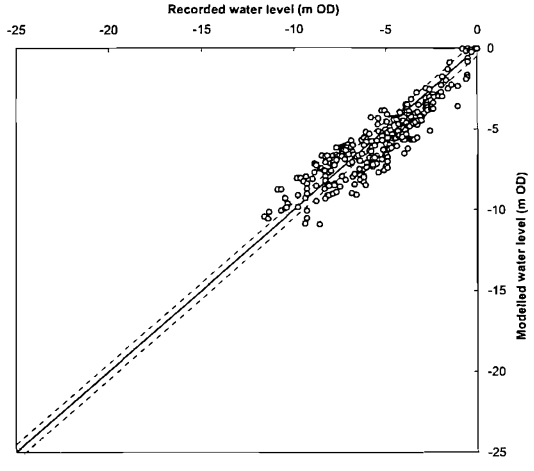

(b) External piezometers

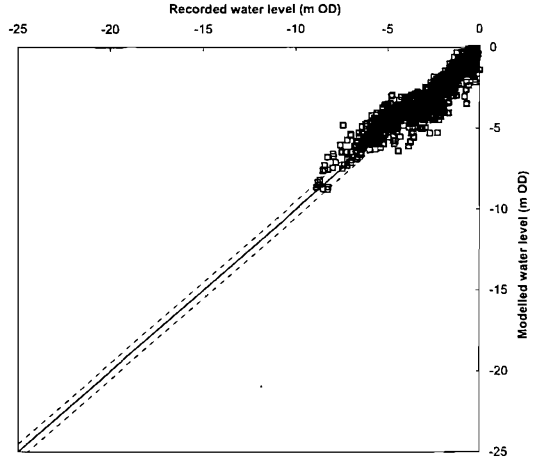

(c) Remote piezometers

Figure 4.32: *Drawdowns at selected remote standpipe piezometers in the chalk*

Table 4.12: *Summary table of statistics for the transient model simulation (n is the number os piezometer readings, M is the mean of residual errors, MA is the mean of absolute residual errors, and R is the correlation coefficient)*

	Internal	External	Remote	Overall
n	150	325	1398	1873
M (m)	0.10	0.34	0.20	0.22
MA (m)	0.96	0.92	0.56	0.65
Linear relationship	$y = 0.989x$	$y = 1.012x$	$y = 1.012x$	$y = 1.001x$
R	+0.97	+0.93	+0.95	+0.98

4.8 Conclusions and implications for practice

The sensitivity analysis of the steady state models suggests that for a mildly complex scheme, a numerical modelling approach is unlikely to provide a unique solution giving the permeability profile of each stratum zone identified. Nevertheless, it provides a useful framework for assembling, analysing and interpreting complex data sets. In the case of the CTRL Thames Tunnel southern approach excavation, the performance of the dewatering system cannot satisfactorily explained without the inclusion of large scale inhomogeneities within a 445 m long excavation including:

- a zone of anisotropic chalk with a ratio k_x/k_z of 350 to 750;
- a zone of isotropic high permeability chalk, where $k_x = k_z = 2.7 \times 10^{-2}$ to 6.8×10^{-2} m/s (2300 to 5850 m/day);
- a transition zone between the anisotropic chalk and high permeability chalk.

4.8.1 Implications for dewatering system design

The chalk features listed above make the site hydrogeology at the case study site far more complex than suggested by the original interpretation of

data from a site investigation. Some evidence of a high permeability zone was available in the form of chalk core samples, but the interpretation of the core data made in this dissertation (see §3.7.2) would have been difficult without the benefit of hindsight or supporting information.

Inhomogeneities might be identified by more thorough site investigation, perhaps including the use of more widespread pumping tests. Pumping tests were carried out in wells significantly distant from the excavation and the high permeability zone, hence the resulting permeability data were clearly not representative of the whole site. In hindsight, individual pumping tests using 3 wells screened in the Chalk and spaced at 200 m centers along the approach excavation would probably have been sufficient to determine the levels of permeability variation.

In contrast to high permeability features, anisotropy can be of great benefit in achievement target drawdowns, as demonstrated in this chapter. Greenwood (1994) provides an example, originally described by Troughton (1987), of a construction dewatering system (at Bank Misr, Cairo) where anisotropy caused by clay layers in sands aided the reduction of internal piezometric levels and minimized external drawdowns. An anisotropy ratio of 100 is shown to be highly influential, confirming the previous study by Powrie et al. (1989). The influence of anisotropy is hard to establish by means of pumping tests, primarily because it becomes more apparent once a barrier to horizontal flow is in place. It may be possible to determine vertical permeabilities from pumping tests by analysing the response of observation wells that are screened at different levels, using a numerical model or analytical approach; a similar approach was used to determine the effect of silt lenses on the vertical permeability of the Norwich Crag sands (Knight et al., 1996). Another solution would be to carry out a pumping test, install a horizontal cut-off perhaps using sheet piles, and then repeat the test. The test could then be replicated in a numerical model to establish an approximate range of anisotropy ratios. Ideally, the depths of the wells and the cut-off would be the same as initially planned for the dewatering system. Such an investigation may also be of benefit for refining the design of cut-off walls, but will be costly and therefore only appropriate for large

scale projects where the potential cost savings may be greater.

While pumping tests can be costly, wells and piezometers used for pumping tests can often be incorporated in to the dewatering system design. The cost of increased site investigation must be weighed against the benefits of having a better optimized design. If there is sufficient flexibility in the construction schedule, modern methods of data collection and review make it is possible to take an observational method approach, which was implemented at the CTRL Thames Tunnel with success and was discussed in Chapter 2.

The level of heterogeneity found in the Chalk means that the equivalent well analysis and cumulative drawdown methods of designing a dewatering system can be inappropriate for this type of ground. A numerical modelling approach is preferable, because distinct zones of permeability can be incorporated and their effect investigated. The success of the design is strongly dependent on the conceptual understanding of the geology and the accuracy of the input parameters. The risk due to uncertainties should be investigated through a rigorous sensitivity analysis.

The transient modelling carried out demonstrates that once a good understanding of the ground conditions and boundary conditions has been achieved, the performance of the dewatering system can be predicted for the period of construction with a fair level of confidence. In reality, ongoing disruptions to the dewatering system for maintenance purposes make predicting remote drawdowns difficult; probably only drawdown trends can be estimated with an accuracy in the order of 1 metre. Models allow monitoring data to be compared to the model outputs at regular stages during the construction; they can be an integral part of the design and review process of the observational method, as shown in Figure 2.12.

4.8.2 Implications for geotechnical design

The performance of a dewatering system can influence other aspects of geotechnical design. It has been demonstrated that anisotropy may help to achieve the required drawdowns within an excavation while minimising the

drawdowns behind a retaining wall. Conversely, unforeseen high permeability features may reduce the head difference between each side a wall. Determining pore water pressure distributions on both sides of a wall is an important task during the design of a dewatering system with the information being used in the final design of the walls and the temporary prop supports. The modelling indicated that the effectiveness of cut-off walls for groundwater control is strongly dependent on the horizontal and vertical permeabilities of the aquifer at the toe; optimization of the cut-off wall design might be improved by fuller investigation of permeability distribution.

Unforeseen large scale inhomogeneities can increase the risk of settlement in areas previously thought to be not at risk, by increasing the distance of influence. Alternatively, anisotropy can aid the mitigation of settlements if external drawdowns are smaller than expected. Preene (2000) recommends carrying out a settlement risk assessment before groundwater lowering, based on uniform aquifer properties and boundary conditions. The assessment of settlements could be less uncertain if good predictions of drawdown responses can be made, which would require detailed aquifer data to be available. Inhomogeneities will also have an influence of the performance on recharge systems; with better site investigation it may be possible to optimise the layout of recharge wells.

4.8.3 Implications for the prediction of environmental impacts

Many larger construction projects require an environmental impact assessment to be carried out prior to any construction activity. This might include the impacts of construction dewatering on the temporary disturbance of the natural groundwater flow regime and levels and the migration of groundwater contaminants. The assessment will be based on the expected performance of the dewatering system, but should also take into account the influence of unexpected ground conditions. The effect of high permeability features and anisotropy add complexity by dramatically

altering the drawdown response and distance of influence. In the Chalk, the low effective porosity enables the transport of contaminants to be very rapid and a deterioration of the groundwater quality can not easily be reversed. The observational method allows a dewatering system to be modified promptly in response to unexpected ground conditions, but the impact of upgrading the system on the remote groundwater environment should also not be forgotten.

Very little information has been published on the environmental impacts of construction dewatering. The next part of this dissertation will consider the changes in groundwater quality that occurred during the dewatering of the CTRL Thames Tunnel southern approach excavation.

Chapter 5

The contaminant transport problem

5.1 Background

5.1.1 Potential impacts

Any change to the natural groundwater regime has the potential to adversely affect groundwater resources. A description of the full range of potential groundwater impacts caused by civil engineering works is provided by Preene and Brassington (2003). The impacts associated with either temporary or permanent abstraction include:

- ground settlement, as discussed in §2.1;
- depletion of groundwater-dependent features such as ponds and wetlands;
- derogation of individual groundwater sources such as boreholes and springs;
- the effects on the water levels and water quality of an aquifer as a whole.

Figure 5.1 shows some of the potential impacts of construction dewatering. Impacts upon regional groundwater resources are only likely to

be observed where large long-term temporary dewatering systems are being operated Preene and Brassington (2003). Such impacts include the degradation of coastal aquifers by saline intrusion and the lateral and vertical migration of leachate or contaminants from areas of historic or current industrial activity or landfilling activity. These are two issues that will be discussed in more detail during the course of this dissertation.

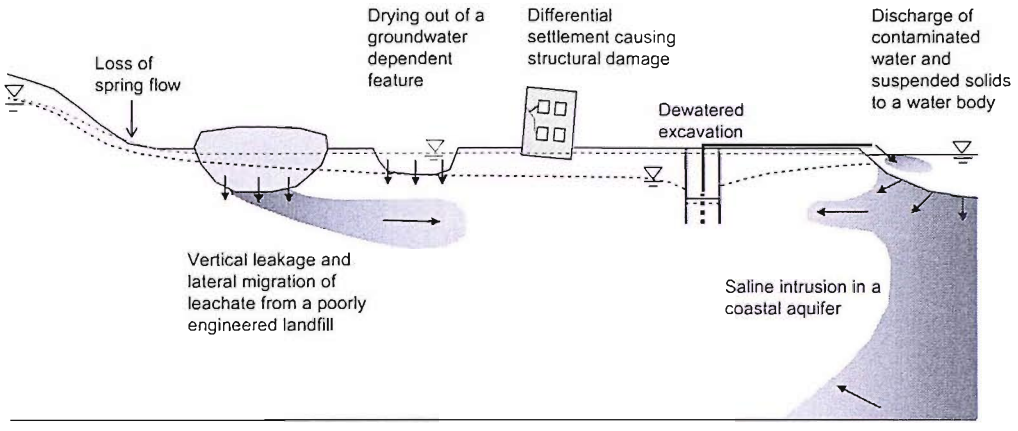

Figure 5.1: *Some potential impacts of construction dewatering*

5.1.2 Groundwater protection

Traditionally hydrogeologists are charged with striking a balance between the exploitation of groundwater for water supply and the protection of future water resources. Only 2.5% of all water on the earth is freshwater and 30% of this is distributed as groundwater (Shiklomanov, 1997). The use of groundwater is increasing due to a rise in world population and economic growth; the loss of surface water due to contamination; the availability of huge quantities; and the high quality of groundwater reserves relative to surface water (Environment-Agency, 1998). In England and Wales groundwater provides 35% of the present demand for public water supply and in some areas it is the only available future resource (Environment-Agency, 1998). Usually little treatment of clean groundwater is required before use for potable supply, because of the high quality. In

addition, groundwater is an important source for industry and agriculture and provides baseflow for many surface water systems. The risk of pollution is increasing due to the disposal of waste materials and from the widespread use of potentially harmful chemicals in industry and agriculture. Once an aquifer becomes contaminated it can be difficult, and in some cases impossible, to successfully clean up.

The Environment Agency (EA) is the statutory body responsible for managing water resources in England and Wales, under the Water Resources Act 1991 and the Environment Act 1995. The EA issued the revised Policy and Practice for the Protection of Groundwater in 1998. The duties of the EA with respect to groundwater quality are to:

- achieve Statutory Quality Objectives;
- control discharges to groundwater through the discharge consent process;
- prevent pollution through regulations set by the Secretary of State;
- enforce against pollution events; and
- take remedial action when pollution has occurred.

The EA is charged with powers to control groundwater abstraction through the abstraction licensing process. Under the Water Resources Act 1991 dewatering has been generally exempt from legal restrictions. Preene and Brassington (2001) explain the recently proposed changes which will require contractors to apply for either an abstraction consent for projects greater than a one month duration, or a abstraction permit for short-term schemes. In addition, a discharge licence is required to allow the discharge of abstracted water to a surface water body.

The risk of activities to groundwater sources is assessed by the EA using source protection zones (SPZ); the source refers to a well, borehole or spring used for public drinking water supply or other potable supply (Environment-Agency, 1998), rather than the source of contamination.

SPZs are defined using groundwater models to delineate the capture zones (area of influence) of abstraction points. The SPZs are categorised as:

- Zone 1 (Inner Source Protection) - this area is defined by a 50 day travel time to the source, which is the standard time for the decay of biological contaminants.
- Zone 2 (Outer Source Protection) - this area is defined by a 400 day travel time to the source, which is time required to provide delay and attenuation of slowly degrading pollutants.
- Zone 3 (Source Catchment) - this area covers the total catchment area for the source. It is defined as the area needed to support the abstraction from long term annual groundwater recharge (effective rainfall). If the aquifer is confined the zone may extend to a considerable distance.

The Chalk is the most important major aquifer within the UK supplying 60% of the groundwater that is used in England and Wales (UK-Groundwater-Forum, 1998). It is also more vulnerable to human activity because of its low effective porosity; both the flow velocity and the area drawn on when pumping on a borehole in the Chalk are much greater than an aquifer with a high storage capacity such as the Triassic sandstones. Therefore, the risk to groundwater resources from large-scale dewatering projects in the Chalk is particularly high, especially in urban areas where there may be numerous potential pollution sources.

5.1.3 Transport processes

The transport processes for a contaminant moving through a porous medium can be explained by considering the principle of conservation of mass to an elemental volume within the flow field, firstly for a conservative (non-reactive) solute:

$$\text{Net rate of accumulation of mass} = \text{Mass flowrate out} - \text{Mass flowrate in} \tag{5.1}$$

In solute transport the movement of solute particles with the average seepage velocity q, as governed by Darcy's Law, is termed advection. For transport along the y axis in Figure 4.1, the net accumulation of solute mass is given by:

$$-\frac{\partial}{\partial y}(q_y C)\Delta x \Delta y \Delta z \tag{5.2}$$

where C is the concentration of a contaminant in units of mass of solute per volume of water. This expression can also be written for flow in the x and z directions. Therefore the net accumulation of solute mass from the elemental volume is given by:

$$-\Big[\frac{\partial}{\partial x}(q_x C) + \frac{\partial}{\partial y}(q_y C) + \frac{\partial}{\partial z}(q_z C)\Big]\Delta x \Delta y \Delta z \tag{5.3}$$

If a sink or source is applied to the elemental volume then the equation becomes:

$$-\Big[\frac{\partial}{\partial x}(q_x C) + \frac{\partial}{\partial y}(q_y C) + \frac{\partial}{\partial z}(q_z C)\Big]\Delta x \Delta y \Delta z + Q_s C_s \tag{5.4}$$

where Q_s is the volumetric rate at which water is added and removed and C_s is the concentration of the water added or removed. The net rate of accumulation of solute mass $\partial M/\partial t$ within the element is given by:

$$\frac{\partial M}{\partial t} = \frac{\partial(\theta C)}{\partial t}(\Delta x \Delta y \Delta z) \tag{5.5}$$

where θ is the effective porosity. Equations 5.4 and 5.5 can be combined to give:

$$-\frac{\partial}{\partial x}(q_x C) - \frac{\partial}{\partial y}(q_y C) - \frac{\partial}{\partial z}(q_z C) + q_s C_s = \frac{\partial(\theta C)}{\partial t} \tag{5.6}$$

Contaminants will also move when groundwater is static. Where there is a concentration gradient the contaminant spreads from its source by diffusion, according to Fick's Law of diffusion in a free solution:

$$F_D = -D^* \frac{\partial C}{\partial y} \tag{5.7}$$

F_D (M T^{-1} L-2) is the diffusive mass flux across a cross-sectional area ($\Delta x \Delta z$) over a distance (Δy) along the y axis and D^* is the effective molecular diffusion coefficient (L^2 T^{-1}). In moving groundwater mechanical dispersion of a pollutant will occur due to microscopic local variations in the groundwater flow velocity. The combined effect of mechanical dispersion and molecular diffusion is termed the hydrodynamic dispersion. For one-dimensional flow along the y axis, the hydrodynamic dispersion D in the direction of the flow is given by:

$$D_y = \alpha_y |v_y| + D^* \tag{5.8}$$

where α_y is the longitudinal dispersion and $|v_y|$ is the magnitude of the average true seepage velocity in the longitudinal direction ($v_y = q_y/[\theta \Delta x \Delta z]$). The contribution to the hydrodynamic dispersion made by molecular diffusion will be high at low seepage velocities, and low at high seepage velocities. The relative contribution is governed by the Peclet number Pe:

$$Pe = \frac{vd}{D^*} \tag{5.9}$$

where d is the average particle diameter. The diffusion process dominates for $Pe \leq 0.4$.

The expression for the difference between mass inflow and mass outflow due to longitudinal dispersion for flow along the y axis is:

$$\frac{\partial}{\partial y}\left(\theta D_{yy} \frac{\partial C}{\partial y}\right) \Delta x \Delta y \Delta z \tag{5.10}$$

Dispersion will also take place in the horizontal transverse and vertical transverse directions to give:

$$\frac{\partial}{\partial y}\left(\theta D_{yx} \frac{\partial C}{\partial x} + \theta D_{yy} \frac{\partial C}{\partial y} + \theta D_{yz} \frac{\partial C}{\partial z}\right) \Delta x \Delta y \Delta z \tag{5.11}$$

The advection-dispersion equation for unidirectional flow along the y axis, where no sources or sinks are present, is found by combining Equations 5.5 and 5.11 and dividing both sides by $\Delta x \Delta y \Delta z$:

$$\frac{\partial(\theta C)}{\partial t} = -\frac{\partial}{\partial y}(qC) + \frac{\partial}{\partial y}\left(\theta D_{yx}\frac{\partial C}{\partial x} + \theta D_{yy}\frac{\partial C}{\partial y} + \theta D_{yz}\frac{\partial C}{\partial z}\right) \tag{5.12}$$

If porosity is assumed to be constant, both spatially and with time, Equation 5.12 can be simplified to:

$$\frac{\partial C}{\partial t} = -\frac{\partial}{\partial y}(vC) + \frac{\partial}{\partial y}\left(D_{yx}\frac{\partial C}{\partial x} + D_{yy}\frac{\partial C}{\partial y} + D_{yz}\frac{\partial C}{\partial z}\right) \tag{5.13}$$

The conservation of mass can also be affected by interactions between the porous media and the contaminant. Contaminants can be adsorbed onto the soil causing a reduction in the rate of the contaminant transport. Where adsorption occurs the advection-dispersion equation is modified by the retardation factor R:

$$\frac{\partial C}{\partial t} = -\frac{v}{R}\frac{\partial C}{\partial y} + \frac{D_{yx}}{R}\frac{\partial^2 C}{\partial x^2} + \frac{D_{yy}}{R}\frac{\partial^2 C}{\partial y^2} + \frac{D_{yz}}{R}\frac{\partial^2 C}{\partial z^2} \tag{5.14}$$

The retardation factor is determined by:

$$R = 1 + \frac{\rho_b}{\theta}K_d \tag{5.15}$$

where ρ_b is bulk density of the soil (kg/m^3) and K_d is the distribution coefficient for a linear isotherm (the mass of solute on the solid phase per unit mass of solid phase divided by the concentration of solute in the solution in m^3/kg). In a field situation, the retardation factor can be interpreted as the observed distance travelled by the front of a non-sorbing solute plume to that of a sorbing solute plume. Adsorbed contaminants will be transferred back into solution as fresh groundwater flows through a contaminated soil, allowing the soil to be cleaned *in situ*. This process facilities the remediation of soils using the soil washing technique.

5.2 The case study site

Dewatering for the CTRL Thames Tunnel southern approach excavation was a concern, because there were several possible sources of groundwater contamination in close proximity. A significant part of the Swanscombe

Peninsula was designated as a Source Protection Zone 3 (Environment-Agency, 2003), Figure 5.2. The closest point of abstraction is approximately 1.5 km to the south-east of the site. Furthermore, when reviewing future water resources in the Southern region, the EA describe the groundwater around Swanscombe as an important option open for investigation' (Environment-Agency, 2003). Therefore, it was particularly important to maintain the quality of this water reserve. Consideration will now be given to the potential sources of groundwater contamination in and around the case study site.

5.2.1 Saline intrusion

The proximity of the southern approach excavation to the Thames was a cause for concern, as the Thames represented a source of brackish or saline water. For a coastal aquifer it is often expected that there is a well defined interface between the saline groundwater and fresh groundwater in accordance with the Ghijben-Herzberg relationship (quoted in Todd (1980)). Figure 5.3 shows the saline wedge for an ideal coastal aquifer under hydrostatic conditions. The Ghijben-Herzberg relationship may be written as:

$$h_s = \left(\frac{\rho_f}{\rho_s - \rho_f}\right) h_f = \alpha h_f \tag{5.16}$$

where h_s is the depth of the freshwater below sea level, ρ_f is the density of freshwater, ρ_s is the density of seawater and h_f is the height of the water table above sea level. The saline-freshwater interface is encountered at a depth below sea level equivalent to α times the height of the water table above sea level, reflecting the hydrostatic equilibrium between the lighter fresh groundwater and heavier seawater. For this pressure balance relationship, a decrease in h_f due to dewatering would see a decrease in depth to saline-freshwater interface (h_s). This would lead to the interface moving closer to the surface, and the interface would migrate inland. Denser saline water typically forms a deep wedge that can extend inland, in some cases up to several kilometres (Bear, 1972). In stratified aquifers there

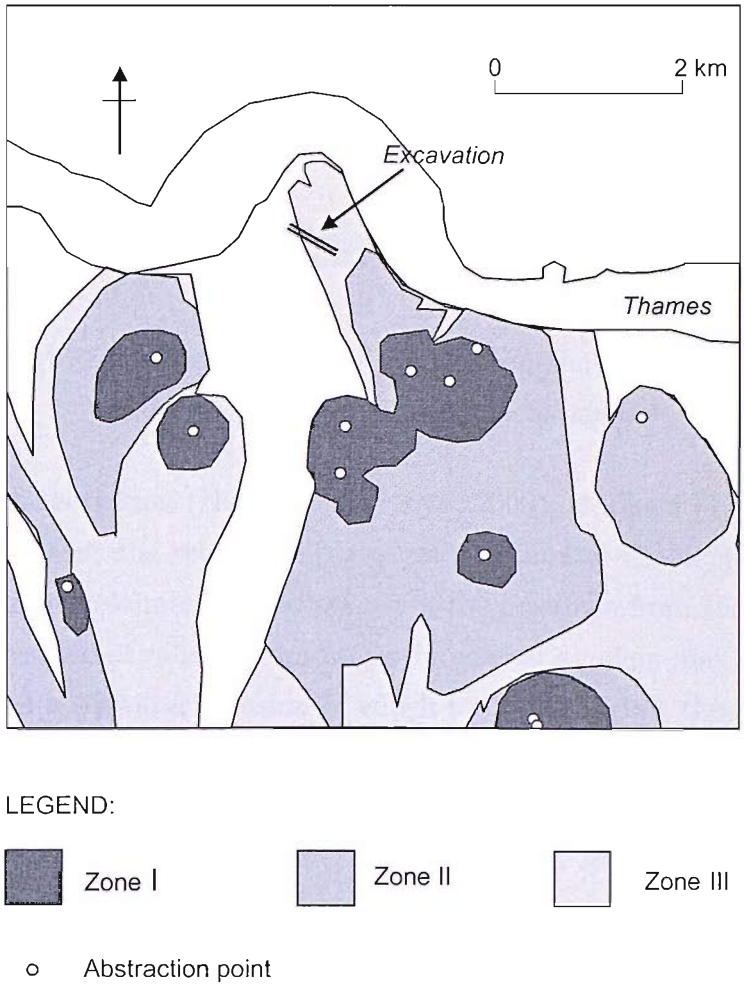

Figure 5.2: *Map of the source protection zones close to the site, as defined by the Environment Agency (2003)*

may be more than one saline wedge.

In reality the interface is not as sharply defined as suggested by Ghijben-Herzberg relationship. The interface will be continually disturbed by both tidal fluctuations and seasonal variations in recharge and discharge, causing significant fluctuations in its position. These fluctuations and the diffusion of salt water will lead to a transitional brackish zone (Stringfield and Legrand, 1971). The sharp interface predicted by the Ghijben-Herzberg equation may be interpreted as the centre of the transition zone, i.e. 50%

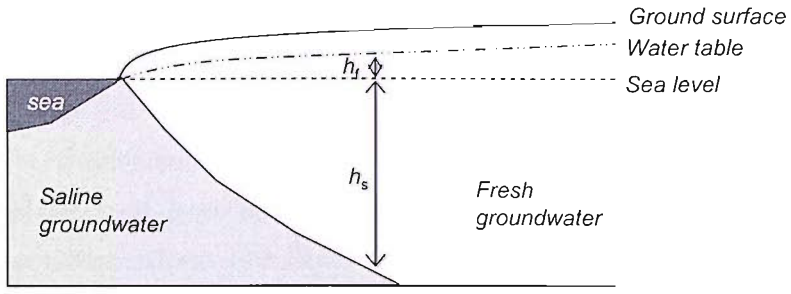

Figure 5.3: *A schematic diagram of the Ghijben-Herzberg hydrostatic relationship for a homogeneous coastal aquifer*

sea water concentration (Herbert and Lloyd, 2000). Hubbert (1940) demonstrated that the relationship also underestimates the depth to the interface and overestimates the distance of the interface from the shoreline.

The presence of saline groundwater in coastal aquifers may represent the residue of a seawater invasion of which took place when the land level was relatively lower. Problems arise when groundwater reserves are heavily exploited by individual coastal wells, which can cause upconing (the rising of deep waters) of connate waters (Bear and Dagan, 1968). More serious is the lowering of the fresh-water piezometric surface that may induce a progressive invasion of saline waters, leading to long-term contamination of the aquifer properties. Studies of saline intrusion usually show significant increases in the aquifer salinity over decades. For example, in the predominantly sandstone coastal aquifer of Israel an increase in chloride concentration of 30 mg/l per year was observed at locations less than 1500 m from the shore between 1980 and 1990 due to exploitation for water supply (Melloul and Goldenberg, 1998). Despite the great concern about saline intrusion there appears to be little published information relating abstraction rates and salinity increases except over very large regional scales. At the case study site, there was a relatively high concentration of pump capacity, compared to individual wells or small groups of wells used for public water supply. Therefore, it was expected that there would be some significant saline intrusion rather than upconing of older saline waters from deep in the aquifer.

Saline water has a higher concentration of major ions, compared to freshwater, which makes it unsuitable for potable water supply, agriculture and many industrial uses. Most commonly chloride is used as a tracer for following the salinisation process, because it behaves conservatively within most groundwater environments. Groundwater can be categorised in terms of chloride concentrations as follows (Stuyzand, 1986):

- Freshwater Cl <300mg/l;
- Brackish water 300< Cl <10,000 mg/l;
- and saline water Cl >10,000 mg/l.

The European Community drinking standard is 150 mg Cl/l, while the World Health Organisation recommend a limit of 200 mg Cl/l for potable water (Custodio and Bruggeman, 1987).

5.2.2 leachate migration

In the local area, there had been considerable quarrying of the Chalk for use in cement production. Cement kiln dust (CKD) is a waste residue of cement production which was deposited in many small landfill sites close to the dewatering works, as shown in Figure 5.4. At sites A and B, disposal was on alluvial deposits, which act as a natural liner between the waste material and the aquifer. Therefore, the risk of leachate migration from these sites was expected to be minimal. However, some deposition took place directly onto the Chalk outcrop at the non-engineered site C, predominantly during the 1950s and 1970s, and in a small area at site D. Site investigation records show that landfill site C was shallow with material deposited to a depth of -1 m OD where the standing groundwater table is at approximately +1 m OD. The lack of a liner significantly increased the risk of leachate migration from these sites.

CKD is a fine, dry alkaline dust composed of oxidised, anhydrous phases, such as lime (CaO), arcanite (K_2SO_4)and sylvite (KCl), which will dissolve completely or precipitate as more stable and less soluble secondary

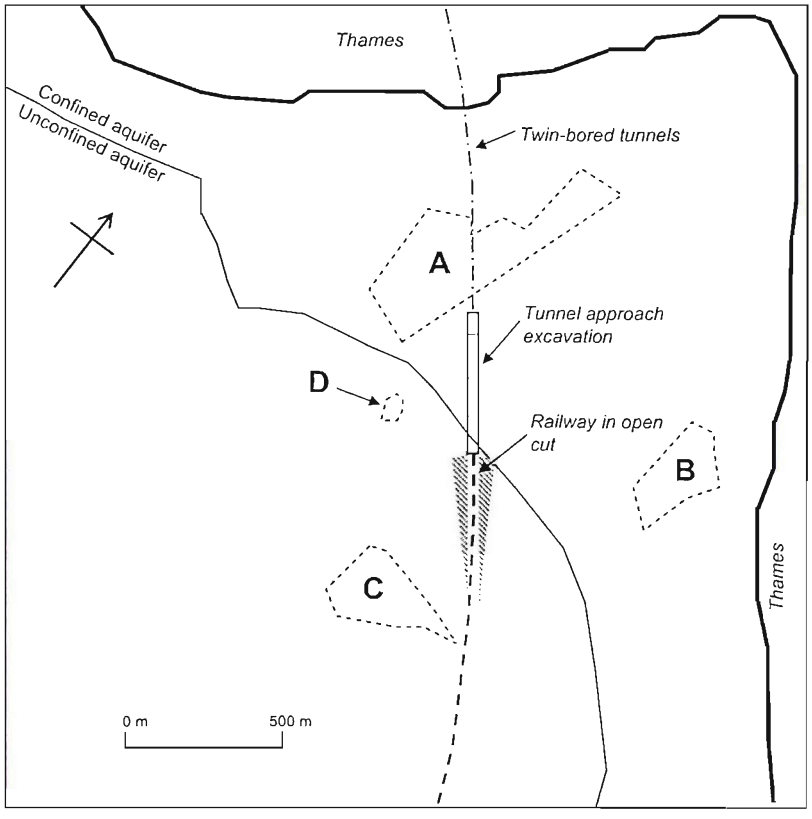

Figure 5.4: *Landfill sites close to the excavation*

phases on contact with water. The most appropriate indicators of CKD are chloride, potassium, sodium, sulphate, pH, electrical conductivity, and total dissolved solids (USEPA, 1998). Experimental leaching tests with CKD gave particularly high concentrations of potassium and sulphate (Duchesne and Reardon, 1998). CKD may contain trace metals including cadmium, lead, mercury, selenium, silver and zinc at levels above those naturally found in soils. Furthermore, high levels of arsenic and strontium have also been found in CKD (USEPA, 1993).

CKD is often mixed with different wastes to increase the bearing strength and reduce leachability before landfilling (Shively, Bishop and Gress, 1986). Permeabilities of the the materials range from 2.6×10^{-10} m/s, equivalent to an unweathered clay, to 1.2×10^{-7} m/s, equivalent to a silty sand (USEPA, 1998). The description of the deposited material at the case study site ranges from sandy gravel to clay. A summary of various case

histories of CKD impacts on groundwater is given in USEPA (1998), including discharges of contaminants to groundwater fed water bodies. The risk from CKD landfills tends to be particularly high because most sites are in contact with karstic, or highly fractured aquifers, where there is potential for rapid transport.

5.3 Monitoring

5.3.1 Monitoring programme

An array of monitoring wells was used used to monitor groundwater quality during the dewatering operation. The location of monitoring wells, shown in Figure 5.5, was decided by the main contractor in consultation with the Environment Agency (EA). The wells were largely concentrated in the unconfined area to the south of the excavation. The monitoring wells in the unconfined area defined the acceptable landward limit of any saline intrusion experienced as a result of the dewatering. Monitoring wells were also located close to or within the landfills sites A, B, and C. Limited monitoring resources meant that no monitoring was carried out close to the Thames boundary in the northern area of the site.

The monitoring array consisted of existing site investigation piezometers and new monitoring wells drilled specifically for the purposes of collecting samples (the NBH series). Typically, the monitoring wells were drilled to a maximum depth of about -20 m OD using the cable percussion method, although some shallower gravel piezometers were used in the confined aquifer. The wells were generally installed with a 25 to 50 mm diameter slotted PVC screen of variable length and an annular pea gravel filter. A bentonite seal, of at least 2 m in depth, was used to prevent vertical migration of contaminants between strata or from the surface. Boreholes were fitted with covers at the ground surface to minimise ingress of surface water into the well.

Samples were taken for a full laboratory analysis every month, while weekly or fortnightly field measurements were made of the general water

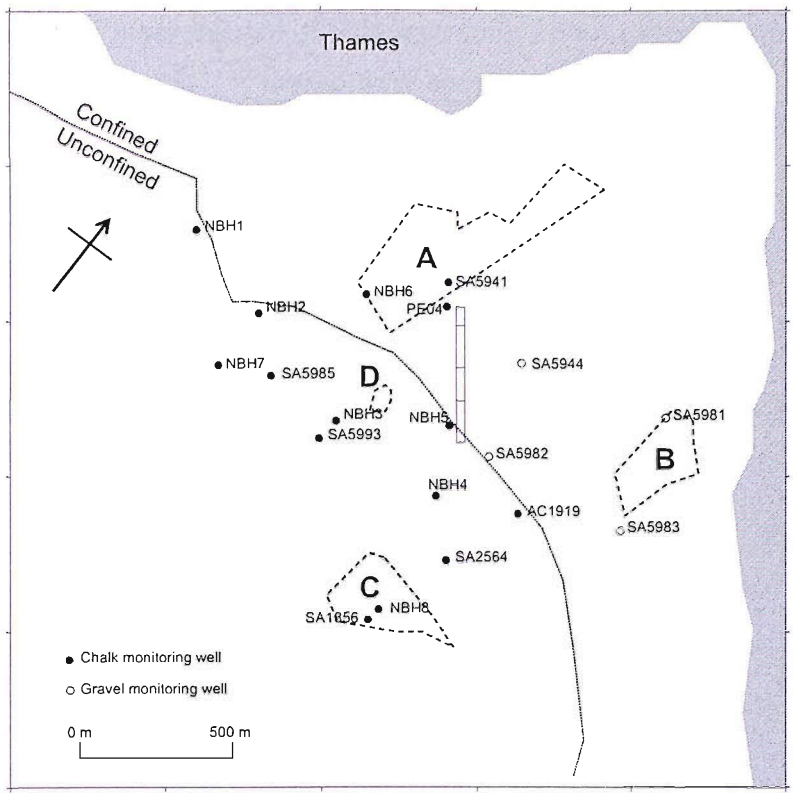

Figure 5.5: *Location of monitoring wells*

quality parameters including pH and electrical conductivity. The full test suit is shown in Table 5.1. The monitoring programme was regularly reviewed during the dewatering operations by the main contractor and the Environment Agency; it was decided to reduce the numbers of monitoring wells being sampled in order to reduce monitoring costs.

Sampling of abstracted water was also carried out. Initially, field and laboratory testing was carried out monthly at six dewatering wells that were approximately equally spaced along the excavation. Once the system was fully commissioned, it was evident that the inflows were greatest in cells SCC2 and SRC2+SRC3. Fortnightly samples from a single well in each of these two cells was sufficient to satisfy the monitoring requirements of the Environment Agency.

Table 5.1: *The groundwater quality parameters monitored. Units are mg/l except were specified*

	Monitoring wells		Abstraction wells
	Weekly/fortnightly	Monthly	Fortnightly
Field tests			
pH (units)	✓	✓	✓
Redox potential (mV)	✓	✓	✓
Electrical conductivity (μS/cm)	✓	✓	✓
Total dissolved solids	✓	✓	
NaCl	✓	✓	
Dissolved oxygen (% sat.)	✓	✓	
Dissolved oxygen	✓	✓	
Temperature (°C)	✓	✓	
Laboratory tests			
pH (units)		✓	✓
Sodium		✓	✓
Chloride		✓	✓
Potassium		✓	✓
Sulphate		✓	✓
Nitrate		✓	✓
Nitrite			✓
Ammoniacal nitrogen		✓	✓
Total organic carbon		✓	✓
Chemical oxygen demand		✓	✓
Biological oxygen demand		✓	✓
Total petroleum hydrocarbons		✓	✓
Total phenols		✓	✓
Volatile organic carbon (μg/l)		✓	
Iron		✓	✓
Manganese			✓
Magnesium		✓	✓
Calcium		✓	✓
Ionic balance (%)		✓	
Alkalinity		✓	✓
Total suspended solids		✓	
Total dissolved soils		✓	✓

Table 5.2: *Categorisation of the groundwater monitoring wells at the Swanscombe Peninsula. Locations are shown in Figure 5.5*

	Primary wells	Secondary wells
Field tests	Weekly	Fortnightly
Laboratory tests	Monthly	Monthly
Chalk wells	AC1919, NBH1, NBH2, NBH3, NBH4a, NBH5, NBH8	NBH6, NBH7, SA1856, SA2564, SR5941, SA5985, SA5993, PE04
Gravel wells	SA5983	SA5981, SA5982, SR5944

5.3.2 Sampling methods

Groundwater samples taken from the monitoring wells were collected using a Waterra inertial pump, which comprises a foot valve at the base of a length of approximately 20 mm diameter plastic tubing (polyethylene of teflon). To draw flux samples from the borehole the tubing was oscillated upwards and downwards by hand; when the tubing was lowered the water entered the tube as the foot valve was forced open and when the tubing was raised the valve was closed trapping water in the tube. Repeated strokes allowed the water to rise in pulses to discharge at the surface. The pump intake was positioned within the screened section of the well. At least three well volumes were removed from the well and the water level was allowed to recover prior to the collection of the sample for analysis. Each well was supplied with a dedicated pump which was stored permanently inside the well and not cleaned prior to sampling. The samples of abstracted water were drawn directly from the head of the dewatering well via a sampling tap. Field sampling was carried out using handheld meters, which were calibrated before each round of sampling.

All samples were collected in clean sample bottle, which were rinsed three times with sample water before taking the test sample. Samples were

stored in a cool box and delivered the same day to an accredited laboratory for analysis.

5.4 Baseline water quality

Subsurface solute transport problems often concern the input of a groundwater contaminant at a point source into an aquifer with a low background concentration of that contaminant. In such a case the contaminant will migrate as a plume or a front in accordance with the transport processes (advection, dispersion, diffusion). However, at the case study site the problem was more complex because the contaminants were not introduced from a single point source. The main indicators of contaminant migration, as a result of both saline intrusion and migration of CKD leachate, were the major ions, including chloride (Cl), sodium (Na), potassium (K), sulphate (SO_4). The following sections will discuss the Thames water quality, the existing major ion groundwater chemistry and other groundwater quality parameters prior to dewatering.

5.4.1 Thames water quality

It has already been established that the quality of the Thames water may impact upon the groundwater through the saline intrusion process. The salinity of the Thames water was measured by sampling over a single tidal range, from high to low tide, on 27th March 2003. The data suggest the Thames salinity, as indicated by the chloride (Cl) concentration, is greatest approximately one hour after high tide ($\approx$ 7150 mg/l) (Figure 5.6). The low value at 12:30 is unexpected, but is likely to reflect the complicated nature of the estuary mixing. Sulphate (SO_4) concentrations track the changes in salinity closely, as do the magnesium (Mg) values, although the tidal variation is less pronounced.

The sodium (Na) concentrations vary unexpectedly, with the concentration even exceeding that of Cl at 12:30. Typically Na concentrations of saline water bodies are just are approximately equal to

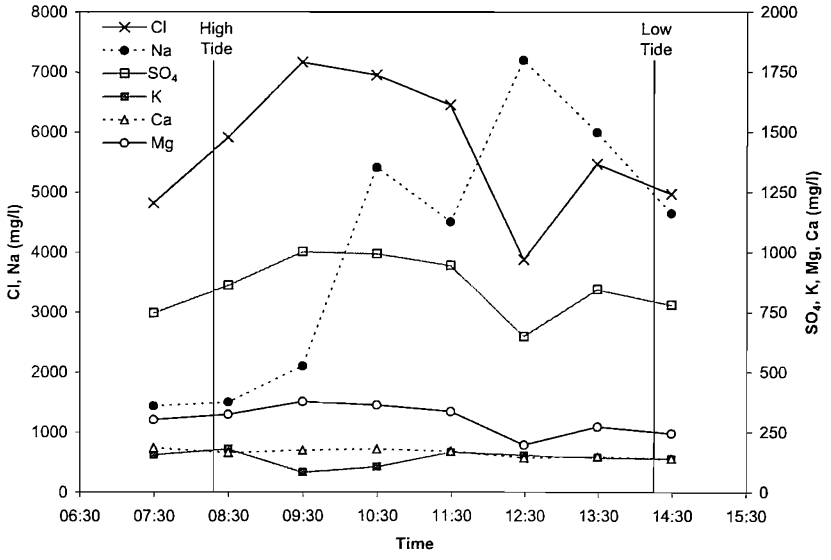

Figure 5.6: *Tidal fluctuations of dissolved major ions in the Thames on 27th March 2003*

Table 5.3: *Representative major ions analyses of seawater and Thames water*

Ion	Seawater (mg/l) (Goldberg, 1963)	Seawater ion ratio $[ion]/[Cl^-]$	Thames water (mg/l) $n = 8$	Thames ion ratio $[ion]/[Cl^-]$
Cl	19000	-	5700	-
Na	10500	0.553	4100	0.719
K	380	0.020	140	0.025
SO_4	2700	0.142	850	0.149
Ca	400	0.021	160	0.028
Mg	1350	0.071	300	0.053

55% of Cl concentrations (Goldberg, 1963), as shown in Table 5.6. The data suggest an error in the analysis of sodium, possibly due to an laboratory error. Calcium (Ca) levels are relatively constant over the tidal range with concentrations in the range to 140 to 185 mg/l. Potassium (K) concentrations are of a similar level, but with reduced concentrations (< 100 mg/l) in the first hours after high tide.

With exception of the Na ratio, the ion ratios of the Thames water are comparable to those of seawater (Table 5.6). The Thames values are based on mean concentrations calculated from the 8 tidal sampling results. The Thames water is significantly less saline than average seawater, however the salinity is determined by the flow regime of the Thames which will change seasonally. The measured chloride concentrations are consistent with the mean monthly concentration for the month of March between 1977 and 1988 recorded by (Attrill and Power, 2000) at West Thurrock. However, Atrill and Power showed that Cl concentrations can be as high as 10,000 mg/l in September, when the freshwater input to the Thames is lowest. The pH of the Thames water was approximately 6.9.

5.4.2 Groundwater characterisation

Some baseline groundwater quality data existed for the case study site with measurements taken as early as December 1996 during an initial site investigation. At this samples were analysed for most of the site investigation piezometers around the Swanscombe Peninusla. Further data were collected by the site environmental team from June 2001 up to the start of the dewatering in November 2001 using the array of monitoring wells described previously, with laboratory analysis carried out at monthly intervals. This meant that typically only 4 or 5 baseline measurements were available, which did not allow the investigation of seasonal variations or the influence of tidal fluctuations at monitoring wells close to the Thames. Nevertheless, it was possible to calculate a set of mean values for each monitoring well. For the majority of the wells the groundwater quality was reasonably stable during the six months prior to dewatering, with the

exception of wells SA5983 and SA5981 where the variation was assumed to relate to tidal influences.

The existing groundwater chemistry was dependent on the proximity of the groundwater to the Thames, the influence of CKD disposal and possibly the geological strata. The concentrations of the major ions Cl, Na, K and SO_4 ions are presented in Figure 5.7. The Ca and Mg analysis was not carried out for the baseline samples and therefore these ions are absent from the figure.

The Cl concentrations of the Chalk groundwater were generally in the order of approximately 60-150 mg/l (Figure 5.7(a)), which is less than the EC drinking water standard of 150 mg/l. Aquifer hydrochemistry is often examined in terms of the ratios of concentrations of major ions to the concentration of chloride (Elliot, Chadha and Younger, 2001). The composition of the fresh groundwater is characterised by high ratios of SO_4/Cl and K/Cl at a lower salinity. With the exception of NBH5, the SO_4/Cl ratios were greater than 1 and are as high as 3.4 (SA2564 and SA5985). With the exception of NBH5 and SA2564, the K/Cl ratios range from 0.2 to 0.4. The Na/Cl ratios range from 0.6 to 1.0.

The piezometers screened in the gravel (SA5981, SA5983 and SR5944) had a Cl concentration approximately in the 1000-2000 mg/l range, indicating brackish groundwater (Figure 5.7(b)). The composition of the brackish groundwater was comparable to that of the Thames, with K/Cl ratios generally below 0.1 and SO_4/Cl ratios below 0.25 except for SR5944. The Na/Cl ratios were between the 0.6-0.7. The data indicate that there was mixing taking place close to the Thames boundary, which sees the dilution of the higher saline Thames water with freshwater. The SO_4 enrichment at SR5944 may have resulted from some localised disposal CKD or migration of leachate.

Groundwater contaminated by CKD is characterised by having a very high proportion of K ions relative to the Cl concentration (Figure 5.7(b)). The Cl, Na and SO_4 concentrations were also high relative to the fresh groundwater, but the high K concentration was probably the most appropriate indicator of CKD leachate. The monitoring well SA1856 is

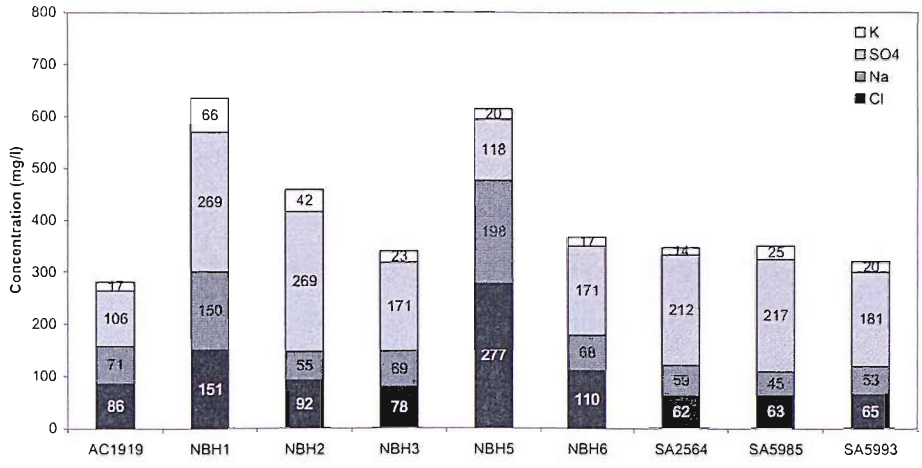

(a) Chalk monitoring wells

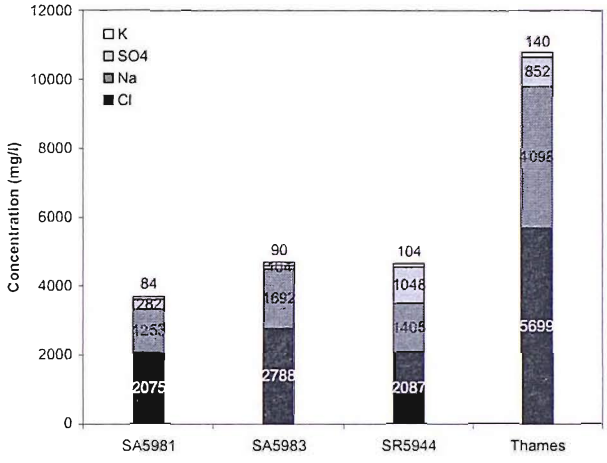

(b) Gravel monitoring wells

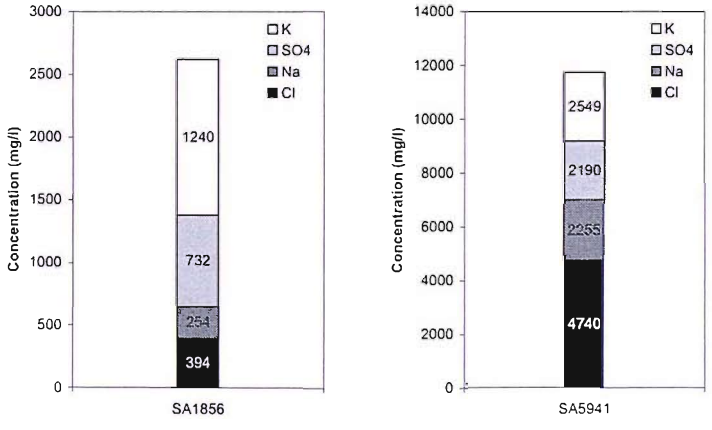

(c) Monitoring wells affected by CKD

Figure 5.7: *Baseline major ion chemistry of monitoring wells around Swanscombe Peninsula*

located in a landfill C area. The well is screened in both the made ground (including landfill material) and the underlying Chalk. Further evidence of CKD leachate is the pH of 12.6 to 12.85 of water sampled from this well as shown in Figure 5.8; the CKD leachates tested by Duchesne and Reardon (1998) had pH of 12.95 to 13.65, with lower values measured for larger water/solid mixtures. The normal pH values for the Chalk groundwater were between 7.0 and 7.2, while for the brackish groundwater the recorded pH values were between 6.8 to 7.0. High pH levels are a concern because they can result in the precipitation of calcium carbonate, which can lead to clogging of wells and pumps, thereby affecting the performance of a dewatering system (Powrie and Roberts, 1995).

The ion concentrations measured for groundwater at the monitoring well SA5941 were significantly higher than expected, particularly the potassium concentration, indicating the presence of CKD leachate (although the pH level was in the normal range). This well is located below landfill A, but the aquifer should be protected from contamination by the alluvial clay confining layer. One explanation for the observed high concentrations may be that the well provides a pathway for the vertical migration of contaminants. Further consideration will be given to this observation in the next section.

Figure 5.8 shows that COD (chemical oxygen demand) levels were generally less than 50 mg/l. Greater COD levels were measured in the brackish groundwater and CKD affected groundwater, reflecting the greater ion concentrations. The BOD levels were generally less than 10 mg/l reflecting the low organic content in the groundwater. However, higher levels of approximately 75 mg/l were found at SA1856 in landfill C where some organic contaminants were also present. Generally, higher ammoniacal nitrogen (NH_4-N) concentrations were found in the brackish and CKD affected groundwater (> 9 mg/l). High concentrations were expected in contaminated areas, but not for the brackish groundwater since the NH_4-N concentrations for the Thames were approximately 0.2 mg/l; it is possible that the high concentrations at wells SA5981 and SA5983 are a result of leachate from Landfill B. Erskine (2000) reports that ammonium has the

Table 5.4: *Summary of the existing groundwater types found at the Swanscombe Peninsula*

Type	Location	Characteristics
Fresh groundwater	- Chalk to the south of the excavation	Cl < 150 mg/l SO_4/Cl > 1 K/Cl 0.2 to 0.4 pH 7.0 to 7.2 COD< 50 mg/l NH_4-N< 2.5 mg/l
Brackish water	- The Thames - Gravels close to the Thames - Chalk to the north of the excavation	Cl > 1000 mg/l SO_4/Cl < 0.25 K/Cl < 0.01 pH 6.8 to 7.0 COD> 200 mg/l
CKD affected groundwater	- Landfills A and C	K/Cl > 3 High ion concentrations pH> 12 COD> 300 mg/l NH_4-N> 10 mg/l

greatest potential of all the common contaminants to impact upon groundwater quality, because the drinking water standard for ammonium is very low (0.39 mg/l), whereas the major ions tend to have much higher acceptability levels.

5.4.3 Initial concentrations

A modelling study was carried out to help interpret the groundwater quality data collected during the dewatering operation. This required a set

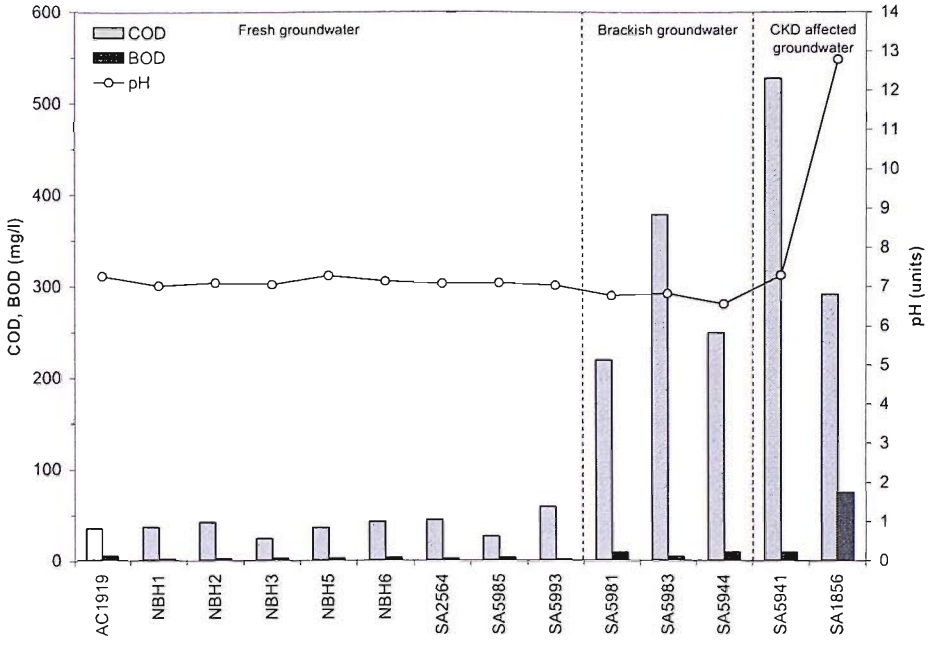

Figure 5.8: *Mean pH, COD and BOD levels before dewatering*

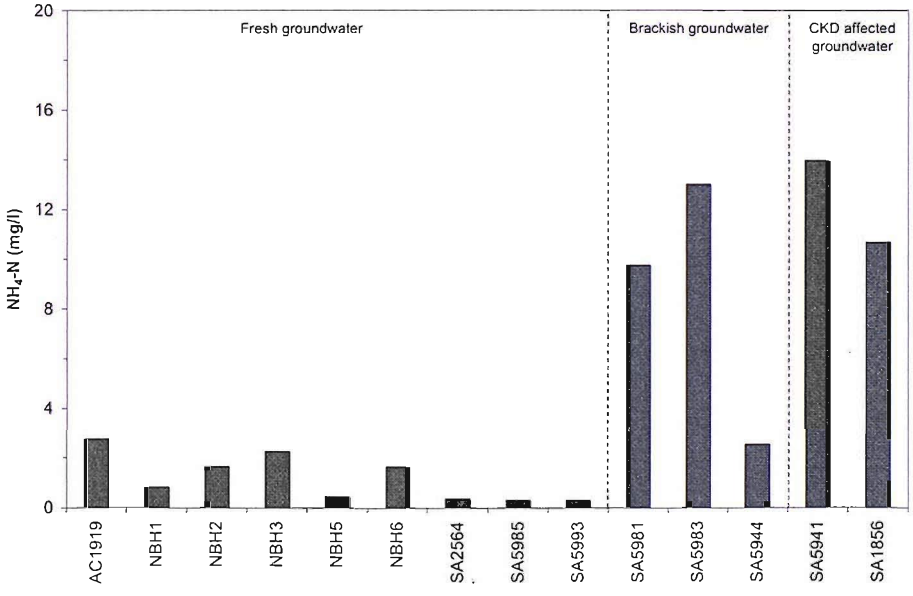

Figure 5.9: *Mean ammoniacal nitrogen levels before dewatering*

of initial concentrations to be prepared for each solute that was to be modelled. Concentration distributions for the site were created using a kriging tool provided by the software SURFER (Golden-Software, 1989), which interpolates the concentrations between measurements and allows contours to be plotted for the model area.

Establishing the baseline groundwater quality across the site was complicated by a number of issues relating to the reliability of the data and the limited data that was available. To provide a sufficient number of data points for the contouring, data from the gravel and chalk strata had to be considered together; the vertical distributions of contaminants were not clear so it was assumed that concentrations did not vary with depth. The number of data points was increased by considering the data collected during site investigation in 1996 and 1997 from site investigation boreholes, in addition to the baseline monitoring data collected 6 months prior to dewatering. For each of the contaminants, a mean value was calculated at each location based on between 2 to 10 measurements.

Unexpectedly high ion concentrations were measured close to landfill A in the gravel and chalk strata despite being separated from the landfill by the alluvial deposits, which should act as a natural liner. Table 5.5 shows the mean groundwater quality measurements for samples taken at the locations shown in Figure 5.10. The concentrations of Cl, Na, SO_4, K and NH_4-H exceeded the upper limit values for four of the six boreholes sampled in the area, where the upper limits represent the normal aquifer groundwater quality with an allowance for any potential saline intrusion that may have existed prior to dewatering. However, with the exception of well SR5941, Ca and Mg concentrations were found to be lower than the normal, which is probably a result of calcite precipitation at high pH levels (Stumm and Morgan, 1996). Typically, COD and BOD levels were also high in these samples.

Table 5.5: *Mean groundwater quality at locations in and around landfill A. The general upper limits for natural groundwater are shown, which allow for some existing saline intrusion. Concentrations are in mg/l. n is the number of measurements available*

	Strata	(n*)	pH	Cl	Na	SO_4	K	NH_4-N	Ca	Mg	COD	BOD
SR2159A	Gravel	2	7.5	338	295	174	18.5	0.1	42	91	97.5	7.8
SR5941	Chalk	6	7.49	**4740**	**2255**	**2190**	**2540**	**24.9**	58	64	**528**	9
SR2158	Chalk	2	7.12	397	215	98	17	5.5	88	47	140	21
SA5940	Chalk	2	**11.72**	**10032**	**4062**	**10540**	**14875**	**47**	5	0.3	**805**	**271**
SA6409	Chalk	2	**10.21**	**5866**	**2875**	**3690**	**8500**	**52.3**	9	5	**501**	**48**
SA6411	Gravel	2	**12.93**	**14162**	**4173**	**11458**	**29172**	**20.9**	14	0.1	**1129**	**134**
Upper limit			7.5	3500	1900	500	130	15	200	100	300	20

The high concentrations of contaminants in the some groundwater samples suggest that vertical migration had taken place between the strata. This is process is commonly referred to as the short-circuiting of flow. Short-circuiting can occur naturally in carbonate aquifers where dissolution features provide a pathway for the rapid transport of contaminants between layers. Short-circuiting can also take place during and after construction of boreholes that act as conduits for vertical flow, which is a more likely explanation for the case study site observations. This is normally a problem associated with unlined boreholes; Price and William (1993) found that natural flow down an open borehole led to rapid changes in the quality of water in some parts of the formation. At waste disposal sites, borehole construction can significantly affect the quality of groundwater (Van Duijvenbooden and Kooper, 1993). Further discussion of short-circuiting effects is given in Chapter 7.

Given the uncertainty of the baseline data, two sets of initial concentration distributions were produced:

- Set A - based on the baseline data excluding the measurements at boreholes where short-circuiting may have taken place.
- Set B - based on all available data and assuming that all measurements are representative of the groundwater quality prior to dewatering.

The initial concentrations of Cl, Na, SO_4, K and NH_4-N are shown in Figures 5.11 to 5.15. To allow the measured concentrations to be gridded realistically, the concentrations at the site boundaries had to be estimated. The boundary concentrations, shown in Table 5.6, represent the existing concentrations of groundwater prior to dewatering, and differ from the boundary concentrations of the contaminant transport model. In contrast to other parameters, there was a distinct difference in the magnesium and calcium concentrations between the gravel and Chalk strata, as shown in Figure 5.16, and therefore it was inappropriate to consider both layers together. There were an insufficient number calcium and magnesium

Table 5.6: *pH levels and concentrations (mg/l) at the site boundaries used for producing initial concentration distributions*

	Thames boundary	Landward boundary
Cl	3500	100
Na	1900	55
SO_4	500	33.33
K	85	15
NH_4-N	0.2	0.8

measurements were made prior to dewatering, hence it is not possible to determine the spatial distribution. For the purposes of modelling, the initial concentrations were assumed to be uniform within each layer at the mean levels shown in Figure 5.16.

5.5 Summary

The potential environmental impacts of construction dewatering at the CTRL Thames Tunnel southern approach excavation included degradation of the aquifer by saline intrusion and the migration of cement kiln dust leachate. Part of the case study site was recognised as a source protection zone by the Environment Agency. The high abstraction rates of the dewatering system, low effective porosity of the Chalk and consequent high rate of groundwater advection meant the risk of further contamination was high.

The principle contaminants of concern were Cl, Na, SO_4, K and NH_4. In addition cement kiln dust leachate was characterised by a pH above 10. Groundwater quality was monitored before and during the construction dewatering using an array of monitoring wells. In addition, samples were taken of abstracted groundwater. The baseline data was used to determine the areal distribution of contaminants but the depth profile could not be established with certainty due to the limited depth of the monitoring wells.

Highly contaminated groundwater was sampled at wells screened in

and around landfill A, despite a significant layer of alluvial clay lining this landfill site. This implies that the drilling of site investigation boreholes might have allowed the vertical migration of leachate, a process commonly called short-circuiting. Two sets of initial concentration distributions have been made to allow the investigation of saline intrusion, leachate migration and short-circuiting effects using a contaminant transport model.

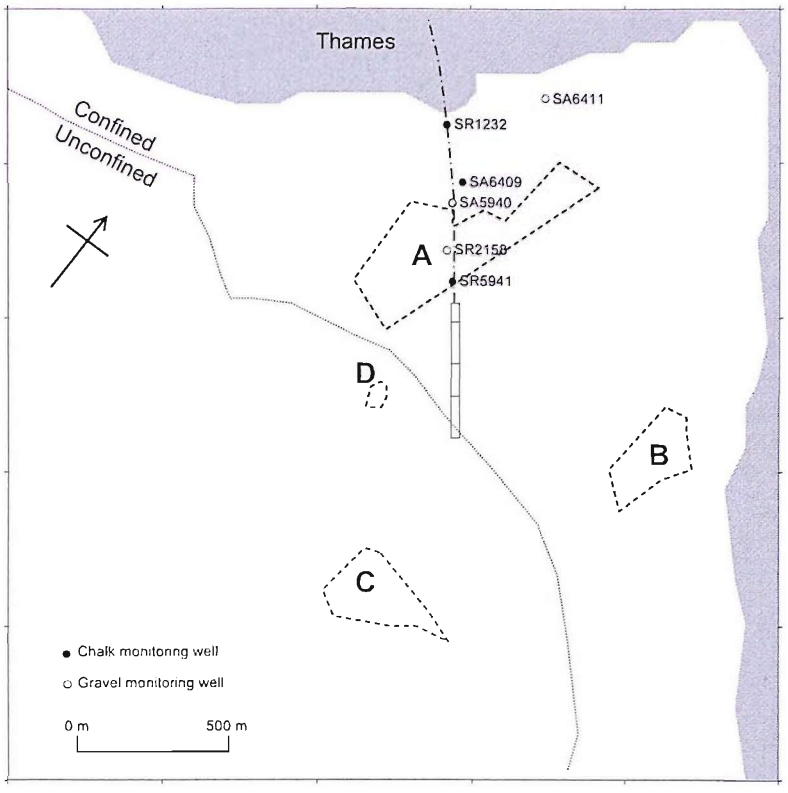

(a) Plan

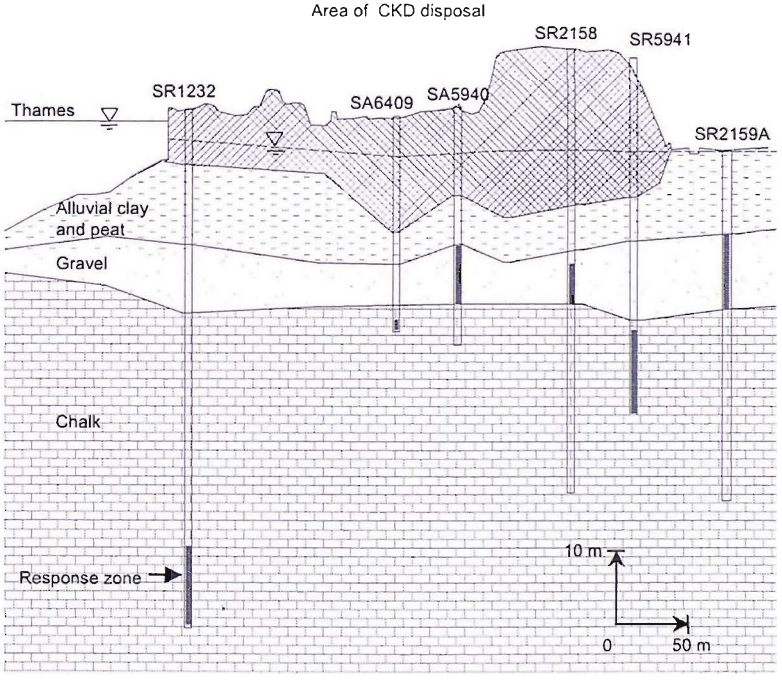

(b) Plan

Figure 5.10: *Site investigation piezometers located in and around landfill A. Cross-section is shown along the tunnel alignment*

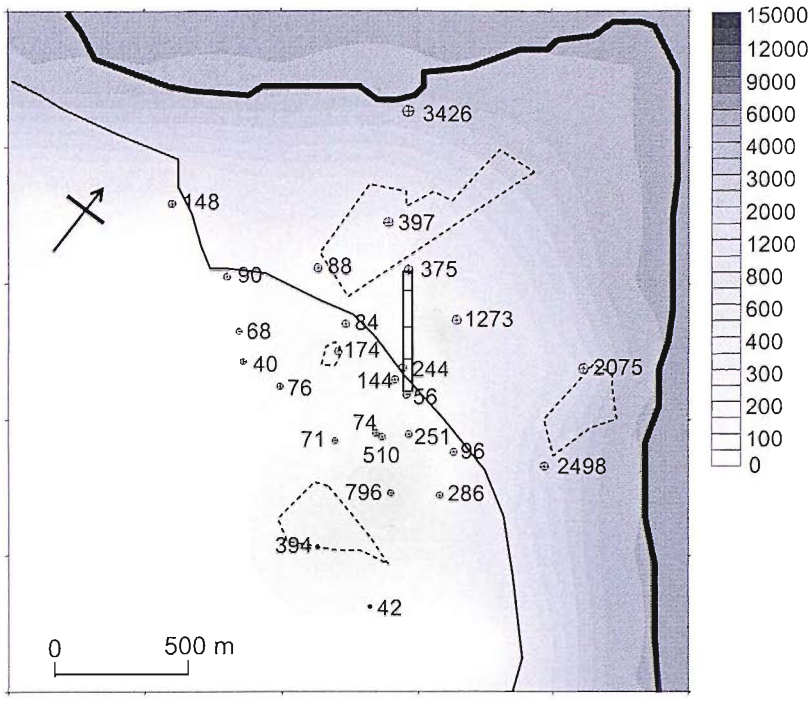

(a) Set A

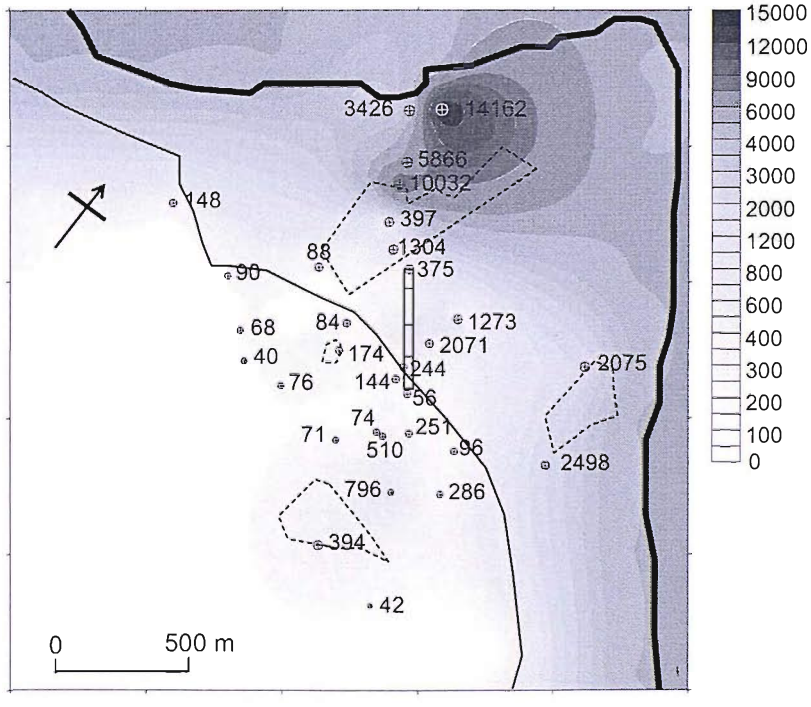

(b) Set B

Figure 5.11: *Initial chloride concentrations (mg/l) in the gravel and Chalk before dewatering. Spot measurements are shown for selected piezometers*

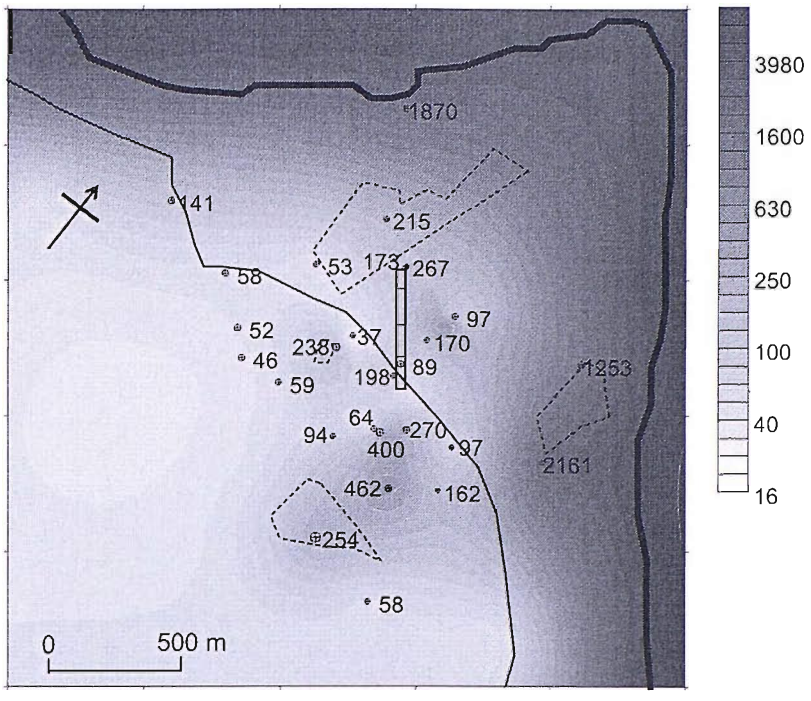

(a) Set A

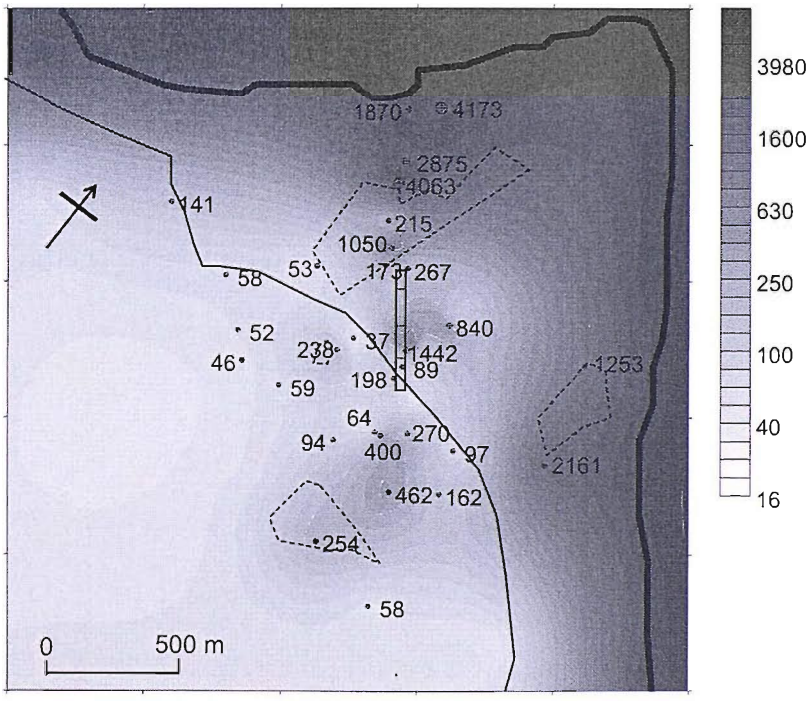

(b) Set B

Figure 5.12: *Initial sodium concentrations (mg/l) in the gravel and Chalk before dewatering. Spot measurements are shown for selected piezometers*

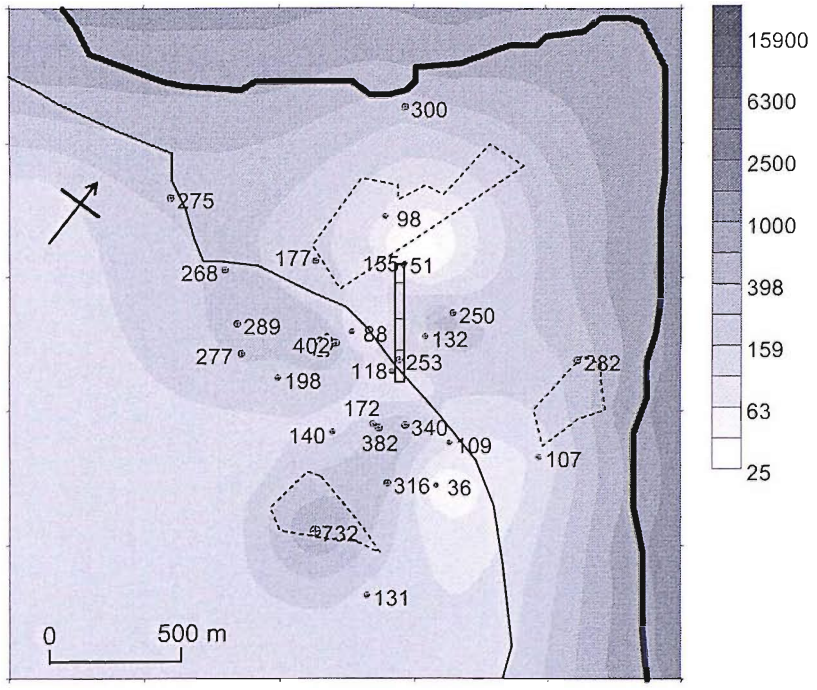

(a) Set A

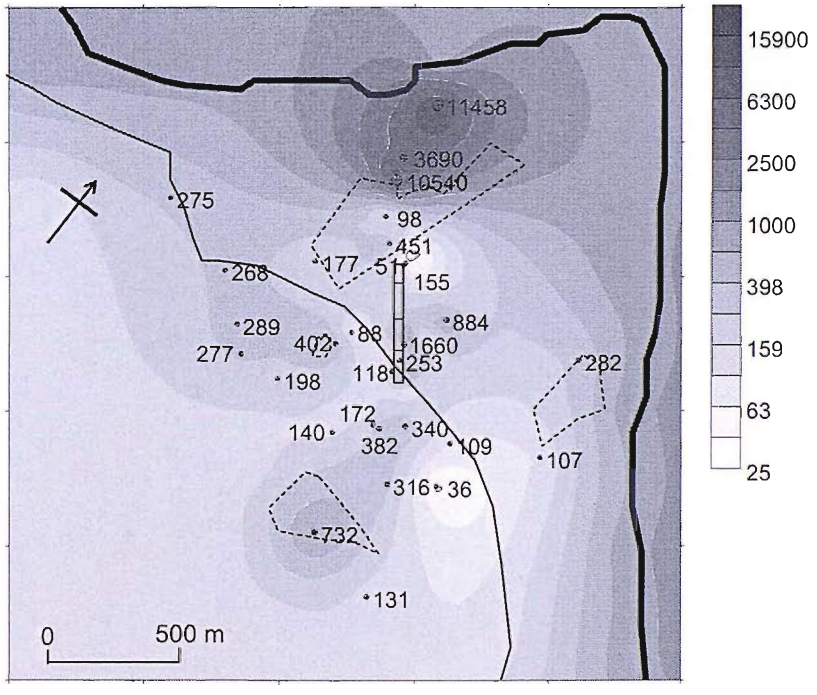

(b) Set B

Figure 5.13: *Initial sulphate concentrations (mg/l) in the gravel and Chalk before dewatering. Spot measurements are shown for selected piezometers*

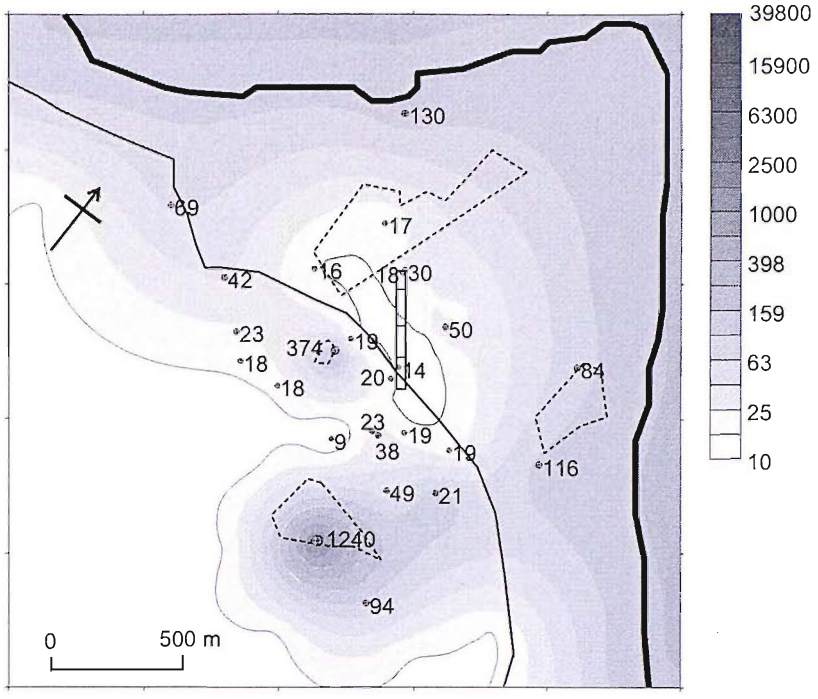

(a) Set A

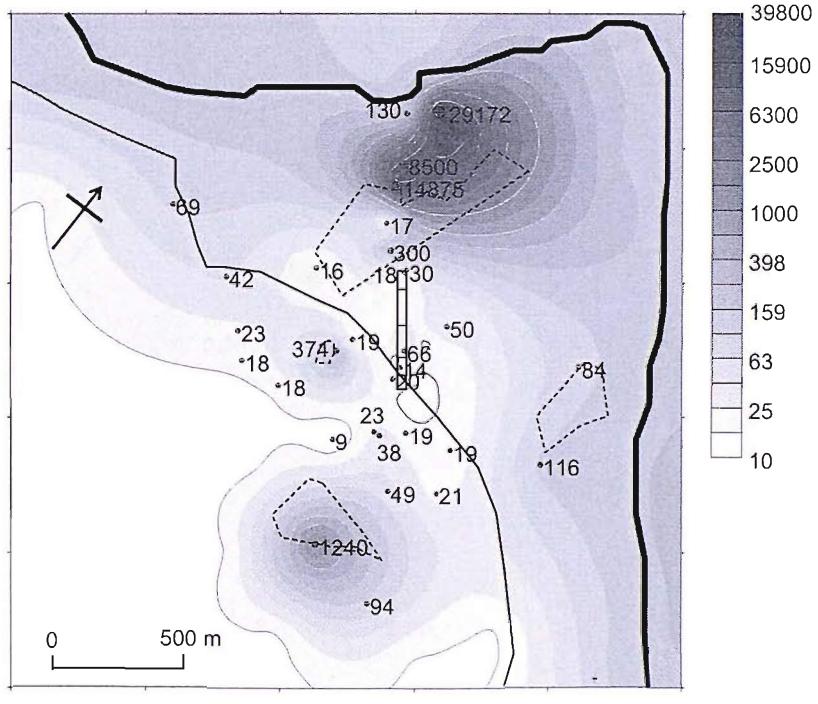

(b) Set B

Figure 5.14: *Initial potassium concentrations (mg/l) in the gravel and Chalk before dewatering. Spot measurements are shown for selected piezometers*

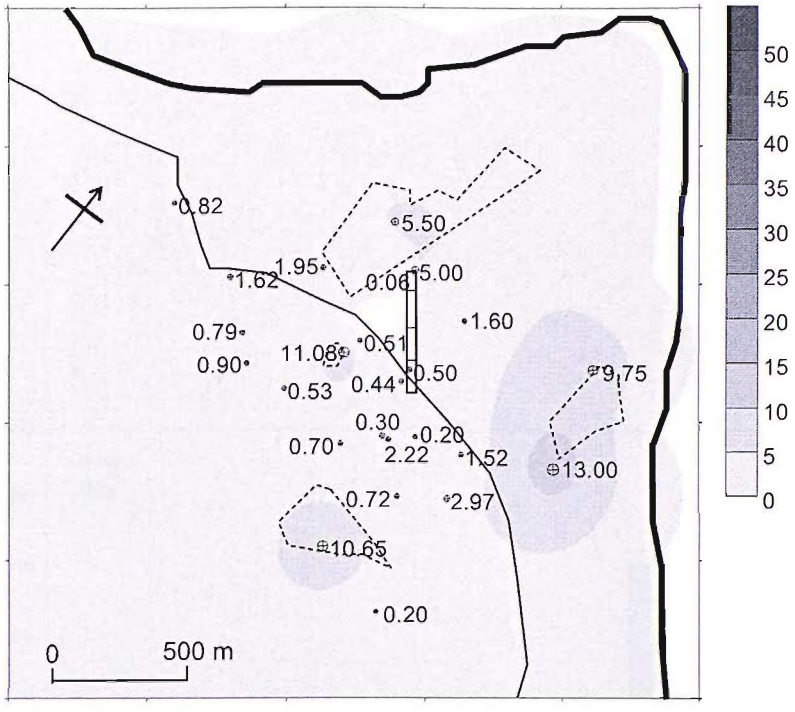

(a) Set A

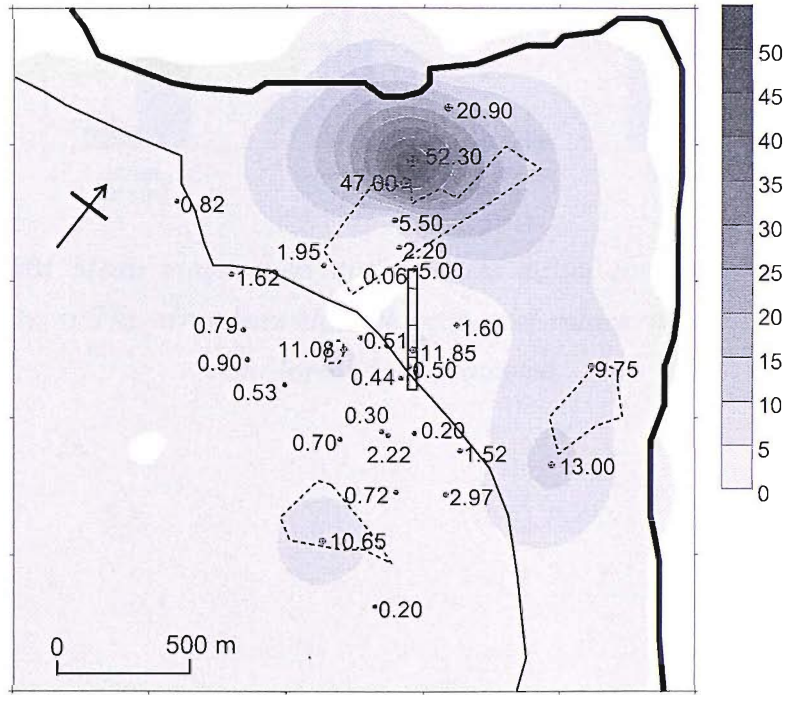

(b) Set B

Figure 5.15: *Initial ammoniacal nitrogen concentrations (mg/l) in the gravel and Chalk before dewatering. Spot measurements are shown for selected piezometers*

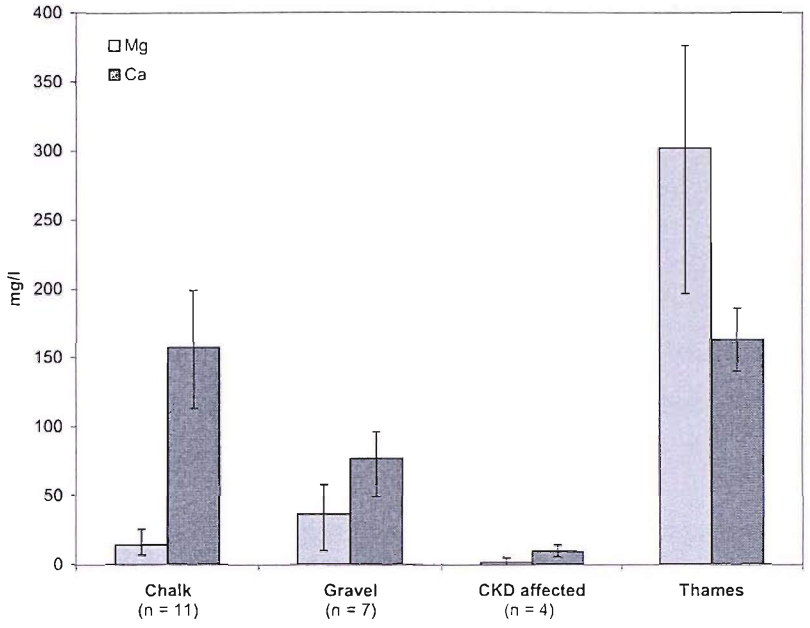

Figure 5.16: *Mean magnesium and calcium initial concentrations of the sampled waters. The error bars show the range of values, n is the number of monitoring wells sampled*

Chapter 6

Contaminant transport modelling

6.1 Modelling aims

The groundwater flow modelling described in Chapter 4 was used as a basis for a series of contaminant transport models. The purposes of the contaminant transport modelling were:

- to investigate the processes of saline intrusion and leachate migration caused by construction dewatering, by aiding the interpretation of the limited groundwater quality data,
- to assess the suitability of the site monitoring programme for protecting the groundwater quality of the aquifer, and
- to investigate whether high contaminant concentrations, probably resulting from short-circuit flow, were representative of the aquifer.

The code MT3D (Zheng, 1999) was used to model the transport of solutes. This code was developed in response to the requirement for a contaminant transport model that was free of numerical errors, efficient with respect to computer and execution time, while being both flexible and simple to use. The model uses a Lagrangian approach to simulate advection, whereby individual particle are tracked through the flow field. A Eulerian

approach is used to model the dispersive and reactive processes, whereby the mass balance of a solute is calculated for a fixed point in space. The mixed Eulerian-Lagrangian approach is favourable for advection-dominated problems with very large Peclet numbers and does not require the very small nodal spacings that are required when using a Eulerian method in order to minimise numerical dispersion. A discussion of the advantages and limitations of the different modelling codes is given by Zheng (2002).

6.2 Model simplification

A simplified transient groundwater flow model was used for the investigation of contaminant transport, which will be referred to as *MODEL CT*. This section describes the key changes that were made to the *MODEL 1* discussed in Chapter 4. The changes relate to a reduced number of nodes of the three dimensional finite difference grid. The period covered by the original transient model was extended to 16th December 2003 giving a total length of time for the simulation of 750 days. A summary of the groundwater flow results is provided here, with further details given in the Appendix.

6.2.1 Grid discretisation

The high number of nodes of the *MODEL 1* meant that execution time for the calculation of solute transport using a standard personal computer was high. The finite difference grid was simplified to 5 layers as shown in Figure 6.1. The numbers of rows and columns were also reduced thereby reducing the total number of nodes by a factor of approximately 4.5 Table 6.1. The main limitation of the new grid design is that the sloping diaphragm wall profile could not be represented as convincingly, although surface area of the walls in the model were close to the actual design (Table 6.2).

The reduced number of layers meant that depths of the strata interfaces in the contaminant transport model were more approximate. The transmissivities of the overall model and the model zones were maintained

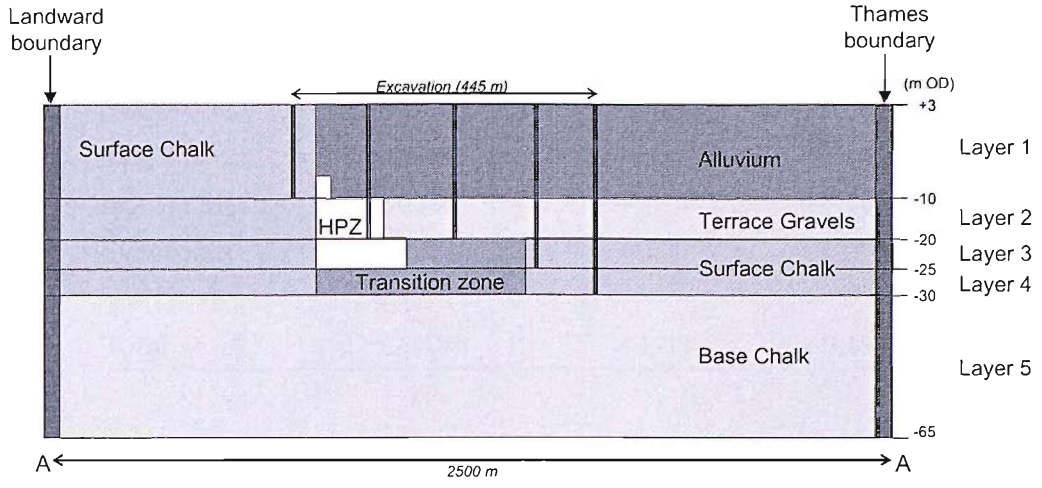

Figure 6.1: *The layers and hydraulic conductivity zones of the simplified model*

Table 6.1: *Comparison of the finite difference grid designs of* MODEL 1 *and* MODEL CT

	MODEL 1	*MODEL CT*
Number of layer	12	5
Number of rows	114	75
Number of columns	83	65
Total number of nodes	113544	24375
Max nodal spacing (m)	33.33	50
Min nodal spacing (m)	4	8

Table 6.2: *Comparison of errors in the diaphragm wall surface area (m^2).*

$$Percentage\ error = 100(1 - \frac{Actual}{Modelled})$$

Cell	Actual surface area	*MODEL 1*	*MODEL CT*
SLC+SCC1	6257	+2.98	-1.77
SCC2	8581	-0.56	+1.03
SCC3+SRC1	6370	+3.73	+0.16
SCR2+SRC2	5273	+0.35	-3.19
Total	26481	+1.53	+0.19

by making small changes to the hydraulic conductivities, as shown in Figure 6.2. The vertical hydraulic conductivities (k_z) were kept the same as those used in *MODEL 1* (Table 4.5).

6.2.2 Results

Table 6.3 gives the statistics describing the fit of the calculated groundwater levels to the recorded levels. There is a slight deterioration of the match for internal and external water levels when compared to the transient model in Chapter 4 (Table 4.12). Water levels at the excavation were difficult simulate accurately because of the simplified representation of the diaphragm wall, as indicated by the mean absolute residual (MA) of 1.40 m for the internal piezometers and 1.05 for the external piezometers. However, a good match of calculated and measured water levels for remote piezometer was achieved.

6.3 Model calibration

6.3.1 Modelling procedure

The first step in the contaminant transport modelling was to determine the appropriate porosities of the geological units. As chloride (Cl) behaves

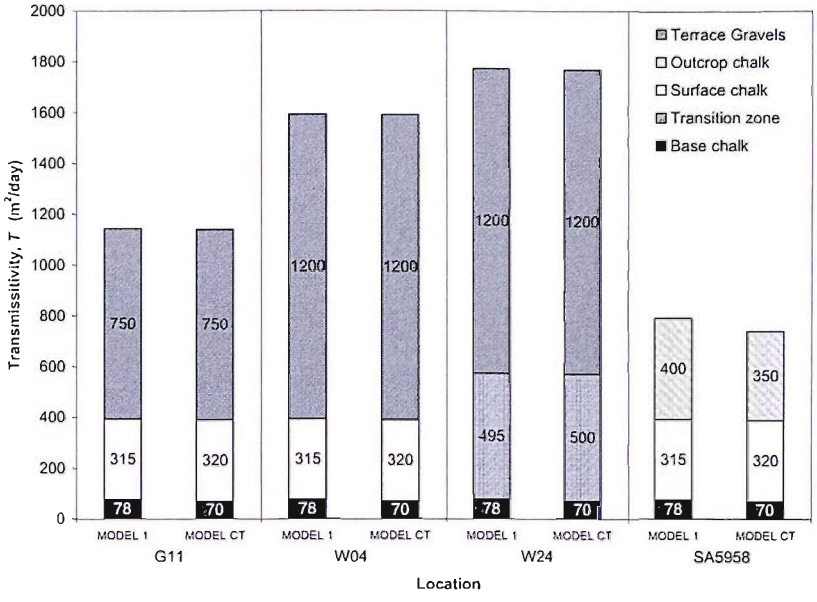

(a) T at different locations

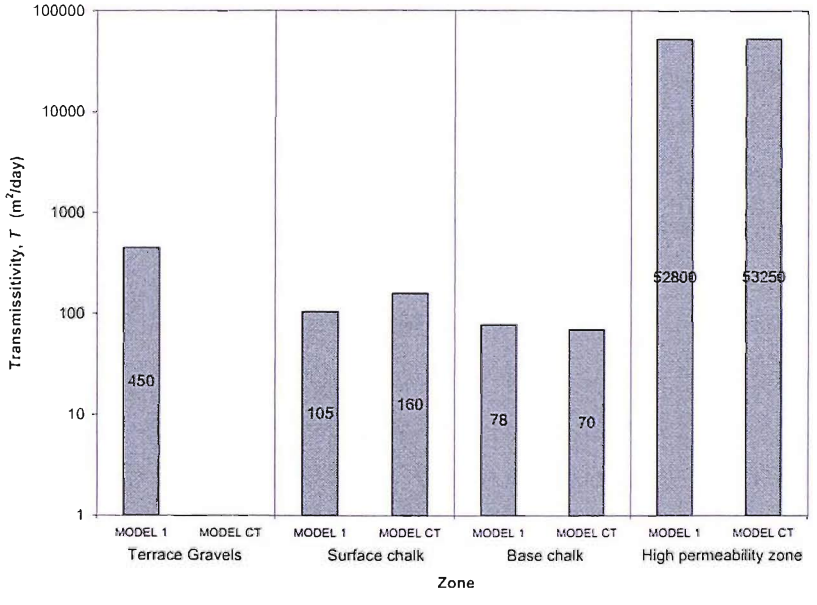

(b) T of zones at well W38

Figure 6.2: *Transmissivities of MODEl 1 and MODEL CT*

Table 6.3: *Summary table of statistics for the water levels of* MODEL CT *(n is the number of piezometer readings, M is the mean of residual errors, MA is the mean of absolute residual errors, and R is the correlation coefficient)*

	Internal	External	Remote	Overall
n	179	369	1751	2299
M (m)	-0.26	0.25	0.18	0.15
MA (m)	1.40	1.05	0.44	0.65
Linear relationship	$y = 0.977x$	$y = 1.029x$	$y = 1.016x$	$y = 0.996x$
R	+0.92	+0.92	+0.96	+0.97

conservatively, it provides a useful natural tracer of groundwater flow. The model was calibrated by achieving a good match between measured and calculated Cl concentrations of abstracted groundwater. During construction dewatering Cl concentration of abstracted groundwater increased, especially in cell SCC2 where concentrations reached 3300 mg/l after 2 years (Figure 6.3). Figure 6.3 is a typical time-series graph used which was used to review the changing groundwater quality as part of the site monitoring programme. It was assumed that measurements from a single well in each of the cells would be representative of the abstracted groundwater for the cell as a whole, and therefore the same well was not sampled on each occasion. The chloride concentration of the first sample drawn from SCC2 (W23) was collected using a Waterra pump as no pumping was taking place. At this time the well had not been developed and the purge volume was less than 3 well volume, hence the high measured concentration (700 mg/l) reflects the stagnant water in the well after installation. The graph implies that there are four distinct stages in the chloride record of the cell SCC2. A possible interpretation may be as follows:

- Stage 1: Saline intrusion through within the low porosity surface chalk leads to an increase in salinity during the first year of dewatering.
- Stage 2: The saline front in the surface chalk reaches the excavation

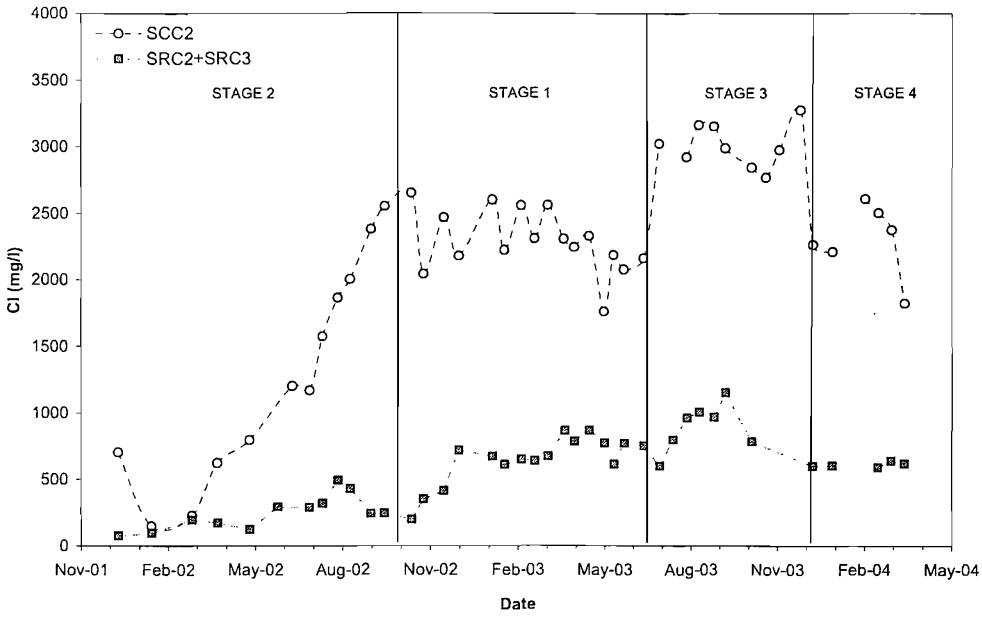

Figure 6.3: *Changes in the chloride concentration of abstracted groundwater in cells SCC3 and SRC2+SRC3.*

and concentration begin to stabilise.

- Stage 3: A second saline front, possibly migrating through the base chalk or the gravels, reaches the excavation leading to higher concentrations

- Stage 4: Concentrations begin to decrease as the water levels are gradually allowed to recover.

The variability of concentrations within small areas of the excavation, and the validity of the above interpretation, could be determined during the modelling. Lower concentrations were measured in cell SRC2+SRC3 where groundwater flow was fed by the high permeability zone, although the increase of 100 to 1000 mg/l is still significant.

6.3.2 Porosities and travel times

The time taken for a particle to flow along a flowpath of length l can be calculated using Equation 6.1, which is based on Darcy's Law:

$$t = \frac{\theta l^2}{kH} \tag{6.1}$$

where H is the head drop along the flowpath, k is the bulk permeability and θ is the effective porosity. Travel time is highly sensitive to values of effective porosity; this is particularly noticeable in the Chalk where relatively small changes can significantly affect the low effective porosity. Figure 6.4 (Reeves, 1979) was used to give an initial estimation of the Chalk porosity. For the surface chalk, with a permeability of 35 m/day and discontinuity spacings between 60 and 200 mm, an effective porosity of 0.03 to 0.008 is indicated. For the base chalk, with a permeability of 2 m/day and similar discontinuity spacings, an effective porosity of 0.01 to 0.004. Johnson (1994) indicates that the effective porosity of a fine to medium gravel is 0.25.

Simple calculations were used to assess the likelihood of saline intrusion in each of the aquifer layers. It was assumed that the head drop between the Thames boundary (0.5 m OD) and the outside the diaphragm wall is 8.5 m over a distance of 1200 m.

- For the surface chalk, if $\theta = 0.01$ and $k = 35$ m/day, then $t = 48$ days.
- For the gravels, if $\theta = 0.25$ and $k = 120$ m/day, then $t = 353$ days.
- For the base chalk, if $\theta = 0.005$ and $k = 2$ m/day, then $t = 424$ days

The results demonstrate the potential for rapid migration of contaminants in the upper layers of the Chalk which is exacerbated during construction dewatering by steep hydraulic gradients.

The calculations assume a reasonably high steady-state drawdown and therefore underestimate the travel time. As the calibration of the *MODEL CT* was to be highly sensitive to the effective porosity of the surface chalk and transition zone, a sensitivity analysis was made using the particle tracking code MODPATH (Pollock, 1990). Figure 6.5 shows the starting locations of 8 particles, offset from the model boundary by approximately 150m. Particles 5, 6 and 8 are the first to arrive at the excavation as they

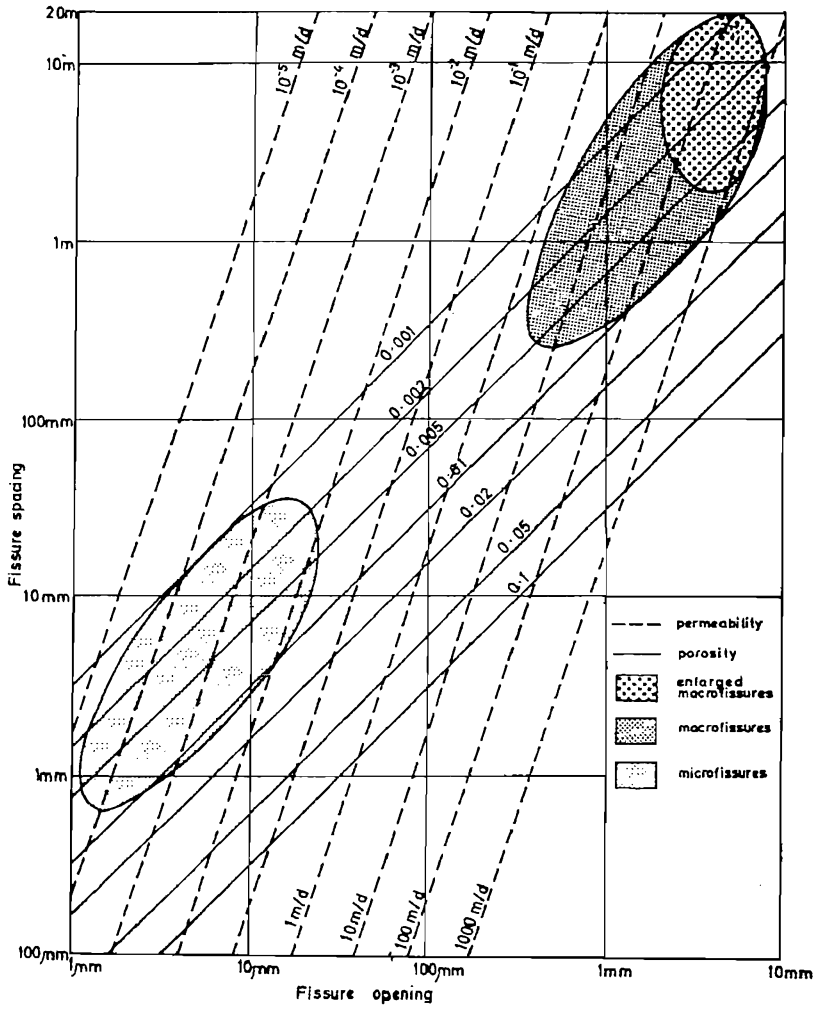

Figure 6.4: *Fissure openings, spacings, permeability and effective porosity relations for the Chalk (Reeves, 1979)*

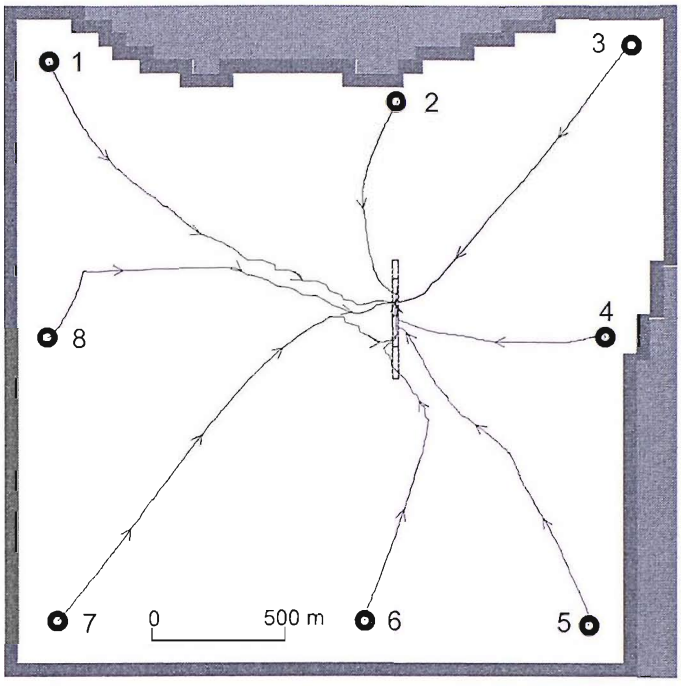

Figure 6.5: *Particle starting locations and flowpaths in model layer 3. Flowpaths are shown after 500 days and θ of the surface chalk/transition zone is 0.03*

become channelled within the high permeability zone (Figure 6.6). Assuming the high permeability zone consist of closely spaced fissures and has a permeability of 4000 m/day, an effective porosity of 0.1 can be estimated from Figure 6.4. Using Equation 6.1, for a head drop (H) of 6 m along a flowpath between the landward boundary and the excavation with a distance of 1500 l, the estimated travel time through high permeability zone is just 7.8 days. This implies that a zone of high permeability Chalk can significantly increase the speed of contaminant migration. Furthermore, it increases the risk that contaminants passing through the aquifer may go unnoticed if the frequency of monitoring is fortnightly or monthly.

Figure 6.6 indicates that a saline front passing through surface chalk layer (from particle locations 2, 3 and 4), will breakthrough at the excavation between 200 and 465 days for the porosities of 0.008 and 0.03. These time are consistent with those suggested by Figure 6.3. Longer travel

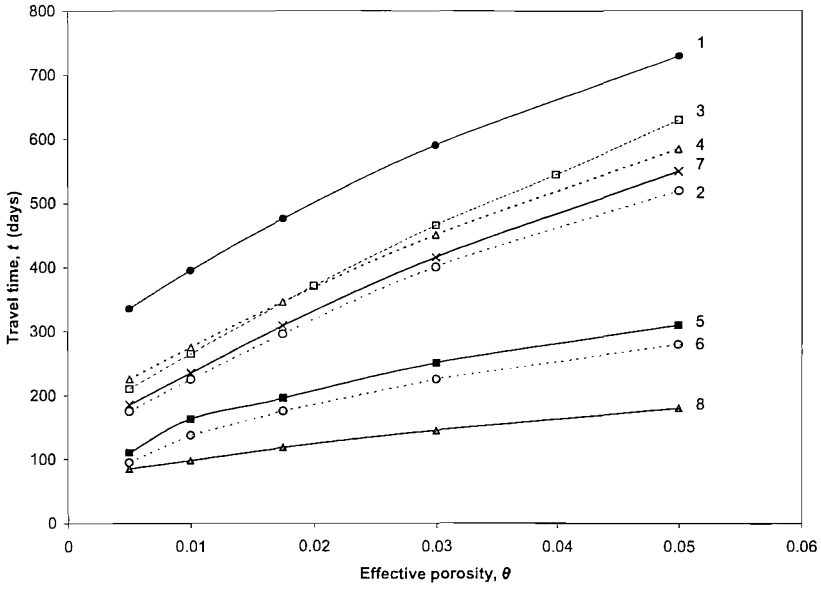

Figure 6.6: *Travel times for contaminant advection through Layer 3 of the model at different effective porosities of the surface chalk/transition zone. The starting locations of particles are shown in Figure 6.5*

times are predicted for groundwater from location 8, because the recharge from the landward boundary (L1) is very low (see §4.4.4). Further MODPATH simulations indicated that the breakthrough of the saline fronts within the gravel and base chalk strata did not occur within the 750 days period represented by the model.

6.3.3 Chloride results

Chloride transport was simulated using the initial concentration distribution set A. No allowance was made in the model for variations in density of the groundwater. Based on the baseline measurements and analysis, the Thames boundary represented a continuous sources loading at a constant concentration of 5700 mg/l; a constant concentration of 85 mg/l was applied for the landward boundary. The model was calibrated by trial-and-error by adjusting the effective porosities to allow a match of the calculated and measured concentrations of groundwater abstracted at the excavation. The best fit was achieved using the porosity values listed in

Table 6.4: *Porosities values used for the calibrated* MODEL CT

Zone	Effective porosity, θ
Alluvium	5
Terrace Gravels	0.25
Surface chalk	0.0175
Transition zone	0.0175
Base chalk	0.008
High permeability zone	0.1

Table 6.4. Choosing dispersivity values for use in field-scale transport simulations is inherently difficult (Zheng, 2002). Values of dispersivity are generally dependent upon the scale of testing; Gelhar, Welty and Rehfeldt (1992) indicates that values of longitudinal dispersivity(α_L) of 10, transverse horizontal dispersivity (α_{TH}) of 0.1 and transverse vertical dispersivity (α_{TV}) of 0.01 are appropriate for the current model area. Figure 6.7 suggests that the model is relatively insensitive to the dispersivity value taken, although at lower dispersivities there is greater variation along the overall trend line caused by sharper concentration fronts.

Figures 6.8 and 6.9 show that the contaminant model could represent the general trends adequately, but could not simulate small variations resulting from fluctuations in well performance and tidal influences. It is evident that there were significant variations, of up to 1000 mg/l, in the concentrations of individual wells located at spacings or approximately 10 m. These localised variations occur because a zone of transition between the saline and freshwater groundwater is formed about the excavation. Figure 6.12(d) shows the development of the diagonal transition zone in the surface chalk layer, which is influenced by the approximately L-shaped Thames boundary. The calculated data suggests that the initial interpretation of the Cl record (§6.3.1)is not accurate and implies that it is not suitable to group the well data together as presented in Figure 6.3.

Sufficient data were available to allow the Cl concentration profile

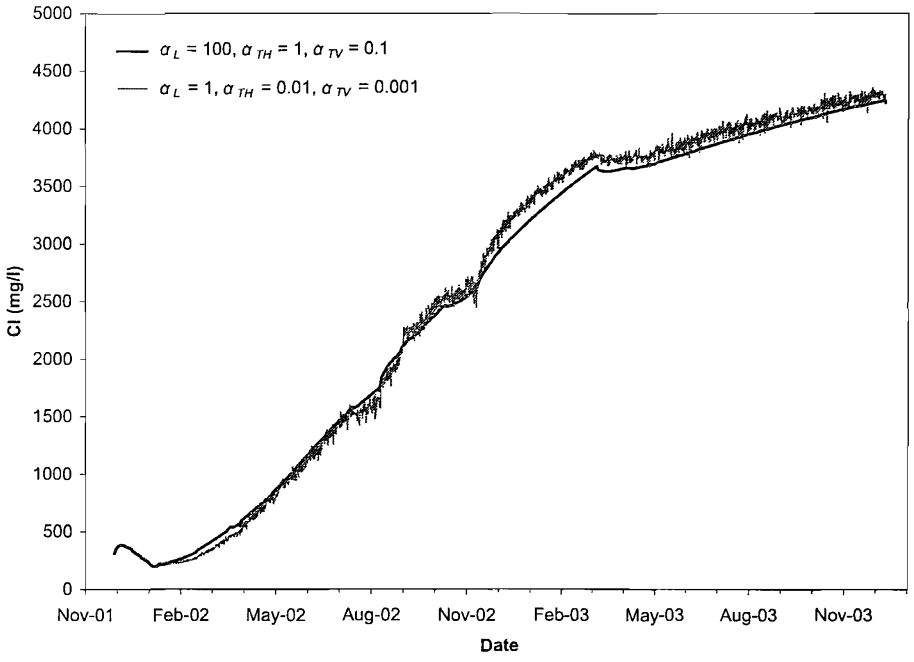

Figure 6.7: *The effect of dispersivity on the calculated chloride concentrations of well 23*

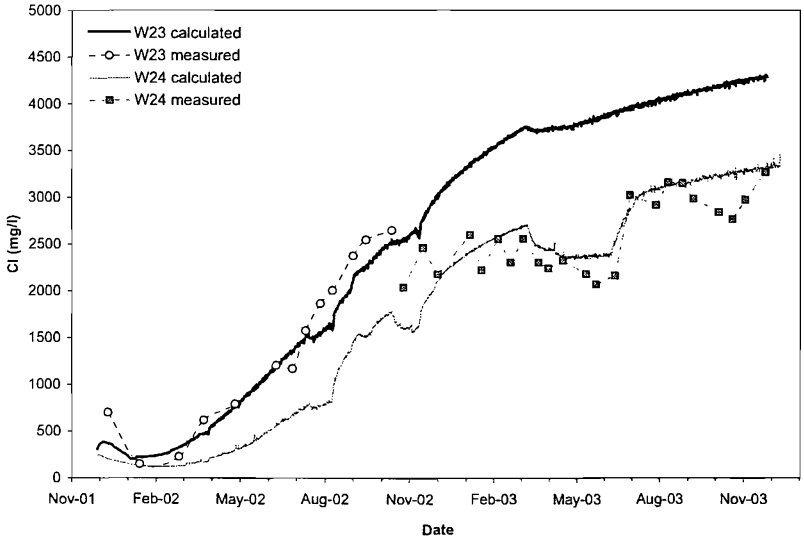

Figure 6.8: *Comparison of measured and calculated chloride concentrations of groundwater abstracted from cell SCC2*

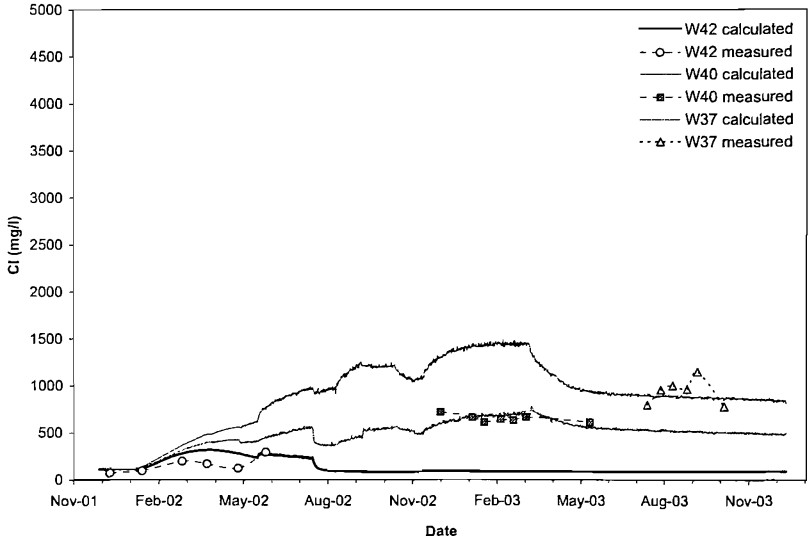

(a) Wells W42,W40 and W37

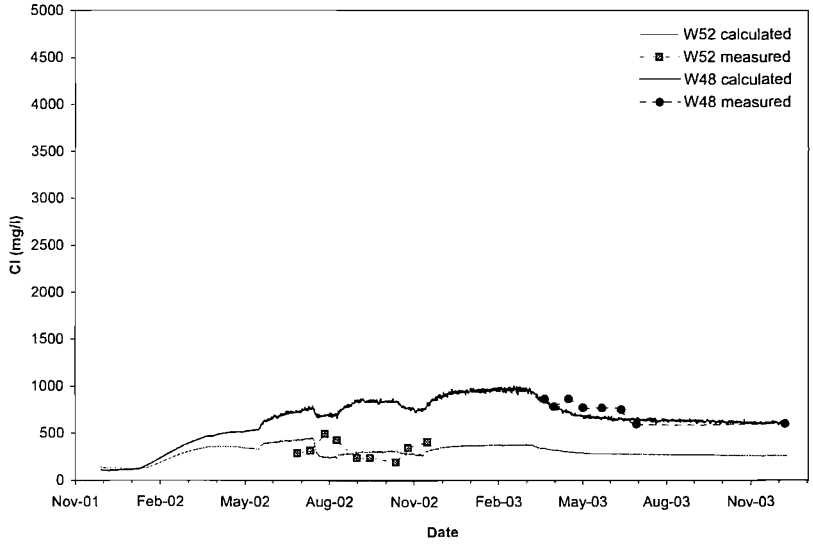

(b) Wells W52 and W48

Figure 6.9: *Comparison of measured and calculated chloride concentrations of groundwater abstracted from cell SRC2+SRC3*

along the length of the excavation to be matched for the first 5 months of dewatering (Figure 6.10). Cl concentrations were generally higher towards the deeper end of the excavation. However, this does not imply that there is increase in salinity caused by depth, instead it is a consequence of the flow pattern with freshwater from the south being channelled towards the shallow end of the excavation by the high permeability zone.

Figures 6.11 and 6.12 show the different migration rates of the saline front for each strata. As expected, the rate of migration was greatest in surface chalk; by 10th April 2003, $t = 500$ days, concentrations at the centre of the excavation were 4000 mg/l for the surface chalk layer, but only 2000 mg/l for the gravel and the base chalk layers (Figure 6.12). Vertical movement of saline waters between layers can be limited by the predominance of bedding plane fissures (implying anisotropic permeabilities) in the Chalk (Lloyd, Howard, Pacey and Tellam, 1982). The lack of monitoring wells of variable depths between the excavation and Thames boundary made it difficult to validate the advancement of the saline front and the apparent variation with aquifer depth. For each layer the advance of the saline front is quickest to the eastern side and northern end of the excavation with slower migration to the north-eastern corner; the relative importance of corner effects during flow towards an excavation is discussed by Powrie and Preene (1992).

Figure 6.13 compares the calculated and measured Cl concentrations at selected monitoring wells screened in the surface chalk. A very close fit to the measured data was achieved for monitoring wells located within the diagonal zone of transition (NBH1, NBH2 and NBH6). After 6 months of dewatering, the main contractor (in consultation with the Environment Agency) reviewed the monitoring data, assessed that there was insignificant change in the groundwater quality, and took the decision to downsize the site monitoring programme. Therefore, data are not available for some monitoring wells after July 2002. Figure 6.13 implies that this decision was premature; A MODPATH simulation for the surface chalk layers indicates particles representing the saline front at location 6 (Figure 6.5) would have only moved 200 m downgradient in the first 6 months of dewatering.

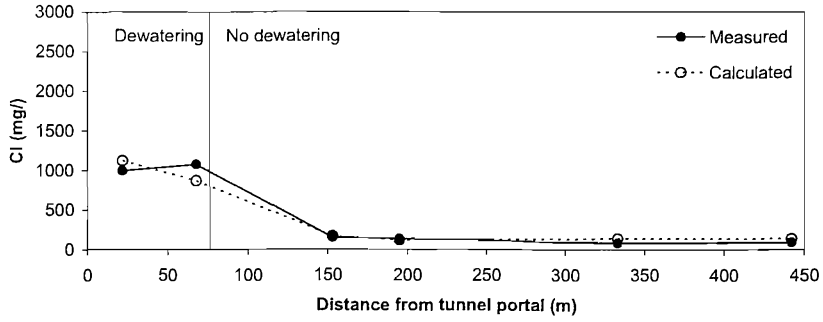

(a) 16th January 2002

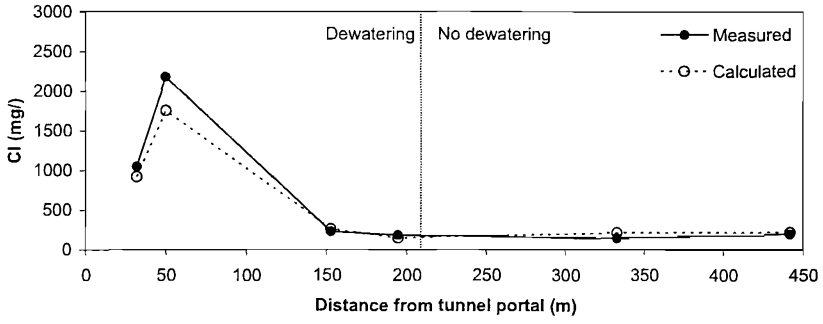

(b) 28th February 2002

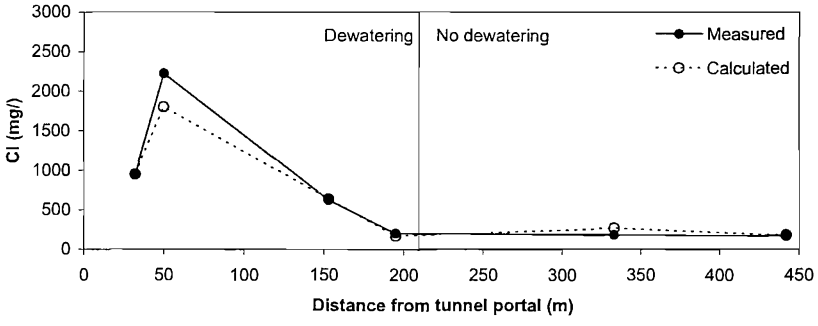

(c) 28th March 2002

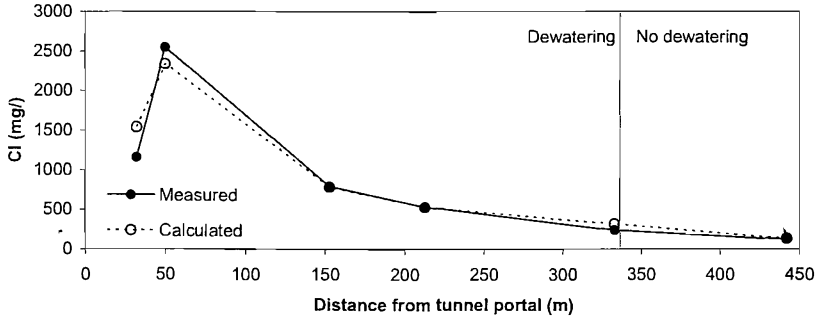

(d) 30th April 2002

Figure 6.10: *Chloride profiles during the early stages of dewatering*

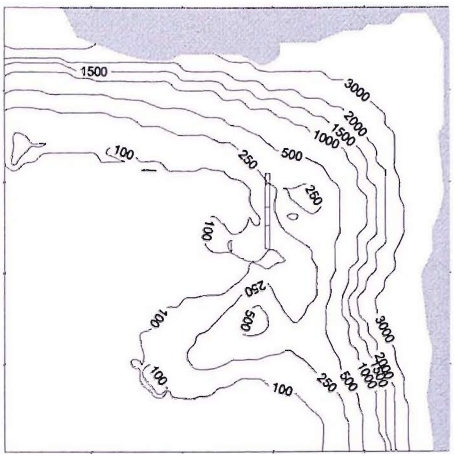

(a) Gravel: 26th Nov 2001

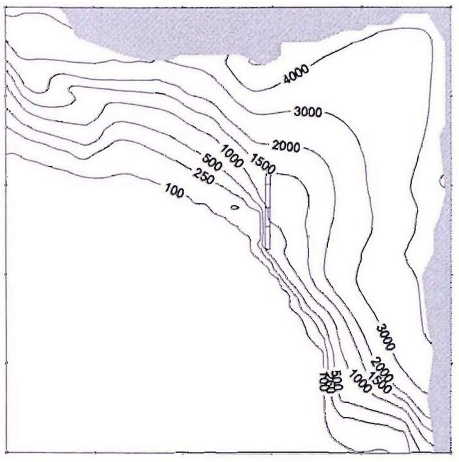

(b) Gravel: 3rd March 2002

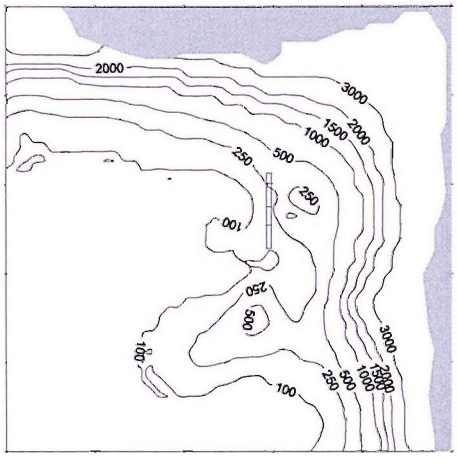

(c) Surface chalk: 26th Nov 2001

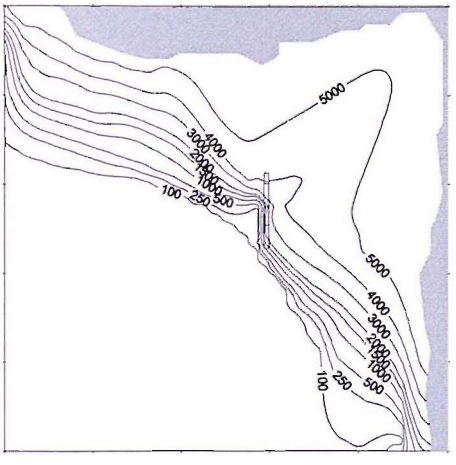

(d) Surface chalk: 3rd March 2002

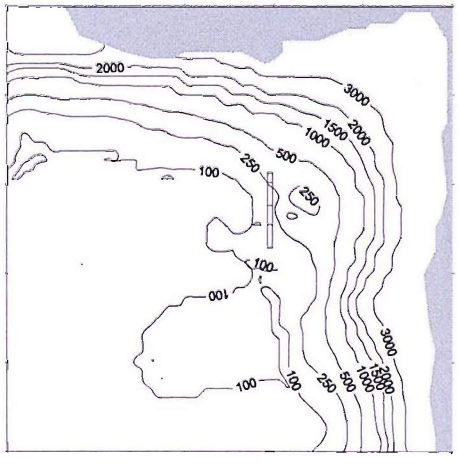

(e) Base chalk: 26th Nov 2001

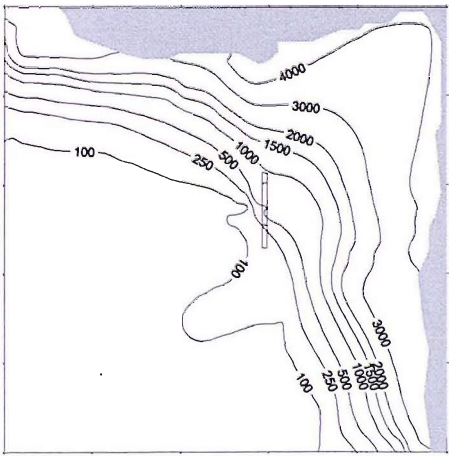

(f) Base chalk: 3rd March 2002

Figure 6.11: *Contours of calculated chloride concentration (mg/l) on 26th November 2001 (t = 0 days) and 3rd March 2002 (t = 250 days)*

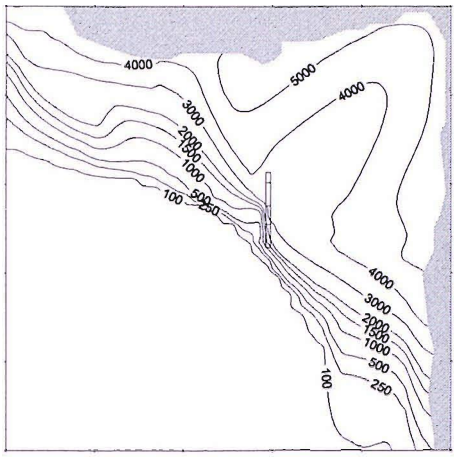

(a) Gravel: 10th April 2003

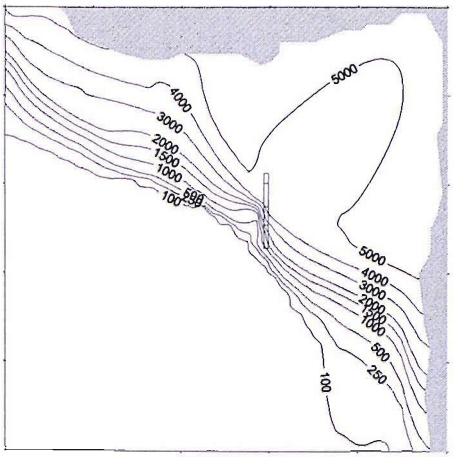

(b) Gravel: 16th Dec 2003

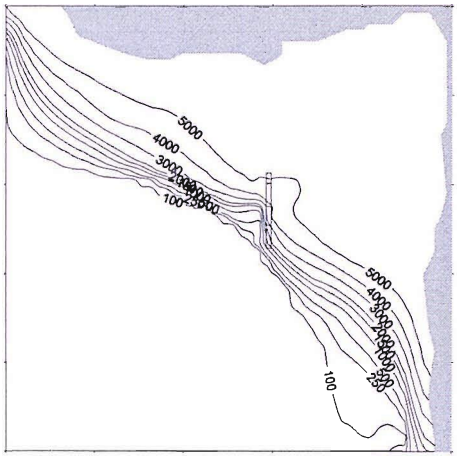

(c) Surface chalk: 10th April 2003

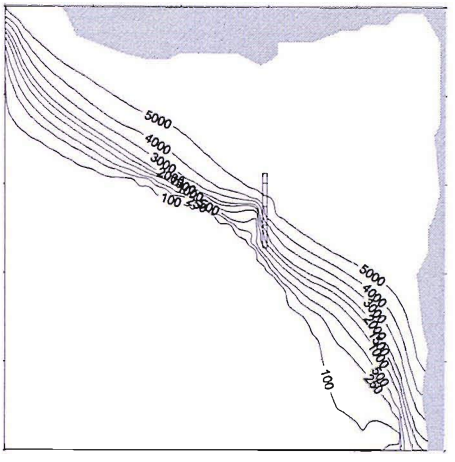

(d) Surface chalk: 16th Dec 2003

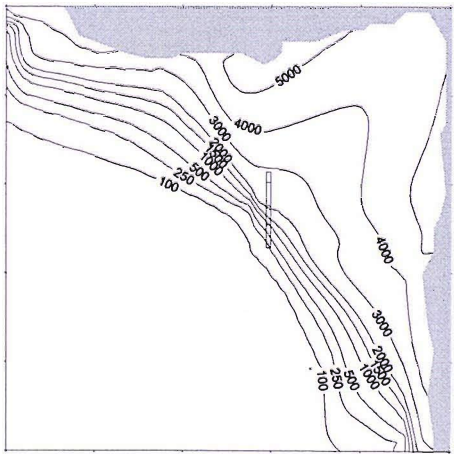

(e) Base chalk: 10th April 2003

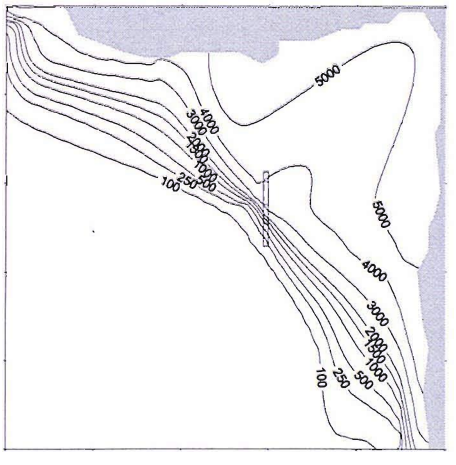

(f) Base chalk: 16th Dec 2003

Figure 6.12: *Contours of calculated chloride concentration (mg/l) on 10th April 2003 (t = 500 days) and 16th Dec 2003 (t = 750 days)*

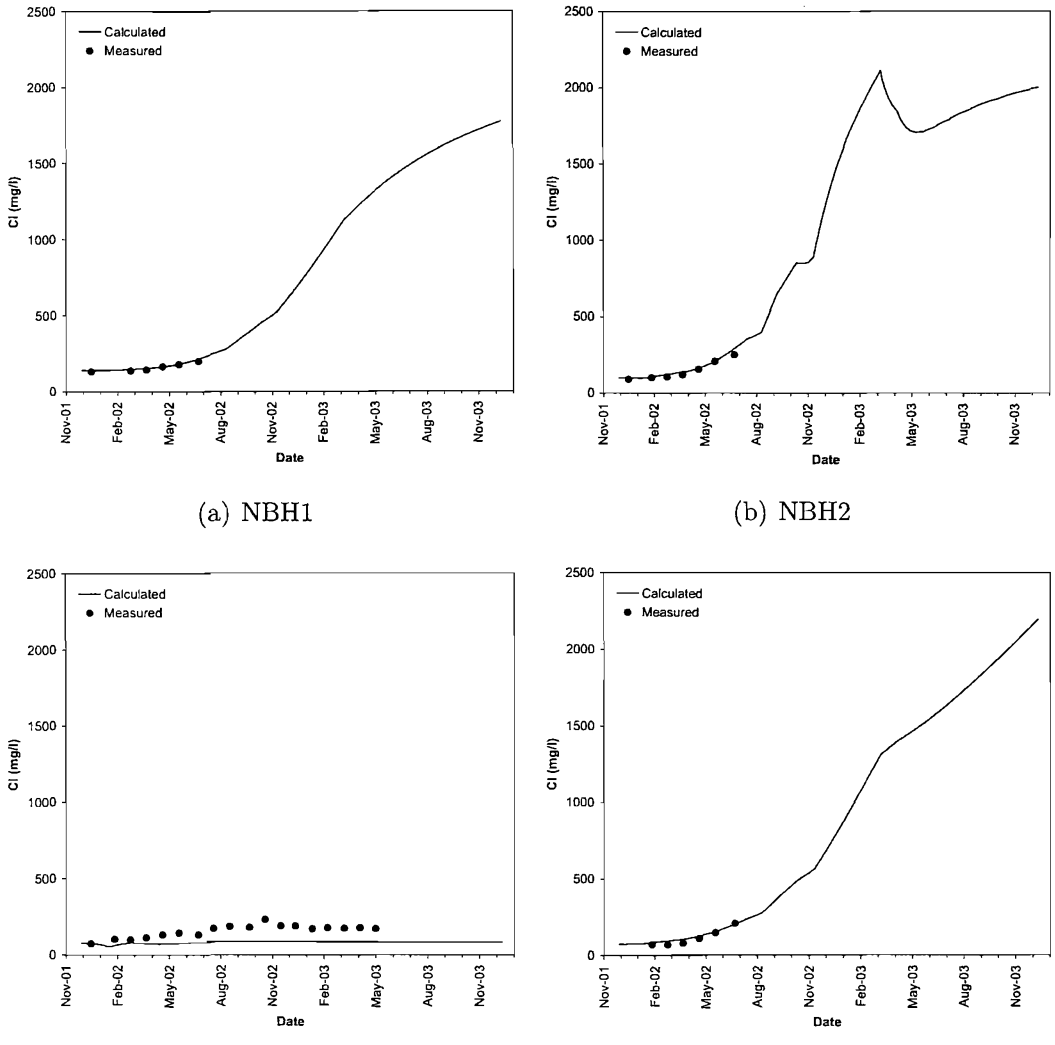

(a) NBH1

(b) NBH2

(c) NBH3

(d) NBH6

Figure 6.13: *Measured and calculated chloride concentrations at selected monitoring wells screened in the Chalk*

Generally, it was hard to match the calculated and measured concentrations of the monitoring wells, as shown in Figure 6.14. This was partly because it was not possible to replicate exactly the small variations in groundwater flow pattern as the dewatering system was fine tuned. In addition, the boundary concentrations were kept constant whereas the quality of the inflowing groundwater would have been more variable with both space and time. The variability of the Thames boundary conditions is indicated by Figure 6.15, where the concentrations of the monitoring wells screened in the gravels are shown close to the boundary. At monitoring well SA5981, the calculated concentrations are representative of the measured data during May 2002 and May 2003, but are significantly greater during the summer months of 2003. The lower measured concentrations over the summer period are interesting as it was expected that higher concentrations would be observed during the summer months in response to the seasonal variation in the Thames salinity described by Attrill and Power (2000). The response of concentrations in the aquifer may be affected by a lag which reflects the leakage through the bed of the Thames. At SA5983 the measured levels are higher than those at SA5981, indicating that in reality the Thames boundary concentrations may vary around the shoreline. The scatter distribution of measured data points suggests that there is a considerable variation in concentrations over tidal cycle; ideally, the effects to tidal influences on concentrations could have been established prior to dewatering as part of the monitoring programme, although this would be a big undertaking.

6.4 Major ion chemistry

This section examines the concentrations of the major ions of the abstracted groundwater, which can be used to validate the flow pattern indicated by the previous groundwater flow modelling.

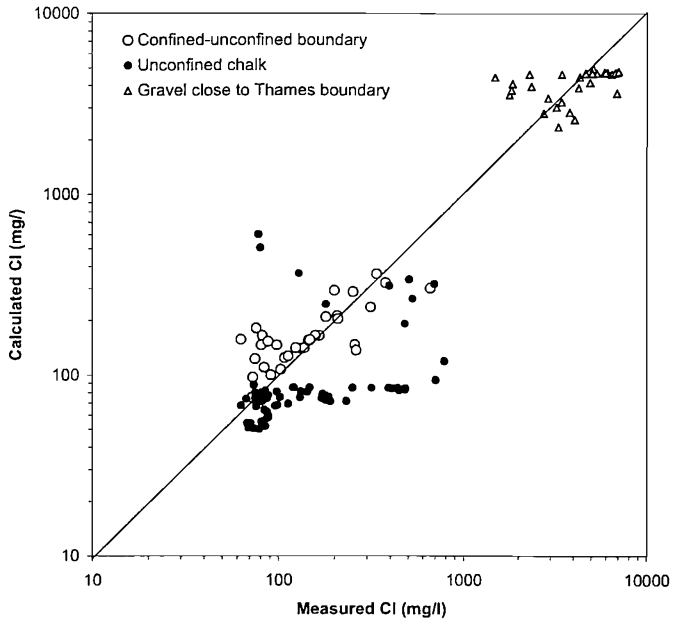

Figure 6.14: *Comparison of measured and calculated chloride concentrations*

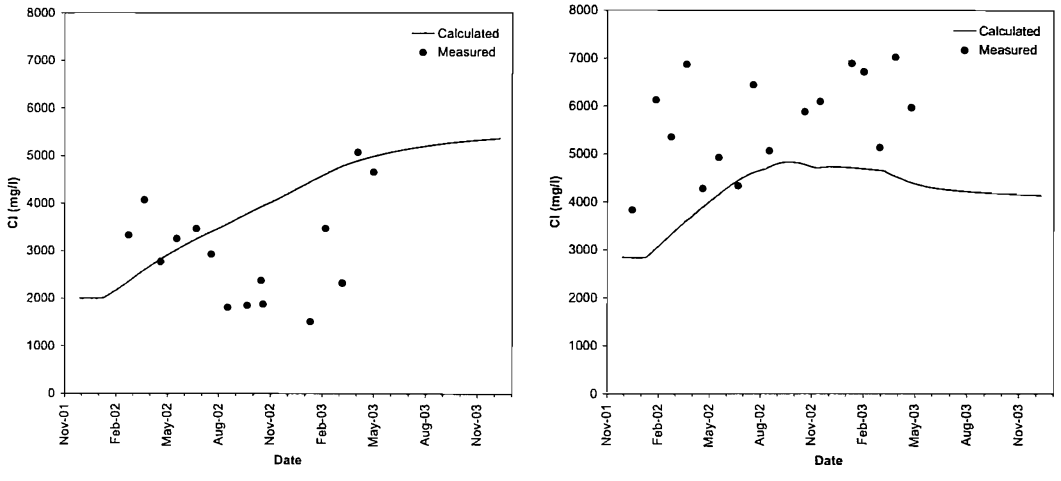

(a) SA5981

(b) SA5983

Figure 6.15: *Measured and calculated chloride concentrations at selected monitoring wells screened in the gravels*

6.4.1 Evidence of ion exchange

The attenuation of solutes as they migrate through an aquifer can take place through dilution, dispersion, degradation and adsorption. Ion exchange is an adsorption process whereby positive ions (cations) are attracted to negatively charged clay-mineral surfaces and are held on these sites. The general ion exchange reaction is expressed as:

$$A^+ + B_{ad} \Longleftrightarrow B^+ + A_{ad} \tag{6.2}$$

Equilibrium is achieved when

$$K_{ex} = \frac{[B^+]N_A}{[A^+]N_B} \tag{6.3}$$

where K_{ex} is the thermodynamic equilibrium constant and N_A and N_B are the mole fractions of the adsorbed ions in the solid phase. The relative strength of adsorption of cations is uncertain, with different version available. Ward and Robinson (2001) suggest a decreasing affinity for cation exchange as follows:

$$Al^{3+} > H^+ > Ca^{2+} > Mg^{2+} > K^+ > NH_4^+ > Na^+ \tag{6.4}$$

This sequence indicates that as water moves through an aquifer, calcium ions would be adsorbed to clay minerals and sodium, potassium and magnesium ions would be released into solution. However, observations of reverse ion exchange are common during the encroachment of modern saline groundwaters in coastal aquifers caused by abstraction. A study by Howard and Lloyd (1983) of the geochemical evolution of saline groundwater in the Chalk aquifer of Lincolnshire and Humberside showed that the exchange between calcium and sodium contributed significantly to the enrichment of calcium. Similar observations were made for the saline intrusion into the Chalk of Essex (Hoather, 1958), although normal ion exchange was found by Elliot et al. (2001) in the Yorkshire Chalk aquifer. Typically older, deeper saline water is not enriched with respect to calcium, nor depleted with respect to the other major cations. In the Chalk, the adsorption sites will be be concentrated on clay minerals on the surface of fissures.

Figure 6.16 compares the concentration of the major ions to the conservative chloride ion for the groundwater abstracted by the dewatering system. The hypothetical mixing of the saline Thames water and clean freshwater is represented by the plotted line. The y-intercept represents the base concentration of the ion in clean fresh chalk groundwater; these are comparable to the concentrations of natural chalk groundwater that are discussed by (Edmunds, Shand, Hart and Ward, 2003). The Thames concentration is based on the data shown in Figure 5.6, with the exception of sodium and potassium for which the general seawater ion ratio is used (as shown in Table 5.3).

The plots for Ca, K and SO_4 suggest two different groundwater compositions for the groundwater abstracted from the two monitored cells. This reflects the groundwater flow pattern (Figure 4.19(a)), whereby the high permeability intercepted and channelled most of the flow through the landward boundary into the cell SRC2+SRC3, so is close to the typical freshwater composition. In contrast, the flow to the cell SCC2 was approximately a diluted form of the Thames water. Calcium is clearly the exception, as significant enrichment is suggested by Figure 6.16(b) in both cells. Calcium concentrations of groundwater abstracted from the cell SCC2 exceeded 200 mg/l, which is greater than both the baseline concentrations and the measured concentrations of the Thames shown in Figure 5.16. The figures indicate that sodium and potassium concentrations for cell SCC2 were slightly depleted (lower than predicted), which would conform to the understanding of reverse ion exchange in modern saline groundwater in the Chalk. Figure 6.16(c) suggests that magnesium may have taken part in the ion exchange, although the interpretation of the data is strongly dependent on the calculated slope of the mixing line, which is true to a certain extent for all the ions. Sulphate concentrations of groundwater from cell SCC2 were well represented by the mixing line, which indicates that no bacterial sulphate reduction occurs in the anoxic sediments at the bed of the Thames; reduction of sulphate to sulphide was significant during saline intrusion into the Mersey Basin sandstone aquifer (Barker, Newton, Bottrell and Tellam, 1998).

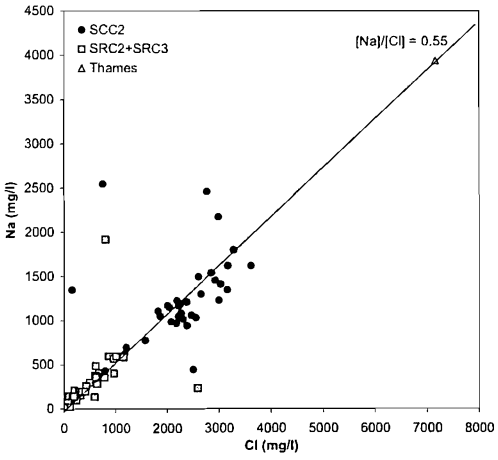

(a) Sodium

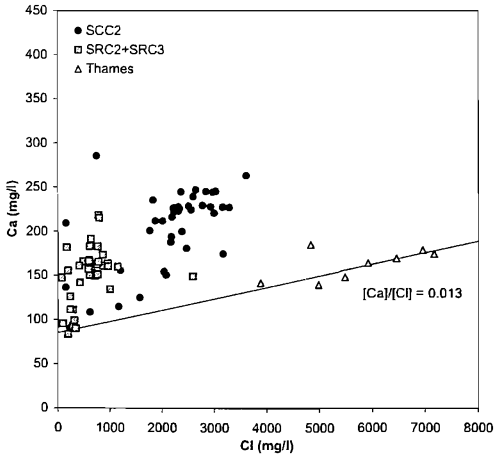

(b) Calcium

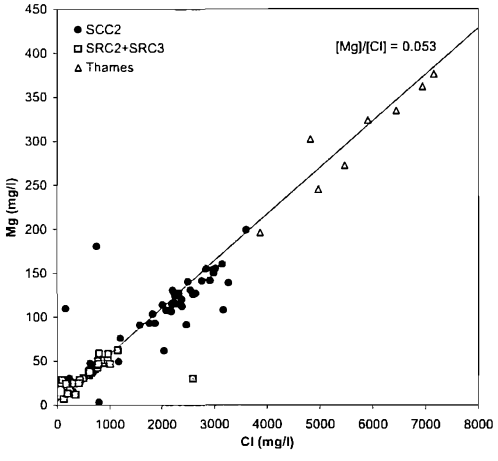

(c) Magnesium

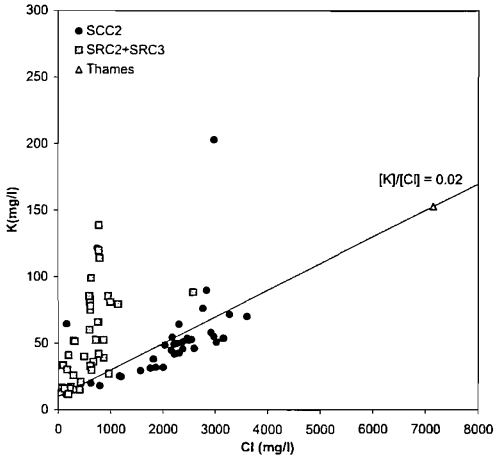

(d) Potassium

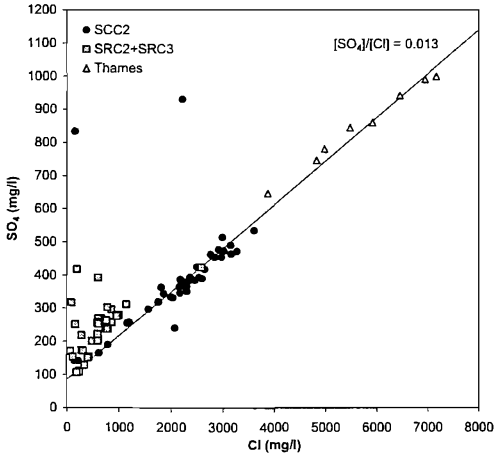

(e) Sulphate

Figure 6.16: *Dilution diagrams for abstracted groundwater. The line is the expected mixing line of fresh and saline waters*

An alternative explanation for the enriched calcium concentration could be the dissolution of calcite. If the saline water from the Thames is undersaturated with respect to calcite, dissolution will take place as the saline water passes through the Chalk aquifer, as described in Equation 3.9 (Plummer, 1975). Barker et al. (1998) suggest that significant calcite dissolution can take place in the oxic zone of estuary sediments where high biological productivity supports a high partial pressure of carbon dioxide (pCO2). However, the low calcium concentrations of the baseline gravel brackish groundwater (Figure 5.16) suggests that the enrichment occurs after the water has entered the aquifer, rather than during the infiltration through the Thames bed.

6.4.2 Modelling ion exchange during saline intrusion

The evolution of saline groundwater between the Thames boundary and the cell SCC2 was investigated using the contaminant transport model. The initial concentrations of each ion were applied based on the set A distributions (§5.4.3). Initially, the calibrated model was used to calculate concentrations by assuming the ions behaved conservatively. Where the model overpredicted the concentrations of abstracted groundwater, it was necessary to apply a retardation factor (R) to simulate the depletion of ions due to adsorption. It was assumed that the relationship between the dissolved and sorbed concentration was described by the linear isotherm, which assumes that the solid matrix has an infinite sorption capacity. This form of retardation is expressed in Equation 5.15. The lack of monitoring well data meant that it was not possible to distinguish between the retardation for the different strata. Instead a general retardation factor was applied to describe the adsorption for the aquifer as a whole. The applied boundary concentrations and the retardation factors (R) are shown in Table 6.5.

The modelling results confirm the understanding of the ion exchange processes that took place during the intrusion of saline water from the Thames boundary. The concentrations of abstracted groundwater are

Table 6.5: *Boundary concentrations and retardation factors used to achieve a good fit of measured and calculated concentrations when modelling saline intrusion. *Enrichment of Ca could not be simulated in the model.*

Contaminant	Thames boundary (mg/l)	Landward boundary (mg/l)	Retardation factor R
Cl	5700	85	1
Na	3125	55	2.95
SO_4	810	120	1
K	115	15	5.80
Mg	300	20	1
Ca*	150	140	-

shown in Figures 6.17 to 6.21. Both SO_4 and Mg behaved conservatively, whereas Na and K was attenuated to different degrees. The modelling suggests a greater attenuation of K ($R = 5.80$) than Na ($R = 2.95$), consistent with a greater affinity for cation exchange sites for K (Equation 6.4). Retardation factors vary on a site by site basis depending on the aquifer material, concentrations and the groundwater flow. For example, DeSimone, Howes and Barlow (1997) found that $R = 1.8$-5.2 for the transport of a waste-water contaminant plume through a sandy and gravel aquifer. In addition to the attenuation in the aquifer, the calculated retardation factors may account for an attenuation of concentrations as the Thames water infiltrates through the bed into the aquifer.

Figure 6.21 shows that the measured concentrations of Ca exceeded those calculated by the model. It was not possible to simulate the enrichment of Ca, but it is apparent that the Ca concentrations might have been increased by a factor of approximately 2 to 2.5 due to ion exchange and/or calcite dissolution.

The contaminant model is unable to replicate the variable Na and K concentrations that were measured at W24. These appear in Figures 6.19(b) and 6.20 as spikes in the concentrations. Similar spikes of the same magnitude were not observed for the conservative ions Cl and SO_4,

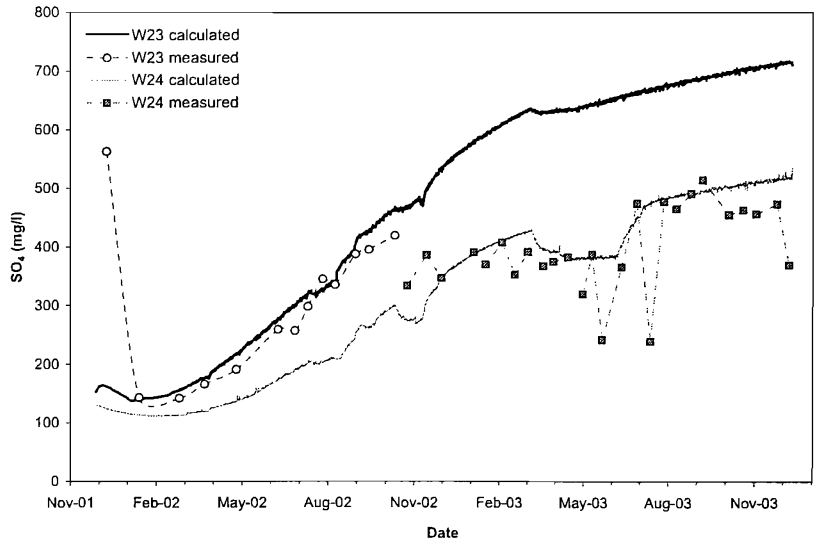

Figure 6.17: *Comparison of measured and calculated sulphate concentrations of groundwater abstracted from cell SCC2. R = 1*

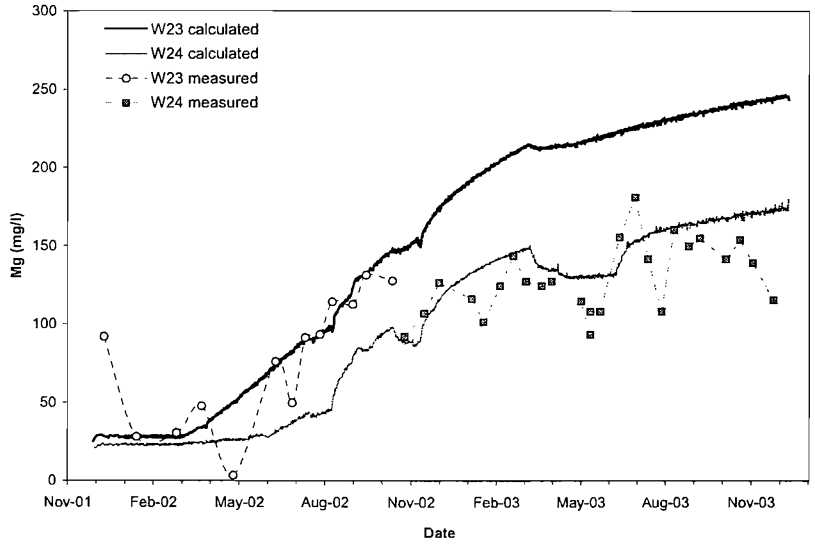

Figure 6.18: *Comparison of measured and calculated magnesium concentrations of groundwater abstracted from cell SCC2. R = 1*

therefore it is unlikely that the spikes represent evidence of cement kiln dust leachate. Instead, they may reflect variations in the degree of ion exchange taking place.

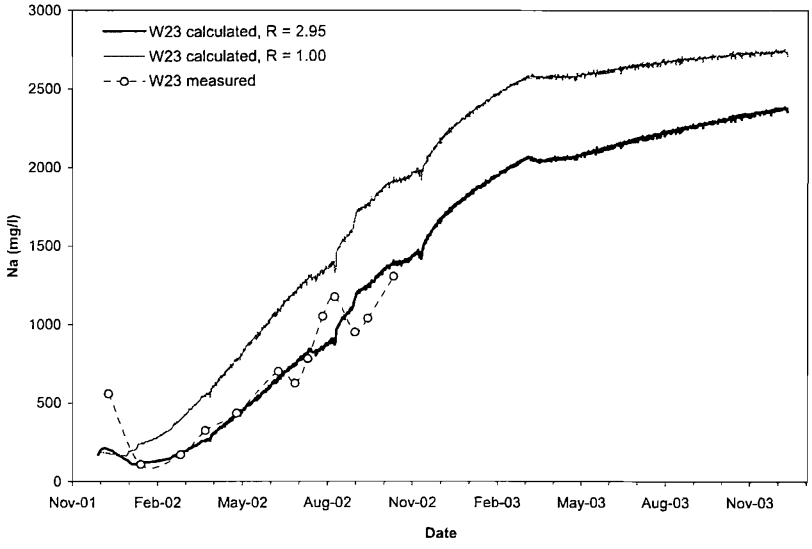

(a) Well W23

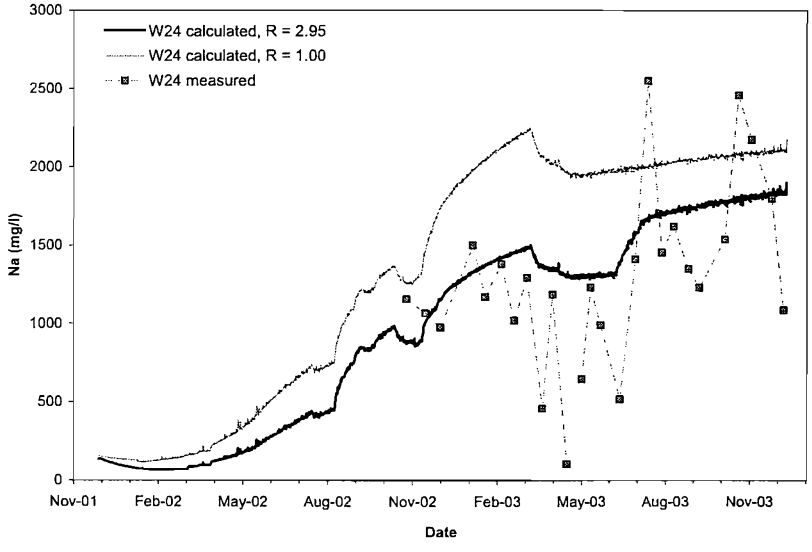

(b) Well W24

Figure 6.19: *Comparison of measured and calculated sodium concentrations of groundwater abstracted from cell SCC2. R is the retardation factor*

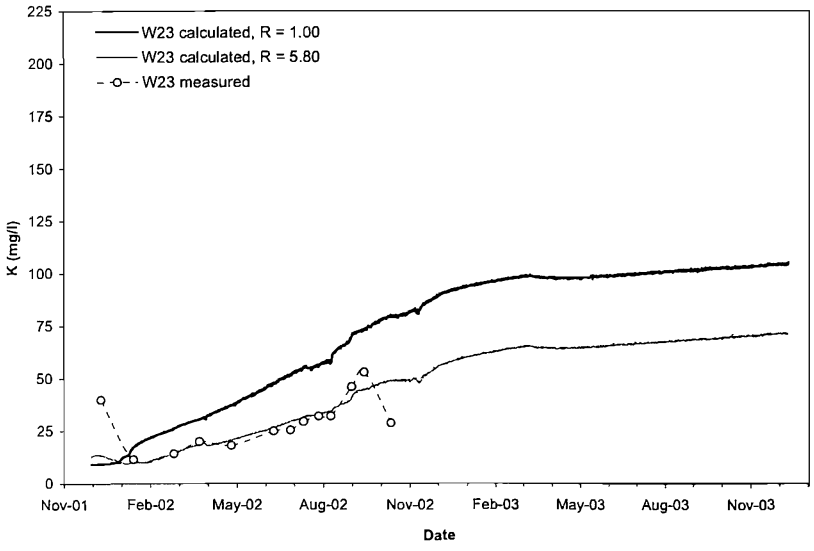

(a) Well W23

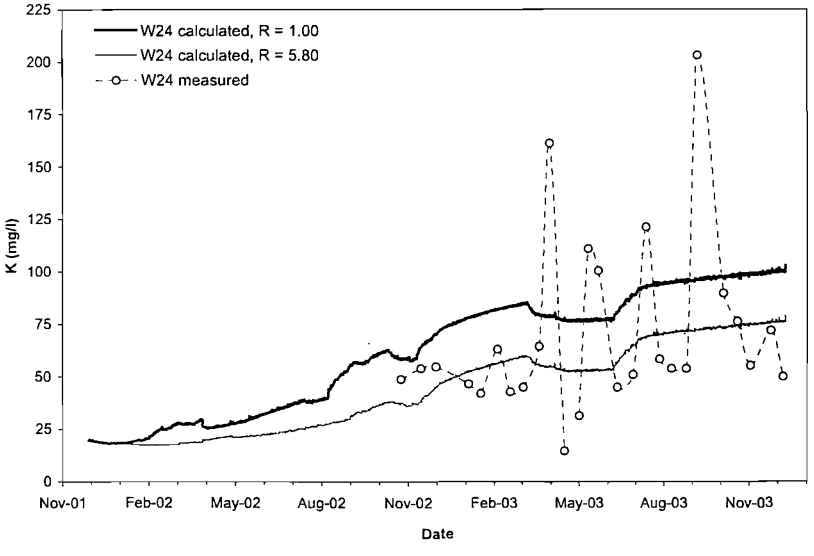

(b) Well W24

Figure 6.20: *Comparison of measured and calculated potassium concentrations of groundwater abstracted from cell SCC2. R is the retardation factor*

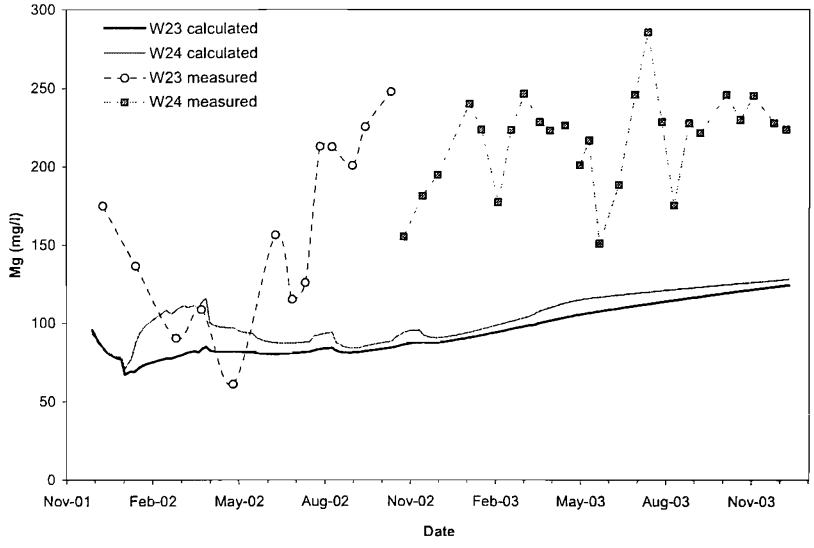

Figure 6.21: *Comparison of measured and calculated calcium concentrations of groundwater abstracted from cell SCC2. R = 1*

6.5 Leachate migration

6.5.1 Migration of leachate from landfill C

A study was made to determine the fate of cement kiln dust (CKD) leachate migrating from the unlined landfill C. Figure 6.22 shows the flowpaths of particles that were tracked from the landfill using MODPATH. Leachate migrating by advection only would have reached the excavation between and 16th February 2002 and 20th March 2002 (82 to 114 days) for an effective surface chalk porosity of 0.0175. Pumping in the cell SRC2+SRC3 did not start until the 1st May 2002, hence the particles are captured by the pumping wells in cell SCC3+SRC1. However, the leachate plume did pass by well W42, which was monitored during this period (samples were drawn using a Waterra pump).

Figure 6.16 indicates that concentrations of SO_4 and K in the groundwater abstracted from cell SRC2+SRC3 were greater than expected for a dilute solution of saline groundwater. It was established in Chapter 5 that SO_4 and K were the primary indicators of groundwater contaminated by CKD. The high Ca concentrations of the abstracted groundwater water

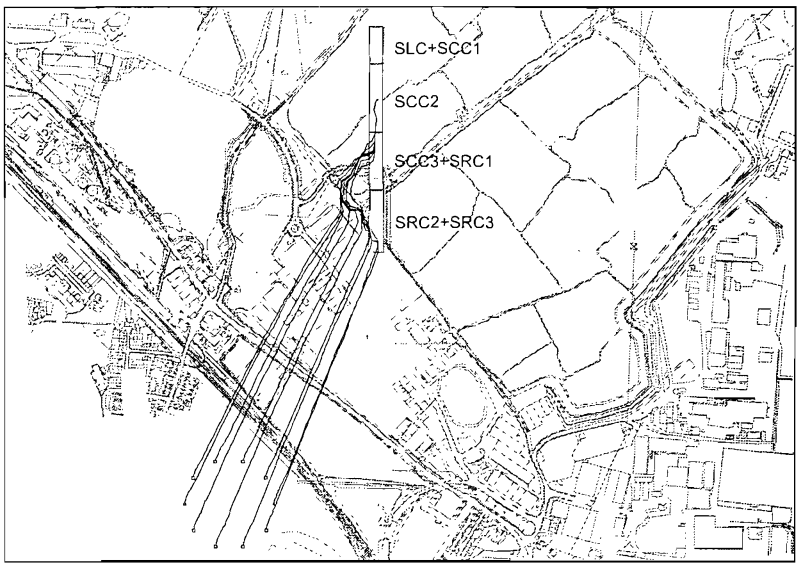

Figure 6.22: *Flowpaths between landfill C and the excavation calulated using MODPATH*

are not associated with CKD leachate, but may be explained by ion exchange or calcite dissolution, as discussed previously. The pH levels of abstracted groundwater exceed the normal baseline levels (Figure 6.23, but not significantly, indicating that a strong plume of CKD leachate was not detected at cell SRC2+SRC3. A small peak in both COD and BOD occurred on 30th April 2002, possibly as a result of leachate (Figures 6.24 and 6.25). The high levels in the initial samples are unreliable because wells were not developed and the purge volumes were inadequate to remove stagnant water.

Modelling was carried out to look in detail at the transport of SO_4 and K from the landfill with the initial concentrations applied using the distribution set A. The boundary conditions were set as listed in Table 6.5. To minimise the computational effort required in the modelling, only the first 500 days of dewatering were simulated. It was assumed that the leachate was only present in layer 1 of the model (+3 to -10 m OD), because of the shallow depth of the landfill. A new concentration distribution was created for the other layers by omitting the monitoring well SA1586.

Figure 6.26 compares the measured potassium concentrations of

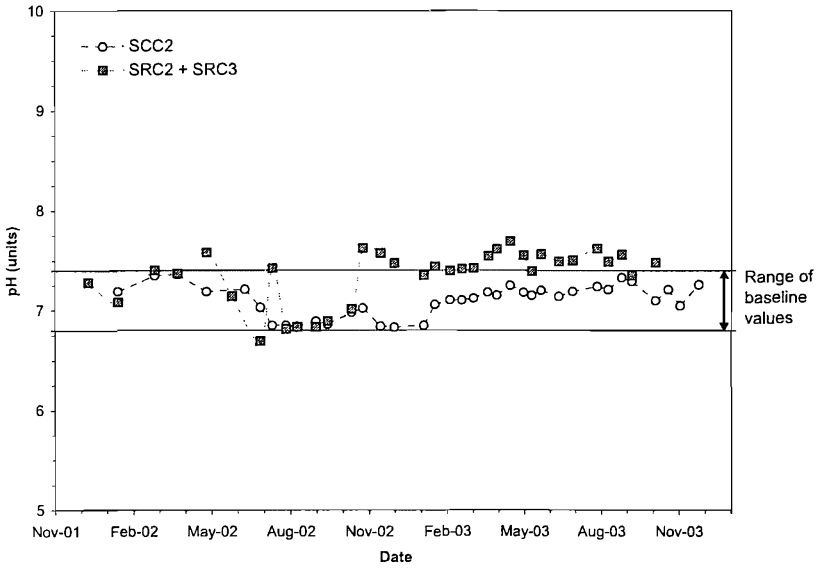

Figure 6.23: *Field measurements of pH of abstracted groundwater*

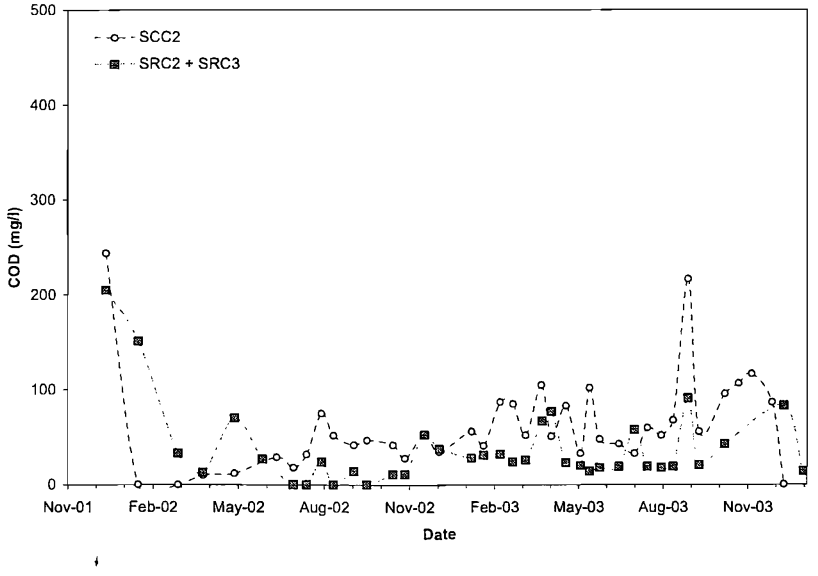

Figure 6.24: *Measurements of COD of abstracted groundwater*

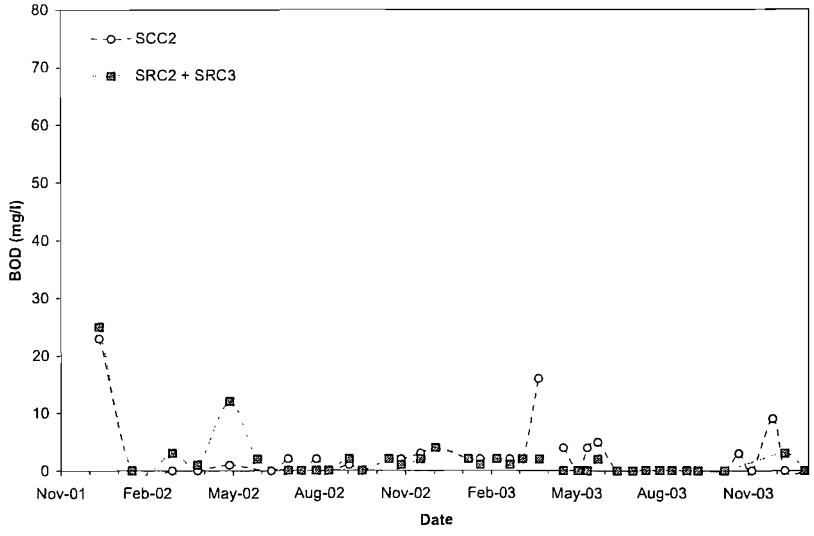

Figure 6.25: *Measurements of BOD of abstracted groundwater*

groundwater abstracted from cell SRC2+SRC3 to the concentrations calculated for an advection-dispersion simulation. A calculated peak concentration of approximately 70 mg/l is evident during April 2002, implying an attenuation of the leachate signal predominantly by mixing with clean freshwater during advection. In the measured data a smaller, later peak occurs during July 2002, which suggests that the attenuation is greater, or perhaps that the leachate remained locked in the pores of the Chalk matrix below the landfill site and therefore could not readily migrate.

In conjunction with the application of a retardation factor, an area of low permeability (0.01 m/day) was created in layer 1 of the model at the site of landfill C. This lower permeability was required to simulate a slow release of leachate from the landfill, which was predominantly above the water table. The fit of the model was improved by applying a retardation factor, $R = 2.3$, uniformly throughout the model account for the observed attenuation (Figure 6.27). The retardation factor is less than the factor calculated during the modelling saline intrusion, suggesting that in reality the influence of ion exchange is variable for different groundwater types and ground conditions across the site.

A good study of leachate migration from landfill site C is hampered by

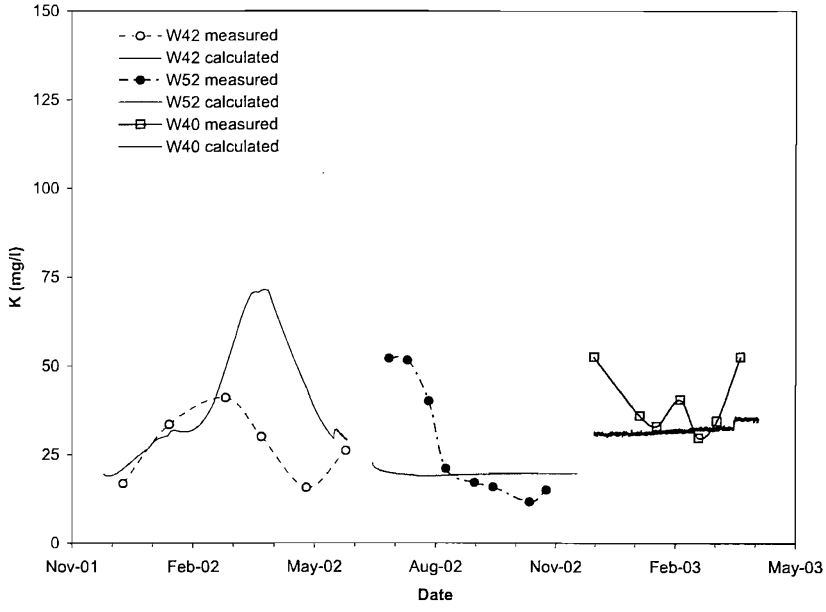

Figure 6.26: *Potassium concentrations in groundwater abstracted from cell SRC2+SRC3. R = 1*

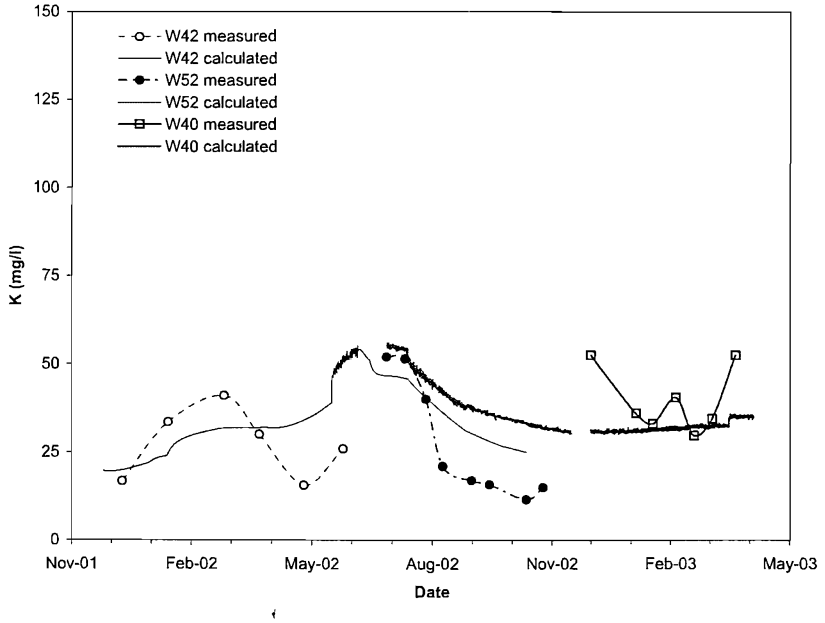

Figure 6.27: *Potassium concentrations in groundwater abstracted from cell SRC2+SRC3. R = 2.3*

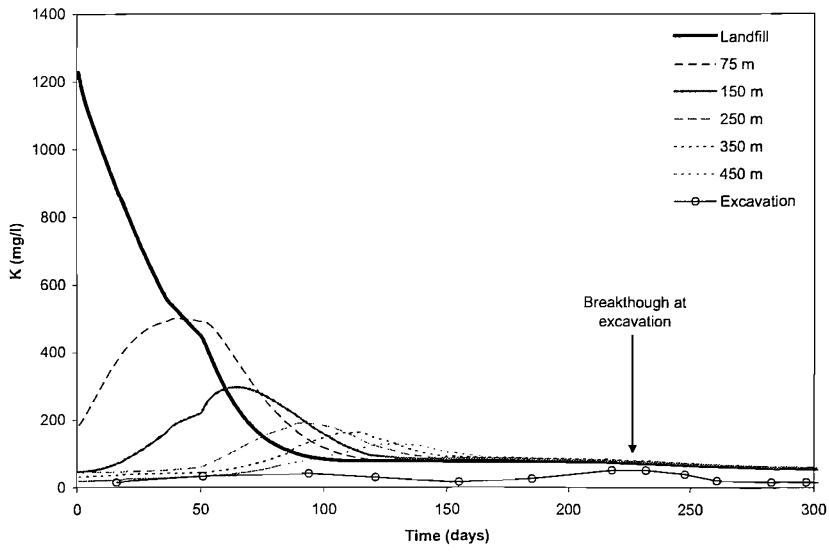

Figure 6.28: *Attenuation of potassium between landfill C and the excavation.* $R = 1$

the lack of groundwater quality monitoring at the source. The monitoring well SA1586 was drilled to a depth of -0.5 m OD (ground level +6.2 m OD), which meant that it was dry during dewatering. A well drilled as a replacement, NBH8 to a depth of -9 m OD did not detect any CKD leachate suggesting that the leachate was only present at very shallow depths. Modelling shows that even when no retardation is assumed, the attenuation of K is still very significant, with the leachate signal reduced to approximately 25% of the source concentration within 150 m of the landfill site (Figure 6.28). This makes detection at the point of abstraction very difficult, especially when there are other sources of the contaminant such as saline intrusion.

Where there is not a constant input of leachate, soils can be cleaned up during construction dewatering caused by freshwater groundwater flowing from a recharge boundary flushing the aquifer. This is likely to have been the case for landfill C.

Figure 6.29 shows a peak concentration of sulphate during February 2002. As SO_4 behaves conservatively there is no retardation and the peak concentration is detected much earlier than for potassium (Figure 6.27). It

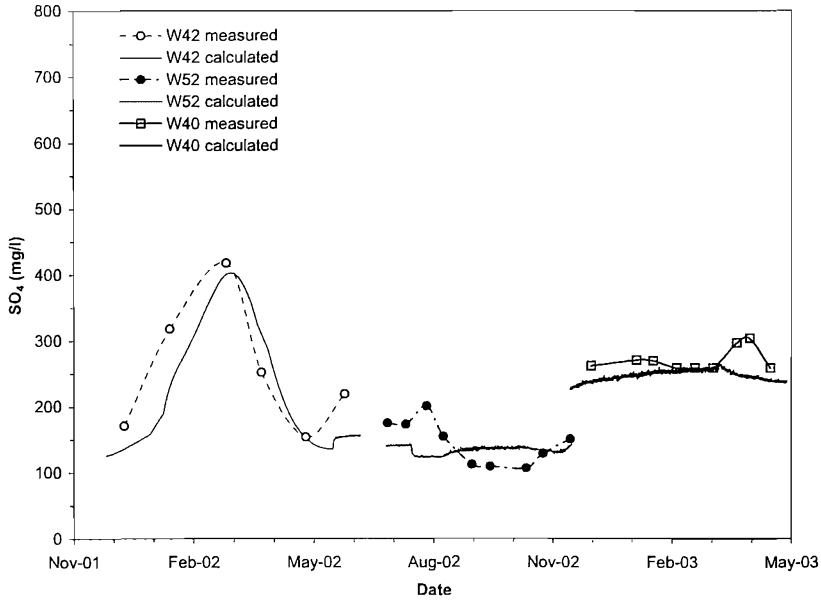

Figure 6.29: *Sulphate concentrations in groundwater abstracted from cell SRC2+SRC3. R = 1.0*

is important to be aware when formulating a monitoring strategy that different contaminants will be retarded at different rates. Unfortunately, published estimates of distribution coefficients (K_d) are few in number and vary with lithology.

6.5.2 Short circuiting

A MODPATH particle tracking simulation was carried out to determine the movement of potentially contaminated groundwater resulting from short-circuit flow within monitoring wells. The model suggested that the contaminated groundwater would have been abstracted in the cell SCC2 (Figure 6.30). The model was run to investigate the migration of Cl, Na, K, SO_4 and NH_4-N using the distribution set B. The boundary concentrations and retardation factors listed in Table 6.5 were applied to the model.

Figures 6.32 to 6.35 show a significant overestimation of the abstracted concentrations. The results imply that the quality of water sampled from monitoring wells installed below an area of waste disposal can be unrepresentative of the true quality of groundwater within the aquifer. Such

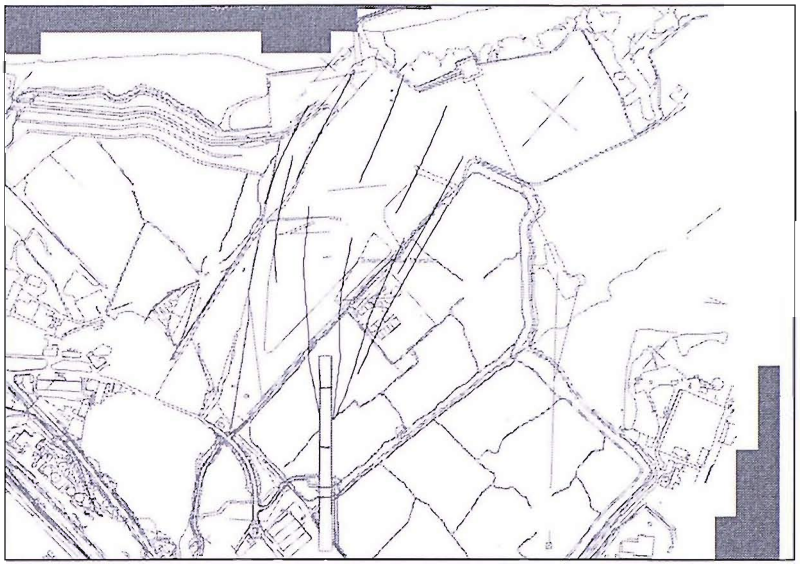

Figure 6.30: *Flowpaths of potentially contaminated groundwater due to short-circuiting*

samples reflected the groundwater quality within the well and the immediately outside the well screen. Small volumes of leachate around the well screen may have migrated during dewatering, but evidence of contaminants in the abstracted groundwater were possibly masked by the effects of saline intrusion. This is an extreme example of how short-circuiting can lead to unrepresentative groundwater samples; it is important to be aware that the influence of short circuiting may be more subtle and therefore harder to distinguish when analysing groundwater quality data.

6.6 Summary

A contaminant transport model was constructed based on the hydrogeology of *MODEL 1*. The effective porosities of the model zones were determined by matching the measured and calculated concentrations chloride, which behaved conservatively. The model showed that significant saline intrusion occurred within the surface chalk layer due to its low effective porosity and

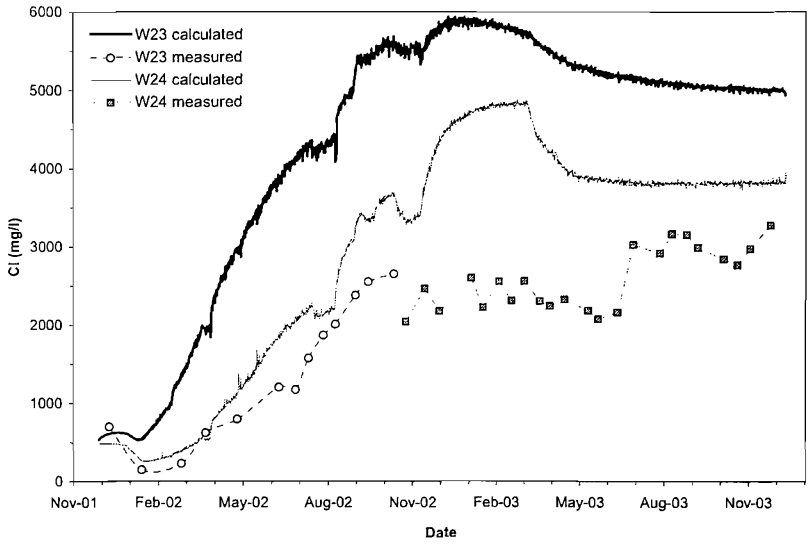

Figure 6.31: *Comparison of measured and calculated chloride concentrations of groundwater abstracted from cell SCC2 using distribution set B. R = 1*

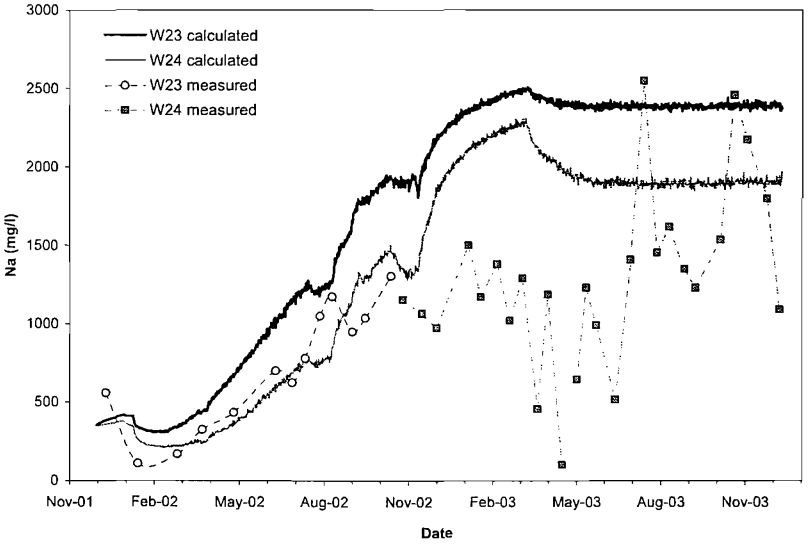

Figure 6.32: *Comparison of measured and calculated sodium concentrations of groundwater abstracted from cell SCC2 using distribution set B. R = 2.95*

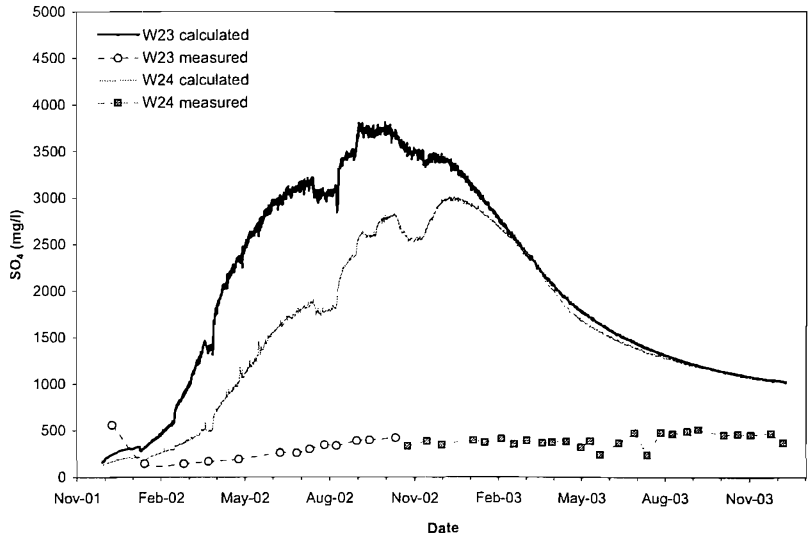

Figure 6.33: *Comparison of measured and calculated sulphate concentrations of groundwater abstracted from cell SCC2 using distribution set B. R = 1*

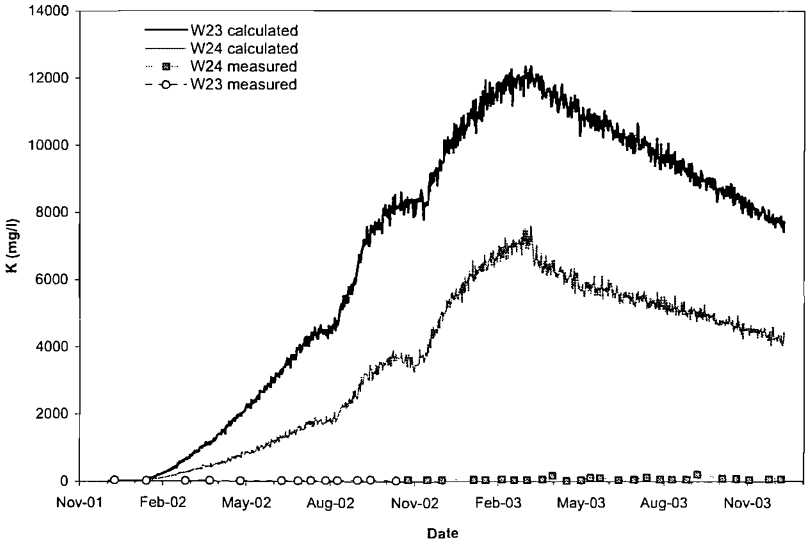

Figure 6.34: *Comparison of measured and calculated potassium concentrations of groundwater abstracted from cell SCC2 using distribution set B. R = 5.80*

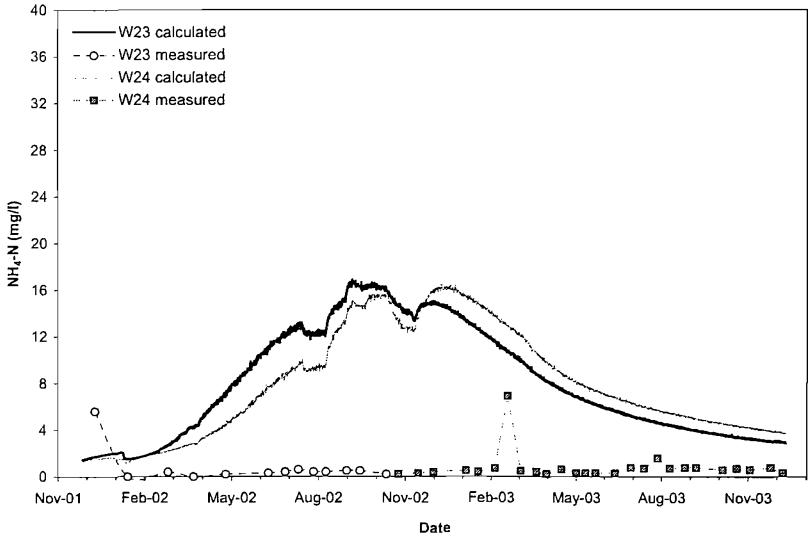

Figure 6.35: *Comparison of measured and calculated ammoniacal nitrogen concentrations of groundwater abstracted from cell SCC2 using distribution set B. R = 2.10*

relatively high permeability. The saline intrusion also occurred through the gravel and base chalk, but advance of the saline front was much slower. A zone of transition between freshwater and saline groundwater developed diagonally across the excavation, leading to variations in the quality of groundwater abstracted between individual wells.

Evidence of ion exchange was found by plotting ion concentration against chloride concentration. Concentrations of sodium and potassium were depleted while calcium was enriched. Retardation factors for sodium and potassium were estimated by modelling the breakthrough of major ions at the excavation. Modelling suggested that attenuation of cement kiln dust leachate from an unlined landfill took place by mixing with freshwater. Further attenuation of potassium may have been caused by adsorption. Groundwater samples from monitoring wells drilled through a landfill lined by naturally occurring alluvial clay layer were contaminated by cement kiln dust leachate. Modelling was used to show that these samples were unrepresentative of the true groundwater quality.

The following chapter will consider the implications of the results for

the assessment of environmental impacts of construction dewatering. In addition, the adequacy of the groundwater quality monitoring programme will be discussed, and recommendations will be made for the designs of future monitoring networks.

Chapter 7

Implications of the modelling results

7.1 Implications for environmental impact assessment

The contaminant transport modelling suggested that significant migration of saline water occurred during construction dewatering. The rate of saline intrusion varied considerably with the aquifer depth in accordance to the effective porosities and the permeabilities of the aquifer layers. The limited vertical flow of groundwater, caused by anisotropy in the chalk layers, may have helped to maintain the stratified salinity depth-profile (Lloyd et al., 1982). It was not possible to validate the depth-profile because of a lack of monitoring wells situated between the Thames boundary and the excavation at variable depths.

The transport of conservative contaminants during construction dewatering was controlled by advection. The saline front advanced quicker towards the sides of the excavation than the corners. Simple calculations, for example using Equation 6.1, can be used to give a reasonable estimates of travel times for groundwater contaminants of different strata. These are particularly useful when considering smaller dewatering projects, where a numerical modelling study is probably unwarranted. In variable ground

conditions, such as the Chalk, it is important to be aware of the range of possible permeabilities and porosities.

Where the site hydrogeology is mildly complex, as was the case study site, making predictions of aquifer contamination requires a comprehensive conceptual understanding of both the ground conditions and the recharge boundaries. Spatial variations in the lateral recharge from boundaries will affect the rate of advection of contaminants. The degree of hydraulic continuity between a saline water body and the aquifer will control the potential for saline intrusion. During construction of the Medway immersed tube tunnel, alluvial clay sealing the base of the river limited the leakage of saline water into the aquifer (Leiper et al., 2000). The modelling suggested moderate inflows from Thames, but increases in the groundwater salinity were still observed. It is unlikely that detailed information of the site boundaries will be available prior to dewatering, so predictions will be based on idealized conditions. During a numerical modelling study, a comprehensive sensitivity analysis should be carried out to determine the effect of changes in both the ground conditions and boundary conditions. The model can then be used as a tool for developing a monitoring policy for a site.

The modelling suggests that a zone of transition between saline and fresh groundwater developed centered around excavation. Clearly, the saline intrusion caused by any construction dewatering activity will be limited to the aquifer between the excavation and the saline source. When the dewatering system is de-commissioned and the water levels are allowed to recover, the new hydraulic gradient will determine if further landward migration takes place, or if freshwater discharging to the river pushes back the saline front. The potential for recovery of groundwater quality will depend on the groundwater conditions of individual sites. The cleaning of an aquifer may require the flushing of a number of pore volumes of freshwater, especially in the Chalk because of its dual-porosity nature.

For small dewatering projects, in which the abstraction lasts for a few months, rather than years, the advance of saline water is likely to be negligible even in low porosity aquifers.

Construction dewatering will also induce the migration of existing leachate plumes within the distance of influence. The modelling showed how the concentrations of contaminants were significantly attenuated during advective transport by mixing. Potassium, an indicator of cement kiln dust leachate, was also attenuated by adsorption, leading to a delay of the contaminant breakthrough at the excavation. Good estimates of retardation factors (R) are required to predict the travel time of non-conservative contaminants.

Baseline groundwater quality data indicated that some short circuiting of flow took place between a landfill lined by a natural alluvial clay layer area and the aquifer. It is expected that short-circuit flow resulted from the construction of site investigation piezometers and monitoring wells. The groundwater quality measurements taken at these locations were found to be unrepresentative of the general aquifer water quality, indicating that contamination due to short-circuiting is limited to inside the well and immediately around the well screen.

7.2 Implications for future monitoring

7.2.1 Evaluation of the site monitoring programme

A number of failings were evident in the site monitoring programme, which limited the the detail of contaminant transport study. These are summarised using categories suggested by Streetly (1998):

No data: An insufficient number of monitoring wells were located between the excavation and the Thames boundary, making it impossible to track saline intrusion into the aquifer. Only one chalk monitoring well, SR5941 (Figure 3.7, was located to the north of excavation and this well showed effects of short-circuiting. In addition, the salinity depth profile could not be established.because the monitoring wells were generally less than 20 m deep and only screened in a single stratum. The nature of cement kiln dust leachate plume at landfill C was not established prior to dewatering.

Incorrect data: As previously discussed, short-circuiting effects gave unrepresentative samples at locations in and around landfill A.

Infrequent data: The influence of tide on groundwater quality was not established for each monitoring well prior to dewatering. Therefore it is difficult to distinguish long term changes from tidal fluctuations, particularly at monitoring wells SA5981 and SA5983. Sampling at many monitoring wells was stopped in June 2002, approximately 6 months after the start of dewatering. The modelling results imply that adequate consideration had not been given to the travel times of the saline fronts. Data are missing because some monitoring wells went dry (AC1919, SA1856, and SA5982) and drawdowns at some wells restricted purge volumes (SA5981 and SA5983). Low purge volumes increased the risk of drawing an unrepresentative sample from the well. Drawdowns were higher than expected, due to the inhomogeneity of the aquifer (discussed in Chapter 4).

Inadequate baseline period Seasonal effects on groundwater quality could not be established from the baseline data, because only 4 to 6 months of background monitoring was carried out.

The methods used to sample monitoring the wells were evaluated using in accordance with headings suggested by Lerner and Teutsch (1995) (Table 7.1). The pumping equipment (Waterra pump) is a low cost technology, which relies on the effort of the operator to raise the water. Therefore, sampling sufficient volumes to purge the volume and collect the sample was time consuming. Furthermore, the ball valve at the pump intake had a tendency to clog with fines, so the pump had to be lifted out of the well for cleaning. The monitoring wells also functioned as piezometers; many were not originally installed for the purposes of groundwater sampling.

The following sections will discuss aspects of the monitoring programme that need to be considered carefully during the design. There is clearly no single sampling method fit for use on all monitoring projects, instead sampling procedures should be decided on a case by case basis (Lerner and Teutsch, 1995).

Table 7.1: *Evaluation of the sampling methods using monitoring wells at the case study site. (After Lerner and Teutsch (1995))*

Category	Comments
Environment	
Hydrogeology	Gravel and Chalk
Type of well	Screened with filter pack
Short circuiting and mixing	Within strata and within well
Investigation type	Long term monitoring
Sampling equipment	
Capital costs	Very Low
Running cost	Low cost of parts, but high labour costs
Ease of use	Specialist staff not required
Availability	Commercially availbale
Decontamination	Not required
Performance	
Level accurate	Within strata
Maximum sample depth	No limit, but time and costs of sampling increases with depth
Volume sampled	2.5 litres
Flushing ability	3 well volumes, where possible
Effect on sample	Possible degassing and sorption to sampling equipment
Multi-purpose use of well	Used for site investigation and monitoring piezometers

7.2.2 Monitoring well construction

Drilling in contaminated land can result in the migration of contaminated water between geological strata particularly where there are significant vertical concentration gradients. Short-circuit flow can be prevented by a number of measures taken during borehole construction. These include the use of a temporary casing to line the borehole during drilling. When drilling through an alluvial clay layer it is recommended that multiple casings should be used. For this method, an initial borehole should be drilled to the base of the clay layer, this borehole should be backfilled with grout with the steel casing in place. A smaller diameter borehole should be drilled through the grout into the underlying aquifer.

Keely and Boateng (1987) discuss the merits of different drilling methods. Mud rotary drilling is unsuitable for the drilling of monitoring wells and site investigation boreholes in contaminated land, because the circulation of drilling fluids may result in cross contamination from one strata to another, as well as the introduction of non-native fluids. The use of bentonite drilling fluids can lead to raised COD levels of groundwater samples. In some geological formations these effects may be long lasting and might not be eliminated simply by well purging (Brobst and Buszka, 1986). Air rotary drilling eliminates the need for drilling fluids by using compressed air to cool the drill bit. However, if water or foam are added to the air stream, some non-native fluids may also invade the environment around the borehole. Cable percussion drilling is the most appropriate method, because no drilling fluid or water is generally required. Furthermore, steel casing will reduce the likelihood of cross contamination. However, the cable percussion method can be more expensive, particularly if deep monitoring wells are required, and progress on the borehole can be slow.

Commonly an annular bentonite seal is used to prevent vertical flow between the borehole wall and the well liner. However, the bentonite itself may be a cause of contamination; the gypsum content of bentonite can contribute to sulphate concentrations of the groundwater. Furthermore,

bentonite may alter the natural concentration of ions (Remenda and van der Kamp, 1997), and therefore bentonite seals should be placed no closer than 1 to 1.5 metres above the well screen to limit contamination of water at lower depths. There is some evidence that the effectiveness of bentonite seals can be inhibited where groundwater has a high total dissolved solids (TDS) content above 5000 mg/l or a high chloride concentration (Nielsen and Schalla, 1991).

It is important for the monitoring well to be well developed after construction to remove any foreign contaminants derived from the construction process. Development will also allow the removal of both soil and rock smeared on the borehole wall during drilling. Smearing will restrict water inflow (Palmer, 1981) and therefore impact upon how groundwater samples represent the true groundwater quality. It is unclear what method was used to develop monitoring wells at the case study site. Development by airlift is not practical in small diameter wells less than 50mm, so a purging method is more appropriate although this is maybe less effective at bringing fines to the surface.

7.2.3 Monitoring well design and sampling

When designing a monitoring well consideration should be given to the purge volumes required to remove stagnant water from the well. Barcelona and Helfich (1986) suggest that the adequacy of purging is the dominant factor affecting the precision of samples. Scalf, McNabb, Dunlop, Cosby and Fryberger (1991) state that four to ten well volumes is a commonly used guide, but standardized guidelines fail to account for differences between the hydraulic and geological settings of individual wells at different sites. Hart, Tomlinson and Chaseling (2000) suggest that electrical conductivity (EC) should be measured during purging with a handheld meter. Samples should be collected once the EC readings have stabilised. Purge volumes and the amount of well development required can be minimised by using a fine uniform gravel or sand well filter in preference to pea gravel (Keely and Boateng, 1987). The use of finer material enables a

more effective filtering of the inflowing water. Minimising the purge volume is helpful if the intention is to sample at shallow depths at which the water level is close to the base of stratum thereby restricting recharge to the well.

The modelling results show that contaminant transport occurs at different rates in different layers of an aquifer. Future modelling designs should consider these variations by sampling at different depths. Lerner and Teutsch (1995) discuss the advantages and disadvantages of different multi-level sampling technologies.

7.2.4 Monitoring well locations

For future monitoring investigations, greater emphasis should be placed on monitoring close to the source of the contamination. Figure 7.1 shows an ideal layout of monitoring wells for a homogeneous aquifer, preferably using piezometer nest arrangements. An array of primary monitoring wells should be used to monitor groundwater quality (and drawdowns) at and near the contamination source. Ideally, monitoring wells would be located along the predicted flowpaths between the source and the excavation. These can be estimated reasonably well using a simple groundwater model. If contaminant migration is detected at the primary monitoring wells, additional secondary wells can be constructed closer to the excavation. These wells can be targeted at specific depths depending on the nature of the contaminant plume or front. Secondary monitoring wells should also be used to monitor groundwater changes at the expected distance of influence. Accessibility issues may place restrictions on the locations of the monitoring wells.

Monitoring of selected dewatering wells should also take place, although it is important to be aware that significant differences in the groundwater of individual wells can exist. All wells should be fitted with a sampling point, allowing regular field measurements of general water quality parameters in order to gauge the variability. The overall quality of the abstracted water should be monitoring of the discharge quality, and will probably be a requirement of the Environment Agency.

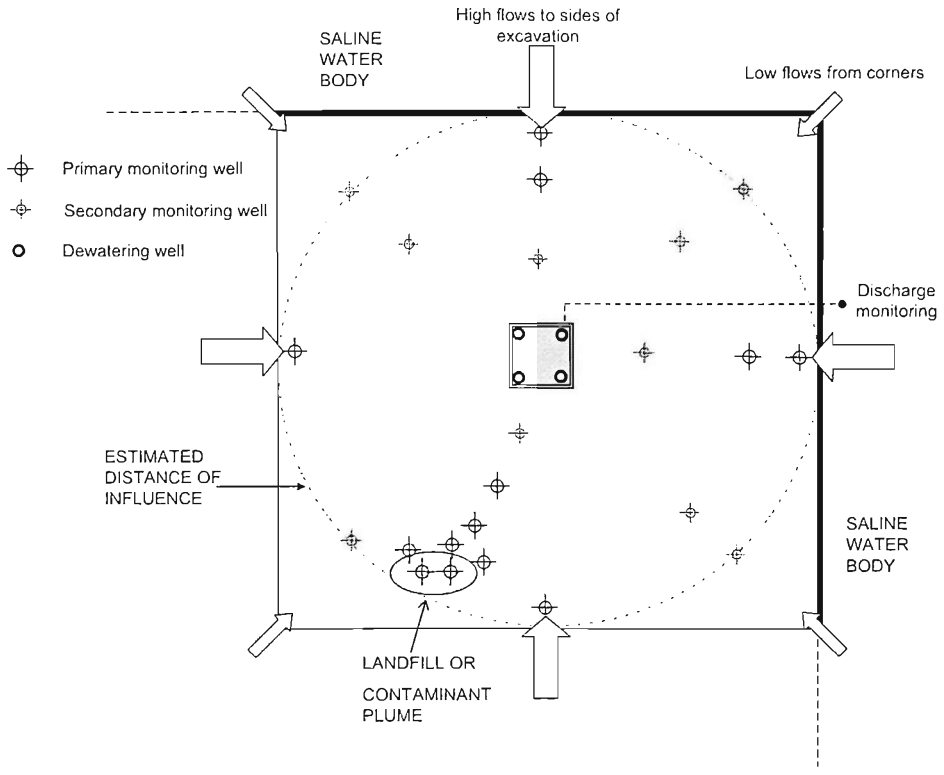

Figure 7.1: *Possible arrangement of monitoring wells*

For a large scale dewatering scheme, it is recommended that a numerical contaminant transport model is developed during the design phase to predict the movement of contaminants. Once a groundwater flow model has been developed, the modelling of conservative contaminants, such as chloride, can be done relatively easily. Monitoring near the source in the first months of dewatering will provide useful data to allow the model to be re-calibrated and in turn, improved long-term predictions can be made. Sampling frequencies should reflect the likely rate of migration, but should be reviewed in light of new data. Providing the key sources of contamination are well monitored, it should be possible to take an observational approach to the monitoring of groundwater quality.

7.3 Summary

In light of evidence that construction dewatering resulted in both saline intrusion and leachate migration at the case study, a review of the site monitoring programme was made. The key failings of the monitoring programme were a lack of monitoring wells able detect the advance of a saline front in the different strata, a premature reduction in the scale of the monitoring programme, and a poor design of some monitoring wells.

Short-circuiting of flow in wells can be prevented by the use of additional drilling casings and the careful placement of bentonite seals. Fine gravel or sand should be used as a filter material, rather than pea gravel, to help minimise the required purge volumes. A greater emphasis should be put on monitoring groundwater quality close to the sources of contamination. For large scale dewatering projects, contaminant transport models can be used as a tool to review and interpret data.

Chapter 8

Conclusions

8.1 Project overview

A good understanding of ground conditions is essential for the design of a successful construction dewatering system. The design engineer is required to make judgements about any site investigation information that is available. A valid assessment of the potential environmental impacts of the construction dewatering requires good predictions of the groundwater flows and remote drawdowns.

The reserach focused on the case study of the CTRL Thames Tunnel southern approach excavation, which required a large-scale deepwell construction dewatering system. A large volume of monitoring data was collected during construction which was analysed using numerical models in order to determine:

- The potential scale of inhomogeneities that may be encountered during construction dewatering and how these can affect groundwater flows.
- The magnitude of groundwater quality changes during the operation of a major construction dewatering scheme with respect to saline intrusion and leachate migration .
- The limitations of a groundwater quality monitoring programme and how future monitoring can be improved.

A number of important conclusions were made in the previous chapters. The key findings are now summarised below.

8.2 The influence of inhomogeneities

- Substantial modifications were required to the construction dewatering system design in order to cope with variable Chalk permeabilities. At the deepest part of the excavation wells were made redundant because of unexpected low inflows. Conversely, near the shallow end of the approach additional wells were required to achieve the necessary drawdown.

- Numerical modelling showed that the performance of the dewatering system could not be satisfactorily explained without the inclusion of large scale inhomogeneities within a 445 m long excavation. These included a zone of anisotropic chalk (k_x/k_z of 350 to 700), causing low inflows, and a zone of isotropic high permeability chalk ($k = 2.7 \times 10^{-2}$ to 6.8×10^{-2} m/s) causing high inflows.

- The site investigation data was inadequate to allow differentiation between the Chalk zones during the design phase. Some evidence of a high permeability zone was available in the form of chalk core samples, but the interpretation of the core data would have been difficult without the benefit of supporting information. Pumping tests were carried out in wells significantly distant from the excavation and the high permeability zone, hence the resulting permeability data were clearly not representative of the whole site.

- High permeability features can significantly increase the distance of influence of a construction dewatering system. Consequently, environmental impacts and ground settlements may be affected at more remote locations.

- Anisotropy can be helpful in achieving target drawdowns using a relatively low pumping capacity. However, the influence of anisotropy

is hard to establish by means of pumping tests, primarily because it becomes more apparent once a barrier to horizontal flow is in place.

- Anisotropy can reduce the distance of influence of a construction dewatering system. Therefore, environmental impacts and ground settlements could be less significant than expected where anisotropic effects are encountered.

- The modelling indicated that the effectiveness of cut-off walls for groundwater control is strongly dependent on the both horizontal and vertical permeabilities of the aquifer at the toe. Optimization of a groundwater cut-off design could be improved by detailed investigation of the vertical permeability.

- If there is sufficient flexibility in the construction schedule, modern methods of data collection and review make it is possible to take an observational method approach. Numerical modelling could be a useful tool in reviewing monitoring data.

- Numerical modelling is a preferable method of design if ground conditions are potentially variable. Distinct zones of permeability can be incorporated and their influence investigated through rigorous sensitivity analysis.

8.3 Environmental impact assessment

- Many larger construction projects require an environmental impact assessment to be carried out prior to any construction activity. This might include the impacts of construction dewatering on the temporary disturbance of the natural groundwater flow regime and levels and the migration of groundwater contaminants.

- The contaminant transport modelling suggested that significant migration of saline water occurred during construction dewatering, with increases in chloride concentrations from 100 mg/l to 5000 mg/l.

- The modelling suggested that rate of saline intrusion varied considerably with the aquifer depth in accordance to the effective porosities and the permeabilities of the aquifer layers. In addition, the limited vertical flow of groundwater, caused by anisotropy in the chalk layers, may have helped to develop the stratified salinity depth-profile. It was not possible to validate the depth-profile because of a lack of monitoring wells situated between the Thames boundary and the excavation at variable depths.

- The modelling suggested that a zone of transition between saline and fresh groundwater developed centered around excavation. The saline intrusion caused by any construction dewatering activity is likely to be limited to the part of the aquifer between the excavation and the saline source.

- For small dewatering projects, in which the abstraction lasts for a few months, rather than years, the advance of saline water is likely to be limited in distance, even in low porosity aquifers.

- To make reliable predictions of saline intrusion the degree of hydraulic continuity between a saline water body and the aquifer will need to be investigated.

- Construction dewatering can induce the migration of existing leachate plumes within the distance of influence. The modelling showed how the concentrations of contaminants were significantly attenuated during advective transport by mixing.

- Potassium, an indicator of cement kiln dust leachate, was also attenuated by adsorption, leading to a delay of the contaminant breakthrough at the excavation. Good estimates of retardation factors (R) are required to predict the travel time of non-conservative contaminants.

- Baseline groundwater quality data indicated that some short circuiting of flow took place between a landfill lined by a natural

alluvial clay layer area and the aquifer. It is expected that short-circuit flow resulted from the construction of site investigation piezometers and monitoring wells.

- Contaminant transport modelling provided a useful tool for the interpretation of groundwater quality data collected during the construction dewatering operations at the case study site.
- Good predictions of contaminant migration require a comprehensive conceptual understanding of both the ground conditions and the recharge boundaries. A comprehensive sensitivity analysis should be carried out to investigate uncertainties.

8.4 Monitoring of groundwater quality

A number of failings were evident in the site monitoring programme, which limited the detail of contaminant transport study. The key failings of the monitoring programme were:

- A lack of monitoring wells able detect the advance of a saline front in the different strata. Distinct vertical groundwater quality variation is likely during construction dewatering as flow is predominantly horizontal.
- A premature reduction in the scale of the monitoring programme. The use of contaminant transport models would allow a more detailed review of data during the construction.
- Poor design of some monitoring wells leading to wells going dry. Careful consideration should be given to the remote drawdown levels to enure that wells penetrate to sufficient depth. Fine gravel or sand could be used as a filter material, rather than pea gravel, to help minimise the required purge volumes.
- Short-circuiting effects were evident in wells drilled below a landfill. Care should be taken to minimise the potential for short-circuiting by

the use of additional drilling casings and the careful placement of bentonite seals.

- A lack of monitoring wells were situated at or close to the source. A greater emphasis should be put on monitoring groundwater quality close to the sources of contamination during the early stages of construction.

8.5 Recommendations for future work

This research has drawn attention to the problems of uncertain ground conditions faced when designing a construction dewatering in the Chalk. It has been shown that anisotropy can have great influence on the performance of a construction dewatering system. The investigation and determination of vertical permeability through field tests is one area that should be given further consideration.

Vertical permeabilities may be determined by conducting a series of pumping tests at multiple levels and monitoring the response using observational wells screened at different levels within the aquifer. Estimates of vertical permeability could be obtained by analysing pumping test data using groundwater models. Alternatively, carrying out pumping tests in conjunction with a groundwater cut-off could give a more reliable estimate of vertical permeability, but would be costly. The challenge remains to find a cost-effective way of determining levels of anisotropy during a site investigation.

The second part of this research has dealt with the migration of contaminants during a period of intensive groundwater abstraction during which significant saline intrusion took place. Further work should be carried out to establish the longer term impacts on the groundwater quality. It is unclear whether saline intrusion is reversed following the de-commissioning of the dewatering system. Post-dewatering monitoring is equally as important as monitoring during the abstraction phase and efforts should be made to collect and interpret data and draw conclusions.

It has been demonstrated that construction dewatering on a relatively large scale may pose a significant risk to the quality of groundwater resources. However, the level risk is dependent on ground conditions encountered. Therefore, it is inappropriate to make general statements on the environmental impacts of construction dewatering works, instead a case by case approach is needed. The monitoring requirements imposed by the regulatory body (Environment Agency) means that monitoring data will be readily available and this data could form the basis of future environmental impact assessments for proposed projects. However, it has been shown that more rigorous monitoring will be required to make a complete scientific investigation of the environmental impacts.

Appendix A

Appendix: Details of *MODEL CT*

A.1 Model development

This section gives details of how *MODEL 1* (Chapter 4) was simplified to *MODEL CT*. The reduction in the number of layers from 12 to 5 meant that the diaphragm wall profile could only be represented approximately. However, the surface areas of the modelled walls were closely comparable to the installed walls (Table 6.2).The diaphragm wall profile is shown in Figure A.1.

Despite the more approximate representation of the strata interfaces in *MODEL CT*, the transmissivity of the overall model and the model zones were maintained (Figure 6.2). The hydraulic conductivity values are compared in Table A.1.

The model was used to simulate the performance of the construction dewatering system for a period of 750 days from 26th November 2001 to 16th December 2003. This required 21 stress periods and the pumping rates were fixed for each period to match the abstraction flow record (Figure A.2) using the analytical well function in Groundwater Vistas. As with the previous models no surface recharge was applied. The lateral recharge was calculated by the model using the boundary conductances specified in Table 4.3.

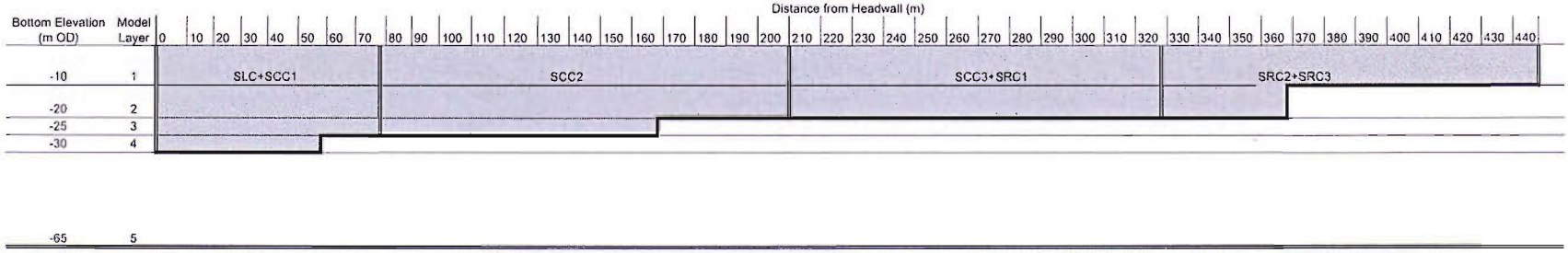

Figure A.1: *Layer discretisation and the stepped diaphragm wall profile*

Table A.1: *Values of hydraulic conductivity (m/day) for each of* MODEL 1 *and* MODEL CT

Zone	*MODEL 1*		*MODEL CT*	
	k_x	k_z	k_x	k_z
Alluvium	0.1	0.01	0.1	0.01
Terrace Gravels	150	150	120	120
Surface chalk	35	0.1	32	0.1
Transition zone	55	36.5	50	33
Outcrop chalk	50	5	32	0.1
High k zone	4800	4800	3550	3550
Base chalk	2	0.02	2	0.02

A.2 Results

The figures in this section show the good match of recorded and modelled drawdowns. The results are briefly discussed in §6.2 and a summary of statistics is provided in Table 6.3.

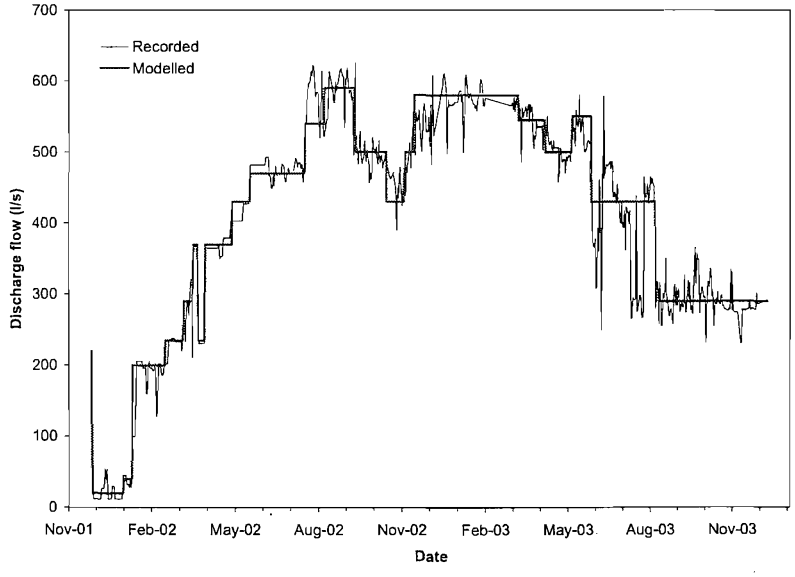

Figure A.2: *Modelled and recorded total abstraction record for* MODEL CT

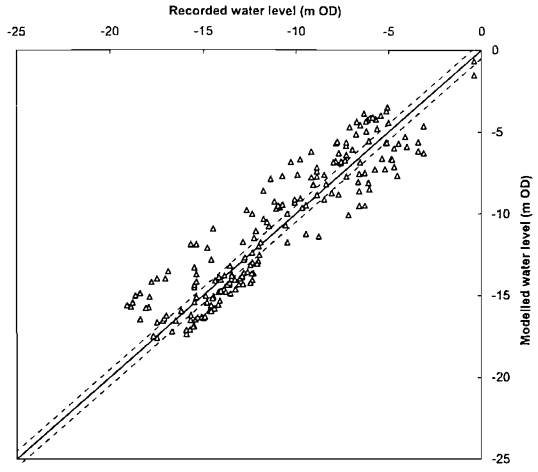

(a) Internal piezometers

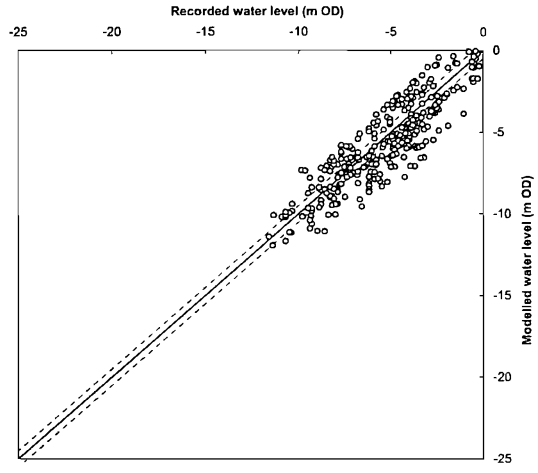

(b) External piezometers

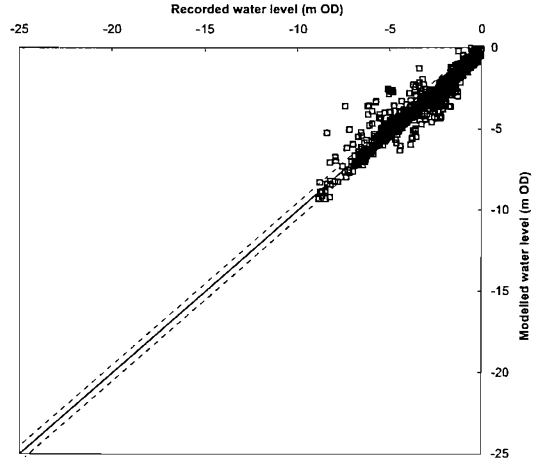

(c) Remote piezometers

Figure A.3: *Drawdowns at selected remote standpipe piezometers in the chalk*

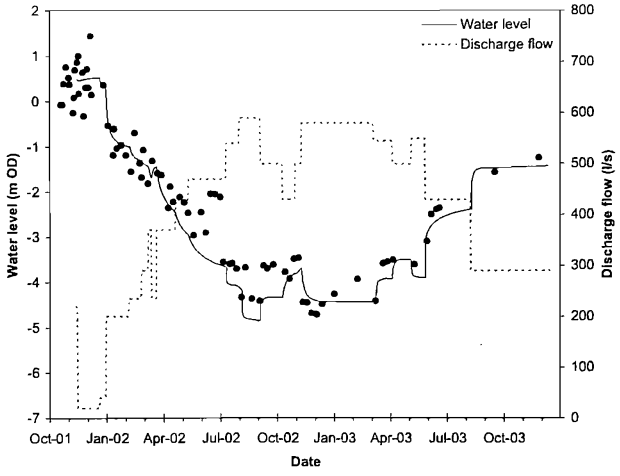

(a) G11

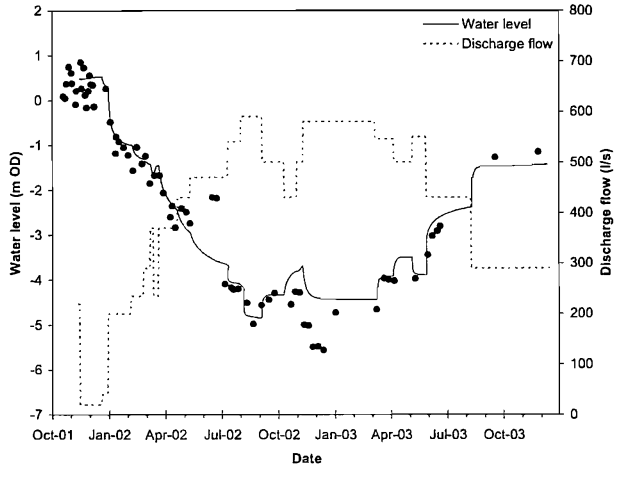

(b) G15

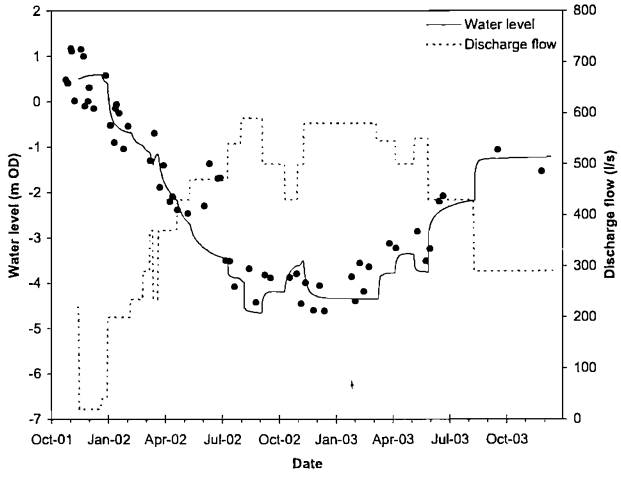

(c) SA5981

Figure A.4: *Modelled (solid line) and recorded (dots) drawdowns at selected remote standpipe piezometers in the gravel*

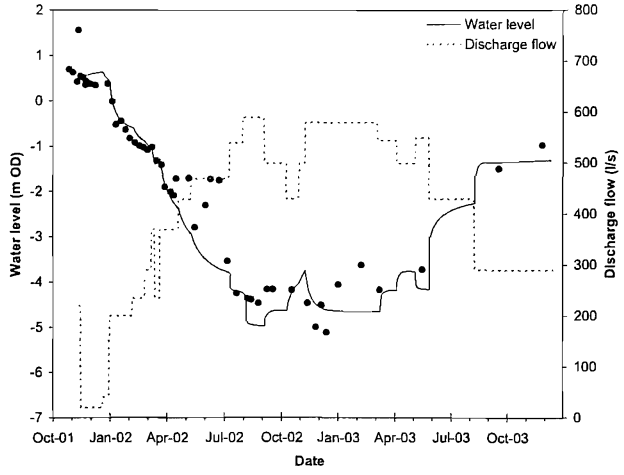

(a) NBH1

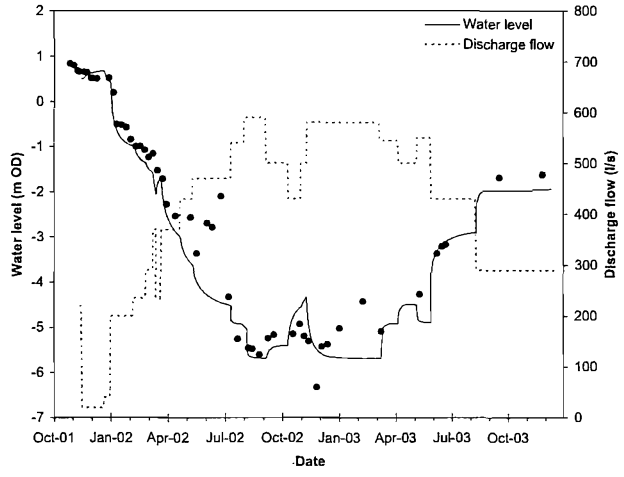

(b) NBH3

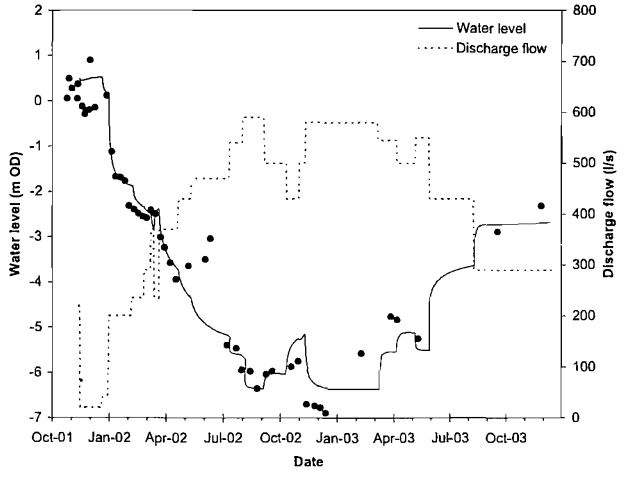

(c) SA5943

Figure A.5: *Modelled (solid line) and recorded (dots) drawdowns at selected remote standpipe piezometers in the Chalk*

References

Anderson, M. and Woessner, W. (1992). *Applied Groundwater Modelling*, Academic press, San Digo.

Attrill, M. and Power, M. (2000). Modelling the effect of drought on estuarine water quality, *Water Research* **34**(5): 1584–1594.

Banks, D., Davies, C. and Davies, W. (1995). The chalk as a karstic aquifer - evidence from a tracer test at stanford-dingley, berkshire, uk, *Quarterly Journal of Engineering Geology* **28**(S1): S31–S38.

Barcelona, M. and Helfich, J. (1986). Dewatering and environmental monitoring for the extractive industry, *Environmental Science and Technology* **20**(11): 1179–1184.

Barker, A., Newton, R., Bottrell, S. and Tellam, J. (1998). Processes affecting groundwater chemistry in a zone of saline intrusion into an urban sandstone aquifer, *Applied Geochemistry* **13**(6): 735–749.

Bear, J. (1972). *Dynamics of Fluids in Porous Media*, American Elsevier, New York.

Bear, J. and Dagan, G. (1968). Solving the problem of local interface upconing in a coastal aquiferby the method of small perturbations, *Journal of Hydraulic Research* **6**(1): 16–44.

Bell, F. and Mitchell, J. (1986). Control of groundwater by exclusion, *in* B. F. Cripps, J.C. and M. Culshaw (eds), *Groundwater in Engineering Geology*, number 3, Geological Society Engineering Geology Special Publication, pp. 429–433.

BGS (1997). *Geological map of the Lower Thames Valley*, British Gelogical Society, London.

Bogli, A. (1964). Mixed-water corrosion, *International Journal of Speleology* **1**: 61–70.

Brobst, R. and Buszka, P. (1986). The effect of three drilling fluids on ground water sample chemistry, *Ground Water Monitoring Review* **6**(1): 62–70.

Cedergren, H. (1989). *Seepage, drainage and flownets*, 3rd edn, Wiley, New York.

Clayton, C. (2001). Managing geotechnical risk: time for change, *Proceedings of the Institution of Civil Engineers, Geotechnical Engineering* **149**(1): 3–11.

Clayton, C., Matthew, M. C. and Simons, N. E. (1995). *Site Investigation*, Blackwell Science, Cambridge.

Connorton, B. (1976). The development of the chalk as an aquifer by solution: a mechanism, *Technical report*, Thames Water Authority, Reading.

Custodio, E. and Bruggeman, G. (1987). *Groundwater Problems in Coastal Areas*, Studies and Reports in Hydrology, UNESCO, Paris.

Darcy, H. (1856). *Les fontaines publiques de la ville de Dijon*, Dalmont, Paris.

DBC (2002). Eastern quarry -planning brief, supplementary planning guidance, *Technical report*, Dartford Borough Council.

DeSimone, L., Howes, B. and Barlow, P. (1997). Mass-balance analysis of reactive transport and cation exchange in a plume of wastewater-contaminated groundwater, *Journal of Hydrology* **203**: 228–249.

Duchesne, J. and Reardon, E. (1998). Determining conrols on element concentrations in cement kiln dust leachate, *Waste Management* **18**: 339–350.

Dupuit, J. (1863). *Etudes theoriques et pratiques sur le movement des eaux*, Dunod, Paris.

Edmunds, W., Shand, P., Hart, P. and Ward, R. (2003). The natrual baseline quality of groundwater: a uk pilot study, *The Science of the Total Environment* **310**: 25–35.

El-Naqa, A. (1994). Estimation of transmissivity from specific capacity data in fractured carbonate aquifer, central jordan, *Environmental Geology (New York)* **23**(1): 73–80.

Elliot, T., Chadha, D. and Younger, P. (2001). Water quality impacts and palaeohydrology in the yorkshire chalk aquifer, uk, *Quarterly Journal of Engineering Geology and Hydrogeology* **34**: 385–398.

Environment-Agency (1998). *Policy and Practice for the Protection of Groundwater*, The Stationary Office, London.

Environment-Agency (2003). www.environment-agency.gov.uk, july 2003.

Erskine, A. (1990). The effect of tidal fluctuation on a coastal aquifer in the uk, *Ground Water* **29**(4): 556–555.

Erskine, A. (2000). Transport of ammonium in aquifers: retardation and degradation, *Quaterly Jounral of Engineering Geology and Hydrogeology* **33**: 161–170.

Fabbri, P. (1997). Transmissivity in the geothermal euganean basin; a geostatistical analysis, *Ground Water* **35**(5): 881–887.

Ferris, J. (1951). Cyclic fluctutaions of water level as a basis for determining aquifer transmissivity, *International Association of Scientific Hydrology* **Publ. 33**: 148–155.

Forth, R. and Thorley, C. (1994). Ground movements due to dewatering for the construction of deep excavations and tunnels in hong kong, *in* W. Wilkinson (ed.), *Groundwater Problems in Urban Areas*, Thomas Telford, London, pp. 31–42.

Gelhar, L., Welty, C. and Rehfeldt, K. (1992). A cririca l review of data on field-scale dispersion in aquifers, *Water Resources Research* **28**(7): 1955–1974.

Gibbard, P. (1994). *The Pleistocene history of the Lower Thames valley*, Cambridge University Press, Cambridge.

Goldberg, E. (1963). Chemistry-the oceans as a chemical system, *in* M. Hill (ed.), *Composition of seawater, comparative and descriptive oceanography of the sea*, Interscience, New York.

Golden-Software (1989). *SURFER Version 4.0*, Golden, CO.

Greenwood, D. (1994). Engineering solutions to groundwater problems in urban areas, *in* W. Wilkinson (ed.), *Groundwater Problems in Urban Areas*, Thomas Telford, London, pp. 369–387.

Hart, B., Tomlinson, R. and Chaseling, J. (2000). Using the stabilisation plateau to estimate optimum well purge volume, *Ground Water Monitoring and Remediation* **20**(3): 113–121.

Haswell, C. (1969). Thames cable tunnel, *Proceedings of the Institution of Civil Engineers* **44**: 323–340.

Hazen, A. (1892). Physical proerties of sands and gravels with reference to their use in filtration, *Technical report*, Report to Massachusetts State Board of Health.

Herbert, G. and Lloyd, J. (2000). Approaches to modelling saline intrusion for assessment of small island water resources, *Quaterly Journal of Engineering Geology and Hydrogeology* **33**: 77–86.

Hoather, R. (1958). Increase in hardness by cation-exchange associated with the infiltration of seawater into chalk under woolwich and reading beds, *Ground Water* **12**: 54–69.

Howard, K. and Lloyd, J. (1983). Major ion characterization of coastal saline ground waters, *Ground Water* **21**(4): 429–437.

Hubbert, M. (1940). The theory of groundwater motion, *Journal of Geology* **48**: 785–944.

Ineson, J. (1962). A hydrogeological study of the permeability of chalk, *Journal of the Institute of Water Engineers* **16**: 449–463.

Johnson, S. (1994). Rising groundwater levels: engineering and environmentl implications, *in* W. Wilkinson (ed.), *Groundwater Problems in Urban Areas*, Thomas Telford, London, pp. 285–298.

Keely, J. F. and Boateng, K. (1987). Monitoring well installation, purging, and sampling techniques - part 1: Conceptualizations, *Ground Water* **25**(3): 300–313.

Knight, D., Smith, G. and Sutton, J. (1996). Sizewell b foundation dewatering - system monitoring, construction and performance monitoring, *Geotechnique* **46**(3): 474–490.

Leiper, Q., Roberts, T. and Russell, D. (2000). Geotechnical engineering for the medway tunnel and approaches, *Proceedings of the Institution of Civil Engineers, Transport* **141**(1): 35–42.

Lerner, D. and Teutsch, G. (1995). Recommendations for level-determined sampling in wells, *Journal of Hydrology* **171**: 355–373.

Lloyd, J., Howard, K., Pacey, N. and Tellam, J. (1982). The value of iodide as a parameter in the chemical charcterisation of groundwaters, *Journal of Hydrology* (57): 247–265.

Logan, J. (1964). Estimating transmissibility from routine production tests of water wells, *Ground Water* **2**: 35–37.

Lord, J., Clayton, C. and Mortimore, R. (2002). *Engineering in Chalk*, Report No. C574, CIRIA.

MacDonald, A. and Allen, D. (2001). Aquifer properties of the chalk of england, *Quarterly Journal of Engineering Geology and Hydrogeology* **34**: 371–384.

MacDonald, A., Brewerton, L. J. and Allen, D. J. (1998). Evidence for rapid groundwater flow and karst-type behaviour in the chalk of southern england., *in* R. N. S. (editor) (ed.), *In: Groundwater Pollution, Recharge and Vulnerability.*, Vol. Special Publication, 130, Geological Society,, London,, pp. 95–106.

Mace, R. E. (1997). Determination of transmissivity from specific capacity tests in a karst aquifer, *Ground Water* **35**(5): 738–742.

Marsland, A. (1986). Floodplain deposits of the lower thames, *Quarterly Journal of Engineering Geology* **19**: 223–247.

Marsland, A. and Randolph, M. (1978). A study of the variation and effects of water pressures in pervious strata underlying crayford marshes, *Geotechnique* **28**: 435–464.

McDonald, M. and Harbaugh, A. (1988). A modular three-dimensional finite- difference groud-water flow model, *Technical report*, United States Geologcal Survey.

Melloul, A. and Goldenberg, L. (1998). Early-indicator signals of groundwater contamination: the case of seawater encroachment, *Environmental Geology* **33**(4): 279–288.

Monkhouse, R. (1995). Prediction of borehole yield in the confined chalk of the london basin, *Quarterly Jounrnal of Engineering Geology* **28**: 171–178.

Morgan, H. and Bubbers, B. (1969). Station construction, *in* H. Follenfant (ed.), *The victoria Line*, Lewis Publishing, Proceedings of the Institution oc Civil Engineers, pp. 453–475.

Nielsen, D. and Schalla, R. (1991). Design and insatllation of ground-water monitoring wells, *in* D. Nielsen (ed.), *Practical handbook of groundwater monitoring*, Lewis Publishing, Michigan.

Owen, M. and Robinson, V. (1978). Characteristics and yield of fissured chalk, *Thames Groundwater Scheme*, Institution of Civil Engineers, London.

Palmer, C. (1981). *Principles of contaminant hydrology*, Lewis Publishing, Michigan.

Peck, R. (1969). Advantages and limitations of the observational method in applied soil mechanics, *Geotechnique* **19**(2): 171–187.

Pickles, A., Lee, S. and Norcliffe, B. (2003). Groundwater and ground movement around deep excavation, *Proceedings of the Institution of Civil Engineers, Geotechnical Engineering* **156**(GE3): 147–158.

Plummer, L. (1975). Mixing of seawater with calcium carbonate groundwater, *in* E. Whitten (ed.), *Quantitative Studies in the Geological Sciences*, Geological Socitey of America, London, pp. 219–236.

Pollock, D. (1990). User's guide to modpath:, *USGS*.

Powers, J. (1992). *Construction dewatering*, 2nd edn, Wiley, New York.

Powrie, W. (1994). Ground movements due to construction dewatering, *in* W. Wilkinson (ed.), *Groundwater Problems in Urban Areas*, Thomas Telford, London, pp. 237–250.

Powrie, W. (2004). *Soil mechanics*, 2nd edn, Spon Press, Oxon.

Powrie, W. and Preene, M. (1992). Equivalent well analysis of construction dewatering systems, *Geotechnique* **42**(4): 635–639.

Powrie, W. and Roberts, T. (1990). Field trial of an ejector well dewatering system at conwy, north wales, *Quarterly Journal of Engineering Geology and Hydrogeology* **23**: 169–185.

Powrie, W. and Roberts, T. (1995). Case history of a dewatering and recharge system in chalk, *Geotechnique* **45**(4): 599–609.

Powrie, W., Roberts, T. and Moghazy, H.-D. (1989). Effects of high permeability lenese on the efficiency of wellpoint dewatering, *Geotechnique* **3**: 543–547.

Preene, M. (2000). Assessment of settlements caused by groundwater control, *Proceedings of the Institute of Civil Engineers, Geotechnical Engineering* **143**: 177–190.

Preene, M. and Brassington, R. (2001). Environmental regulation of groundwater abstraction for dewatering works, *Proceedings of the Institute of Civil Engineers, Geotechnical Engineering* **149**(2): 75–76.

Preene, M. and Brassington, R. (2003). Potential groundwater impacts from civil-engineering works, *Water and Environmental Management Journal* **17**(1): 59–64.

Preene, M. and Powrie, W. (1993). Steady-state performance of construction dewatering systems in fine soils, *Geotechnique* **43**(2): 191–205.

Preene, M. and Roberts, T. (1994). The application of pumping tests to the design of construction dewatering systems, *in* W. Wilkinson (ed.), *Groundwater Problems in Urban Areas*, Thomas Telford, London, pp. 121–133.

Preene, M. and Roberts, T. (2002). Groundwater control in the lambeth group, *Proceedings of the Institution of Civil Engineers, Geotechnical Engineering* **155**(4): 221–227.

Price, M. (1987). Fluid flow in the chalk of england, *in* J. C. G. Williams and B. P. J. (eds), *Fluid flow in sedimentary basins and aquifers*, Spec. Pubn 34, Geol. Soc., London, pp. 141–156.

Price, M. and William, A. (1993). Influence of unlined boreholes on groundwater chemistry: A comparative study using pore-water

extraction and packer sampling, *Journal of the Institution of Water and Environment Management* **7**(6): 651–659.

Price, M., Bird, M. and Foster, S. (1976). Chalk pore-size measurements and their significance, *Water Service* **October**: 569–600.

Price, M., Downing, R. and Edmunds, W. (1993). The chalk as an aquifer, *in* M. P. R. A. Downing and G. P. Jones (eds), *The Hydrogeology of the Chalk of North-West Europe*, Clarendon Press, Oxford, pp. 35–58.

Razack, M. and Huntley, D. (1991). Assessing transmissivity from specific capacity in a large and heterogeneous alluvial aquifer, *Ground Water* **29**(6): 856–861.

Reeves, M. (1979). Recharge and pollution of the english chalk: some possible mechanisms, *Engineering Geology* **14**: 231–240.

Remenda, V. and van der Kamp, G. (1997). Contamination from sand-bentonite seal in monitoring wells installed in aquitards, *Ground Water Monitoring Review*.

Reynolds, R. (1987). Diffusivity of a glacial-outwash aquifer by the wylw technique, *Ground Water* **25**(3): 290–299.

Rhoades, R. and Sinacori, M. (1941). Pattern of ground-water flow and solution, *Journal of Geology* **49**: 785–794.

RLE (2001). Drawing: Plan and long section showing route alignment and gelogical information, *Rail Link Engineering*.

Roberts, T. and Deed, M. (1994). Cost overruns in construction dewatering, *in* B. Skipp (ed.), *Risk and reliability in ground engineering*, Thomas Telford, London, pp. 254–265.

Roberts, T. and Preene, M. (1990). Case studies of construction dewatering in chalk, *Chalk* pp. 571–575.

Roberts, T. and Preene, M. (1994). Design of groundwater control systems using the observational method, *Geotechnique* **44**(4): 727–734.

Robinson, V. (1976). The hydrogeological model of the kennet chalk aquifer, *Technical report*, Unpublished Note,Thames Water Authority, Reading.

Rumbaugh, J. and Rumbaugh, D. (1996). Groundwater vistas.

Sargent, D., Beckie, R. and Smith, G. (1998). Design and performance of deep well dewatering: A case study, *Canadian Geotechnical Journal* **35**(1): 81–95.

Scalf, M., McNabb, J., Dunlop, W., Cosby, R. and Fryberger, J. (1991). *Manual of groundwater sampling procedures*, National water well association.

Scanlon, B., Mace, R., Barrett, M. and Smith, B. (2003). Can we simulate regional groundwater flow in a karst system using equivalent porous media model? case study, barton springs edwards aquifer, usa, *Journal of Hydrology* **276**: 137–158.

Searle, T. and Gammon, J. (1993). Geotechnical aspects of groundwater problems and their classification, *in* W. Wilkinson (ed.), *Groundwater Problems in Urban Areas*, Thomas Telford, London, pp. 31–42.

Shiklomanov, I. (1997). World freshwater resources, *in* P. Gleick (ed.), *Water in crisis: A guide to the world's freshwaterwater resources*, Oxford University Press, New York, pp. 13–24.

Shively, W., Bishop, P. and Gress, D.and Brown, T. (1986). Leaching tests of heavy metals stabilised with portland cement, *Journal of Water pollution Control Federation* **58**: 234.

Sichardt, W. and Kyrieleis, W. (1930). *Grundwasserabsenkungen BEI*, Fundierungsarbieten, Berlin.

Skempton, A. and Chrimes, M. (1994). Thames tunnel: geology, site investigation and geotechnical problems, *Geotechnique* **44**(2): 191–206.

Spink, T. (2002). The ciria chalk description and classification scheme, *Quarterly Journal of Engineering Geology and Hydrogeology* **35**(4): 363–369.

Stevenson, M. and De Moor, E. (1994). Limehouse link cut-and-cover tunnel: design and performance, *Proceedings of the 13th International COnference on Soil Mechanics and Foundation Engineering, New Delhi* **2**: 887–890.

Streetly, M. (1998). Dewatering and environmental monitoring for the extractive industry, *Quaterly Journal of Engineering Geology* **31**: 125–127.

Stringfield, V. and Legrand, H. (1971). Effects of karst features on circulation of water in caronate rocks in coastal areas, *Journal of Hydrology* **14**: 387–404.

Stumm, W. and Morgan, J. (1996). *Aquatic chemistry*, J. Wiley and Sons, New York.

Stuyzand, P. (1986). A new hydrochemical classification of water types: principles and applications to the coastal dunes aquifer system of the netherlands, *Proceedings of the Nineth Salt Water Intrusion Meeting, Delft* pp. 641–655.

Terzaghi, K. (1936). The shearing resistance of saturated soils, *Proceedings of the First International Conference on Soil Mechanics* **1**: 54–56.

Thames-Water (2003). Hydrogeological study of the swanscombe area and eastern quarry, *Technical Report CR/03/183C*, British Geological Survey.

Todd, D. (1980). *Groundwater hydrology*, John Wiley and Sons, New York.

Toynton, R. (1983). The relation between fracture patterns and hydraulic anisotropy in the norfolk chalk, england, *Quarterly Journal of Engineering Geology* **16**(3): 169–185.

Troughton, V. (1987). Groundwater control by pressure relief and recharge, *Proceedings of the 9th European Conference on Soil Mechanics, Dublin* **1**: 259–264.

UK-Groundwater-Forum (1998). *Groundwater our hidden asset*, British Geological Society, Keyworth.

USEPA (1993). Report to congress on cement kiln dust, volume ii: Methods and findings, *Technical report*, Office of Soild Waste, US Environmental Protection Agency.

USEPA (1998). Technical background documenet on groundwater controls at ckd landfills (draft), *Technical report*, Office of Soild Waste, US Environmental Protection Agency.

Van Duijvenbooden, W. and Kooper, W. F. (1993). Effects on groundwater flow and groundwater quality of a waste disposal site in noordwijk, the netherlands, *Science of the Total Environment* **21**: 85–92.

Ward, R. and Robinson, M. (2001). *Priniples of hydrology*, London, 4th edn, McGraw-Hill.

Warren, C. and Mortimore, R. (2003). Chalk engineering geology -channel tunnel rail link and north downs tunnel, *Quarterly Journal of Engineering Geology and Hydrogeology* **36**: 17–34.

WeatherOnline (2006). www.weatheronline.co.uk, march 2006.

Whitaker, D. (2004). Groundwater control for the stratford ctrl station box, *Proceedings of the Institution of Civil Engineers, Geotechnical Engineering* **157**(GE4): 183–191.

White, J. and Roberts, T. (1993). The significance of groundwater tidal fluctutations, *in* W. Wilkinson (ed.), *Groundwater Problems in Urban Areas*, Thomas Telford, London, pp. 31–42.

Williams, R. (1987). Frost weathered mantles on the chalk, *in* J. Boardman (ed.), *Periglacial Processes and Lanforms in Britain and Ireland*, Cambridge University Press, Cambridge, pp. 127–133.

Younger, P. (1989). Devensian periglacial influences on the development of spatially variable permeability in the chalk of southeast england, *Quarterly Journal of Engineering Geology* **22**(4): 343–354.

Younger, P. and Elliot, T. (1995). Chalk fracture system characteristics: implications for flow and solute transport, *Quarterly Journal of Engineering Geology* **28**: S39–S50.

Zheng, C. (1999). Mt3d: A modular three-dimesional transport model for simulation of advection, dispersion and chemical reactions of contaminats in groundwater systems, *Technical Report SERDP-99-1*, U.S. Army Engineer Reserach and Development Center, Vicksburg, MS.

Zheng, C. adn Bennett, G. (2002). *Applied contaminant transport modelling*, Wiley-Interscience, New York.